Feasibility Studies on Ultra High Molecular Weight Polyethylene/Multi Walled Carbon Nanotubes Composites for Total Joint Replacements

A Thesis Submitted in Partial Fulfillment of the Requirements for the Award of the Degree of

DOCTOR OF PHILOSOPHY

by

P. S. Rama Sreekanth

(Roll No. 09610313)

DEPARTMENT OF MECHANICAL ENGINEERING

INDIAN INSTITUTE OF TECHNOLOGY GUWAHATI

GUWAHATI -781039

July 2013

Department of Mechanical Engineering

Indian Institute of Technology Guwahati

Guwahati-781039, Assam, India

Certificate

It is certified that the work contained in the thesis entitled "**Feasibility Studies on Ultra High Molecular Weight Polyethylene/Multi Walled Carbon Nanotubes Composites for Total Joint Replacements"** submitted by **Mr. P.S. Rama Sreekanth** to the Indian Institute of Technology Guwahati for the award of degree of Doctor of Philosophy has been carried out under my supervision in the department of mechanical engineering, Indian Institute of Technology Guwahati. This work has not been submitted elsewhere for the award of any other degree or diploma.

Dr. S. Kanagaraj
Associate professor
Department of Mechanical engineering
Indian Institute of Technology Guwahati

Acknowledgements

I would like to express my gratitude to my supervisor Dr. S. Kanagaraj for his confidence, kindness, and patience with me for all these years. I would also thank my Doctoral committee members for continually reviewing the progress of my work with valuable suggestions and constructive criticism to improve the quality of the thesis. I also deeply acknowledge Prof. D. Chakraborty and Prof. P. Mahanta for extending various facilities in the department of mechanical engineering during the tenure of my research work.

I wish to express my sincere thanks to the technical staff from department of Mechanical engineering and Central instruments facilities for their timely help. I am greatly indebted to M/s Ticona, Germany for supplying UHMWPE, M/s Microtrol Sterilizations Pvt. Limited, Bangalore, for helping in sterilizing the test samples, Mr. Ravi Sarangapani, M/s Shusrut –Alder surgicals. I also thank Prof. J.A.O. Simoes for supplying the material during the initial stages of my work, which helped me gain hands on experience with several analytical tools and experimental setups.

The support received from Mr. Kiran, Mr. Balaji, Mr. Ravindar Reddy, Dr. Mangala Lahkar, Dr. Anuradha at different stages of my work is also acknowledged. I would like to thank my friends Naresh, Santosh, Shravan,Pitambar, Raju, Kiran, Anand, Janaki Ram, Sekhar, Ravi, Arun, Priya, Sridhar, Saumes, Mantulal, Saptarshi who made my work memorable.

I would like to thank my wife Radhika and my daughter Sudha for supporting me in the completion of this thesis in various ways. Their unconditional love and support inspired me to do hard work with dedication. My family has been my strength throughout these years. I especially thank my father for inspiring for hard work, patience and teaching me Indian culture and

philosophy. I don't know how to thank my mother for her love and belief without bothering what kind of science I do. I am also thankful to my brother and my in-laws for their well wishes. Finally, I express my sincere thanks to all who helped me in whatever form during my stay at IIT Guwahati and successful completion of this thesis.

I gratefully thank the supreme Almighty God, who has showered his blessings on me in various ways to make me stand for what I am today.

P. S. Rama Sreekanth

25th July, 2013 IIT Guwahati

Abstract

Ultra high molecular weight polyethylene (UHMWPE) has been the prime choice for total joint replacements (TJRs) owing to its unique attributes like good mechanical properties and wear resistance compared to most of the commonly used engineering polymers. However, some of the critical issues like osteolysis, wear debris generation, and property degradation after irradiation still remain prime concern. In order to seek a solution for some of the problems, it is proposed to develop multi walled carbon nanotubes (MWCNTs) based UHMWPE composites having improved mechanical properties and wear characteristics compared to that of UHMWPE. The MWCNTs were chemically functionalized and physically blended with UHMWPE in a ball milling machine for 45 minutes to form homogeneous mixture with different concentrations such as 0.5, 1.0, 1.5, 2.0, 2.5 and 5.0 wt. % of reinforcement. In order to compare the antioxidant activity of MWCNTs with currently employed antioxidant, UHMWPE was blended with 0.1, 0.3 and 0.5 wt. % of alpha-Tocopherol (α_T). The physically blended powders of UHMWPE/MWCNTs and UHMWPE/α_T were then compression moulded to obtain the test sample in the form of a sheet having the dimension of 20 mm × 20 mm and 0.5 mm thick.

The mechanical properties of the composites and α_T blends were studied according to ASTM D1708 standard. The optimum concentration of MWCNTs in UHMWPE was found to be 2 wt. %, where the work to failure, fracture stress, strain at fracture, and yield stress of the medical grade UHMWPE were enhanced by 176, 93, 70 and 44 %, respectively. However, the presence of α_T was not found to influence the mechanical properties of UHMWPE. The mechanisms related to the enhancement of mechanical properties of UHMWPE upto an optimum concentration of MWCNTs were identified as inherent properties of reinforcement, homogenous dispersion of MWCNTs in UHMWPE, effective stress transfer from UHMWPE to MWCNTs,

and the improved crystallinity of the composites. The hardness and Young's modulus of UHMWPE were found to be enhanced by 75 and 170 %, respectively, whereas the plasticity index was reduced by 17 % for 2 wt. % composites.

In order to estimate the antioxidant potentialities of MWCNTs and compare them with that of α_T, the composites and blends were gamma irradiated at 25, 50, 75 and 100 kGy doses. The mechanical properties of all the test samples were evaluated on a time scale of within 10 days, 60 and 120 days after irradiation. The work to failure and yield stress of the composites and α_T blends were increased with irradiation dose within 10 days after irradiation, whereas they were continuously decreased after 60 and 120 days of irradiation due to free radical induced oxidation. The strain at fracture of irradiated composites and α_T blends was also decreased continuously with ageing. The degradation of mechanical properties of UHMWPE was increased with irradiation dose but it was decreased exponentially with an increase of MWCNTs concentration, whereas a linear decreasing trend was observed in case of α_T blends. The mechanism related to the role of MWCNTs acting as an antioxidant has been confirmed. The crosslink density and radical concentration studies revealed that the presence of MWCNTs has not restricted the crosslinking of the polymer, whereas the presence of α_T showed an opposite trend. The electron spin resonance (ESR) studies revealed that the free radical concentration was found to be reduced with an increase of MWCNTs and α_T concentration in UHMWPE. The antioxidant activity exhibited by 2 wt. % MWCNTs in UHMWPE was similar to that of 0.1 wt. % α_T in UHMWPE. Wear studies on composites and α_T blends were performed using a pin-on-disc Tribometer for the sliding distance of 20 km before and after irradiation. The wear factor of unirradiated UHMWPE was reduced to 71, 59, 44 and 27 % upon adding 2 wt. % MWCNTs, 100 kGy irradiated 0.1 wt. % α_T, 100 kGy irradiation and a combination of 2 wt. % MWCNTs

and 100 kGy irradiation, respectively. The biocompatibility of 2 wt. % composite was studied, where the bone bonding ability, anti-platelet adhesion, and non-irritant behavior of composites were confirmed by *in vitro* and *in vivo* studies. Based on the above study, it is concluded that the MWCNTs reinforced UHMWPE composites can be explored as a potential alternative for total joint replacements to enhance the longevity of the implant material by reducing the material related implant failures.

Contents

List of Figures

List of Tables

Nomenclature

A	Projected area
H	Hardness
L	Sliding distance
P	Applied load
S	Stiffness
V	Wear volume
A_{max}	Maximum contact area
A1	Plastic work done
A2	Elastic work recovered
E^*	Reduced Young's modulus
H_F	Final height
H_0	Initial height
H_s	Heat of fusion of sample
H_f	Heat of fusion of 100 % crystalline polymer
H_r	Resonance frequency
P_{max}	Maximum laod
d	Interplanar spacing
g	Spectral splitting factor
n	Order of diffraction
q_s	Swell ratio
h_{max}	Maximum depth

h_c	Contact depth
h_r	Residual depth
β	Bhor magneton
ν	Indenter shape parameter
ν_d	Crosslink density
λ	Wave length
θ	Angle of incidence
$Ø_1$	Molar volume
χ_1	Flory interaction parameter

Chapter 1

Introduction

1.1 Definition of a Biomaterial

Biomaterial is a material used to make devices to replace a part or a function of the body in a safe, reliable, economic, and physiologically acceptable manner, Hench et al. [1982]. Materials of a wide variety are being used for different devices and the treatment of disease or injury. These primarily include simple and common items such as sutures, needles, catheters, plates, tooth fillings and the devices for complete heart replacement, lung assist devices and total joint replacements. A good number of definitions has been proposed for the term biomaterials over the years. In a simple term a *biomaterial* can be defined as "A synthetic material used to replace part of a living system or to function in intimate contact with living tissue and does not trigger any adverse biological reactions", Black [1992].

Biomaterials are classified primarily in three ways, Park et al. [2003]. First, the biomaterials may be considered from the point of view of the problem that is to be solved, e.g. replacement of diseased or damaged part, assist in healing, improve functionality and correct cosmetic problems. Second is based on tissue level, organ level or a system level, e.g. Heart, lung, eye, ear and bone. Third is the classification of materials in order to meet the requirements specified as above, e.g. Polymers (nylon, silicone rubber, polyester, polyethylene, etc.) are used in sutures, blood vessels, hip socket, ear, nose and other soft tissues; Metals (Ti and its alloys, Co-Cr alloys, Stainless steels, Au, Ag, Pt, etc) are used in joint replacements, bone plates and screws, dental implants, pacer and suture wires; Ceramics (Alumina and Zirconia) are used in dental implants, femoral head in hip prosthesis and other orthopedic applications. The following two parameters are required to be considered when a material is intended to be used as a biomaterial: (i) the effect of

the body environment on the material and (ii) the effect of the material on the biological system, Park et al. [2003].

The field of biomaterials has evolved over the past 50 years from the innovation of individual medical devices to the most sophisticated equipments to save the lives of the patients by integrating science and technology for the betterment of the overall medical service systems. The number of medical devices used in the USA and globally is given in Table 1.1, Ratner et al. [2004], and the illustration of various devices and implants that are intended to use in the human body is shown in Figure 1.1, Park et al. [2007]. Although a number of devices used for blood bags, catheters and contact lenses is several times more compared to cardiovascular and orthopedic devices, nonetheless, the revenue involved with them is relatively less. The revenue involved in cardiovascular devices was about 6 billion USD in 2002 and that of orthopedic devices was 4.7 billion USD in 1998, Ratner et al. [2004], which is significantly higher than most of the other medical devices. It is observed from Table 1.1 that the number of hip/knee implants for global use was 750,000 and it is also seen from the literature that the number of replacement surgeries was also increased globally. Thus the proposed research work is focused on the longevity enhancement of ultra high molecular weight polyethylene (UHMWPE) used as one of the articulating components in hip joint replacement.

Table 1.1 Number of various medical devices used in USA and globally, Ratner et al. [2004]

Device type	Number of devices (US)	Number of devices (Global)
Intraocular lenses(2003)	2,500,000	7,500,000
Contact lenses2000)	30,000,000	90,000,000
Vascular grafts	300,000	900,000
Heart valves	100,000	300,000
Pacemakers	400,000	1,200,000
Blood bags	40,000,000	1,200,000,000
Breast prostheses	250,000	750,000
Catheters	200,000,000	600,000,000
Heart-Lung (Oxygenators	300,000	900,000
Coronary stents	1,500,000	4,500,000
Renal dialysis	320,000	960,000
Hip prostheses (2002)	250,000	750,000
Knee prostheses (2002)	250,000	750,000
Dental implants (2002)	910,000	2,730,000

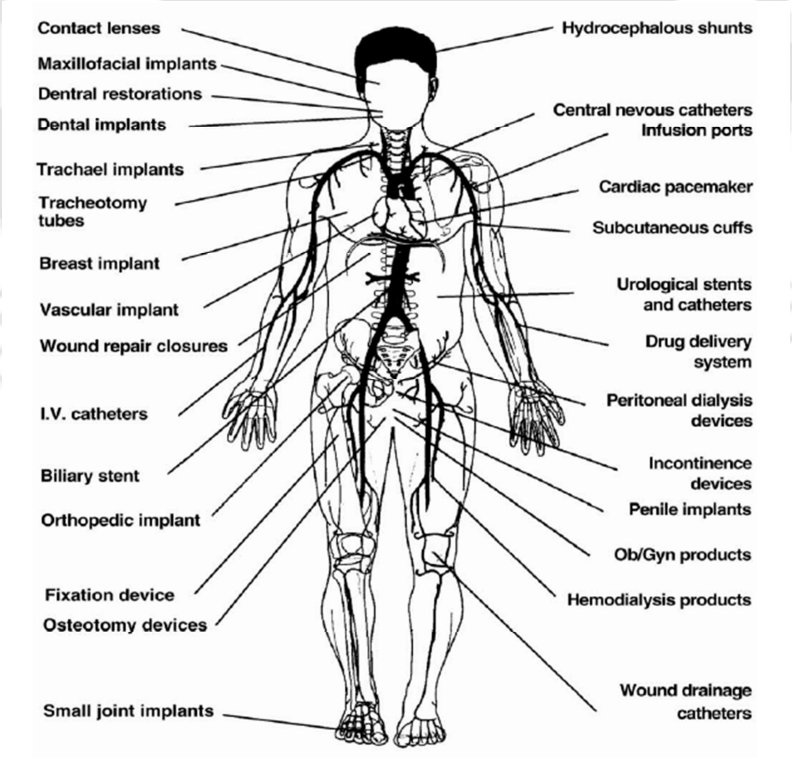

Figure 1.1 Schematic diagram of a human body showing various implant devices and materials. Park et al. [2007]

1.2 Understanding structural anatomy of Human joints and artificial prosthesis.

Human joints have a crucial role to play in the overall functioning of the body and carry out routine activities allowing bones to articulate on one another. Joints allow a wide variety of stability and motion options, which vary depending on their location, position and function. For example, the hip joint can be compared to a ball- on- socket joint allowing motion in three axes, and the knee joint acts as a disk-on-plate allowing restricted type of motion. Besides, the human joints are also classified as load bearing joints and non-load bearing joints. Hip, knee and ankle joints are among the primary load bearing joints and these are also called synovial joints. Most of the other joints such as elbow, shoulder, wrist etc. pertain to non-load bearing class. Typical anatomy of synovial joints is shown in Figure 1.2. The joints may vary in their shape, size and loading pattern but their typical lubrication mechanism remains the same. The articulating surfaces of the bones are covered with articular cartilage preventing their direct physical contact. The assembly is encapsulated by ligament and joint capsule, which is lined with synovial membrane and filled with synovial fluid, Sokoloff [1978]. The tribological behaviour of the natural joints is extremely good due to the presence of synovial fluid, which allows the joints to work under a wide range of loading conditions without causing damage to the bones. The excellent lubrication of joints is due to very low coefficient of friction of bone, (0.003 – 0.015), which usually last for over 70 years, Dumbleton [1981]. However, the joint may lose its natural lubricating function due to accident or some degenerative joint diseases like arthritis or due to excessive wear leading to severe pain in the joint location. Now, the patient needs to be operated for joint replacement with artificial implant materials paving a way for Total Joint Replacements (TJRs) surgeries. Although TJRs are common in case of knee, shoulder, elbow, wrist, ankle and finger joints, these are the recent developments compared to that of hip joints.

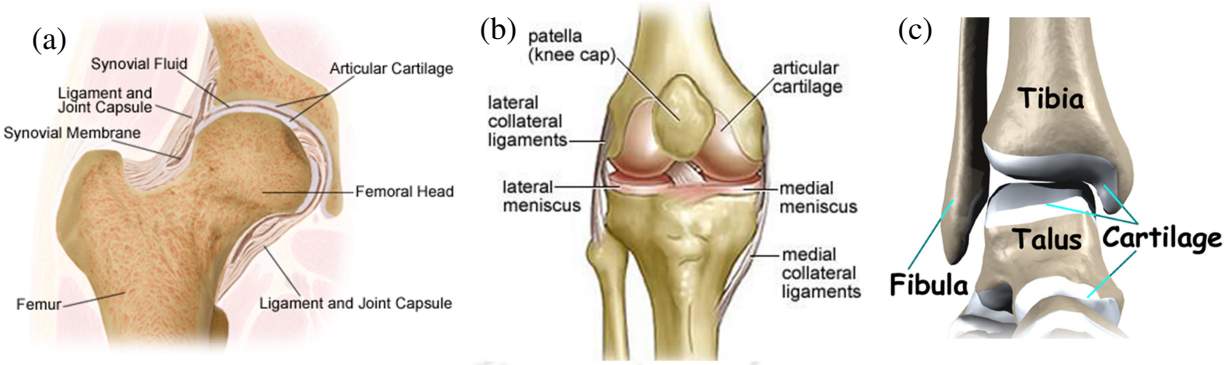

Figure 1.2. Anatomy of load bearing joints (a) Hip joint (b) Knee joint (c) Ankle joint [http://]

The details of the different parts used in total hip replacement are shown in Fig 1.3. A total hip prosthesis consists of 4 major components namely femoral stem, femoral head, acetabular cup and metallic back up fitted into the pelvis. Acetabular cup is fit into the metallic back up either by mechanical fixation or by using PMMA bone cement, Ritter [1995]. The femur bone is sectioned at the greater trochanter at a suitable angle and the femoral stem is fixed either by press fit or cemented fixation, Ducheyne [1988]. The femoral head is fixed on the stem and then anatomically positioned into the acetabular cup.

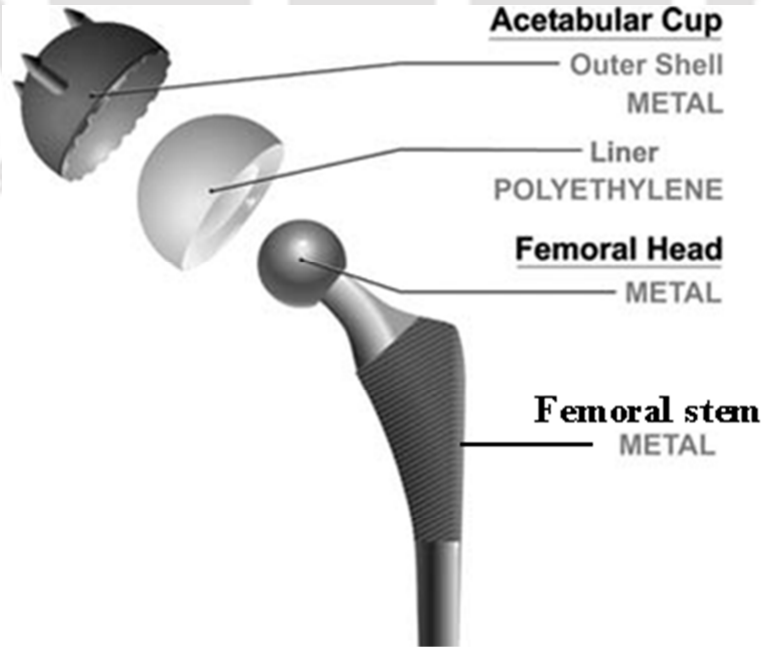

Figure 1.3 Assembly of artificial hip prosthesis, Narayan [2009]

1.3 Importance of the selected problem

Arthritis is a degenerative joint disease resulting in severe pain to the patients. More than 230 000 total hip arthroplasty (THA) and 490 000 total knee arthroplasty (TKA) were performed annually in USA alone, Kurtz et al. [2007] and the number of TJRs was expected to increase substantially for the next 2 decades, Kurtz et al. [2005]. Though it is originally intended for older patients, THA is now being used in younger and much more active patients, who require prosthesis that can last longer and endure a much more active lifestyle without the need for a revision. Thus, the design goals have been advanced from simply alleviating pain and discomfort for older patients to returning physically demanding life styles including sports activities for young active patients, Lewis [2001]. Davidson et al. [2003] reported that the total number of revisions resulting from the wear of an acetabular cup was more than 10000 per year.

Figure 1.4a shows the projection of both total hip and total knee replacements from 2005 to 2030, where the total hip revisions are projected to grow from 40,800 to 96,700 corresponding to an increase of 174 % and the total knee revisions are expected to increase by 673 %. Figure 1.4b shows the possible reasons for failure of an implant, where it is observed that the probability of implant failure due to infection was prominent during the initial 3 years period but later it was reduced to zero at 5 years. However, the failure of an implant due to other factors like loosening, fracture and wear are also found to increase over time. The rising prevalence of TJRs is a clear indication of the severity of the problem and thus it necessitates for a high-end engineering solution to enhance the longevity of the implant.

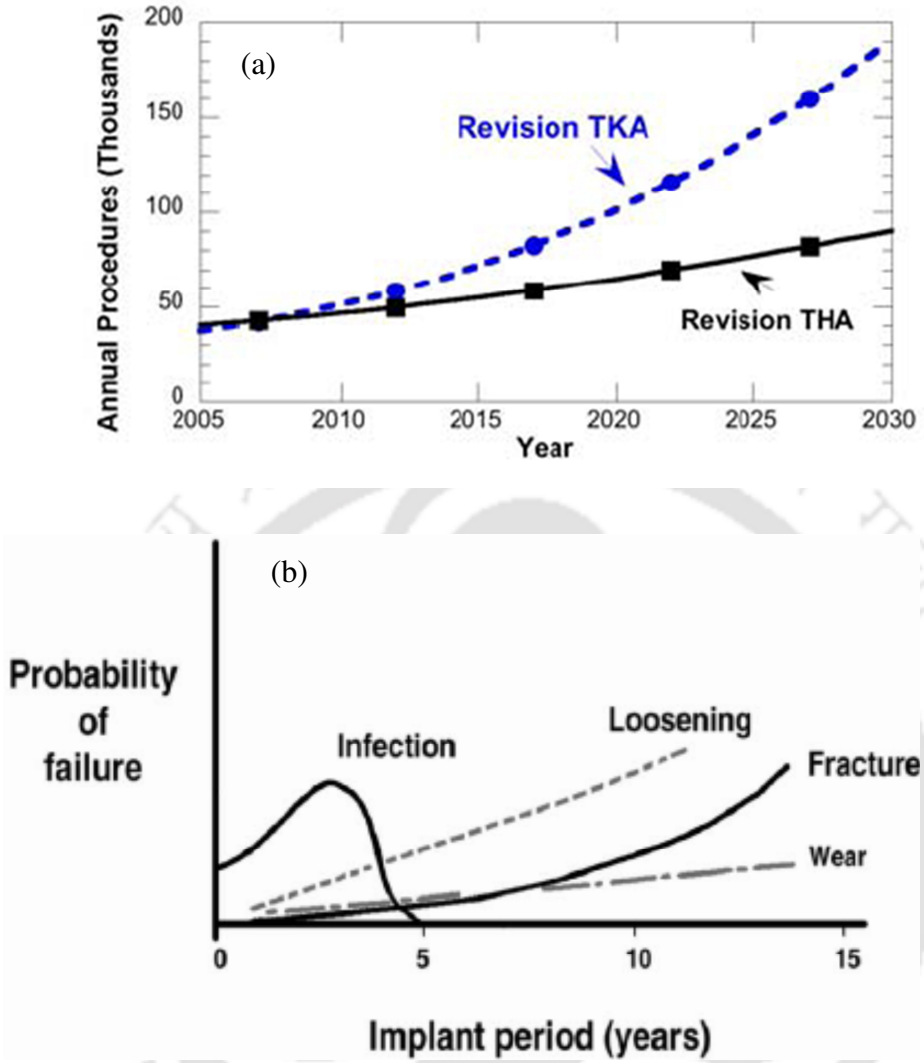

Figure 1.4 (a) Projected revisions of THA and TKA in USA, Kurtz et al. [2007] (b) Possible reasons for implant failure, Park et al. [2007]

1.4 Reasons for revised surgery

The objective of THA is to relieve the pain in the joint location and restore its original mobility. The shape, size and design of the implant depend primarily on the location at which it is used in the body. The typical arrangement of different material combination currently used for THA along with fixation technique used for femoral stem and acetabular components is shown in Figure 1.5.

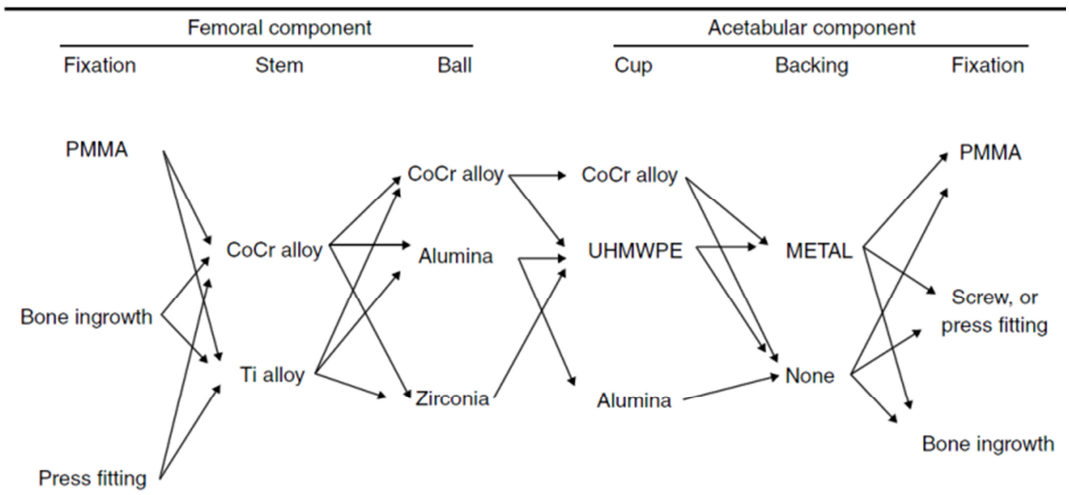

Figure 1.5 Possible combinations of different materials used in THA, Wong et al. [2007]

Based on different combinations, the prosthesis can be made of a Metal- on- metal or ceramic - on - ceramic or Metal - on - polyethylene or ceramic on polyethylene. Though different combination of materials are used in THR, the artificial hip prosthesis implanted in the patient is not once in a lifetime procedure, the chances of revised surgery may vary depending on the life style, activities and other post operative care of the patient. Various factors that enforce primary surgeries are given in Figure 1.6a, where the main reason for primary hip surgeries is observed to be Osteoarthritis, which constitutes 87.7 % of the total surgeries performed. Figure 1.6b shows the possible reasons for the revision surgeries, where the aseptic loosening, implant breakage and wear of acetabular caused 58 % of total revisions. During hip surgery, the synovial membrane needs to be cut to access the joint and it is not known from the available literature that whether the synovial membrane functions correctly or not after the surgery, Burger et al. [2007]. If it does not function properly, it leads to direct mechanical contact of the articulating surfaces and causes asperity contacts, which generate heat and wear debris. Local bone resorption resulting from the

polyethylene wear debris is one of the primary causes for loosening of the component in hip replacement surgery.

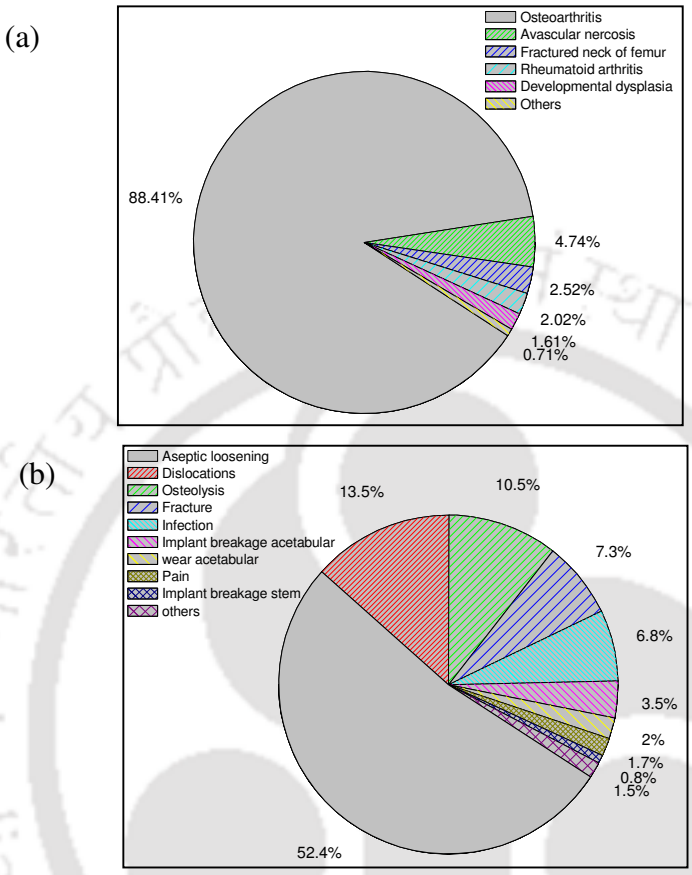

Figure 1.6 Statistics showing various factors leading to (a) Primary (b) Revision of Hip surgeries, Davidson et al. [2003]

1.5 Why is wear of acetabular cup so prominent?

Concerns have been raised about the biological influence and lifetime effects of the wear debris. Wear has been accepted as a major cause of osteolysis in THA. Submicron wear particles migrate into the effective joint space and stimulate a foreign-body response resulting in bone loss, Zhu et al. [2001]. In many patients, the bone around the implant became worn away leading to reduced joint function, which was caused by wear debris induced osteolysis in the implant, Amstutz et al. [1992]. In a normal metal-on-polymer bearing couple, the wear debris is generated

from the acetabular cup against femoral head and it can cause serious damage to the living tissues. Though UHMWPE is biologically an inert material, presence of large amount of biologically an inactive particulate material can trigger an exceptionally strong macrophage response, which leads to osteolysis around the implant in general and bone- implant interfaces in particular, Peter et al. [1996]. It was also observed from four to seven-year follow-up studies that metal- on- metal articulation was appeared to be effective in order to reduce the wear and loosening of the implant compared to that of metal-on-polyethylene, Dorr et al. [2000]. However, the metal debris generated during usage can become ionized and travel anywhere in the body, Zhu et al [2001]. Though there is no strong link between metal ions and health problems, patients with metal-on-metal implants have shown high metal levels in their blood and organs, and there is a lot of concern about systemic health effects, Harris [1995]. Thus, there has been increased focus on the development of alternative materials or improvement of wear resistance of existing materials for the total joint replacements in order to reduce the number of costly revision surgery often necessitated by the osteolysis triggered by the wear debris.

1.6 Motivation of work

UHMWPE has been in use as a biomaterial for TJRs since 1961. From the date of its inception as a material for acetabular cup by Dr. Sir Charnley, it has become a cynosure of all biomaterial scientists due to its chemical resistance, lubricity and extraordinary resistance to wear, which are all crucial parameters in increasing the longevity of the implant. However, even after 50 years (1961-2011) of its usage in TJRs, the number of revised surgeries being performed due to material related problems is a major concern among the material science and medical community. The statistical projections of the TJRs discussed in Figure 1.4a and Figure 1.4b indicated a mammoth increase of the replacement surgeries and related material problems caused

about 58 % of revised surgeries. An increase of number of revised surgeries enforces increased economic, hospital infrastructure and professional burden and the total expenditure for the joint replacement surgeries is also expected to increase. According to Kim [2008], the total annual hospital cost for primary and revision hip and knee arthroplasty procedures in the USA was estimated to be $9.1 billion in 2004 and is expected to exceed $80 billion by 2015.

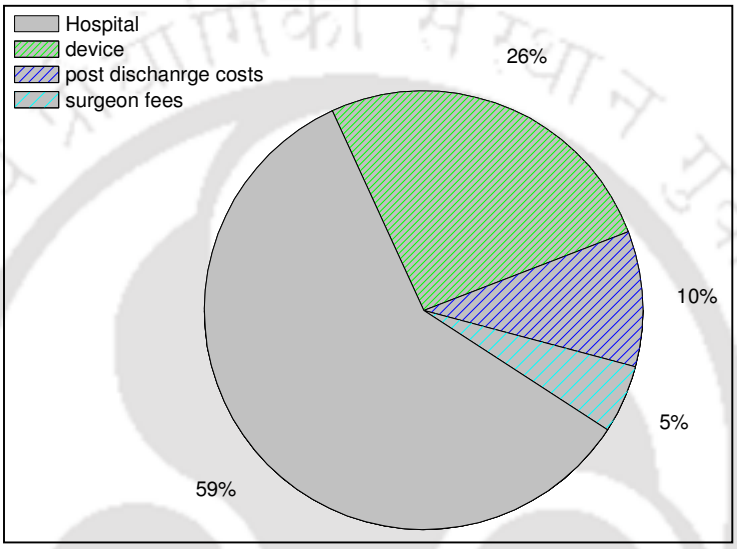

Figure 1.7 Breakdown of an expenditure for the total hip arthroplasty, Lavernia et al. [2007]

Figure 1.7 shows the breakdown of an expenditure for the THA surgery, where it is observed that about 59 % of the total cost goes to hospital facilities and infrastructure, Lavernia et al. [2007]. An increase of TJRs is not only a burden to the patient but also to the government and medical care units to meet the economic factors surrounding the THR and provide the necessary facilities to improve the patient comfort standards. Thus, there is a need for the researchers in orthopedics to envisage the economic impact that a hip arthroplasty can have for the society. The demands and challenges have kept the research activity still open for providing a permanent solution for the aforementioned problems with an uncompromising implant life for the TJRs. Thus, an

attempt is being made in that direction to develop a UHMWPE based composite material for acetabular cup component with improved longevity addressing to the present and future challenges faced by the patient and medical care units.

1.7 Organization of thesis

The present thesis is organized into five chapters. Chapter 1 gives the definition of a biomaterial and its classification with an emphasis on orthopedic implant materials and its importance. Basic anatomy of human joints, its functionality, and the role of joint prosthesis were also covered. The significance of the selected problem, its causes, necessity and motivation to carry out the present work are also briefly described.

Chapter 2 presents a literature review in the field of radiation crosslinking, α-tocopherol (vitamin E) blends with UHMWPE, composites, antioxidant activity of MWCNTs, and finally the biocompatibility of MWCNTs. The technical gaps present in the above referred field were identified and the objectives for the present work were framed.

Chapter 3 gives a detailed description of the techniques involved in the sample preparation and its coding. Methods used for the characterization of the processed samples for assessing their mechanical properties, wear characteristics, network parameters and biocompatibility were presented in a methodical way.

Chapter 4 describes the results and discussion on the role of MWCNTs in enhancing the properties of UHMWPE, the synergy between the matrix and reinforcement in the presence of gamma irradiation, the mechanism and reason behind the influence of MWCNTs on the network parameters and the comparison of results with that of conventional antioxidant. The wear

behaviour of the composites at different doses of irradiation and finally the biocompatibility of composites were also deliberated at length.

Chapter 5 presents a gist of the overall work, prominent results obtained and salient findings from the thesis work. A conclusion note and the future direction for the present work were also briefed.

Chapter 2

Literature review

UHMWPE is being used as a biomaterial for joint arthroplasty due to its remarkable properties. Ever since its inception, it is being continually evolved through the ages to stand as an immediate alternative for total joint replacements. From the nascent stages of virgin polyethylene to recent developments like surface modification and carbon nanotube composites, UHMWPE has undergone a gradual transition in improving its wear resistance to assist the longevity of implant. The success of an implant used as an articulating surface is influenced by the number of wear debris generated from it and many attempts are being made, which are discussed below, to reduce the same. This chapter is broadly divided into two divisions: (i) a critical review of the reports on the various techniques to reduce the wear volume and enhance the longevity of UHMWPE, and (ii) identifying the underexplored zones in the field of proposed research. The literature review has been broadly categorized into 5 subsections, which are as follows:

i) Effects of gamma radiation on the mechanical properties and wear resistance of UHMWPE
ii) Vitamin E as an antioxidant used in UHMWPE
iii) Effects of reinforcement on the mechanical properties and wear resistance of UHMWPE
iv) Antioxidant activity of MWCNTs and their influence on composites
v) Biocompatibility of MWCNTs

Various literature available under each subsection has been discussed in chronological order detailing their advantages and limitations.

2.1 Effects of gamma radiation on mechanical properties and wear resistance of UHMWPE

The molecular chain architecture of UHMWPE imparts many unique attributes, including toughness, and wear resistance, Lewis [2001]. Over the years, a good amount of expertise has been invested in studying the wear phenomenon of UHMWPE and developing strategies for reducing *in vivo* wear of virgin UHMWPE bearing components. However, the high demands of 'zero wear' are not yet fulfilled by UHMWPE and hence it necessitates the structural modification of UHMWPE in order to improve its characteristics.

Crosslinking of the polymer chain is the first step towards achievement of the goal. Three classes of methods are being used for crosslinking the polymers: radiation-induced crosslinking, chemical-induced crosslinking, and silane compound-induced crosslinking. Among these three methods, radiation induced crosslinking has dominated in medical applications as the other crosslinking techniques influenced the biological reaction in the body, Aquino [2012]. Gamma irradiation of UHMWPE induced several changes in its structure. The properties of irradiated UHMWPE was influenced by the irradiation dose and its environment. Premnath et al. [1999] reported that the crosslinking of UHMWPE dominated when irradiation was done in absence of air, whereas chain scission of polymer was observed to dominate when irradiation was done in air environment. Oonishi [1995] attempted highly crosslinked UHMWPE by over 1000 kGy of gamma irradiation in air for orthopedic applications.

Costa et al. [1997] showed that oxidation of polymer took place even during manufacturing. In order to confirm the same, they tested commercially available 2 samples: (i) ram extruded and (ii) compression moulded UHMWPE. It was confirmed that primary dialkyl peroxides were formed in different concentrations during the mechano-oxidative degradation of UHMWPE. Costa et al. [1998] compared the oxidation level of UHMWPE sterilized by gamma irradiation

and ethylene oxide (ETO). It was reported that the amount of oxidation was found to be higher in gamma sterilized samples compared to ETO. Their studies also proved that all the samples showed surface oxidation, which was formed during the processing condition. It was concluded that the oxidation of UHMWPE due to gamma sterilization led to inhomogeneous distribution of reactive species in polyethylene, which caused unpredictable *in vivo* performance of UHMWPE. Muratoglu et al. [1999] studied the influence of irradiation dose on the mechanical properties, and wear resistance of UHMWPE. They observed that the ultimate tensile strength and yield strength of UHMWPE were reduced by 52 and 10 %, respectively at 300 kGy irradiation dose compared to that of unirradiated sample. It was also concluded that the molecular weight between the crosslinks strongly influenced the wear resistance of the sample. Edidin et al. [2000] reported that the mechanical properties of UHMWPE were significantly reduced after accelerated ageing for 4 weeks. They observed that the crystallinity of aged UHMWPE was found to be higher than that of virgin polymer. Puertolas et al. [2001] characterized UHMWPE, which was subjected to gamma irradiation after a shelf ageing for a period of 6 years. It was reported that the fracture stress and strain of aged sample were reduced by 20 and 97.1 %, respectively compared to unaged sample. Lewis [2001] reviewed the properties of crosslinked UHMWPE, where the mechanism involved for the degradation of properties after irradiation was deliberated. It was concluded that the crosslinking improved the wear resistance of the polymer but there was a concomitant depreciation of its mechanical properties. Kang et al. [2001] studied the effect of gamma irradiation on the thermal and mechanical properties of UHMWPE. The crystallinity of the sample was reported to be increased with irradiation dose. The strain at fracture and wear volume of UHMWPE were reduced by 54 and 40 % at 250 kGy compared to that of unirradiated sample. Suarez et al. [2003] irradiated UHMWPE from 100 to 2000 kGy

doses to confirm its loss of ductility. It was reported that the relative intensity of free radicals was increased from 12 to 145 at 100 and 200 kGy dosage, respectively. The strength and fracture strain of UHMWPE were found to be reduced by 21.5 and 93 % compared to unirradiated polymer at 250 kGy. Maadeed et al. [2006] reported that the density, crystallinity and shore hardness of UHMWPE were increased after irradiation and subsequent shelf ageing. Oral et al. [2007] reviewed the effects of radiation crosslinking on UHMWPE. The primary conclusion from their review was that the crosslinking of UHMWPE increased its wear resistance but it also left with long-lived residual free radicals in the polymer causing the reduction of its mechanical properties.

Oonishi et al. [1997] studied the wear resistance of irradiated UHMWPE against an alumina ball using a sphere-on-plate reciprocating testing machine. It was reported that the wear resistance of UHMWPE was increased with irradiation dose in comparison to that of unirradiated specimens. However, the coefficient of friction of the test sample was not influenced by the irradiation, but the hardness of the samples was increased. Lee et al. [2009] performed scratch and wear tests on a prosthetic femoral head against crosslinked UHMWPE sockets using a 8-station hip wear simulator for 2 million cycles. They reported that abrasive wear of UHMWPE was reduced by 97 % against Zirconia toughened alumina compared to CoCr. In case of oxide coated Zirconium-Niobium femoral head, the abrasive wear resistance of UHMWPE was increased by 161 % compared to CoCr. Bashyal et al. [2011] opined that the benefits of improved wear resistance and low rate of osteolysis of highly crosslinked polyethylene outweighed the concerns of ageing degradation of the properties.

Sugano et al. [2004] studied the wear rate of 1000 kGy irradiated UHMWPE acetabular cup retrieved after 25 years of its usage under *in vivo* condition. It was reported that the wear rate

of retrieved cup was found to be 0.04 mm/year whereas the conventional cup under *in vitro* condition had the wear rate of 0.06 mm/year.

Muratoglu et al. [2002] irradiated UHMWPE using 2 MeV electron beam at 140 ^{o}C to obtain the limited penetration effect of irradiation. The wear studies on irradiated sample using a 12-station hip simulator showed that there was no significant mass loss after a million cycles whereas the conventional material showed the wear rate of 27 mg/million cycles. It was concluded that the high crosslink density near the articulating surface of the sample improved the wear resistance of the acetabular liner significantly.

The prime purpose of irradiation is to enhance the wear resistance of UHMWPE, but nonetheless it has detoriating effects on the mechanical properties. A few studies on the wear rates of conventional and crosslinked UHMWPE are shown in Table 2.1.

Table 2.1 Influence of irradiation on wear rate/wear factor of UHMWPE

Irradiation process & Dosage	Wear rate/wear factor		Type of wear tester	Reference
	Virgin	Irradiated		
Lupersol 130	4.1 mm^3/y	1.1 mm^3/y	Hip joint simulator	Shen et al. [1996]
Gamma irradiated 1000 kGy	17.1 mm^3	3.23 mm^3	Sphere on disc	Oonishi et al. [1997]
Gamma-irradiated 105 kGy		CoCrMo[cf] 6.19 ± 4.43 Alumina[cf] 8.31 ± 3.21 Zirconia[cf] 0.12 ± 0.14	12-station hip joint simulator	Wang et al. [2003]

Gamma irradiation in air 75 kGy	51 mm^3/y	5.62 mm^3/y	Hip joint simulator	Essner [2005]
Gamma irradiation 100 kGy	0.649×10^{-6} mm^3/Nm	0.449×10^{-6} $mm^3/N\text{-}m$	Multidirectional pin-on-disk	Burroughs et al. [2006]
50 kGy of electron-beam radiation	$0.375mm^3$ /250000 cycles	$0.225mm^3$ /250000 cycles	Dual axis simulator	Schwartz et al. [2007]
Highly cross-linked (100 kGy)	6.8×10^{-7} $mm^3/N\text{-}m$	3.94×10^{-7} mm^3/Nm	6-station pin-on plate	Kang et al. [2008]
Highly crosslinked (500 kGy)	15×10^{-6} $mm^3/N\text{-}m$	12×10^{-6} $mm^3/N\text{-}m$	Ball on disc	Kang et al. [2001]
Gamma irradiation in air 90 kGy	26.8 mm^3/y	17.7 mm^3/y	Knee simulator	Wang et al. [2008]
Gamma irradiation 100 kGy	9 $gm/10^6$ cycles	1.8 $gm/10^6$ cycles	Bi-directional pin-on disc	Otal et al. [2007]
E-beam 72 kGy	14.2 mg/y	4.1 mg/y	Knee simulator	Stoller et al. [2011]

cf- Counter face

It is observed from Table 2.1 that crosslinking had tremendous effects on the wear rate of the polyethylene ensuring its longevity by significantly improving the wear resistance of the UHMWPE. A similar trend was observed both in conventional wear testing machines and wear simulators as well. The literature points out that the higher dose of irradiation led to better wear resistance and thus it may increase longevity.

However, it is a known fact that the mechanical properties of UHMWPE are relatively degraded due to the oxidation of the polyethylene by the irradiation generated free radicals. Oxidation of the polymer was found to be one of the major problems encountered as a consequence of crosslinking. In order to overcome the same, the irradiation process was combined with thermal treatment as a technology to improve the wear and oxidation resistance of UHMWPE, Muratoglu et al. [1999], McKellop et al. [1999], Muratoglu et al. [2001]. Nakamura et al. [1998] reported that the relative intensity of radicals generated in UHMWPE was reduced with heat treatment parameters for both gamma and electron beam irradiated test samples. They have also reported that the Young's modulus of 25 kGy irradiated sample in air and annealed for 4 hours at 120 ^{o}C showed an enhancement of 43 % in comparison with unirradiated sample, whereas the same sample irradiated in N_2 environment under same heat treatment condition showed 12.3 % less than that of unirradiated sample. They concluded that the heat treatment of UHMWPE minimized its oxidation and wear volume. Medel et al. [2004] irradiated UHMWPE at 25 kGy dose and thermally aged at 120 ^{0}C for different time periods upto 36 h. The stress and strain at fracture after 36 h of ageing were found to be reduced by 61.8 and 82 %, respectively, where the difference between short and long ageing period was easily observed. Gencur et al. [2006] studied the influence of 100 kGy irradiation dose on the fatigue crack resistance of UHMWPE after thermal treatments. It was concluded that the crosslinking was detrimental to the ability of UHMWPE to resist the crack inception and propagation under cyclic loading compared to that of unirradiated UHMWPE. The findings also suggested that highly crosslinked UHMWPE had better resistance to crack propagation in annealed condition than the remelted condition. Oral et al. [2006] studied the mechanical properties and fatigue crack resistance of irradiated and melted UHMWPE. The samples were irradiated from 25 to 100

kGy and later melted at 170 ^{0}C for 2 hours. The crystallinity of virgin UHMWPE was increased from 63 to 69 % upon irradiation at 100 kGy dose, while that of irradiated melted samples was reduced to 58 % leading to reduced strength of the sample. It was observed that resistance to fatigue crack propagation was decreased with an increase of radiation dose. Burroughs et al. [2006] stored UHMWPE in vacuum at 70 ^{0}C prior to gamma irradiation at 40 and 100 kGy doses in order to remove the trapped oxygen in the polymer leading to the reduction of oxidation and the increase of crosslink density of polymer during the irradiation process. The wear rate of vacuum treated test sample was reduced by 20 % in comparison with the sample obtained from pre-irradiation treatment. Kilgour et al. [2009] used a six-station wear simulator and assessed the influence of 100 kGy crosslinked, 150 ^{0}C remelted UHMWPE using linear and elliptical wear profiles. It was reported that the elliptical wear path produced higher wear rate compared to linear wear path. However, the wear volume of crosslinked UHMWPE on the elliptical profile was observed to be reduced by 92 % after completion of three million cycles.

The effect of irradiation on mechanical properties of UHMWPE were summarized below in Table 2.2.

Table 2.2. Influence of irradiation on mechanical properties of UHMWPE

Dosage	Young's modulus	Fracture stress	Yield stress	% Strain at fracture	Researcher
200 kGy in air	-	Reduced from 46 to 29 MPa, i.e. 37%	Reduced from 22 to 19 MPa, i.e. 13.6 %	-	Muratoglu et al. [1999]
100 kGy after 6	-	-	Reduced 30.3 to	Reduced from 4.27	Puertolas et

years of *in vivo* ageing			24.7 MPa, i.e. 8.5 %	to 0.12, i.e. 97 %	al. [2001]
500 kGy irradiation in air	-	Reduced from 37 to 33 MPa, i.e.10.8 %	-	Reduced from 50 to 23, i.e. 54 %	Kang et al. [2001]
250 kGy irradiation in air	-	Reduced from 53.4 to 33 MPa i.e. 58.2 %	-	Reduced from 711 to 32 i.e. 95 %	Suarez et al. [2003]
25 kGy irradiation at 100 ^{0}C	Increased from 0.81 to 0.87 GPa i.e. 8 %	Increased from 47.7 to 53.3 MPa i.e. 12 %		Reduced from 3.67 to 3.10 i.e. 15 %	Nakamura et al. [1998]
Gamma irradiation 25 kGy and accelarated aged for 36 hrs	-	Reduced from 37 to 14.1 MPa i.e. 61.8 %	Reduced from 18.6 to 16.7 MPa i.e. 10.2 %	Reduced from 5.31 to 0.92 i.e. 82 %	Medel et al. [2004]

The mechanical test data shown in Table 2.2 confirms that the irradiation led to reduction of mechanical properties. The amount of degradation of the mechanical properties typically depends on the dose of irradiation and the ageing period. It is pointed out in the literature that the irradiation usually led to improvement of strength of the material immediately after irradiation, but it gradually reduced due to oxidation of the material. Post irradiation thermal treatments are used to minimize the loss of mechanical properties by mobilizing the trapped free radicals in

UHMWPE, but it leads to the reduction of fatigue and fracture toughness of the polymer. The beneficial effects of radiation crosslinking in terms of increased the wear resistance can be sufficiently extracted if the problem of oxidation is counteracted. In order to overcome the same, α-tocopherol (α_T, Vitamin E) is being added to UHMWPE. The pros and cons of addition of vitamin E in UHMWPE from various literature have been discussed in the next section.

2.2 Vitamin E as an antioxidant

The recent growth in awareness of vitamin E in orthopedics is attributed to the efforts of Prof. Luigi Costa, who has organized the first meeting on improving UHMWPE for orthopedic applications in 2003, Kurtz [2009]. Since then, the number of research articles based on α_T is gradually increasing. Doping the irradiated polyethylene with α_T is the only known solution so far to prevent the oxidation. The use of α_T as an anti-oxidative and biocompatible additive for UHMWPE has been suggested as an alternative method to improve the wear resistance of polymer without altering its mechanical strength. The rationale and mechanism behind the use of α_T as UHMWPE additive to restrict the degradation are discussed as below.

The most abundant and effective chain breaking antioxidant in the human body is α_T, Burton et al. [1981]. The oxidation of polyunsaturated fatty acids results in active free radicals, which are stabilized by abstracting hydrogen from the OH group of the chroman ring of α_T. Figure 2.1 shows the typical structure of α_T molecule with its phytyl tail and chroman head, Oral et al. [2006]. The free radicals present in the crystalline phase of UHMWPE react with diffused Oxygen to form peroxy radicals that attack other polyethylene chains. It triggered an oxidative cascade leading to oxidative embrittlement and reduction of the mechanical properties of UHMWPE, Reno et al. [2006]. The above said problem can overcome by the addition of α_T in UHMWPE, Oral et al. [2006]. However, an addition of α_T in UHMWPE has associated

problems: a) the presence of α_T in UHMWPE restricted the degree of crosslinking in the polymer by absorbing the free radicals generated during the irradiation which are necessary to form crosslinks between the polymer chains, Kurtz [2009], b) uniform doping of α_T in an irradiated UHMWPE. Various literature discussing the properties of UHMWPE doped with α_T are presented below:

Oral et al. [2004] irradiated UHMWPE at 65 and 100 kGy dose and subsequently doped with α_T for 16 hours. These samples were further subjected to sterilizing dose of 27 kGy and the final dose of 92 kGy and 127 kGy. The α_T blended samples showed low oxidation indices compared to unblended sample. The fatigue strength of α_T doped UHMWPE was found to be 27 % higher than that of 100 kGy sample. It was also reported that the wear rate of the α_T-92 and α_T-127samples was not changed upon ageing. Oral et al. [2005] blended UHMWPE with 0.1 and 0.3 wt. % α_T and gamma irradiated at 100 kGy dose. It was concluded that the presence of α_T increased the oxidation stability of UHMWPE but decreased its crosslink density and resistance to wear. The mechanical properties of UHMWPE were preserved due to the presence of α_T after accelerated ageing. Shibata et al. [2005] studied the fatigue and oxidative resistance of UHMWPE with 0.3 wt. % α_T and 0.3 wt. % Tocopherol acetate after 25 kGy irradiation dose. It was reported that the oxidation index of γ -irradiated UHMWPE was extremely higher compared to that of blends. Though severe fatigue damage was observed in γ-irradiated UHMWPE, no surface asperities were observed in α_T blended specimens. It was concluded that the long-term fatigue performance and the lifetime of UHMWPE components were prolonged by the addition of α_T compared to tocopheryl acetate blended samples.

.

(a)

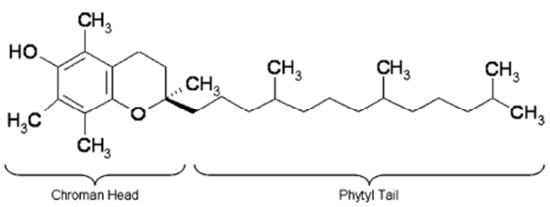

(b) 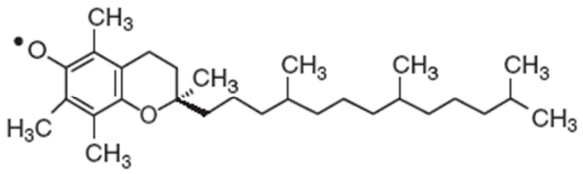

Figure 2.1 a) Structure of α-Tocopherol molecule b) α-Tocopherol free radical after hydrogen abstraction from the chroman head, Oral et al. [2006]

Oral et al. [2006] studied the effect of α_T on oxidation and residual radical transformation of irradiated UHMWPE. The samples were aged at 22 and 40 ^oC in air and 40 ^oC in water for 7 months. It was reported that the α_T doped irradiated UHMWPE showed surface oxidation at the initial period of testing, whereas irradiated UHMWPE was reported to exhibit subsurface oxidation, which was increased with time. It was reported that the presence of α_T helped in faster decay of the radicals leading to its reduced oxidation. Oral et al. [2006a] reported that the average wear rate of irradiated UHMWPE liners was decreased by 10-fold with respect to the unirradiated UHMWPE under serum lubrication. It was concluded that α_T doped irradiated UHMWPE has improved properties than the irradiated cum melted UHMWPE. Bracco et al. [2007] blended UHMWPE with α_T upto 0.5 wt. % and irradiated at 30 and 100 kGy doses. It was reported that blending of α_T in UHMWPE resulted the formation of quinonoid products, which were responsible for its stabilizing activity and improved oxidation resistance. Ridley et al. [2007] doped α_T with UHMWPE and then gamma irradiated in different environment. It was reported that the ESR spectra of the samples were identical irrespective of their irradiation environment and presence of α_T. However, the order of magnitude of radical concentration was found to be less in α_T blend samples than the virgin UHMWPE.

Oral et al. [2008] blended UHMWPE with 0.1, 0.3, and 1.0 wt. % α_T and irradiated at 25, 65, 100, 150 and 200 kGy. It was observed that the crosslink density of virgin UHMWPE was

increased with irradiation dose but it was not changed significantly above 150 kGy. The crosslink density of α_T blend was less than that of virgin UHMWPE and it was decreased with increasing the α_T concentration. It was reported that the strain at fracture was reduced with an increase of irradiation dose but increased with α_T content at any given dosage. Oral et al. [2009] investigated the wear and fatigue resistance of high pressure crystallized UHMWPE blended with α_T with different concentration. It was reported that the presence of α_T during high pressure crystallization (HPC) increased the crystallinity of UHMWPE significantly. The wear rate of virgin UHMWPE was increased significantly after HPC, whereas no significant change in the wear rate was observed in the α_T blended UHMWPE. Lerf et al. [2010] showed that presence of 0.05 wt. % α_T effectively protected highly crosslinked UHMWPE from the oxidative degradation. Haider et al. [2012] characterized the highly crosslinked UHMWPE/α_T blend irradiated at 32 kGy dose in air. It was reported that the α_T doped UHMWPE showed lower wear volume compared with the irradiated UHMWPE.

Even though crosslinking has shown the reduced wear rate of UHMWPE, it caused the reduction of various mechanical properties due to oxidation. UHMWPE doped with α_T has reduced the problem of oxidation and exhibited better properties compared to that of irradiation crosslinked polymer. Further enhancement on the mechanical properties of UHMWPE can be achieved by reinforcing the polymer with different fillers. The influence of different reinforcing filler materials on the properties of UHMWPE and its wear behaviour are discussed in the next section.

2.3 Effects of reinforcement on mechanical properties and wear resistance of UHMWPE

The selection of the reinforcing material used to prepare composite material is based on the requirement of the final product in biomedical application. This section is devoted to bring out

and discuss the potentiality of UHMWPE to improve its mechanical properties, wear resistance, infection retardant and biocompatibility using various fillers as reinforcing materials. A variety of fillers and blends used with UHMWPE is tabulated in Table 2.2. Although a wide variety of filler materials is listed in Table 2.2, the mechanical properties and/or tribological characteristics of few composites are discussed below:

Table 2.3 List of different fillers/blends used with UHMWPE

Filler/Blend	Reference
UHMWPE fibers	Cohen et al. [1997], Deng et al. [1997]
Quartz	Liu et al. [1999], Xie et al. [2003]
High density polyethylene (HDPE)	Jacobs et al. [2000], Lucas et al. [2011]
Polypropylene (PP)	Hasmi et al. [2001]
Carbon nanotube (CNT)	Ruan et al. [2003], Xue et al. [2006], Bakshi et al. [2007, 2007a], Morlanes et al. [2011], Samad et al. [2011, 2011a], Maksimkin et al. [2012]
Carbon fiber	Wood et al. [2011], Dangsheng [2005], Sui et al. [2009a]
Hydroxyapatite (HA)	Fang et al. [2005, 2006], Long et al. [2008], Wang et al. [2009a], Xiong et al. [2009]
Wollastonite	Tong et al. [2003]
Coconut shell	Pradhan et al. [2004]
Kaolin	Guofang et al. [2004]

Epoxy	Chand et al. [2007]
Silver	Morley et al. [2007]
Zirconium	Schwartz et al. [2007], Plumlee et al. [2009]
Natural coral	Ge et al. [2009]

Hashmi et al. [2001] reported that the wear volume of PP was reduced significantly by blending UHMWPE. At 0.28 m/s sliding speed, the wear rate of PP was observed to be reduced by 98 % by blending 15 wt. % of UHMWPE. Tong et al. [2003] reinforced UHMWPE with wollastonite fibers having the aspect ratio of 10:1, 15:1 and 20:1. It was observed that the addition of wollastonite fibers upto 20 wt. % improved the abrasive wear resistance of UHMWPE significantly. Xie et al. [2003] investigated the physical, physiological, mechanical properties and the wear resistance of UHMWPE/quartz composites, where these properties were found to be increased with concentration of reinforcement. They also reported the mild toxicity of wear debris generated from the composites. Guofang et al. [2004] studied the tribological characteristics of kaolin filled UHMWPE composites obtained by different processing technique under dry condition. It was concluded that the wear rate was much lower for the polymerization based composites because of the smaller crystal size and strong interface than the melt mixing one but a reverse trend was observed in case of strength of the composites. Fang et al. [2005] reinforced UHMWPE with sintered HA particles. They reported that the chain mobility of UHMWPE and UHMWPE/HA composites was increased by swelling them in paraffin oil and the resulted composite showed a 90 % increase in Young's modulus and a 50 % increase in the yield strength compared to that of unfilled UHMWPE. Fang et al. [2006] prepared UHMWPE/HA composites up to 22.8 vol. % of reinforcement. They observed that the Young's

modulus and tensile strength of UHMWPE/HA composite were increased by 788, and 5 % respectively, while the fracture strain was reduced by 22 % compared to that of virgin UHMWPE at 22.8 vol. % of reinforcement. It was also reported that the stiffness of the composite was closer to the lower bound value of cortical bone. Xiong et al. [2009] reinforced UHMWPE with nano hydroxyapatite upto 7 wt. %. The hardness of the composites was found to be maximum at 1 wt. % of filler content and 50 kGy irradiation dose. The average friction coefficient was found to be reduced by 22 % and the wear volume was reduced by 27 % at 0 kGy and 81 % at 150 kGy irradiation doses by the addition of 1 wt. % reinforcement into pure UHMWPE. Ge et al. [2009] used 5–30 wt. % of natural coral particles of < 50 μm size as a reinforcement with UHMWPE and studied the wear resistance of the composites in a hip simulator lubricated with bovine serum against CoCrMo femoral head. It was reported that the hardness and wear resistance were increased by 95 and 70 %, respectively at 30 % natural coral composite as compared to virgin UHMWPE. They concluded that the reinforcement of natural coral particles in UHMWPE changed the severity of adhesive wear of UHMWPE acetabular cups and it had less number of micro-cracks generated on the worn surface. Plumlee et al. [2009] prepared UHMWPE/Zr composites with 10 and 20 wt. % Zr. A dual axis wear simulator was used to study the wear behavior of the composites for 250000 cycles. They observed that the wear volume of the composites was reduced with an increase of Zr concentration. It was concluded that the optimum inclusion of 10 wt. % Zirconium particles into UHMWPE matrix effectively reduced the wear rate of the component without the reduction of impact toughness.

Morley et al. [2007] studied tribological characteristics of UHMWPE/Ag nanocomposites using a horizontal Tribometer under synovial fluid condition with different sliding velocities. It

was reported that no detectable variation of either temperature or friction coefficient was observed over the range of sliding velocity (10-80 mm/s).

Wood et al. [2011] observed improved wear strength and mechanical properties of UHMWPE–carbon nanofibers (CNF) composites. Though the stiffness of the polymer was not influenced by the reinforcement, the yield load, fracture load and toughness of the composites were increased by 13, 10.7 and 10.8 %, respectively at 3 wt. % of CNF in UHMWPE. The static coefficient of friction was also reported to be reduced by 78 %. Ruan et al. [2003] reported that the Young's modulus and yield stress of UHMWPE were increased by 38 and 50 %, respectively by reinforcing 1 wt. % MWCNTs. A significant increase of ductility and ultimate tensile strength of the composite was also observed. Xue et al. [2006] blended UHMWPE (80 %) with HDPE (20 %) and the blend was reinforced by MWCNTs (0.2 – 2.0 wt. %) in order to improve the creep and wear resistance of the test sample. It was concluded that the presence of MWCNTs has not shown any significant influence on the creep but the wear resistance of the composites was found to be improved. The yield strength and Young's modulus of the blend were enhanced by 20 and 26 %, respectively at 2 wt. % MWCNTs in the polymer blend. Bakshi et al. [2007] tested UHMWPE/MWCNTs (5 wt. %) nanocomposite films prepared by electrostatic spraying technique. The Young's modulus of the composite was increased by 82 %, but failure stress and strain were decreased by 13 and 64 %, respectively. Bakshi et al. [2007a] also evaluated the UHMWPE/MWCNTs nanocomposites using a Nanoindenter, where it was reported that the hardness and Young's modulus of the nanocomposites were increased by 11 and 10 %, respectively at 5 wt. % of MWCNTs in UHMWPE. It was observed that the plasticity index of the polymer was not influenced by the presence of MWCNTs. Morlanes et al. [2011] irradiated 3 wt. % UHMWPE/MWCNTs composites at 90 kGy in air and it was observed that the Young's

modulus, yield stress and fracture stress of composites were increased by 34, 10 and 4 %, respectively, whereas the fracture strain was reduced by 44 % compared to that of unirradiated composites. Fonseca et al. [2011] reported that the Young's modulus, strain at fracture and toughness of 0.2 wt. % of MWCNTs in UHMWPE were increased by 80, 26 and 35 %, respectively. Maksimkin et al. [2012] reinforced UHMWPE with 1 wt. % MWCNTs and reported that the ultimate strength and yield strength were increased by 286 and 35 %, respectively compared to that of virgin UHMWPE. Tribological tests showed a decrease of dry friction coefficient from 0.24 to 0.14 for 1 wt. % UHMWPE/MWCNTs composites.

The influence of reinforcement of the mechanical properties and wear characteristics are tabulated for easy readability and are given below in Tables 2.4 and Table 2.5

Table 2.4. Influence of different fillers on mechanical properties of UHMWPE

Filler/Blend	Young's modulus	Fracture stress	Yield stress	% Strain at fracture	Toughness	Researcher
Wollastonite (10%)	Increased from 510 to 630 MPa i.e. 23.5 %	Reduced from 32 to 25 MPa i.e. 21 %	-	-	Reduced from 68 to 40 kJ/m^2 i.e. 41 %	Tong et al. [2003]
Quartz (20%)	Increased from 1.2 to 1.45 GPa i.e. 20.8%	Increased from 21-24 MPa i.e. 14.2 %	-	-	Increased from 60 to 81 kJ/m^2 i.e. 35%	Xie et al. [2003]
HA (sintered and parrafin treated)	Increased from 781 to 1370 MPa i.e. 75.4 %	-	Increased from 6.7-11.5 MPa i.e.	-	-	Fang et al. [2005]

			71.6 %			
HA (22.8 wt. %)	Increased from 0.9 to 8 GPa i.e. 788 %	Increased from 27.2 to 28.4 MPa i.e. 4.4 %	-	decreased from 484 to 358 i.e. 26 %	-	Fang et al. [2006]
CNF At 3 wt. %	-	Increased from 41 to 60 MPa i.e. 46.3 %	-	-	Increased from 259 to 289 mJ i.e. 11.5 %	Wood et al. [2011]
MWCNTs (1 wt. %)	Increased from 0.977 to 1.352 GPa i.e. 38.3 %	-	Increased from 8.27 to 12.38 MPa i.e. 49.7 %	Increased from 4 – 9 i.e. 125 %	-	Ruan et al. [2003]
MWCNTs (5 wt. %)	Increased from 682 to 1240 MPa i.e. 81.8 %	Reduced from 14.3 to 12.4 MPa i.e. 9.7 %	-	Reduced from 3.9 to 1.4 i.e. 64.1 %	-	Bakshi et al. [2007]
MWCNTs (3 wt. %)	Increased from 248 to 342 MPa i.e. 37.9 %	Increased from 26.7 to 28.8 MPa i.e. 7.8 %	Increased from 19.9 to 20.7 MPa i.e. 4.0 %	Reduced from 571 to 509 i.e. 10.8 %	Reduced from 121 to 115 mJ i.e. 4.9 %	Morlanes et al. [2011]
MWCNTs				Increased	Increased	Fonseca et

(0.2 to 1 vol. %)	-	-	-	from 275 to 360 i.e. 30.9 %	from 50 - 70 J/gm i.e. 40 %	al. [2011]
MWCNTs (0- 4 wt. %)	-	Increased from 22 to 27 MPa i.e. 22.7 %	Increased from 20 - 22 MPa i.e. 10 %	-	-	Maksimkin et al. [2012]

It can be inferred from Table 2.4 that the presence of reinforcement, in general, has improved the Young's modulus of the UHMWPE. An increase of the modulus was attributed to the effective load transfer from matrix to filler. The strain at fracture and fracture stress, both were either increased or decreased depending on the type of the filler and its concentration. It is observed that the fracture strain was reported to be increased where MWCNTs were used as reinforcement, however an opposite trend was observed in few cases. It is a well known fact that unmodified MWCNTs led to agglomeration causing the reduction of strain at fracture.

Table 2.5. Influence of filler and other parameters on the wear characteristics of UHMWPE

Filler/blend	Wear volume/ factor	Counter face	Type of wear tester	Test conditions	Contributor/researcher
Wollastonite	Reduced from 2.5 mm^3 to 1.3 mm^3 i.e. 48 %	Grey cast iron	Block-on-ring	Sliding velocity 0.53 m/s, normal load (40-160 N)	Tong et al. [2003]
Quartz	Reduced from 630µg/hr -580		Ball-on-disc	30N, 21mm/s,	Xie et al. [2003]

	µg/hr, 550 µg/hr - 500 µg/hr i.e. 8 %, 9 %, respectively			distilled water, bovine serum	
Kaolin	Increased from 4.532×10^{-4} to 9.72×10^{-4} mm^3/m i.e. 114 %	ASTM 1045 steel	Ring on block	Normal load (105-465N) Speed 0.42 – 0.84 m/s)	Guofang et al. [2004]
Nano HA	Wear rate Reduced from 11 to 8.5 $\times10^{-6}$ mm^3/Nm i.e. 22.7 % Friction coeff reduced from 0.12 to 0.08 i.e. 33.3 %	CoCrMo alloy	Ring on block	196 N, 0.304 m/s, water lubrication	Xiong et al. [2009]
Natural Coral	Reduced from 200 to 60 $mg/10^4$ cycles i.e. 70 %	CoCrMo ball	Four-station ball-in socket wear simulator	25% bovine serum, 784 N, 1 Hz.	Ge et al. [2009]
Zirconium	Wear rate Reduced from 0.494 to 0.310 $mm^3/2.5\times10^5$ cycles i.e. 37.2 %	CoCrMo alloy	Dual axis wear simulator	70N ,38 mm/s for 250000 cycles	Plumlee et al. [2009]
CNF At 0.5 wt.%	Wear rate reduced from 2.25 to 1.3×10^{-7} mm^3/Nm i.e. 42.2 %	Carbon steel disk	Pin-on-disk apparatus	57 N, 67.5 m/s for 72 hr.	Wood et al. [2011]

	Friction coff reduced from 0.24 to 0.13 i.e. 45 %				
HDPE (20 %) with MWCNTs (0- 2 wt. %)	Wear rate reduced from 40 to 15 × 10^{-8} mm^3/Nm i.e. 62.5 % Friction coff reduced from 0.14 to 0.09 i.e. 45.8 %	Steel	Ball-on-prism	21.2 N, 28.2 mm/s	Xue et al. [2006]

The wear results shown in Table 2.5 indicate that the wear volume/ wear rate/ mass loss of the virgin UHMWPE was reduced significantly by reinforcing it with different fillers. However, the comparison of the wear data would be difficult, as the resultant wear volume/ wear rate depends on the test condition such as sliding speed, lubricant type, load applied, surface properties of test sample, counter face and others. In general, it can be inferred that the reinforcement technique is often used to improve the wear resistance of UHMWPE. It is important to note that none of the reinforced composites were clinically successful till date.

2.4 Antioxidant activity of MWCNTs and their influence on composites

It was reported by Iijima et al. [1992] that the as-grown carbon nanotubes (CNTs) had a number of defects and impurities. Different defects like point defects e.g. vacancy and interstitial defects, strains, adatoms, pentagon-heptagon pairs, pentagon-octagon-pentagon pairs etc were among those that were observed so far in the CNT walls and tips, Dresselhaus et al. [2001]. These defective sites of CNTs are more reactive than the perfect nanotubes due to their high electron affinities, Zhou et al. [2003] and Chakrapani et al. [2003].

It is noted that the defects in CNTs were created only if the incident particle was energetic enough to displace Carbon atoms and the minimum incident electron energy required to remove a Carbon atom by a knock-on collision was found to be 86 keV, Koutsky et al. [1994], and Smith et al. [2001]. Cataldo [2000] discussed that the γ-radiation on graphite induced the development of disorder band in Raman spectra showing a significant amount of radiation damage in solid graphite. It was also reported that the γ radiation resulted in the rotation of graphite planes and also the formation of domains of hexagonal diamonds.

Krasheninnikov et al. [2002] irradiated single walled carbon nanotubes (SWCNTs) on different substrates and studied the formation and evolution of irradiation induced defects. It was reported that the number of defects was increased with the energy of irradiation. The irradiation resulted in the formation of vacancy and vacancy related defects and some complex defects. They concluded that the pinning of nanotubes to both metallic and graphite substrates happened after irradiation through the formation of chemical bonds between the nanotube and substrate atoms. Schultz et al. [2009] reported about the antioxidant ability of SWCNTs and performed a comparative study on the free-radical scavenging activity of pristine, functionalized and ultra-short SWCNTs with derivatives of the phenolic antioxidant. Their results revealed that all types of SWCNTs were found to be extremely effective antioxidants and the oxygen-radical scavenging activity of the SWCNTs was reported to be about 40 times greater than that of the radio-protective dendritic fullerene.

Charlier [2002] reported that the irradiation of CNTs extracted atoms from their honeycomb lattice continuously or at random, which caused the formation of vacancies on their surface. These vacancies would further cluster and forms into large holes in the structure resulting the formation of a three-coordinate, highly defective carbon network. Cooper et al. [2002] and Hu et

al. [2003] reported that the defects formed on the CNTs due to irradiation were expected to increase the CNT-polymer adhesion and thus significantly improved the mechanical properties of the composites. It was also reported that the irradiation not only produced the defects but also formed covalent bonds between the tubes of CNTs. Watts et al. [2003] reported that CNTs acted as polymer antioxidants due to their high electron affinity. It was observed that PP composites showed higher Oxygen intake temperature by about 20 ^{o}C by adding CNTs due to their ability to take up Oxygen and prevent the oxidation of polymer. They concluded that addition of CNTs was not contributed to the polymer degradation but they helped to stabilize them in the presence of Oxygen. Krasheninnikov et al. [2004] reported that subjecting CNTs into irradiation resulted either the displacement of surface atoms or the incident atoms get absorbed on the surface forming the interstitial atom. Along with simple defects, a number of more complex defects associated with a rotation of a bond in the CNT atom network and other topological defects were formed in the graphitic network. They concluded that the irradiation induced defects formed bonds with the substrates and increased the CNT- substrate adhesion. Kis et al. [2004] confirmed that the irradiation of CNT bundles followed by mechanical testing improved the mechanical properties of nanotube bundles. It was resulted due to irradiation-induced inter-tube links, which provided load transfer and enhanced the shear modulus in the bundle. Sammalkorpi et al. [2004] studied the mechanical properties of CNTs having vacancies and other related defects. Their results indicated that the Young's modulus of nanotubes having defects was essentially the same unless the vacancy concentration was extremely high. However, the tensile strength was reported to be influenced by the defects. Ritter et al. [2006] studied the radiation damage on MWCNTs and their Raman vibrational modes. It was concluded that the number of defects in the CNTs increased with irradiation dose leading to accumulation of vacancies causing weakening of the

inter carbon bonds. They also reported that the growth of the concentration of non-equilibrium vacancies resulted mutual recombination with interstitial carbon atoms. Zeynalov et al. [2008] proved the antioxidant capability of CNTs by examining their anti-oxidative effect of MWCNT on platelet structure by means of the model reaction of cumene initiated oxidation. They concluded that the purified CNTs were reported to have shown more profound inhibition of oxidation in comparison with unpurified ones. It was also reported by Galano [2010] that the antioxidant activity of functionalized CNTs were increased significantely compared to that of un-functionalized CNTs.

Recent studies on MWCNTs and their composites have shown that they exhibited antioxidant characteristics due to their high electron affinities and thus they acted as radical scavengers in polymers, Morlanes et al. [2012] and Sreekanth et al. [2012].

2.5 Biocompatibility of MWCNTs

The success of any material intended to be used under *in vivo* medical applications depends on its biocompatibility. As discussed in Chapter 1, the failure of TJRs was influenced by the wear debris generated from the polymer implant. Though it is biocompatible in bulk form, concerns have risen about the biological influence and lifetime effects of the wear debris, which is accepted as a major cause of osteolysis in total hip arthroplasty. The local inflammation due to the wear debris depends on its particle size, total volume of the debris, aspect ratio, and its chemical reactivity. The degradation products of any orthopaedic implant include two types of debris: particles and soluble debris. Particulate wear debris includes metals, ceramics, or polymers, which are in the range of nanometers to millimeters. The “metal ions” exist in soluble forms in serum protein. The response to implant debris is dominated by local immune activation,

e.g., macrophages. The effects of systemically elevated amounts of metallic and polyethylene wear particles in the liver, spleen, and other tissues of patients have not been associated with remote toxicological or carcinogenic pathology to date, Hallab et al. [2009].

MWCNTs reinforced composites are very promising for orthopedic load bearing applications like TJRs due to their attractive properties. In spite of such attractive features, the toxicity of CNTs is still a debatable issue, with several research groups pointing to their similarity to asbestos fibers, Poland et al. [2008], while others confirm their non-toxicity. CNTs toxicity in both *in vivo* and *in vitro* studies depends on several factors, such as length, type of functionalization, concentration, and even the dispersant used to solubilize the nanotubes. Yet many studies suggested that CNTs toxicity is unfounded. UHMWPE is being used as an articulating surface material in TJRs and its longevity can be enhanced by reinforcing MWCNTs. However, the success of the UHMWPE/MWCNTs composites depends on their biocompatibility. As the present study is intended to use MWCNTs, literature relevant to its potential effects on biological system is discussed here.

The ability to functionalize the sidewalls of CNTs led to their biomedical application, Guzman et al. [1996]. It is generally agreed that the functionalized CNTs constituted a major improvement over unmodified, non-functionalized CNTs, as the latter are often reported to cause adverse reactions from living tissue, whereas the former could be much less toxic due to more biocompatible functional groups attached on their surface, Bicano et al. [2003]. Lam et al. [2004] instilled 0, 0.1, and 0.5 mg of untreated carbon nanotubes intratracheally in mice. It was reported that if the untreated CNTs reached the lungs, it could cause serious toxic effects. It was concluded that CNTs with impurities were expected to cause potential health hazards. Studies of

Koyama et al. [2006] confirmed that the implanted CNTs with impurities in mice induced immunological toxicity, whereas the CNTs without any impurity showed good biocompatibility. Wang et al. [2004] injected SWCNTs in male mice at a dose of 1.5 μg/mouse. They reported that SWCNTs accumulated in bone, but they exhibited good biocompatibility. Cherukuri et al. [2006] tested the systemic toxicity effect of Pristine SWCNTs in a rabbit by Intravenous injection at a dose rate of 7.5 mL for 20 μg/kg body mass and reported that there was no toxic effect. Koyama et al. [2009] conducted toxicity studies on CNTs in mice and concluded that the toxic effect and biological response of CNTs were very much lower than the asbestos. They also reported that the animal mortality and chronological changes in body weight were not observed even 3 months after post-implantation period. Sato et al. [2005] reported that shorter CNTs (~0.22 μm in length) were found to be better integrated into macrophages and phagocytes than the longer (~ 0.8 μm) one. The length and shape of the CNTs also influenced and determined the resulting immunologic response of macrophages, Nel et al. [2006]. However, later studies by Poland et al. [2008] showed that the nontoxic length of CNTs was asserted to be ~10 μm. Schultz et al. [2009] carried out cytotoxicity assays, which showed that concentration of both non-functionalized and derivatized SWCNTs had little or no deleterious effects on cell viability.

Recent studies by Reis et al. [2010] on UHMWPE/MWCNTs and Ormbsy et al. [2012] on PMMA/MWCNTs also confirmed the cytocompatibility of wear debris generated from the nanocomposites with osteoblast like MG63 cells. Cells had grown on CNTs, thus they appeared to have no toxic effect, potentially giving rise to applications such as coatings for prosthetics.

Based on the above literature, it can be inferred that the toxicity of CNTs is not an intrinsic property but it rather depends on the aspect ratio, length and the type of functionalization. The impurities, and not CNTs themselves, were responsible for the reported toxicity, Lacerda et al.

[2006]. The exploration of CNTs in biomedical application is underway. Since a large part of the human body consists of carbon, it is generally thought to be a very biocompatible material and it has a significant potential, Drexler [1992]. In any case, the studies on CNTs aimed at biomedical applications are still active area of research.

2.6 Closure on literature

Based on the deliberation on several topics detailed above, it can be inferred that in spite of several attempts to address the primary concerns of UHMWPE, there are some persistent problems associated with each of the techniques employed thereof. Radiation crosslinking, which is employed to increase the wear resistance of UHMWPE, has some serious side effects such as oxidation of the polymer, which leads to deterioration of mechanical properties and make the material easily prone to failure.

Post irradiation treatment such as melt annealing has emerged as a solution to the above mentioned problem, but it has associated problems of its own. Although melt annealing reduces the amount of free radicals and thus limits the degradation of mechanical properties due to oxidation, nonetheless, it leads to reduction of fracture toughness of the material.

In order to address to the above problems, researchers have tried to introduce α_T doped irradiated UHMWPE. Although it has partially solved the problem of oxidation, it has brought a new set of associated problems. i.e. presence of α-Tocopherol in UHMWPE during the irradiation process restricts the degree of crosslinking in the polymer. However, in spite of having such limitations, α_T doped irradiated UHMWPE still remains a choice of surgeons owing to its antioxidant properties.

UHMWPE reinforced with wide variety of fillers is yet another choice to achieve the desired properties. Fillers of various choices have been used by different researchers, but none of them

were a clinical success. Although Carbon fiber reinforced UHMWPE clinically used due to its superior wear behavior, Farling [1977], it was later withdrawn due to reduced ductility, decreased crack resistance, and the fiber-matrix interface of the composite.

MWCNTs are having extraordinary mechanical properties and also possess good antioxidant characteristics with biocompatibility, when free from impurities. In order to increase the success rate of UHMWPE as an articulating surface, MWCNTs can be selected as a reinforcement material. The present thesis is an attempt in the direction to explore the feasibility of MWCNTs as a reinforcement material with UHMWPE to address to the above discussed problems.

2.7 Objectives of the present work

UHMWPE reinforced with MWCNTs has been a subject of recent interest and a very few studies were reported in this direction more of which are random. Thus, a systemic study is proposed on the influence of MWCNTs on the properties of UHMWPE with the following as the primary objectives.

(i) Identify the optimum concentration of MWCNTs in UHMWPE and study the mechanisms involved for enhanced properties upto an optimum concentration and the reduction thereafter.

(ii) Study the variation of surface properties of composites using Nanoindentation technique.

(iii) Study the effects of irradiation on the mechanical properties of UHMWPE/MWCNTs composites at different irradiation doses and ageing periods.

(iv) Compare the role of MWCNTs and α_T in limiting the ageing degradation of the mechanical properties of γ-irradiated UHMWPE.

(v) Study and compare the wear behaviour of UHMWPE, UHMWPE/MWCNTs composites and α_T blended samples under dry sliding condition before and after the gamma irradiation.

(vi) Study the biocompatibility of UHMWPE/MWCNTs composites.

Chapter 3

Materials and methods

The characterization of composites involves several analytical tools and experimental techniques in order to confirm whether the desired properties are achieved or not. The chapter 3 is focused on discussing the techniques used and methods employed for the preparation of composites beginning with the materials used, design of compression moulding die, method used to blend the powders and consolidate them in the form of sheets of desired thickness. A series of different analytical instruments/techniques is used at various stages of developing and testing the composites, which are discussed below.

3.1 Multi walled carbon nanotubes (MWCNTs)

The MWCNTs were purchased from M/s Shenzhen Nanotech Port Co., Ltd., China. The specifications of as-received MWCNTs are as follows: outer diameter 40-60 nm, length 5- 20 µm, purity - 95 wt. %, ash content < 1.5 %, density – 2160 kg/m^3, special surface area > 200 m^2/g.

3.2 Ultra high molecular weight polyethylene (UHMWPE)

UHMWPE was received from M/s Ticona, Germany, grade GUR 1020 having the molecular weight of 4 x 10^6 g/mol with an average particle size of 140 ± 20 µm and the density of 930 kg/m^3.

3.3 α-Tocopherol (α_T)

α_T having the density of 0.950 g/mL at 20 °C and the molecular weight of 430.71 g/mol was purchased from M/s Sigma Aldrich, Germany.

3.4 Chemical treatment of MWCNTs

MWCNTs are known to have very high specific surface area and they tend to agglomerate, which acts as a defect and stress raiser in the composites leading to the reduction of the overall properties of them. Thus, the as-received MWCNTs were required to undergo a suitable surface modification by which certain functional groups were attached on the surface of MWCNTs. The presence of functional groups on MWCNTs facilitated the chemical bonding with polymer and also allowed homogeneous dispersion of them in the polymer matrix, Datsyuk et al. [2008]. Concerning the usage of MWCNTs as a reinforcement in polymeric materials, the incorporation of the functional groups on the surface of MWCNTs is a very crucial step for the enhancement of interfacial adhesion and stress transfer. As a result, the unique mechanical properties of the MWCNTs can be transferred to the composites.

The chemical treatment of MWCNTs was performed as described by Esumi et al. [1996], which is briefly discussed here. Figure 3.1 shows the setup used for the chemical treatment, where a glass beaker containing MWCNTs and acid mixture, silicon oil heating bath and temperature sensor are shown. The required sample of MWCNTs was suspended in the mixture of concentrated nitric acid and sulphuric acid by the volume ratio of 1:3 and boiled at 140 ^{0}C for 40 minutes. The solution was then allowed to cool to room temperature and the chemically treated nanotubes were washed with deionized water until the supernatant attained a pH around 7. The sample was then dried in a hot air oven at 100 ^{0}C in order to remove the moisture content in the sample. Various functional groups such as carboxyl, carbonyl, and hydroxyl were attached on the MWCNTs surface and the schematic representation of the chemical reaction is shown in Figure 3.1b. Figure 3.2a shows the Thermo Fisher IS10 Fourier transform infrared spectroscope (FTIR) used in the study to obtain the spectra of the treated and untreated MWCNTs, which are

shown in Figure 3.2b. The peaks are identified at 1360, 1710, and 3403 cm^{-1}, which characterize C-O, C=O and O-H bonds, respectively in the chemically modified MWCNTs. Peaks at 1710 and 3453 cm^{-1} are attributed to acidic groups like carbonyl, phenol and lactol. Peak at 1576 cm^{-1} assigns to C=C bond in MWCNTs.

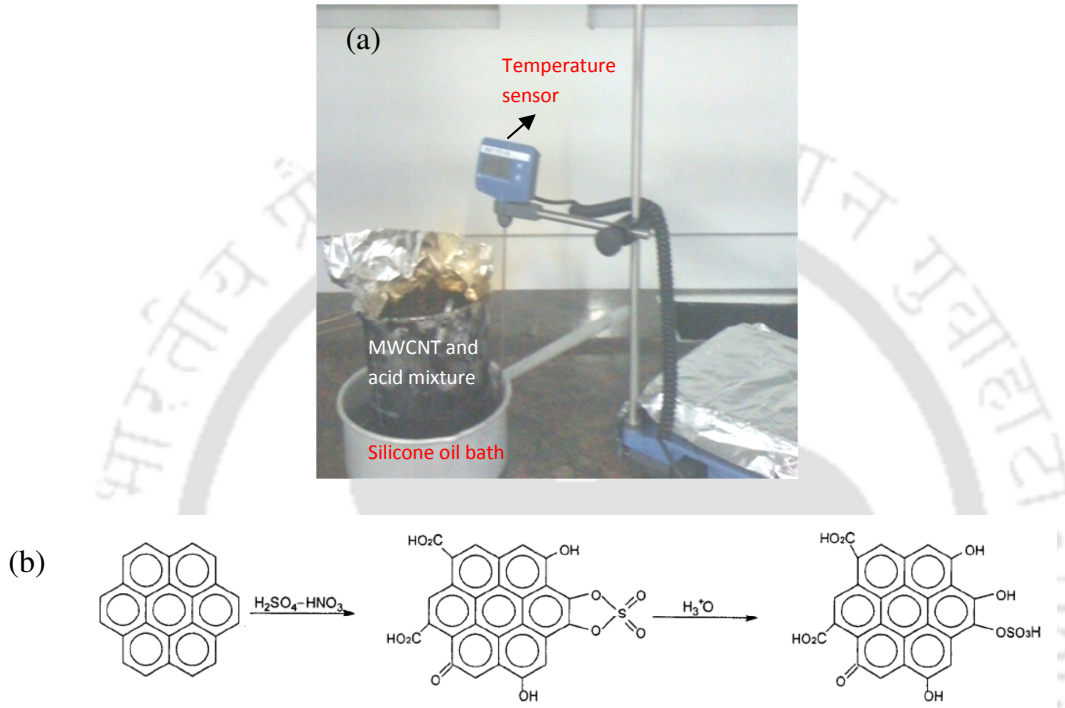

Figure 3.1 a) Chemical treatment setup b) Possible functional groups attached on the surface of MWCNTs

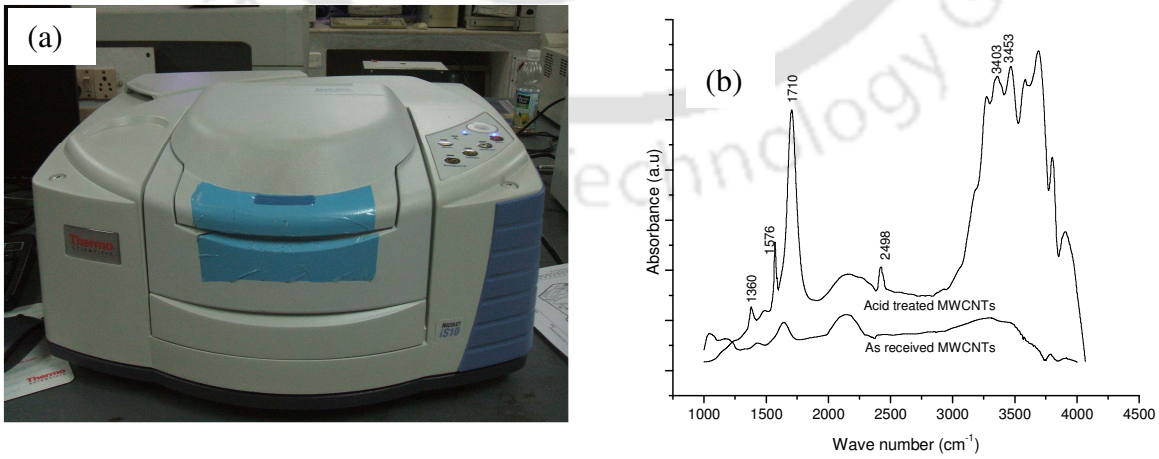

Figure 3.2 a) FTIR spectrometer b) FTIR spectrum confirming the functionalization of chemically treated MWCNTs

3.5 Physical blending of UHMWPE/MWCNTs powder

UHMWPE was physically blended with chemically treated MWCNTs at different concentrations, such as 0.5, 1.0, 1.5, 2.0, 2.5 and 5.0 wt. %, in this case, in a ball milling machine Fritsch, planetary mono mill Pulverisitte 6.0. The optimum ball milling time was chosen as 45 minutes based on the available literature published by our collaboraters, Fonseca et al. [2011]. The ball milling machine and the blend of UHMWPE/MWCNTs are shown in Figure 3.3a and 3.3b, respectively.

3.6 Blending of UHMWPE/α_T

α_T was physically blended with UHMWPE powder at different weight fractions (0.1, 0.3 and 0.5 wt. %) in the same way as that of UHMWPE and MWCNTs mixture. As α_T is highly viscous in nature, it tends to form lumps in the UHMWPE powder and leads to highly localized concentration of α_T after consolidation. Thus, the milling time was increased to 90 minutes to ensure proper blending of them. Figure 3.3c shows α_T in UHMWPE prior to ball milling.

Figure 3.3 a) Ball milling machine b) MWCNTs blended UHMWPE c) α_T lumps in UHMWPE prior to ball milling

3.7 Consolidation of blended powders using a compression moulding machine

The obtained raw material mixture was then processed in a compression moulding machine, M/s Saumya, 25 T capacity. The mixture was filled in the die cavity and the thickness of the sample was controlled by removing the excess material in the die cavity using a stepped strike-off bar. The consolidation pressure of the mixture was kept at 10 MPa, and the temperature of the upper and lower heating plate was at 230 and 220 ^{0}C, respectively for 60 min. The mould was then allowed to cool to room temperature by circulating water into the dies. The cooling

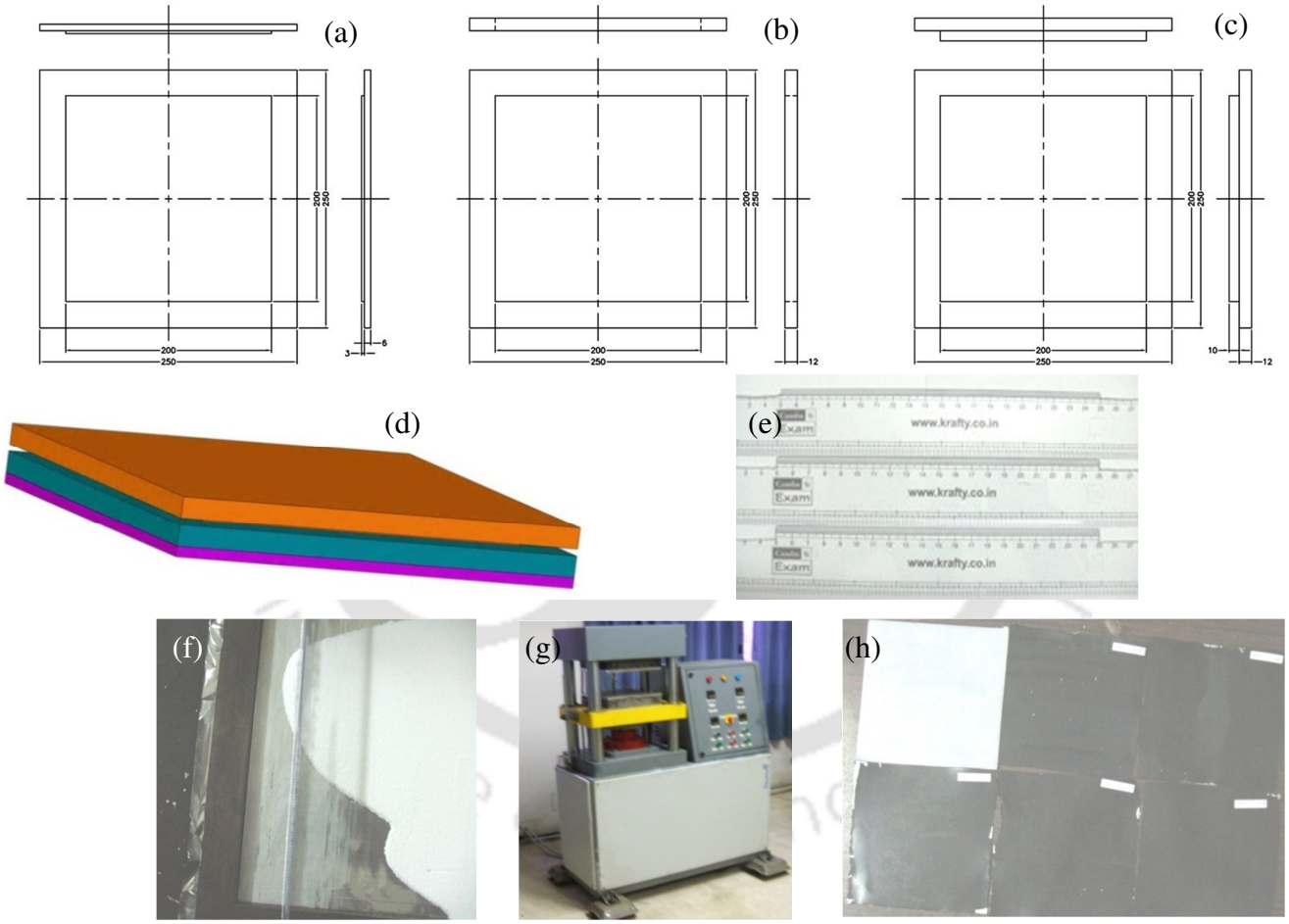

Figure 3.4 a) Lower plate of the die b) Middle plate of the die c) Upper plate of the die d) Die assembly e) Stepped strike-off bars f) UHMWPE being spread in the die cavity using stepped strike-off bar g) Compression molding machine h) Consolidated pure polymer and composites sheets

medium was chosen based on the literature, which reported that the best properties of composites were obtained by water cooling compared to air or liquid nitrogen cooling, Fonseca et al. [2008]. The obtained test samples were in the form of sheet having the dimension of 0.5 mm thick and 20×20 cm cross section. Figure 3.4 shows the compression moulding die, stepped strike-off bar, compression moulding machine, and the obtained sheet. The composites and α_T blends were designated as NC(wt. %) and α_T(wt. %), where wt. % represents the weight fraction of MWCNTs or α_T in UHMWPE.

3.8 Tensile testing of microtensile test specimen

The microtensile test specimens were cut from the sheets obtained from the compression moulding machine and tested according to ASTM D 1708-10 standard. The sample dimension, composite and α_T blend test specimens are shown in Figure 3.5a, 3.5b and 3.5c, respectively. The test was performed in a digitally controlled closed loop servo hydraulic universal testing machine, INSTRON 8801, having the dynamic load capacity of ± 100 kN with load cell accuracy of 0.005 % and it is shown in Figure 3.5d. The test was conducted at a cross head speed of 1 mm/min. in the temperature range of 20 – 24 ^{0}C. In order to ensure the repeatability of the results, five samples were tested per material type and the average of the results is reported.

(a)

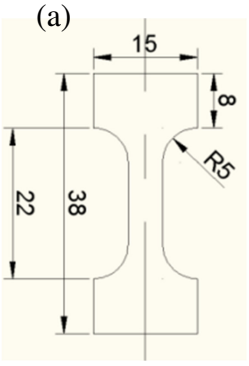

(b)

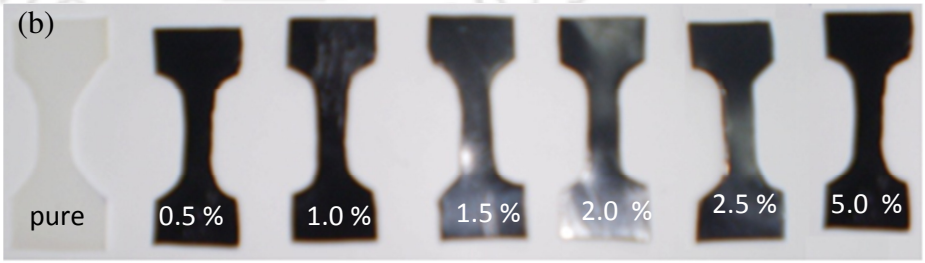

All dimensions are in

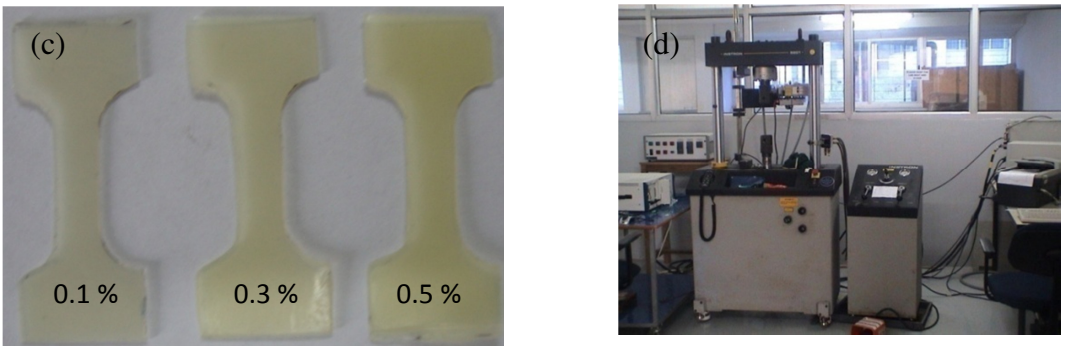

Figure 3.5. a) ASTM D1708 microtensile test specimen b) Microtensile test specimens of composites obtained from the consolidated sheets c) Microtensile test specimens of α_T blends obtained from the consolidated sheets d) INSTRON-8801 universal testing machine with closed loop servo hydraulic system

3.9 Nanoindenter

The Nanoindentation experiments were carried out using a CETR, UMT-2 Nanoindenter. The diamond Berkovich tip, which is a 3-sided pyramid with a total included angle of 136^o, was used in this study. The indenter setup is inbuilt with a capacitive transducer having the load resolution of ~ 150 nN, and the depth resolution of ~ 1 Å. As the tip defect may greatly affect the evaluation of the mechanical properties of the test surface, the accuracy of the instrument was tested by performing the tip shape and frame stiffness calibration using the fused Silica sample, which has the constant elastic modulus at different depth, Oliver et al. [1992].

The load was applied at a rate of 0.5 mN/s to the maximum load of 10 mN, where it was held for 10 s (creep time) to avoid the 'nose problem' and then unloaded to 10 % of the maximum load at the same rate as that of loading and maintained for 10 s (thermal drift time) to compensate the error, which arises due to thermal drift within the indenting system and then finally it was unloaded. Allowing creep at the maximum load aids in mechanical stabilization of the indent and hence improves accuracy of the contact area and depth used for the calculation of hardness and

Young's modulus, Briscoe et al. [1998]. The load as a function of the indenter displacement is obtained during loading and unloading conditions, which are recorded for data analysis. Figure 3.6 shows the Nanoindenter setup used in the present study.

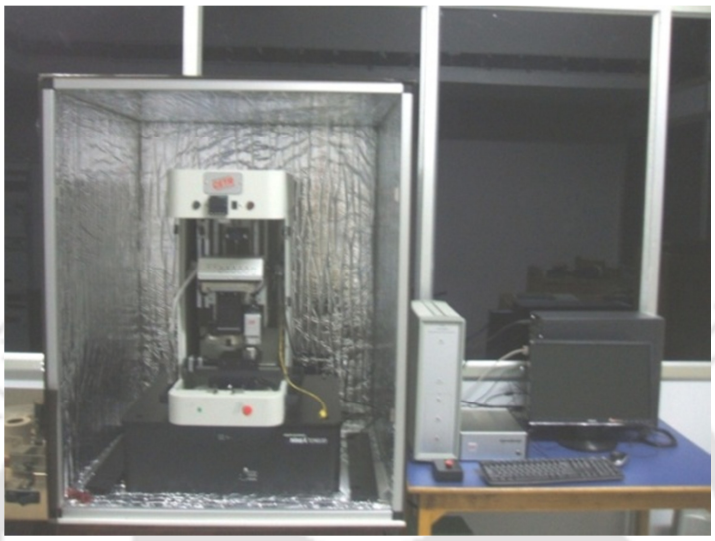

Figure 3.6. Nanoindenter

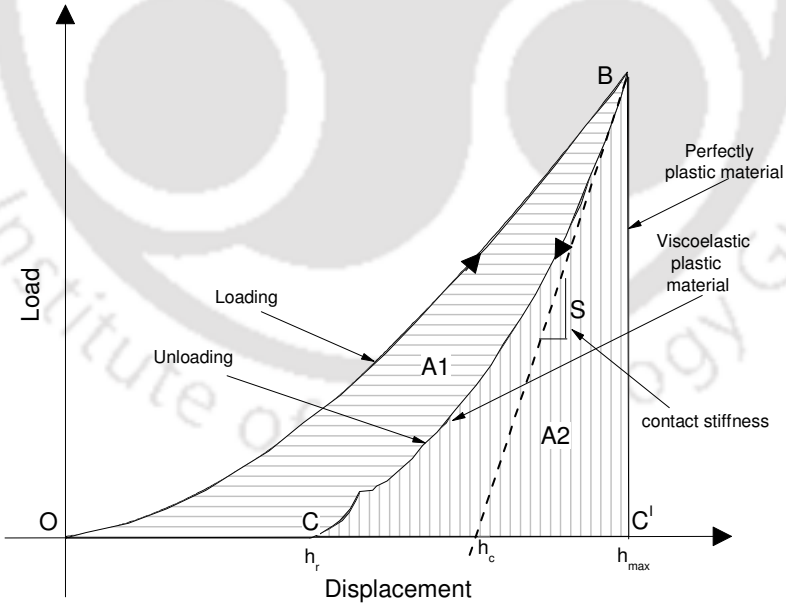

Figure 3.7. Schematic representation of a typical load- displacement curve obtained from the Nanoindentation test (h_r – residual depth, h_c – contact depth, h_{max} – maximum depth of penetration, A1- plastic work done, A2- elastic work recovered)

Figure 3.7 shows the typical load vs. displacement curve, which includes both loading and unloading data for a general viscoelastic–plastic material. The curve OBCO represents the loading, unloading and thermal drift segments to elucidate the calculations involved in estimating the plasticity index of the material. The data obtained by the unloading curve provides information about elastic, visco-elastic and plastic behavior of the material. The load corresponding to the point B in the plot is the maximum load, P_{max}, and the corresponding displacement is obtained at C^1, maximum displacement, on the X-axis as h_{max}. The residual displacement after removing the indenter tip is denoted as h_r. The intercept of the tangent line drawn from the first part of the unloading curve describes the elastic deformation effects, Oliver et al. [1992], and the intercept in the displacement axis is represented as h_c. The difference between $h_c - h_r$ represents the viscoelastic recovery, which follows the immediate elastic depth recovery. The slope of the line evaluated at the maximum displacement represents the contact stiffness, *S*, Oliver et al. [2004]. In case of a perfectly plastic material, there is no displacement of the material during the unloading condition and thus the curve assumes a vertical line and intersecting at C^1 in the displacement axis. In case of a visco-elastic material, the curve traces along BC during the unloading segment and the material rebounces to h_r at C. The plastic work done in the visco-elastic material is represented by area A_1 (OBC), and the elastic work recovered during the unloading condition corresponds to area A_2 (CBC^1).

The relationship between stiffness and elastic modulus at the maximum penetration depth for any indenter geometry is defined as follows, Pharr et al. [1992]:

$$S = \frac{2\nu}{\sqrt{\pi}}\sqrt{A_{max}}E^* \qquad \ldots 3.1$$

where A_{max} is the projection of contact area between the material and indenter tip at h_{max}, ν is the parameter related to indenter geometry ($1< \nu < 1.034$) and E^* is the reduced elastic modulus of the contact. The hardness and plasticity index of the test sample were calculated using the equation 3.2 and 3.3, respectively, Briscoe et al. [1998].

$$H = \frac{P_{max}}{A} \quad \ldots 3.2$$

$$\Psi = \frac{A_1}{A_1 + A_2} \quad \ldots 3.3$$

where P_{max} is the load at the maximum displacement and A is the projected area supporting the load. A_1 and A_2 have been described earlier with reference to Figure 3.7. The tests were conducted on the AS Processed samples (ASP W hereafter, where W stands for wt. % of the MWCNTs) and the surface layer removed samples (SLR W hereafter), where the layer was removed upto 100 μm.

3.10 Rheometer

The viscosity of the composites under melt condition was tested using an Anton Parr Rheometer, Physica MCR 101 model. The test sample was a circular disc of 25 mm diameter and 0.5 mm thickness. The tests were conducted using a parallel plate (PP25) technique under the oscillatory mode with constant shear strain amplitude of 5 %, and an angular frequency of 10 rad/s. As the melting temperature of polymer is about 135 ^{0}C [Ticona data sheet], all the tests were performed in the temperature of 135 to 200 ^{0}C at a heating rate of 1 ^{0}C/min. The PP25 plate was set for zero gap and the heating plate was pre-heated to the required temperature of 135 ^{0}C and maintained for 15 minutes prior to placing the sample. The prepared samples, parallel plate (PP25) and the Rheometer used to characterize the test samples are shown in Figure 3.8. The

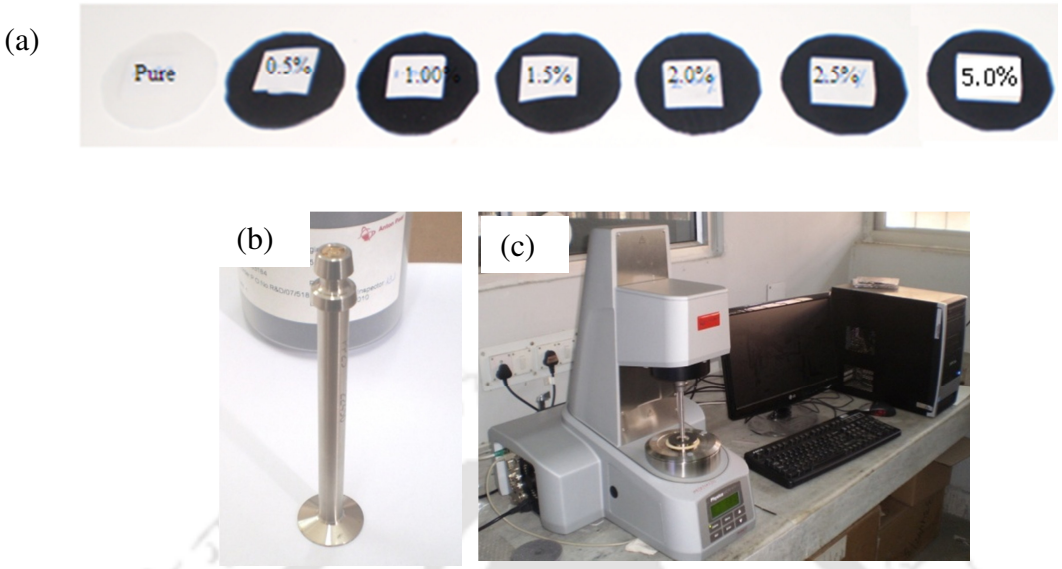

Figure 3.8 a) Polymer and composite test samples b) Parallel plate (PP25) measuring system c) Anton-Paar Rheometer

homogenous dispersion of MWCNTs in UHMWPE was ensured by estimating the rheological percolation of the composites by varying the angular frequency from 0.1 to 100 rad/s at the shear strain amplitude of 5 % at a constant temperature of 160 ^{o}C. The parameters for the rheological studies were chosen based on the results reported by Huang et al. [2006] and Grady [2011].

3.11 Differential scanning calorimeter (DSC)

Thermal characterization by DSC is the most widely used technique to estimate the degree of crystallinity of polymers. A Netzsch simultaneous thermal analyser, model STA 449F3 having the DSC resolution of < 1µW, microbalance resolution of < 1µg and the heating rate accuracy of 0.001 K/min. was used for the calorimetric analysis of the test samples according to ASTM F2625-10 standard. The test was performed from room temperature to 200 ^{o}C at a heating rate of 10 K/min. The sample holder, made of Alumina, was heated in a muffle furnace upto 1200 ^{0}C to remove the contaminants from the pan, if present, later it was sonicated in an ultrasonic bath and dried in an oven to ensure contaminant and moisture free sample holder. The Alumina pan with

perforated lid was used with a sample weighing 5-6 mg. The height of the sample was maintained within 1 mm, and the base of the samples was ensured to have a complete contact with the base of the pan in order to avoid any thermal gradient in the sample and maintain uniform heat flow. Argon was used to purge the sample chamber and the furnace at 20 and 60 ml/min., respectively. The test set up was calibrated with Indium standard at a heating rate of 10 K/min. prior to testing the sample. The DSC set up used in the present study is shown in Figure 3.9. The melting endotherm was recorded and the area under endotherm was calculated by integrating from the beginning of the fusion process to the end of it. The area represents the heat of fusion of the material per unit mass of the sample. The percentage crystallinity of the material is obtained by normalizing the heat of fusion of the sample (H_s) with that of the heat of fusion of 100 % crystalline polymer (e.g. H_f =289.3 J/g for polyethylene-ASTM F2625-10).

$$\% \text{ Crystallinity of polyethylene} = \frac{H_s}{H_f} \times 100 \quad \ldots 3.4$$

Figure 3.9 Differential scanning calorimeter

3.12 Gamma irradiation

Gamma irradiation of all the test specimens has been performed in air by Co^{60} source at a dosage rate of 2.5 kGy/h for the cumulative dosage of 25, 50, 75 and 100 kGy at M/s Microtrol Sterilization Private Limited, Bangalore, India. As the mechanical properties and wear resistance of the polymer saturate at above 100 kGy irradiation, Kurtz [2009], the irradiation study was carried out up to 100 kGy dosage level. The irradiated samples were designated as GI(dose)NC(wt. %) for composites or GI100α_T(wt. %) in case of α_T blends; say a 50 kGy gamma irradiated 2 wt. % composite is represented as GI50NC2.0. Similarly a 50 kGy gamma irradiated α_T0.1 sample is represented as GI100α_T0.1. No post irradiation treatments were performed on the test samples in order to understand the interaction between MWCNTs or α_T and the free radicals. It also helps to estimate the role of MWCNTs in reducing the deteriorating effects of irradiation process. The mechanical properties of irradiated samples were characterized at definite period such as within 10 days, 60 and 120 days after irradiation process.

3.13 Scanning electron microscope (SEM)

Figure 3.10 Scanning electron microscope

The surface morphology of the polymer blends and composites at different stages of the experimentation was studied using Leo 1430 VP SEM with a maximum magnification of 100 kX and the spatial resolution of ~10 nm. The test specimen was sputter coated with Au in order to make a conductive surface on the sample. Figure 3.10 shows the pictorial view of the SEM.

3.14 Transmission electron microscope (TEM)

A 200 kV Transmission Electron Microscope, JEOL JEM 2100, was used to identify the defects formed on the surface of MWCNTs after the irradiation process. High resolution TEM and selective area electron diffraction (SAED) were also used to obtain the crystal planes of MWCNTs. Figure 3.11 shows the pictorial view of TEM.

Figure 3.11 Transmission electron microscope

3.15 Laser micro Raman spectroscope

The stress transfer from polymer to reinforcement was confirmed by Raman spectra using a laser micro Raman (Jovin Yvon, Triax 550) in the backscattering mode equipped with 488 nm blue laser (Argon) and a CCD detector coupled with a monochromator having the XY step

resolution of 0.1 μm, wave number accuracy of ± 1 cm^{-1} and its resolution is 0.5 cm^{-1}. The equipment was also used to study the irradiation induced defects on the surface of MWCNTs. Figure 3.12 shows the pictorial view of micro Raman spectroscope.

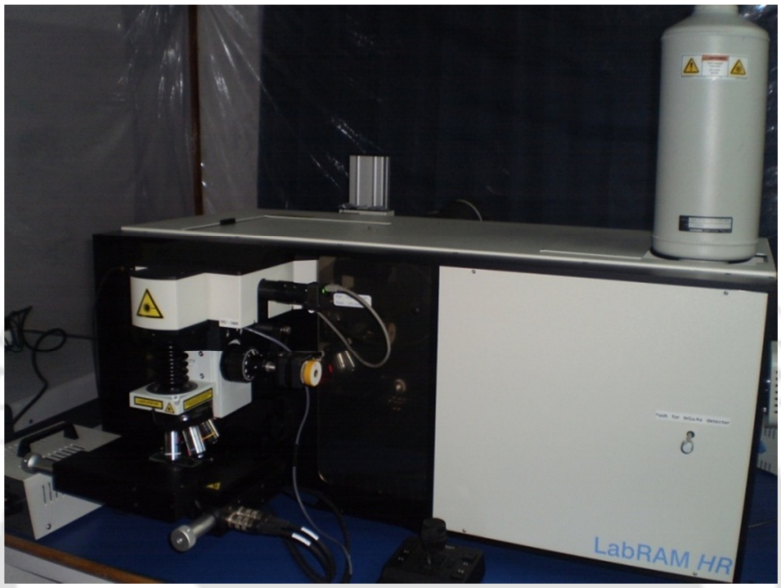

Figure 3.12 Laser micro Raman spectroscope

3.16 Electron spin resonance (ESR) spectroscope

ESR is a technique used to detect and quantify the unpaired or odd electrons in atomic or molecular systems. The identification of a particular species of radical is depending on the spectral splitting factor or the g- value, which is given by the equation 3.5.

... 3.5

Where 'h' is the plank's constant (6.63×10^{-34} J.s)

f – is the frequency band of the ESR spectroscope, 9 GHz,

β – is the electron Bhor magneton (9.27×10^{-24} J/T)

H_r is the resonance frequency of the external magnetic field obtained from the spectrum

The g-value of organic or polymeric radicals varies slightly from the free electron value of g = 2.0023.

The various parameters used during the sample testing were given below:

Magnetic field parameters: Center field- 350 mT, Sweep width- 25×, Time- 30 seconds;

Current parameters: Modulation width- 0.35×1, Time constant- 0.3, Microwave power- 1mW;

Acquisition parameters: Total sweep- 1.

The experimental spectrum is a first derivative curve and its intensity is directly proportional to the radical concentration present in the test sample. The area under the integral curve is called as an absorption curve. As the radical concentration depends on the mass of the sample, which was kept in the range of 5.0 ± 0.1 mg. Figure 3.13 shows the pictorial view of the ESR spectroscope.

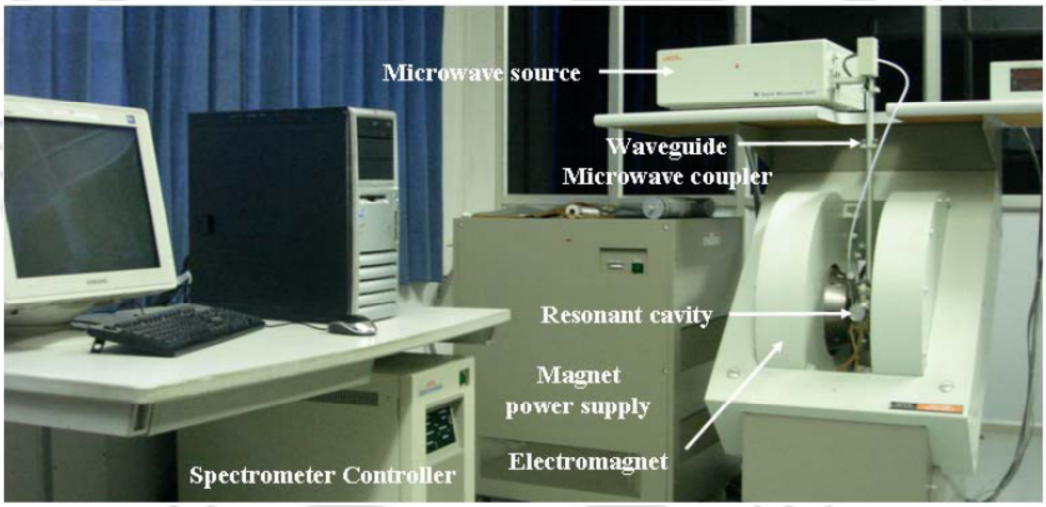

Figure 3.13 ESR spectroscope

3.17 X-Ray diffractometer (XRD)

Powder XRD is a nondestructive tool used to obtain the information about interlayer spacing, structural strain and the impurities in MWCNTs. It was used to monitor the structural modification and changes in lattice strain of the irradiated samples. Bruker D8-Advanced tools

XRD was used to characterize the sample and it is shown in Figure 3.14. The d- spacing was calculated using "Bragg's law" given in equation 3.6

$$2d \sin\theta = n\lambda \quad \ldots 3.6$$

Where d is the interplanar spacing between the diffracting adjacent planes, θ is the angle of the X-ray beam with the lattice plane, n represents the order of diffraction (1) and λ is the wavelength of the X-ray used (1. 5405 Å for Cu $K_{\alpha 1}$).

Figure 3.14 X-Ray diffractometer

3.18 Atomic force microscope (AFM)

The surface topography of wear samples was studied using an atomic force microscope (AFM), Nanosurf, attached to the Nanoindenter supplied by CETR, UMT-2. The AFM has a cantilever tip operated in tapping mode under the dynamic force with tip vibration frequency of 170 kHz, vibration amplitude of 200 mV and the excitation amplitude of 1.3 V. The AFM used in the present study is shown in Figure 3.15.

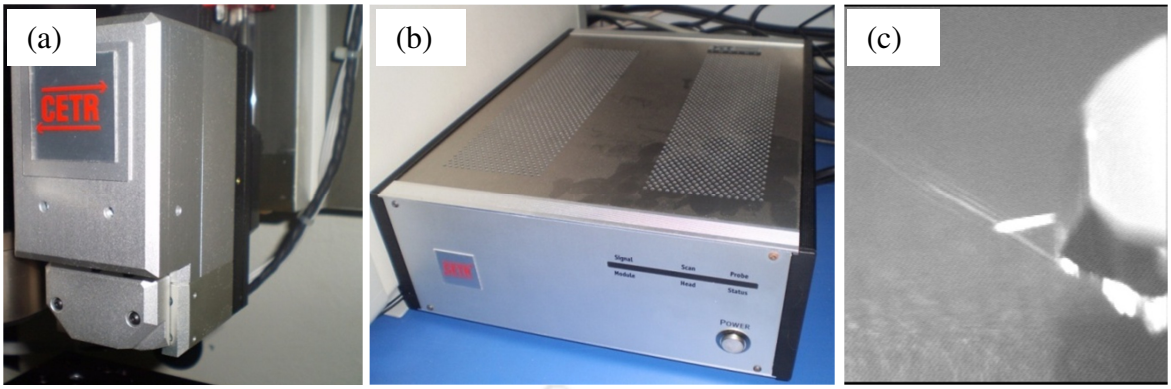

Figure 3.15 a) AFM head b) Controller c) AFM tip

3.19 Swell ratio test

The network parameters of the irradiated UHMWPE, composites and α_T blends were calculated from the swell test, which was carried out according to ASTM F2214-02 standards. The apparatus consists of a round bottom flask, retort stand, oil bath with heating coil, and a water cooled condenser with submersible pump. The samples were in the form of pellets of 6 mm diameter, and 0.5 mm thickness. In order to prevent thermal degradation of the sample, 1.00 wt. % of antioxidant (Irganox) was added into o-Xylene. The sample was immersed in the o-Xylene-antioxidant solution and the same was heated up to 150 ^{0}C. The thickness of the test sample was monitored using the linear variable differential transformer (LVDT) probe at an interval of 15 minutes until an equilibrium swelling of the sample was reached within ± 10 µm accuracy. Then the temperature of the solution was reduced to 50 ^{0}C. The samples, having the signs of cracking and yellowing were discarded from the measurement. The crosslink density (CLD) of irradiated sample (ν_d) was calculated using the equation 3.7, which is given below:

$$\nu_d = -\frac{\ln\left(1-\frac{1}{q_s}\right)+\frac{1}{q_s}+\frac{\chi_1}{q_s^2}}{\emptyset_1\left(\frac{1}{\sqrt[3]{q_s}}-\frac{1}{2q_s}\right)} \quad \ldots 3.7$$

where $q_s = (H_F/H_0)^3$, H_F- final height of sample, H_0 - initial height of the sample, $Ø_1$- molar volume of the solvent (o-Xylene) = 136 [cm^3/mol] and χ_1 - Flory interaction parameter for the

polymer-solvent system, which is given by $\chi_1 = 0.33+0.55/q_s$. The swell test apparatus used to measure the CLD of the test sample is shown in Figure 3.16.

Figure 3.16 Swell test apparatus

3.20 Pin-on-disc (POD) setup

Inorder to study the wear behavior of the test samples under dry sliding conditions a POD wear tester was used. The wear tests of both unirradiated and irradiated test samples were performed using a POD Tribometer, Ducom, TR-20. The sample used for the POD test was a 4 mm diameter circular pellet, which was secured at the end of the pin. The test samples were sonicated for about 15 minutes in an ultrasonic bath and later cleaned with ethanol and dried to remove any surface contaminants prior to testing. The load on the POD wear test sample was 55 N and the test was run at a speed of 0.83 m/s on the track of 80 mm diameter for the sliding distance of 20 km. The linear wear of the sample was monitored by the LVDT probe. The counterface used in the POD test was made of medical grade 316L stainless steel with an average surface roughness of 0.03 ~ 0.04 µm confirming to ISO-5832-1 standards, which was supplied by M/s Shushrut Surgical Pvt. Ltd, Pune, India. The wear factor was calculated using the equation 3.8, which is given below.

… 3.8

Where, V - wear volume (mm^3), P – load applied (N) and L – sliding distance (m). The POD Tribometer and the SS316L counterface used in this study are shown in Figure 3.17.

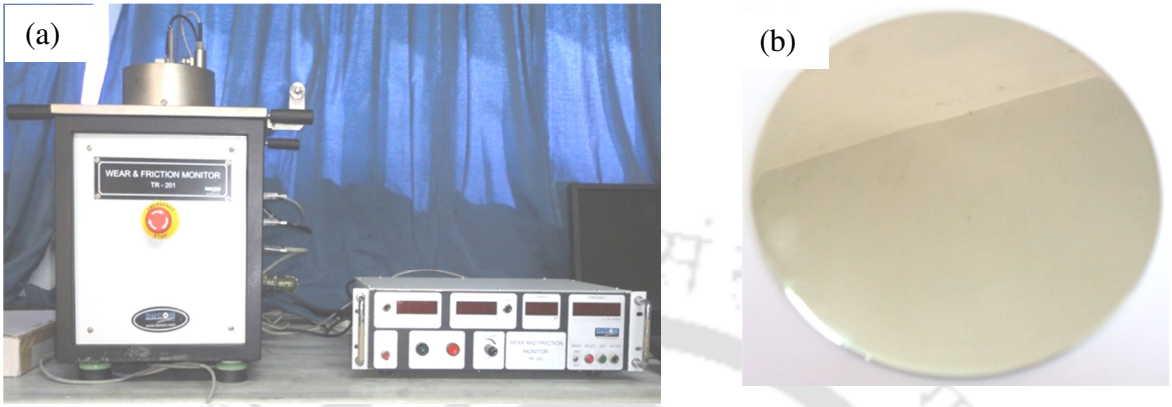

Figure 3.17 a) POD Tribometer b) 316 L stainless steel counter face

3.21 Simulated body fluid (SBF) study

SBF study is a primary and an essential test to establish the biocompatibility of the developed material, where the formation of apatite on the composites was confirmed. The ion concentration of the SBF is almost equal to that of human blood plasma and it is shown in Table 3.1. The SBF solution was prepared by the procedure suggested by Wang et al. [2009] using various chemical reagents listed in Table 3.2. The test samples were soaked in the SBF solution and incubated at 37 ^{0}C. The samples were then taken out of it after 1, 3, 5, 7, 15 and 30 days in order to confirm the rate of deposition of apatite layer on the sample. All the samples were weighed prior to their soaking in the SBF. The weight of the sample and pH value of the SBF solution were monitored regularly using Sartorius: BSA224S-CW weighing balance and Sartorius pH meter model: PB-11, respectively. The formation of hydroxyapatite (HA) was confirmed by energy dispersive X-ray analysis (EDAX) and micro Raman studies. Scanning electron microscope was also used to study the HA coating over the test surface. Figure 3.18 shows the preparation of SBF and the soaked samples in SBF.

Table 3.1. Ion concentration (mmol/L) of SBF and human blood plasma, Sousa et al. [2003]

	Na^+	K^+	Ca^{2+}	Mg^{2+}	Cl^{2-}	HCO_3^-	HPO_4^{2-}	SO_4^{2-}
SBF	142	5	2.5	1.5	147.8	4.2	1.0	0.5
Human Plasma	142	5	2.5	1.5	103.0	27	1.0	0.5

Table 3.2. Reagents used to prepare SBF, Wang et al. [2009]

Sl no	**Name of the Reagent**	**Chemical composition**	**Purity (%)**	**weight**
1	Sodium chloride	NaCl	99.8	8.011 g
2	Sodium hydrogen carbonate	$NaHCO_3$	99.5	0.355 g
3	Potassium chloride	KCl	99.5	0.225 g
4	Di-potassium hydrogen phosphate trihydrate	$K_2HPO_4 \cdot 3H_2O$	99.0	0.231 g
5	Magnesium chloride hexahydrate	$MgCl_2 \cdot 6H_2O$	98.0	0.311 g
6	Hydrochloric acid	1 M HCl	-	39 ml
7	Calcium chloride	$CaCl_2$	95.0	0.292 g
8	sodium sulfate	Na_2SO_4	99.0	0.072 g
9	Tris-(hydroxymethyl) aminomethane	$(CH_2OH)_3CNH_2$	99.0	6.118 g
10	Hydrochloric acid	1 M HCl	-	0-5 ml

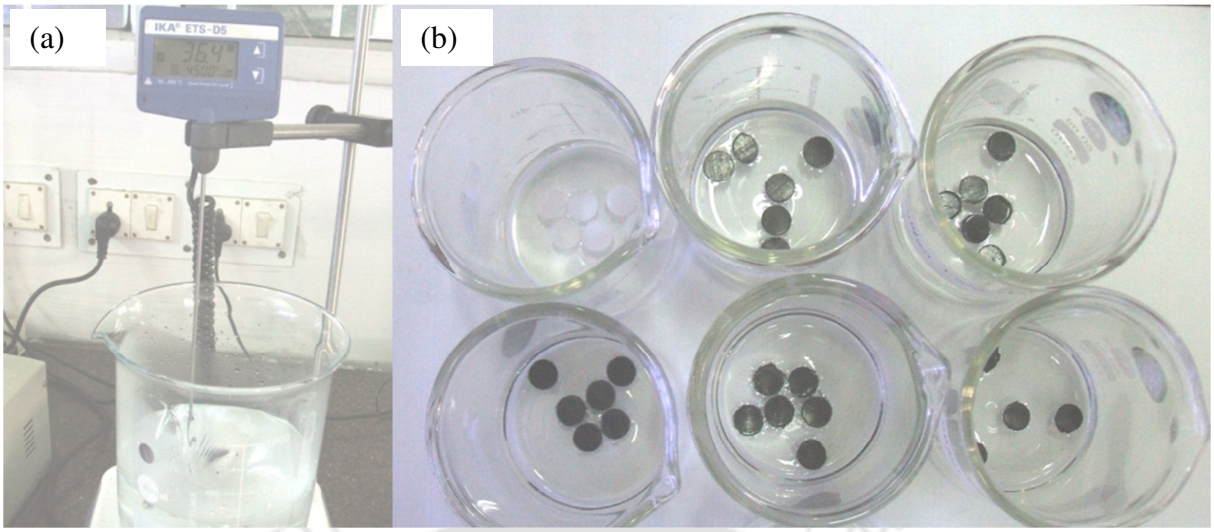

Figure 3.18 a) Preparation of SBF b) Samples soaked in SBF

3.22 Platelet adhesion test

The platelet adhesion test was performed as suggested by Ren et al. [2005]. A 100 ml of fresh human blood was extracted from a healthy adult donor and the sodium citrate was mixed in it with the volume ratio of 9:1 in order to avoid coagulation. The mixture was then centrifuged for about 60 minutes to form platelet-rich plasma (PRP), which contained about 1.078×10^{10} platelets/ml. The polymer and composite test samples were placed in PRP in culture dishes and kept at 37 ^{0}C for 30 min. and 3 hrs. The samples were then removed from the dishes and immersed in a phosphate buffer solution and gently rinsed for 2–3 times to remove the weakly adhered platelets on the test surface. In order to fix the platelets on the test surface, the samples were soaked in 2 % glutaraldehyde for 1 hr and later 5 % glutaraldehyde solution for 12 hrs. The samples were then removed from the solution and rinsed with distilled water. The samples were subsequently dehydrated using gradient alcohol (50, 60, 70, 80, 90 and 100 % ethanol) and then the samples were dealcoholized through isoamyl acetate water solutions (50, 60, 70, 80, 90 and 100 %). The samples were dried and the test surface was observed under scanning electron microscope. Figure 3.19 shows the PRP and the soaked samples.

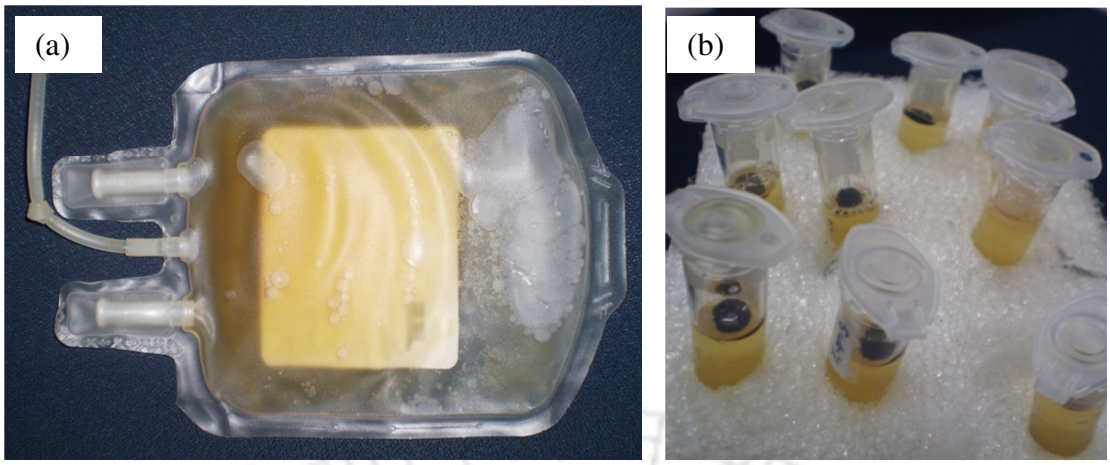

Figure 3.19 a) Platelet rich plasma b) Samples incubated in PRP

3.23 Local effects after *in vivo* subcutaneous implantation

Sprague Dawley rats weighing between 170-210 g were used for the *in vivo* studies. The animals were housed in a bio-safe chamber, where the following conditions were maintained: light/dark cycle for a period of 12 hrs each, temperature 24 ± 3 ^{0}C and relative humidity 55 ± 15%. During the experimental period, the rats were allowed to have free access to food and water at all times. The present study required subcutaneous implantation of the test materials and the reference materials in either side of the subcutaneous pouch of the experimental animals. The specimens were 3 mm radius pellets each weighing 10 mg. The specimens were ultrasonically cleaned in acetone and ethyl alcohol solution for 5 min. and finally rinsed in distilled water and dried. The animals were anaesthetized with ketamine ip administration. The implanted sites were swabbed with alcohol and incised. The test material was inserted in the pouch of subcutaneous region and sutured with non absorbable nylon thread. Figure 3.20 shows the various steps involved in the subcutaneous test process. In order to reduce the number of animals involved in the study, the test was performed using 2 wt. % composite, where the studies on virgin UHMWPE were considered as a standard. Five animals were taken per group and all the animals

were humanely euthanized after 4 weeks and the implant sites were dissected. Histopathological slides were prepared and observed under a digital microscope (Prime star Zeiss) for examination.

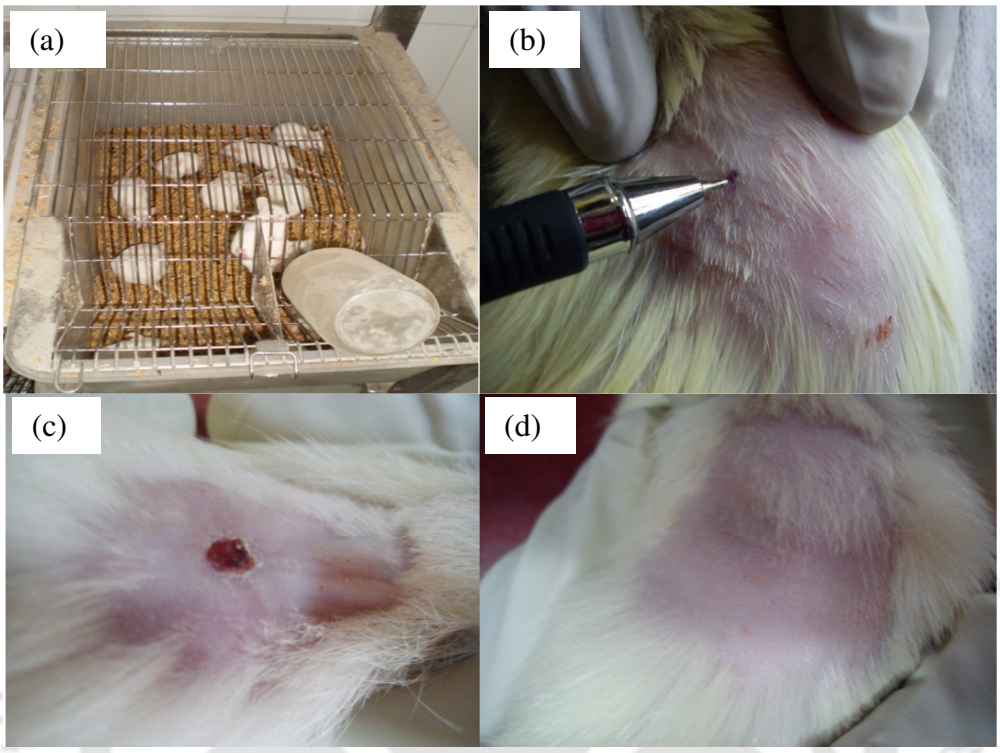

Figure 3.20 a) Test animals access to free food and water b) Location of implantation c) Inscision to place the test sample d) Implanted area after suture

Chapter 4

Results and Discussion

The results and discussion section gives a detailed technical insight into the various experimental outcomes in a sequential order as mentioned below:

1. Mechanical properties of unirradiated UHMWPE/MWCNTs composites and UHMWPE/α_T blends.
2 Mechanical properties of irradiated UHMWPE/MWCNTs composites and UHMWPE/α_T blends.
3 Studies on network parameters and radical scavenging capability of MWCNTs and α_T.
4 Wear studies on composites and α_T blends before and after the irradiation process.
5 Biocompatibility studies on UHMWPE/MWCNTs composites.

4.1 Mechanical properties of unirradiated UHMWPE/MWCNTs composites and UHMWPE/α_T blends

4.1.1 Mechanical properties of unirradiated UHMWPE/MWCNTs composites

Tensile testing of the composites has been performed using the microtensile test specimen having different weight concentrations of MWCNTs such as 0, 0.5, 1.0, 1.5, 2.0, 2.5 and 5 wt. %. The load vs. displacement plots obtained for the test samples are shown in Figure 4.1a. The mechanical properties namely work to failure, strain at fracture, and yield stress cum fracture stress were calculated and plotted in Figures 4.1b, 4.1c and 4.1d, respectively. The work to failure of the material is an indication of its resistance against wear. Although other mechanical

properties are not having any direct influence on the wear resistance of the material, they are expected to influence the resistance of the material against the damage caused by 'impingement' or 'bearing lift off', Kurtz [2009]. It is observed from Figure 4.1 that all the mechanical properties were found to be an optimum at 2 wt. % of MWCNTs in UHMWPE. The work to failure of the pure polymer was increased from 2938 to 8111 mJ, which corresponds to an enhancement of 176 % at 2 wt. % MWCNTs. Similarly other properties namely yield stress, strain at fracture and fracture stress were increased by 44, 70 and 93 %, respectively at an optimum concentration of MWCNTs. Figure 4.2 shows the percentage enhancement of the yield stress, strain at fracture, fracture stress and work to failure of composites compared to that of virgin UHMWPE, where the above observation was inferred. The enhancement of mechanical properties of UHMWPE was increased with concentration of MWCNTs, which is found to be an optimum at 2 wt. % and then it started to decrease.

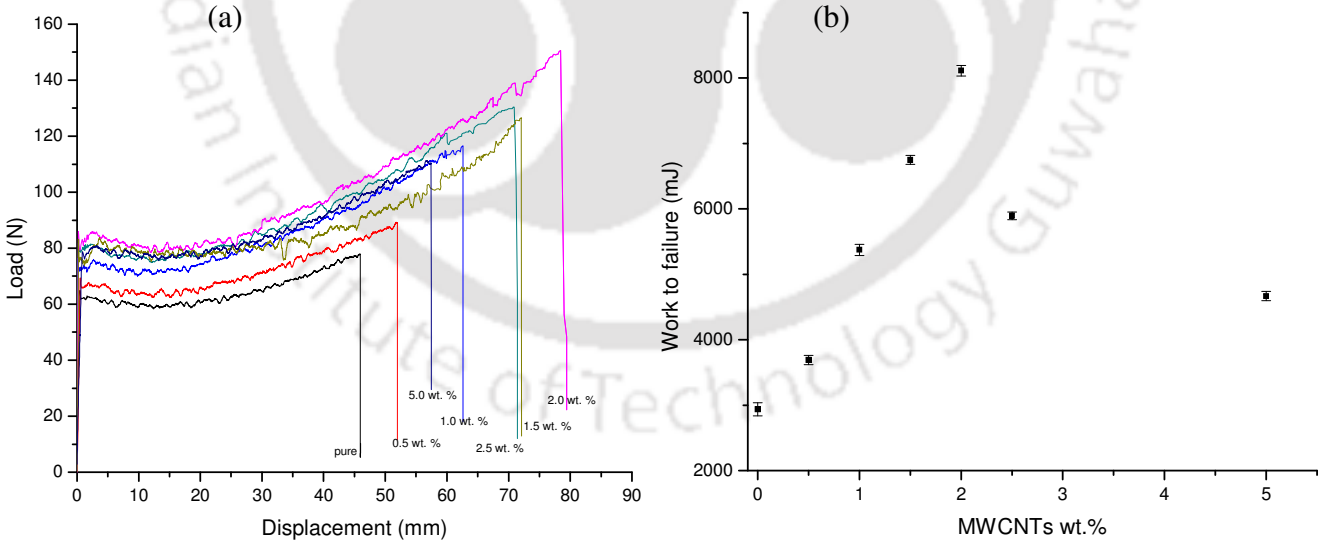

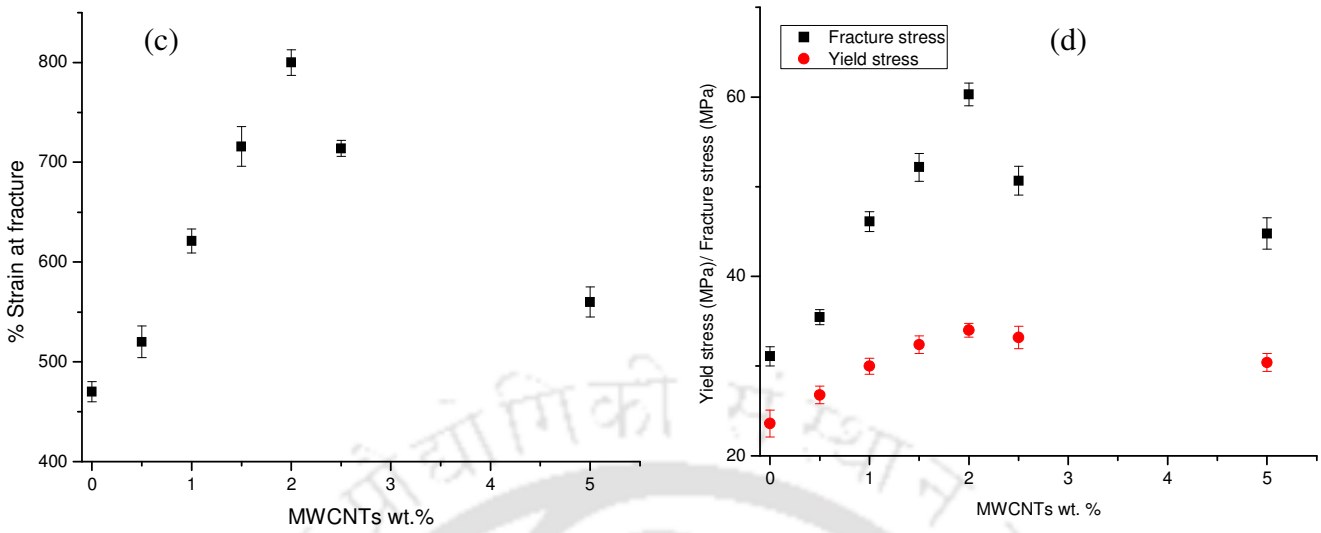

Figure 4.1. a) Load vs. displacement plots b) Work to failure c) Strain at fracture d) Yield stress and fracture stress of the UHMWPE/MWCNTs composites

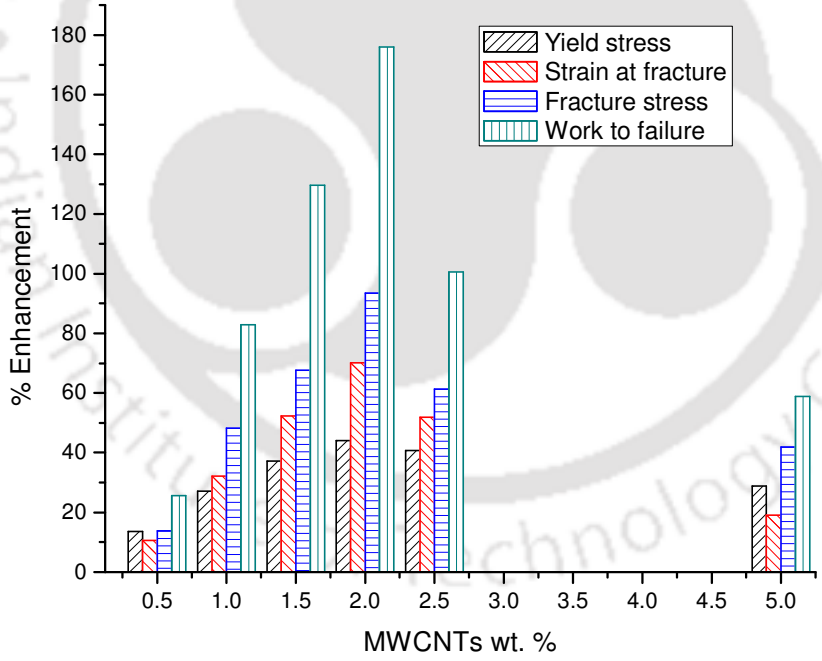

Figure 4.2. Enhancement of the mechanical properties of UHMWPE/MWCNTs composites compared with virgin UHMWPE

4.1.1.1 Mechanisms involved for the enhancement of mechanical properties

The reasons for the enhancement of mechanical properties of the composites up to 2 wt. % of MWCNTs can be explained as follows: (a) MWCNTs are known to have extraordinarily high mechanical properties, Treacy et al. [1996], thus the addition of them would obviously enhance the overall mechanical properties of the composites; (b) functionalization of MWCNTs attaches certain chemical groups on their surface, which bond with the polymer and thus aids in stress transfer from UHMWPE to MWCNTs; (c) homogenous distribution of MWCNTs in UHMWPE; and (d) the addition of MWNCTs increased the crystallinity of the polymer resulting the enhanced mechanical properties, as confirmed by Perepechko [1981]. In order to confirm the above, micro-Raman spectroscopy, rheological percolation and DSC studies were done on the test sample.

Raman spectroscopy has become a first hand and standard tool for the characterization of nanostructures and confirms the stress transfer from the matrix to the filler, Samrutishika [2010]. The Raman spectra of 2 wt. % composites before and after the tensile testing have been studied and shown in Figure 4.3. It is observed that the G- band peak of the test sample before tensile testing was obtained at 1541 cm^{-1}, and it was shifted to 1550 cm^{-1} for the same sample after tensile testing. The G-band observed between 1500 to 1600 cm^{-1} denotes the in Plane vibration of sp^2 carbon-carbon bonds. When MWCNTs are subjected to either tensile or compressive stresses, the C-C bond vibrations change due to the induced strain, which is reflected in the Raman spectra, Cronin et al. [2004]. It leads to a change in either intensity or position of the G - band. Thus, the observed shift in G-band, shown in Figure 4.3, can be used to qualitatively confirm the effective stress transfer from UHMWPE to MWCNTs. According to Minfang et al. [2009], the MWCNTs surfaces provided nucleation sites for the crystallization that subsequently

enhance the MWCNT–polymer interaction leading to effective stress transfer from matrix to reinforcement. Since a shift in G- band confirms the stress transfer. Thus, the enhancement of mechanical properties of the UHMWPE/MWCNTs composites was achieved.

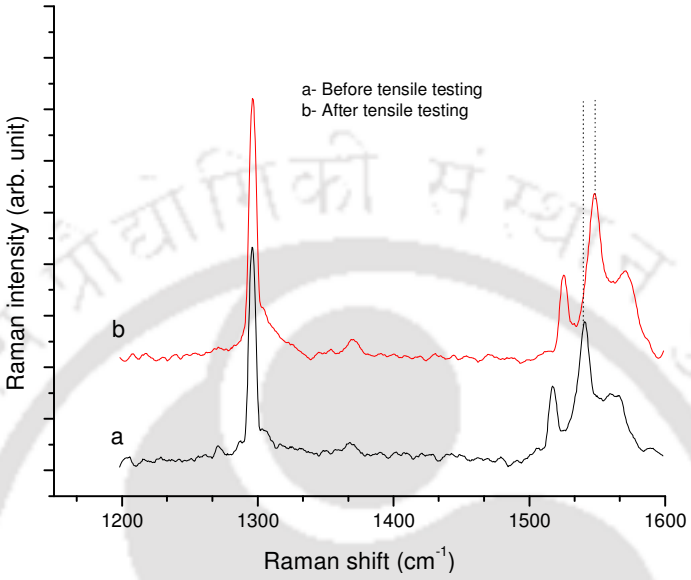

Figure 4.3. Raman spectra of 2 wt. % UHMWPE/MWCNTs composite: before and after the tensile test

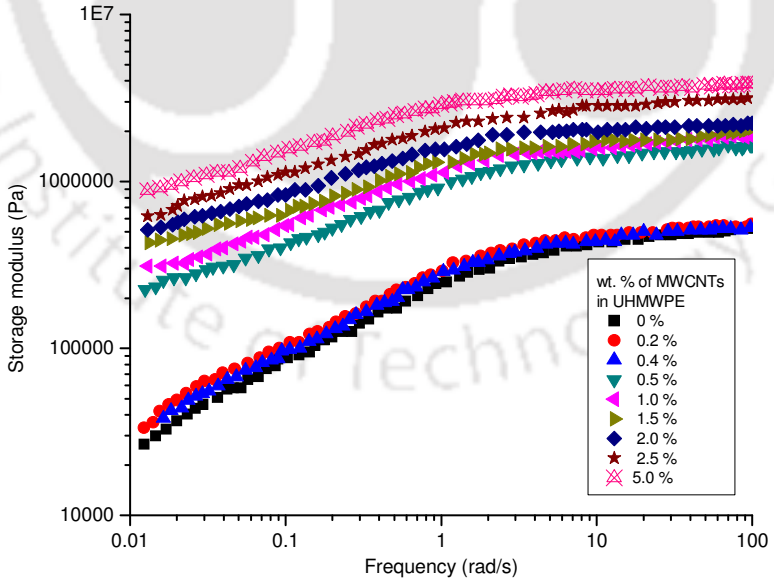

Figure 4.4. Assessment of homogeneous dispersion of MWCNTs in UHMWPE using rheological percolation threshold technique

The homogeneous dispersion of the MWCNTs is confirmed by estimating the rheological percolation of the composites. The term percolation is defined as the concentration of filler material, where a long range connectivity is exhibited by the filler network in the matrix. In rheological experiments, the property that is typically used for estimating the percolation threshold is the storage modulus, Grady [2011]. Figure 4.4 shows the storage modulus of the composites against angular frequency. In order to obtain more accurate threshold value, two additional composites having 0.2 and 0.4 wt. % MWCNTs were prepared and tested. It is observed that no significant change in the storage modulus was observed upto 0.4 wt. % of MWCNTs. The storage modulus of virgin UHMWPE was found to be 26.7 kPa at 0.015 rad/s, which was slightly increased to 33.7 kPa at 0.4 wt. % of MWCNTs. When the concentration of reinforcement was increased to 0.5 wt. %, a very large change in storage modulus was observed and it was increased to 233.2 kPa which is one order higher. However, the change in storage modulus of the composites was not so significant beyond 0.5 wt. %. In other words, the percolation threshold was found to be at 0.4 wt. % above which a significant change in storage modulus was observed. A lower percolation threshold implies better debundling of reinforcement in the matrix. If it is less than 1 wt. %, then the dispersion at nanoscale is considered to be very good, Du et al. [2004]. The rheological studies carried out by Zhang et al. [2006] obtained a threshold limit at 0.6 wt. % of SWCNTs in UHMWPE, whereas the same was found to be 0.4 wt. % in our case. The variation of threshold value may be due to the fact that it varied significantly with type, size, shape and aspect ratio of the filler.

In order to confirm the increase of crystallinity of the composites, DSC studies were performed on the test sample. Figures 4.5a and 4.5b show the DSC thermograms and the crystallinity of the composites, respectively. It is observed from Figure 4.5a that the melting

temperature of the composites was not affected by the presence of MWCNTs. A weak shoulder peak was also observed indicating the presence of small crystals. It is observed from Figure 4.5b that the crystallinity of virgin UHMWPE was found to be 52.5 %, which was increased to 64.7 % upon addition of 2 wt. % MWCNTs corresponding to an enhancement of 23 %. An increase of crystallinity can be attributed to enhance the mechanical properties of composites. It is interesting to note that although optimum mechanical properties were obtained at 2 wt. % composites, the crystallinity was continued to increase to 67 and 72.3 % at 2.5 and 5 wt. % composite, respectively. The reason for the enhanced crystallinity with an increase of MWCNTs concentration is that the MWCNTs acted as sites for nucleation of crystallization of polymer and thus it enhanced the crystallinity of the composite, Sreekanth et al. [2012]. Although the crystallinity of the composites was increased beyond 2 wt. % of MWCNTs, the mechanical properties were found to be reduced. The reasons for the reduction of mechanical properties of the composites beyond 2 wt. % MWCNTs are discussed in the next section

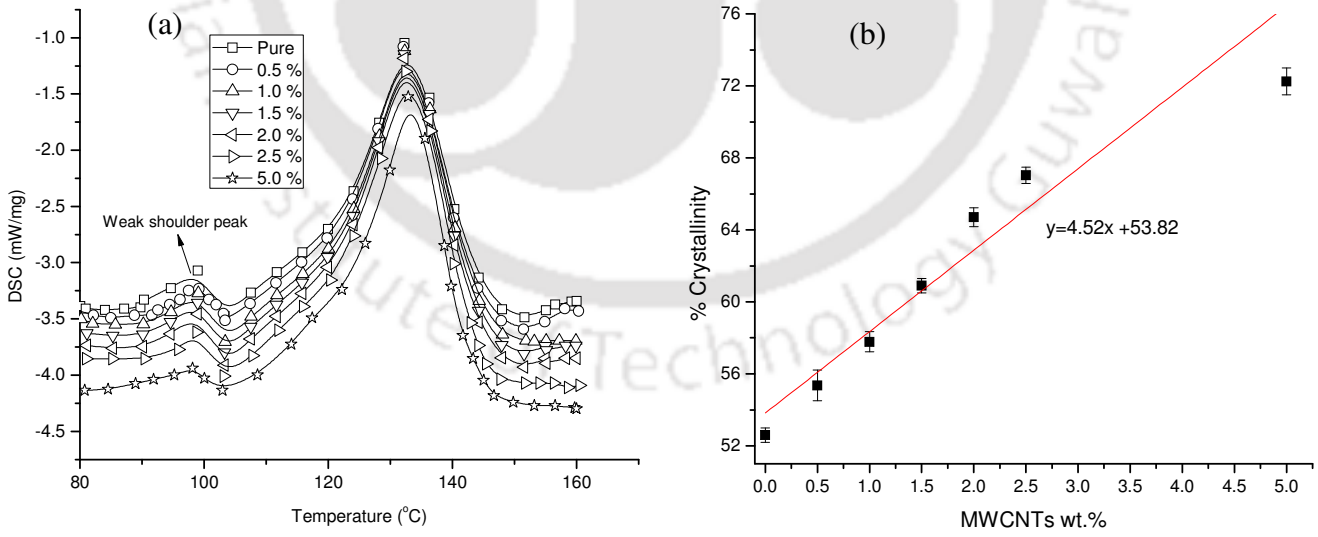

Figure 4.5. a) DSC thermograms and b) Crystallinity of the UHMWPE/MWCNTs composites

4.1.1.2 Reasons for the reduction of mechanical properties of composites beyond 2 wt. % MWCNTs

The reasons for the reduction of mechanical properties could be attributed to the following effects: firstly, there are many studies focused on the rheological characterization of polymer/MWCNTs composites, Chatterjee et al. [2005] and Du et al. [2004], which reported that the viscosity of the composite melt was increased with MWCNTs concentration. It was also found that liquid- like to solid- like transitions of polymer melt were observed with an increase of filler concentration. In order to confirm the above transition behavior, the oscillatory rheometry tests were conducted for all the composites upto 5 wt. % to assess the variation of their complex viscosity with MWCNTs concentration against temperature and the observed results are shown in Figure 4.6. It is observed that the complex viscosity of pure polymer and composites in the temperature range of 135 to 155 ^{0}C was increased by an order of magnitude and it was decreased by upto 5 % when the temperature was raised to 200 ^{0}C. The complex viscosity of

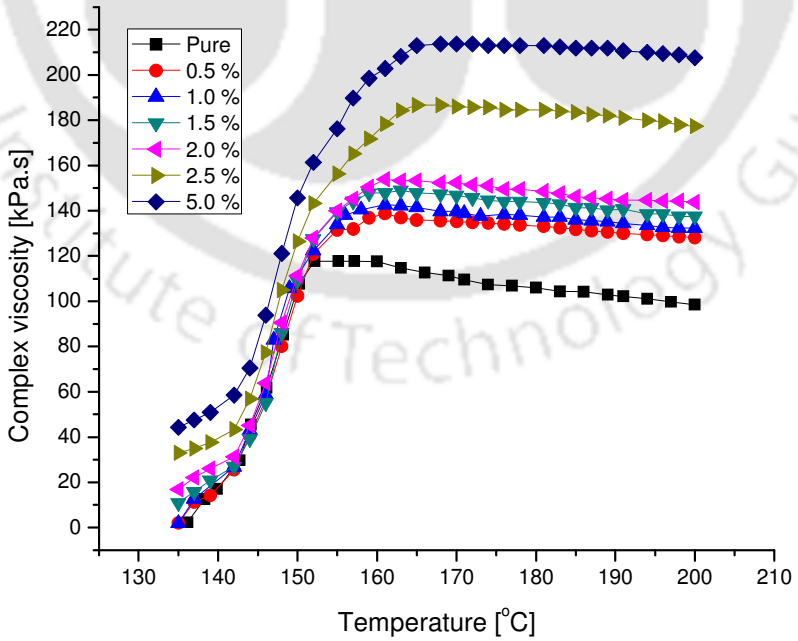

Figure 4.6. Complex viscosity of UHMWPE/MWCNTs composites against temperature

pure polymer at 200 ^{0}C was found to be 98 kPa.s, and the same for 0.5, 1.0, 1.5, 2.0, 2.5 and 5 wt. % composites was increased by 30, 34.6, 39.7, 45, 83.4 and 113 %, respectively compared to pure polymer. As UHMWPE is known to have high melt viscosity, the processibility of the polymer was further reduced due to its enhanced viscosity with an addition of MWCNTs beyond optimum concentration. Secondly, the functionalization of MWCNTs increased their available surface area to interact with polymer, Singh et al. [2008]. In the present study, the surface area of MWCNTs as given by manufacturer is about 200 m^2/g and thus the corresponding amount of polymer available with raw material mixture is not sufficient enough to properly wet the MWCNTs surface leading to the formation of voids in the polymer at higher loading. The severity of the said problem is even higher at 2.5 and 5 wt. % of MWCNTs in UHMWPE. Thirdly, MWCNTs are known to have extraordinary thermal properties in addition to their mechanical properties. The thermal conductivity and specific heat of MWCNTs are 3000 W/m-K, Yang et al. [2009] and 0.71 kJ/kg-K, Pradhan et al. [2009], respectively; while the same for UHMWPE is 0.41 W/m-K, and 1.84 kJ/kg-K [Ticona data sheet]. The heat required for a given temperature raise in the polymer is 2.6 times more than that of the MWCNTs. When equal amount of heat is supplied to MWCNTs and polymer, as in the case of compression moulding, the raise in temperature is higher for MWCNTs than the polymer. As the thermal conductivity of MWCNTs is few order higher than that of the polymer and the maximum heat flow is possible through the path of least resistance, a greater amount of heat is expected to flow through MWCNTs than the polymer. It is evident from the above discussion that although polymer needs higher amount of heat than the MWCNTs for a given temperature raise, but owing to its low thermal conductivity the heat available for its consolidation becomes less. Consequently, it leads to the formation of microvoids in the composites beyond 2 wt. %.

The cumulative effects of increased viscosity beyond 2 wt. % of MWCNTs and higher thermal conductivity and lower specific heat of MWCNTs compared to polymer lead to the formation of microvoids in the composites, which cause the reduction of mechanical properties at higher loadings of MWCNTs. In order to confirm the formation of microvoids with an increase of MWCNTs beyond the optimum concentration, the surface of 5 wt. % composite was also studied in addition to 2.5 wt. %, where a large number of defects and microvoids was observed.

Figures 4.7a–4.7e show the SEM images of the composites at different concentrations to confirm the above observation. The SEM images of 1 and 2 wt. % composites are shown in Figures 4.7a and 4.7b, respectively, where the defect free surfaces were observed. Figures 4.7c and 4.7d show the SEM images of 2.5 wt. % composite, where the presence of microvoids in the range of 0.5 to 2 μm was observed under higher magnification (1000 x). However, the size of the voids for 5 wt. % composites, which is shown in Figure 4.7e, was increased in the order of tens of micron and thus the voids were visible even at lower magnification (100 x). The presence of MWCNTs in large quantity reduces the amount of polymer available to wet the surface of them and the amount of heat available for polymer processing. Thus, it led to incomplete consolidation of the polymer and a large number microvoids with increased dimension. The voids present in the test sample act as defective zones leading to the reduction of mechanical properties at higher concentration of MWCNTs. Due to the above mentioned reasons, the mechanical properties of composites were reduced beyond 2 wt. % of MWCNTs even though the crystallinity was found to be increased.

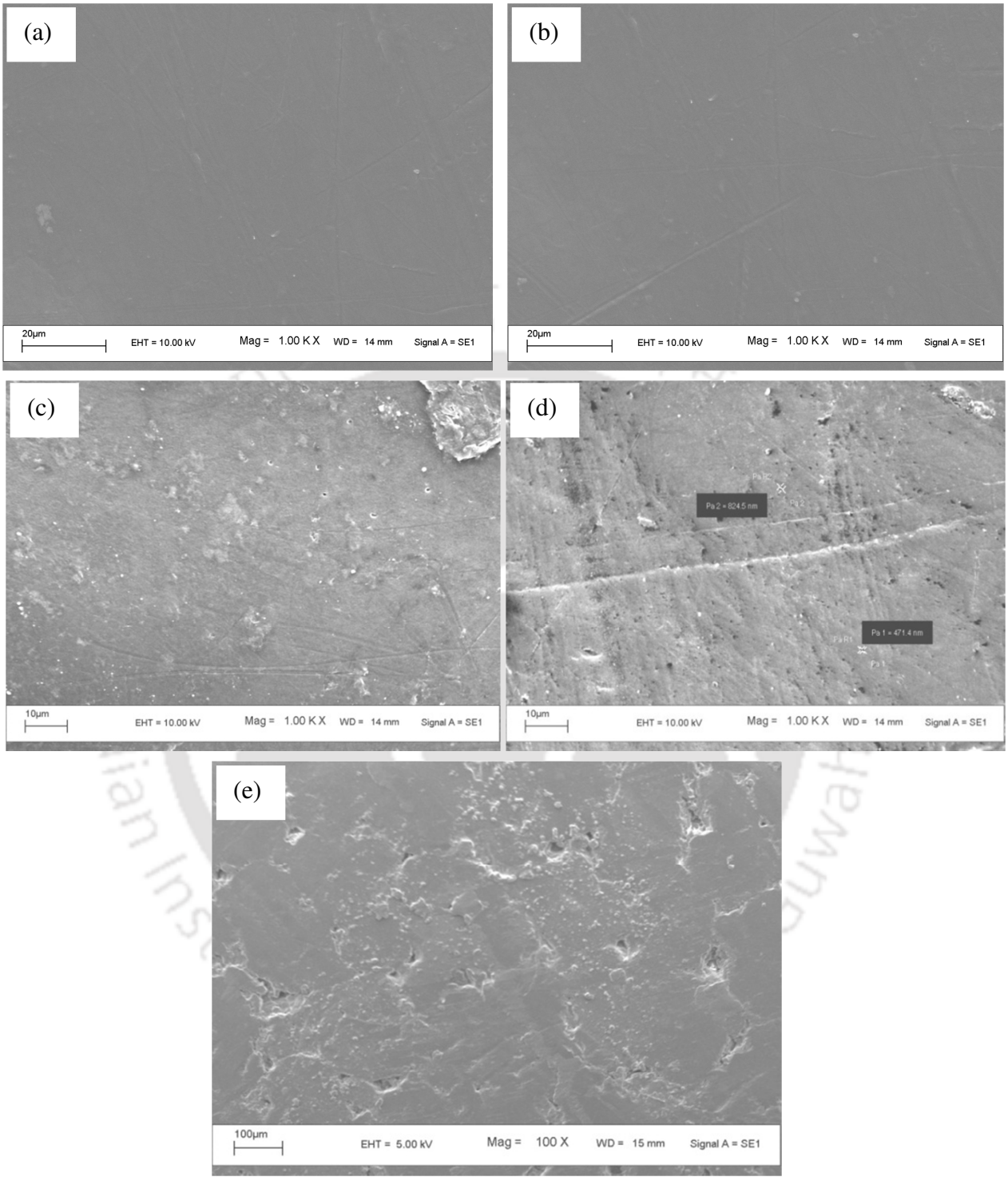

Figure 4.7. SEM images of a) 1 wt. % b) 2.0 wt. % (c) and (d) 2.5 wt. % e) 5 wt. % UHMWPE/MWCNTs composites

4.1.1.3 Surface hardness and plasticity index of composites using Nanoindentation technique

Figures 4.8a and 4.8b show the indenter position obtained against load from the Nanoindentation test with creep segment for ASP and SLR samples, respectively. It is observed from Figure 4.8a that the ascent of loading curve increased with concentration of MWCNTs in the polymer, which implies that the load required to produce same depth of indent in the test sample was increased with MWCNTs concentration. It also confirms that the addition of MWCNTs has hardened the surface of UHMWPE. A similar trend was observed for both ASP and SLR samples. At a peak load of 10 mN, the depth of indent of 0, 1.0 and 2.0 wt. % composites was 3.25, 3.03 and 2.69 μm, respectively for ASP samples. In case of SLR samples, the depth of indent for the same composition of sample at 10 mN was observed to be 3.43, 3.21 and 2.97 μm, which is shown in Figure 4.8b. The depth of indent of 0, 1.0 and 2 wt. % composites of SLR samples was 5, 5.9 and 10.4 % more than that of the respective results obtained for ASP samples, which indicates that the ASP samples are found to have more surface hardness than the SLR samples due to surface oxidation. The comparison of results obtained for ASP and SLR samples in case of 0 and 2 wt. % composites is shown in Figure 4.8c, where it is observed that the depth of indent on ASP samples was lower than that of SLR samples for the same loading condition. The possible reason for the difference in hardness between ASP and SLR samples could be attributed to the oxidation of UHMWPE surface during the processing condition, Costa et al. [1997a]. It is observed from Figure 4.8d that the hardness of ASP sample was increased from 26.1 MPa for pure polymer to 45.7 MPa for 2 wt. % composite samples, which corresponds to 75 % enhancement. The hardness of 2.5 and 5 wt. % composites was observed to be increased by 85 and 116 % compared to that of pure polymer. It a known fact that amorphous polymers

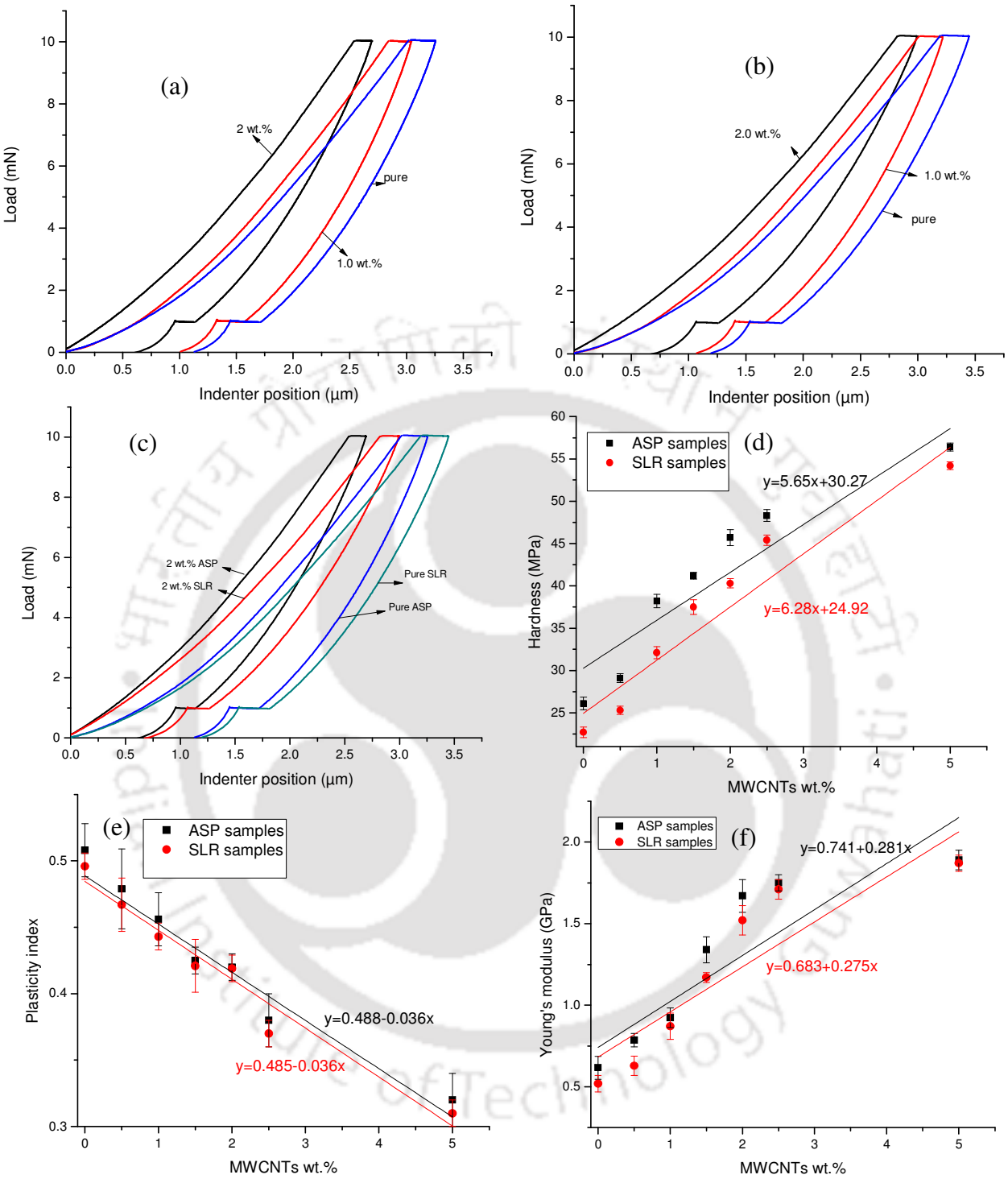

Figure 4.8. a) Indenter position against load for ASP samples b) Indenter position against load for SLR samples c) Comparison of the indenter position for ASP and SLR samples d) Hardness of the test samples e) Plasticity index of the test samples and f) Young's modulus of ASP and SLR samples

are softer than the crystalline polymers, Perepechko [1981], and thus, the hardness of composite was increased due to continuous increase of crystallinity beyond 2 wt. % MWCNTs. In case of SLR samples, the enhancement of hardness was found to be 76 % when the MWCNTs concentration was increased from 0 to 2 wt. %. The hardness of pure polymer was reduced from 26.1 MPa for ASP samples to 22.7 MPa for SLR samples, i.e. 13 % reduction the hardness of 2 wt. % composites was 45.7 MPa for ASP samples and 40.3 MPa for SLR samples corresponding to a reduction of 11.8 %. In the case of 5 wt. % composite, the hardness of ASP and SLR samples was found to be 56.4 and 54.2 MPa, respectively, i.e. a reduction of only 3.9 %. It clearly indicates that the presence of MWCNTs during the consolidation process can also reduce the severity of surface oxidation of the polymer. The hardness of pure polymer observed in this study is ~ 8 % less than that of results reported in the literature i.e. 28.5 MPa, Wang et al. [2007]. The variation between the observed and reported results may be due to different processing parameters employed during the consolidation process of UHMWPE.

Figure 4.8e shows the influence of MWCNTs concentration on plasticity index of the test material, where the creep segment was not considered as suggested by Briscoe et al. [1998]. Plasticity index is the measure of the elastic recovery ability of a material after the deformative load is removed. It primarily depends on surface roughness and hardness of the material and it is usually higher for rough and softer materials, Kogut et al. [2004]. Materials with higher plasticity index generally have high friction, surface temperature and higher wear volume, Nakajima et al. [1998]. As shown in Figure 4.8e, the plasticity index of ASP 2 wt. % composite was observed to be 17.3 % less compared to that of pure polymer and it was further reduced by 25.1 and 35 % for 2.5 and 5 wt. % composites, respectively. A significant reduction of plasticity index beyond 2 wt. % composite is due to the fact that the softer materials have higher plasticity

index than the harder materials, Kogut et al. [2004]. It is noted from earlier discussion that an increase of crystallinity enhanced the hardness, which in turn reduced the plasticity index of composites at higher loadings of MWCNTs beyond 2 wt. %. The observed results of both ASP and SLR samples are found to be not varied significantly because of the fact that the ability of plastic strain recovery of both ASP and SLR sample was close to each other. The reduction of plasticity index with an increase of MWCNTs concentration is due to the fact that MWCNTs are flexible and they do not undergo any plastic deformation at such low load, Briscoe et al. [1998], but UHMWPE is expected to undergo plastic deformation. However, due to strong interfacial bonding between MWCNTs and UHMWPE, as confirmed from the micro-Raman studies, MWCNTs help UHMWPE in elastic recovery and hence it reduces the plasticity index at higher loadings. The reduction of plasticity index of UHMWPE by reinforcing MWCNTs aids in minimizing the problem of deformation induced wear due to cold flow of the material, Rieker et al. [2003], and also lesser wear volume due to reduction in severity of the asperity contact.

Figure 4.8f shows the Young's modulus of ASP and SLR samples. It is observed that the Young's modulus of UHMWPE was observed to be 0.617 GPa, which was increased to 1.67 GPa at 2 wt. % of MWCNTs and the corresponding enhancement was about 170 % for ASP samples. When the MWCNTs concentration was further increased to 2.5 and 5 wt. %, the Young's modulus was observed to be increased by 183.6 and 206.3 %, respectively. Although the bulk mechanical properties were reduced beyond 2 wt. % composite, the Young's modulus was increased up to 5 wt. % composite. It is due to the fact that the surface properties measured using Nanoindenter are not influenced by the formation of voids or any other defects present in the test sample that arise during the consolidation process. The Young's modulus of SLR sample of pure polymer was observed to be 0.52 GPa, which was increased by 200, 229 and 260 % for

2, 2.5 and 5 wt. % composites, respectively. It is also noted that the Young's modulus of ASP samples of pure polymer and 2 wt. % composites was higher by 15 and 8 %, respectively compared to that of respective SLR samples.

Figures 4.9a and 4.9b show the AFM image of the indented surface of pure UHMWPE and 2 wt. % composite, respectively, where the elastic recovery of the material after indentation is confirmed in the composite sample. A triangle is drawn to indicate the actual shape of the indent. It is observed from Figures 4.9a and 4.9b that the elastic recovery of virgin UHMWPE was relatively less compared to that of 2 wt. % composite. It is also observed that the elastic recovery of the test sample was more at the side of the triangle than its vertices. It is due to the fact that the stress concentration was high at the vertices and hence the severity of deformation was found to be high.

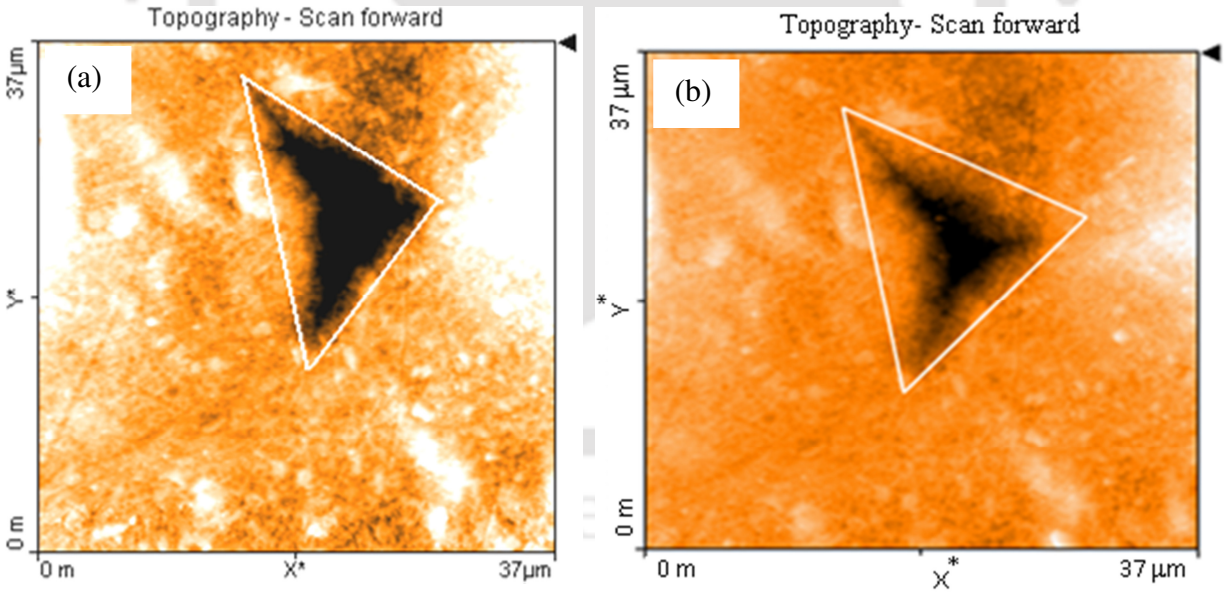

Figure 4.9. AFM image of the indent produced on a) Pure polymer b) 2 wt. % composite

The Young's modulus of the composites obtained from nanoindentation studies is compared with Halpin-Tsai theoretical models. The governing equation for the Young's modulus of the composites using Halpin-Tsai model, Vasiliev [2007], is given below:

Halpin-Tsai equation

$$\frac{E_C}{E_m} = \frac{3}{8}\left[\frac{1+2(l/d)\eta_L V_{cnt}}{1-\eta_l V_{cnt}}\right] + \frac{5}{8}\left[\frac{1+2\eta_T V_{cnt}}{1-\eta_T V_{cnt}}\right] \quad \ldots 4.1$$

Where $$\eta_T = \frac{\frac{E_f}{E_m}-1}{\frac{E_f}{E_m}+2}, \text{ and} \quad \ldots 4.2$$

$$\eta_L = \frac{\frac{E_f}{E_m}-1}{\frac{E_f}{E_m}+2(l/d)} \quad \ldots 4.3$$

E_C- Young's modulus of the composite,

E_f– Young's modulus of the filler (MWCNT- 1340 GPa), Yakobson et al. [2001], Belluci [2005]

E_m – Young's modulus of the matrix (UHMWPE- 0.617 GPa). (obtained from the experimental results)

Density of the filler – 2.16 g/cc (obtained from manufacturer's data)

Density of the matrix – 0.93 g/cc (obtained from manufacturer's data)

(l/d) ratio-86, Kanagaraj et al. [2007]

η_T and η_L are the parameters depending on the elastic modulus of the matrix and filler materials.

The weight fraction of the composites was converted in to volume fraction considering the density of both matrix and reinforcement, and it is given in the Table 4.1.

Table 4.1. Conversion of weight percentage to volume percentage

MWCNTs wt. %	0.5	1.0	1.5	2.0	2.5	5.0
Vol %	0.22	0.43	0.65	0.87	1.09	2.22

As all the results in the thesis were discussed based on the weight fraction, the predicted values of the Young's modulus were plotted against the weight fraction and the results are shown in Figure 4.10, which shows the comparison of the modulus of the composites obtained experimentally and theoretically.

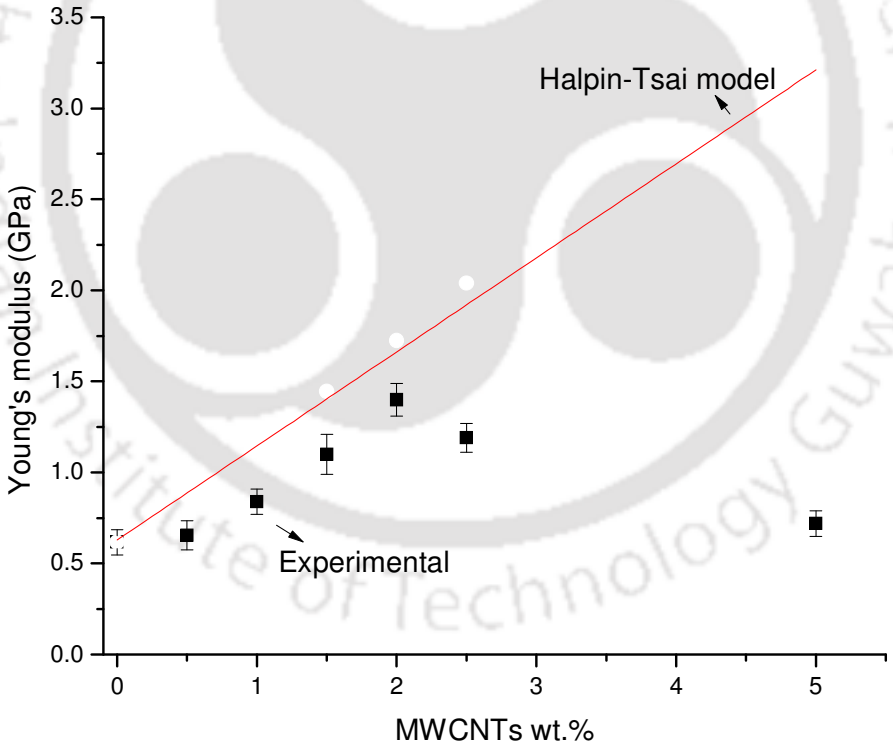

Figure 4.10. Comparison of the theoretical and experimental results of the elastic modulus of the composites

It is observed from Figure 4.10 that the difference between Young's modulus obtained using experimental and HT equation was within 10 % up to 2 wt. % MWCNTs. However, the difference between them is found to increase by 72 and 337 % for 2.5 and 5 wt. % composites, respectively. The increased difference between them is due to the fact that the theoretical models did not consider the experimental anomalies like the possibility of agglomeration, manufacturing difficulties due to increased filler content, micropores, increased viscosity, difficulties in homogeneous dispersion of reinforcement and others.

The mechanical properties of the composites such as work to failure, Young's modulus, fracture stress, strain at failure obtained in the present study were compared with the published literature, and are shown in Figure 4.11a-d. It is observed from Figure 4.11a that the Young's modulus of all the composites with different fillers showed an increasing trend compared to virgin UHMWPE. However, the highest increase of 170 % was obtained in the present study. The fracture stress and strain at fracture shown in Figure 4.11b and 4.11c, respectively, have shown either increasing/ decreasing trend depending on the reinforcement type. However, the fracture stress and strain at fracture of the composites were observed to be increased by 93 and 70 %, respectively in the present study. The yield stress of composites, shown in Figure 4.11d, has exhibited an increasing trend with different fillers, and it is observed that the yield stress was increased by 44 % in the present study.

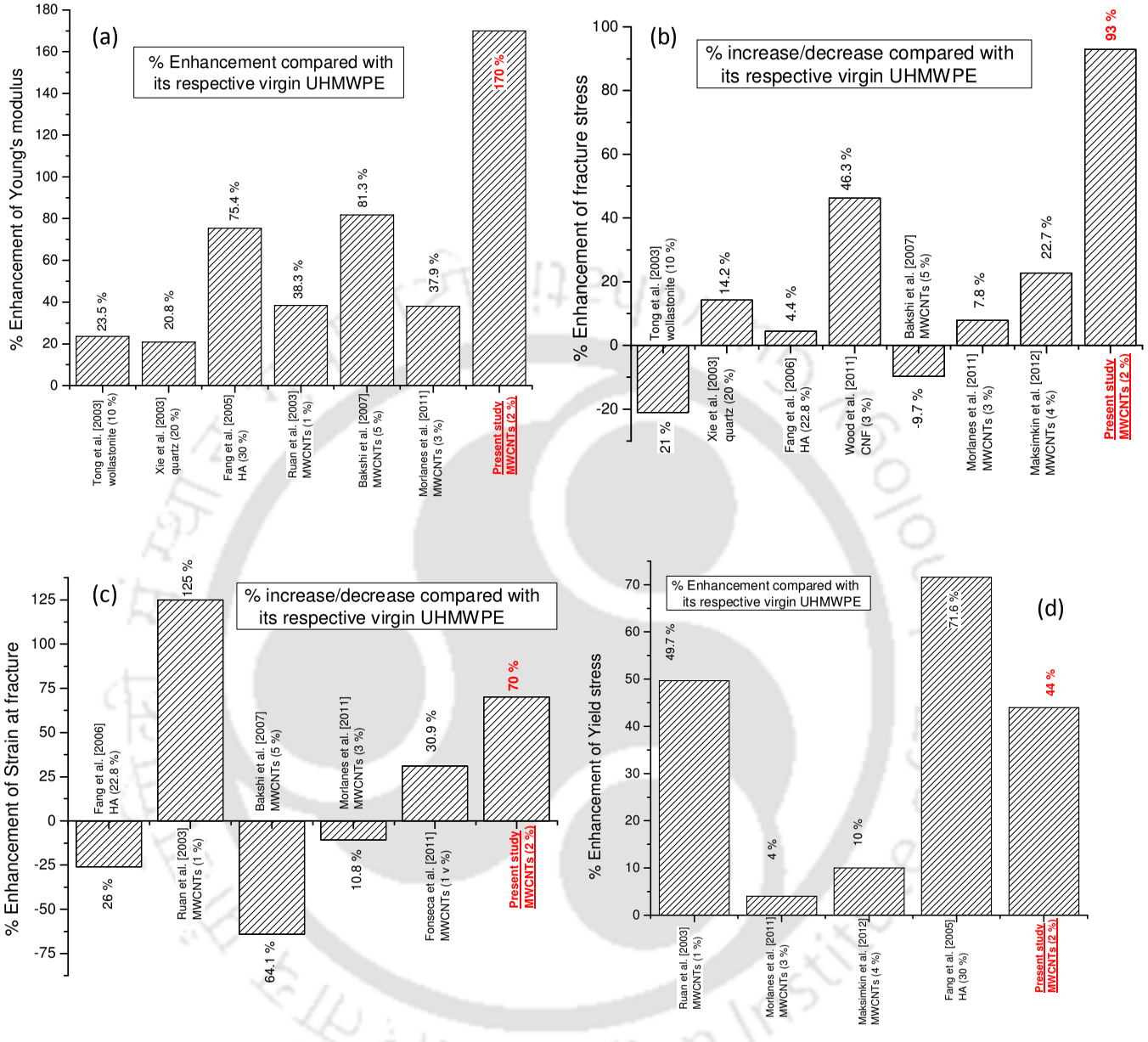

Figure 4.11. Comparison of the mechanical properties obtained from the present study with the published literature a) Young's modulus b) Fracture stress c) Strain at fracture d) Yield stress

4.1.2 Mechanical properties of unirradiated UHMWPE/α_T blends

Figure 4.12 shows the work to failure, strain at fracture, fracture stress and yield stress of UHMWPE/α_T blends. The work to failure of the blend was varied from 2928 mJ for α_T0.1 to 2993 mJ for α_T0.5 and the corresponding enhancement, 2 %, is well within the experimental deviation from that of virgin UHMWPE. Similarly, the strain at fracture was increased from 462 % for α_T0.1 to 473 % for α_T0.5, while the same for virgin UHMWPE was 470 %. The yield stress and fracture stress of UHMWPE/α_T blends were also found to be varied between 24 to 24.5 MPa and 30.4 to 31.3 MPa, respectively, when the α_T content was increased from 0.1 to 0.5 wt. %. In general, it is observed that the properties of unirradiated UHMWPE/α_T blends are not varied significantly compared to that of virgin UHMWPE irrespective of the concentration of α_T. It is due to the fact that α_T acted as an antioxidant and not as a reinforcement material. Moreover, the effects of oxidation during the processing of UHMWPE are negligible on the bulk properties hence the mechanical properties of UHMWPE are not influenced by the presence of α_T.

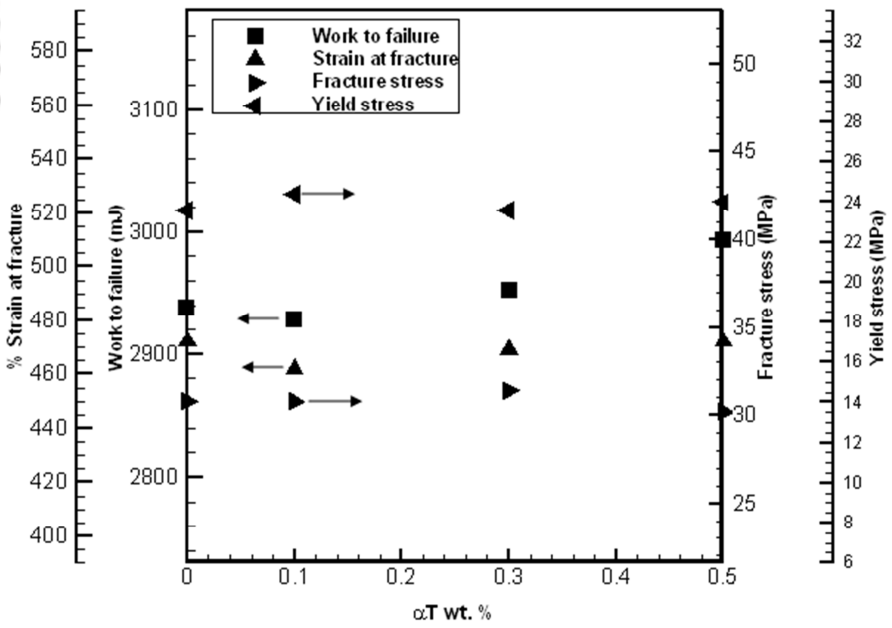

Figure 4.12. Mechanical properties of unirradiated UHMWPE/α_T blends

4.1.3 Summary of the mechanical properties of unirradiated UHMWPE/MWCNTs composites and UHMWPE/α_T blends

The mechanical properties of MWCNTs composites and α_T blends of different compositions were tested according to ASTM D1708 standard. The optimum concentration of MWCNTs reinforcement in UHMWPE was obtained at 2 wt. %, where the work to failure, strain at fracture, yield and fracture stress were increased by 176, 93, 70 and 44 %, respectively, compared to that of pure polymer. The reasons for the enhancement of mechanical properties upto an optimum concentration were attributed to high mechanical properties of MWCNTs, homogeneous dispersion of MWNCTs in UHMWPE, good interfacial stress transfer from polymer to reinforcement, and improved crystallinity. An increased viscosity and the substantial difference in thermal properties of MWCNTs and UHMWPE were found to be primary reasons for the reduction of mechanical properties beyond optimum concentration. These two parameters influenced the formation of microvoids with different dimension. The hardness, Young's modulus and the plasticity index of the composites, both ASP and SLR samples, have been assessed using the Nanoindenter, where a linear trend was observed against MWCNT concentration. The hardness of ASP samples was found to be higher than that of SLR samples. The hardness and Young's modulus of ASP samples were found to be increased by 75 % and 170 %, respectively, whereas the plasticity index was reduced by 17.3 % for 2 wt. % composite compared to pure polymer. The Young's modulus and plasticity index of SLR samples are similar to ASP samples. The mechanical properties of UHMWPE are not influenced by the presence of α_T.

4.2 Mechanical properties of irradiated UHMWPE/MWCNTs composites and UHMWPE/α_T blends

The mechanical properties of the composites irradiated at 25, 50, 75 and 100 kGy doses were studied to understand the role of MWCNTs to restrict the degradation of properties due to shelf ageing. The properties were assessed on a time scale of within 10 days, 60 and 120 days after irradiation. Although an optimum concentration of reinforcement was achieved at 2 wt. % of MWCNTs, other concentrations such as 0.5, 1.0 and 1.5 wt. % were also included in the study to observe the trend followed with increased concentration of MWCNTs. The mechanical properties of UHMWPE/α_T blends having different concentrations such as 0.1, 0.3, and 0.5 wt. % were also studied on the same time scale as that of composites in order to study the individual influence of them.

4.2.1 Mechanical properties of composites and α_T blends within 10 days after irradiation

4.2.1.1 Mechanical properties of composites

The load vs. displacement plots of composites at 25 and 100 kGy irradiation doses are shown in Figures 4.13a and 4.13b, respectively. The trend observed in Figure 4.13 against irradiation dose is similar to that of unirradiated samples shown in Figure 4.1a. The data for the mechanical properties of the test samples at different irradiation doses within 10 days after irradiation was obtained from the load vs. displacement plots and shown in Figures 4.14a – 4.14c. The work to failure of the test samples was evaluated by integrating the area under load vs. displacement plot upto their failure point. It is observed from Figure 4.14a that the work to failure of the polymer was linearly increased with concentration of MWCNTs and irradiation dose. It is noted that the work to failure of unirradiated pure polymer was 2938 mJ, which was

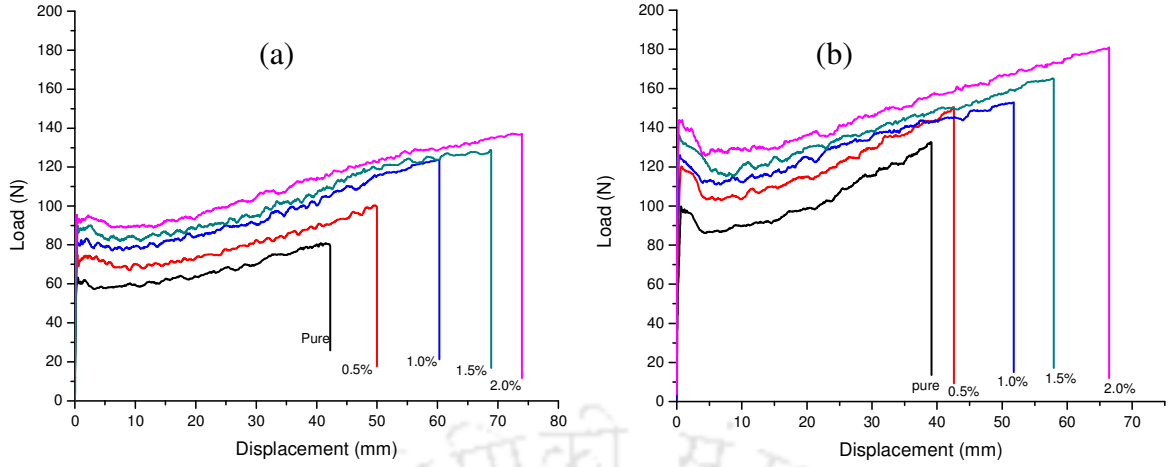

Figure 4.13. Load vs. displacement plots of composites at a) 25 kGy dose b) 100 kGy dose within 10 days of irradiation

increased to 3065, 3243, 3501 and 3979 mJ upon irradiation at 25, 50, 75 and 100 kGy doses, respectively and the corresponding enhancement was 4.3, 10.3, 19.1, and 35.4 %. The work to failure of GI100NC0.5, GI100NC1.0, GI100NC1.5, and GI100NC2.0 was also found to be enhanced by 28, 68, 107, and 149 %, respectively compared to that of GI100NC0.0 test sample. The enhancement of work to failure with irradiation dose is due to the crosslinks formed in the polymer chains using the free radicals formed from C-H cleavage, Kurtz [2009]. The higher irradiation doses usually lead to the generation of more number of free radicals, which take part in the crosslinking process leading to increased work to failure of polymer and composites.

The strain at fracture of composites is shown in Figure 4.14b. It is observed that strain at fracture of the UHMWPE was increased with MWCNTs concentration at any given irradiation dose. However, it was reduced with an increase of irradiation dose at a given MWCNTs concentration. The strain at fracture of pure polymer at 25 kGy irradiation dose was observed to be 440 %, which was reduced to 371 % upon 100 kGy irradiation. In case of GI25NC2.0, the strain at fracture was reduced from 763 to 659 %, when the irradiation dose was increased from

25 to 100 kGy. It is due to the fact that the crosslinking induced by the irradiation process resulted in long molecular chains with infinite mass restricting the mobility of polymer chains, which led to the reduction of fracture strain of the test materials, Premnath et al. [1999]. However, the results obtained by Morlanes et al. [2011] contradicted the above observation, where it was reported that the fracture strain of UHMWPE was reduced with an increase of MWCNTs concentration and irradiation dose. In our case, the strain at fracture of UHMWPE was increased with MWCNTs concentration but reduced with irradiation dose. The probable reason for the same may be due to the fact that MWCNTs were chemically treated, in our case, in order to ensure good interaction between the matrix and MWCNTs, which is very crucial in realizing the fullest potential of MWCNTs. However, no such modification of MWCNTs was reported by Morlanes et al. [2011], which led to the formation of clusters and thus reducing the fracture strain.

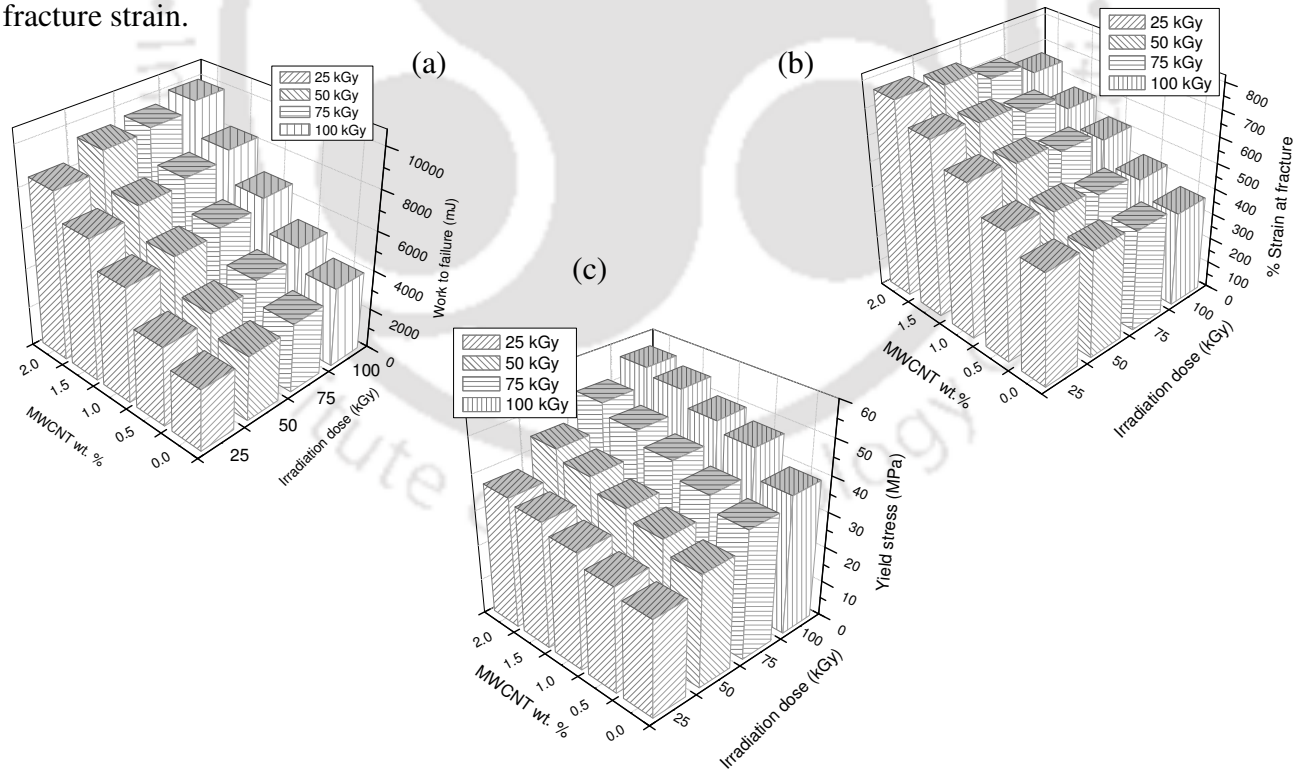

Figure 4.14. Mechanical properties of composites within 10 days after irradiation a) Work to failure b) Strain at fracture c) Yield stress

It is observed from Figure 4.14c that the yield stress of UHMWPE was increased with MWCNTs concentration and irradiation dose. The yield stress of GI25NC0.0 was increased from 27.2 to 37 MPa by adding of 2 wt. % MWCNTs corresponding to an enhancement of 39 %, which was further improved to 44 % at 100 kGy. In case of GI25NC2.0, the enhancement of yield stress was observed to be 48.4 % at 100 kGy dose.

The reasoning for the enhancement of work to failure and yield stress and the reduction of strain at fracture of composites with an increase of irradiation dose could be explained by the mechanism of crosslinking. The gamma radiation of polymer produces excited molecules, both positive and negative ions, which react to form second generation of active intermediates leading to the formation of free radicals, Premnath et al. [1999]. The primary radicals generated during the process of irradiation can occur either by C-C cleavage resulting the breakage of backbone of the polymer or due to C-H cleavage, Lewis [2001]. The C-C cleavage results in a phenomenon called chain scission, while the C-H cleavage leads to crosslinking. During the process of irradiation of polymer, both crosslinking and chain scission processes occur simultaneously. The chain scission process leads to the reduction of mechanical properties as it breaks the backbone of the polymer, while the crosslinking process increased the work to failure and yield stress of the polymer. Higher irradiation dose leads to the generation of more number of free radicals, which take part in the crosslinking process. As the number of crosslinks is increased with irradiation dose, the polymer becomes stiffer and it demands higher loads to deform elastically leading to increased yield stress of the test material. It also causes the reduction of strain at fracture of the composites.

4.2.1.2 Mechanical properties of α_T blends

The load vs. displacement plots of α_T blend samples at 25 and 100 kGy dosage are shown in Figures 4.15a and 4.15b, respectively, where it is observed that the properties are varied with an increase of α_T concentration, unlike in case of the unirradiated condition. The mechanical properties of α_T blends were evaluated from the load vs. displacement plots and are shown in Figure 4.16a – 4.16c. Figure 4.16a shows the work to failure of α_T blends, which was increased with irradiation dose but decreased with raise in α_T concentration. The work to failure of GI25α_T0.1, GI25α_T0.3 and GI25α_T0.5 was observed to be 3005, 2922, and 2841 mJ, respectively corresponding to the reduction of 2, 2.3, and 7.3 % compared to that of 25 kGy irradiated pure polymer. In case of 100 kGy irradiated sample, the respective reduction was observed to be 15, 22.3 and 24 % in comparison with pure polymer. A similar observation was also reported by Oral et al. [2005], where the work to failure of irradiated α_T blended UHMWPE was found to be less than that of irradiated virgin UHMWPE. It is also noted that the work to failure of UHMWPE/α_T blends, irrespective of α_T concentration, at 25, 50 and 75 kGy irradiation doses was found to be varied within experimental deviation compared to that of unirradiated virgin UHMWPE. However, the work to failure of α_T0.1, α_T0.3 and α_T0.5 test samples at 100 kGy dose was found to have an enhancement of 14.9, 5.2 and 2.7 %, respectively compared to that of unirradiated virgin UHMWPE. The reason for the enhancement of work to failure of the UHMWPE/α_T blends with irradiation dose is attributed to be the same as that of composites, as discussed earlier. However, there was no significant influence of 25, 50 and 75 kGy irradiation doses on the work to failure of α_T blend compared to that of 100 kGy dose. It is due to the fact that most of the free radicals generated at low irradiation dose reacted with α_T, thus it left with only fewer radicals available for crosslinking. The situation becomes severe with an increase of

α_T content, consequently the enhancement of work to failure was not observed at higher concentration of α_T in UHMWPE. Figure 4.16b shows the strain at fracture of blend test samples

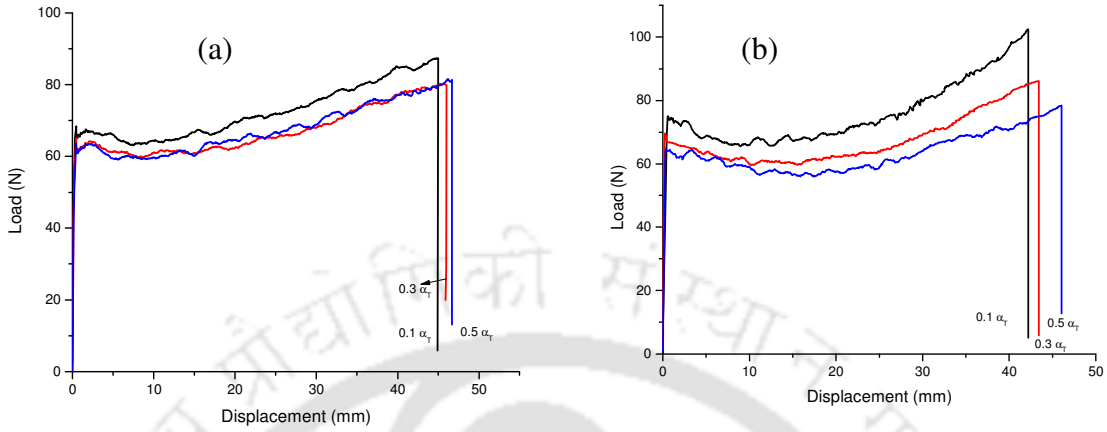

Figure 4.15. Load vs. displacement plots of α_T blends at a) 25 kGy dose b) 100 kGy dose within 10 days of irradiation

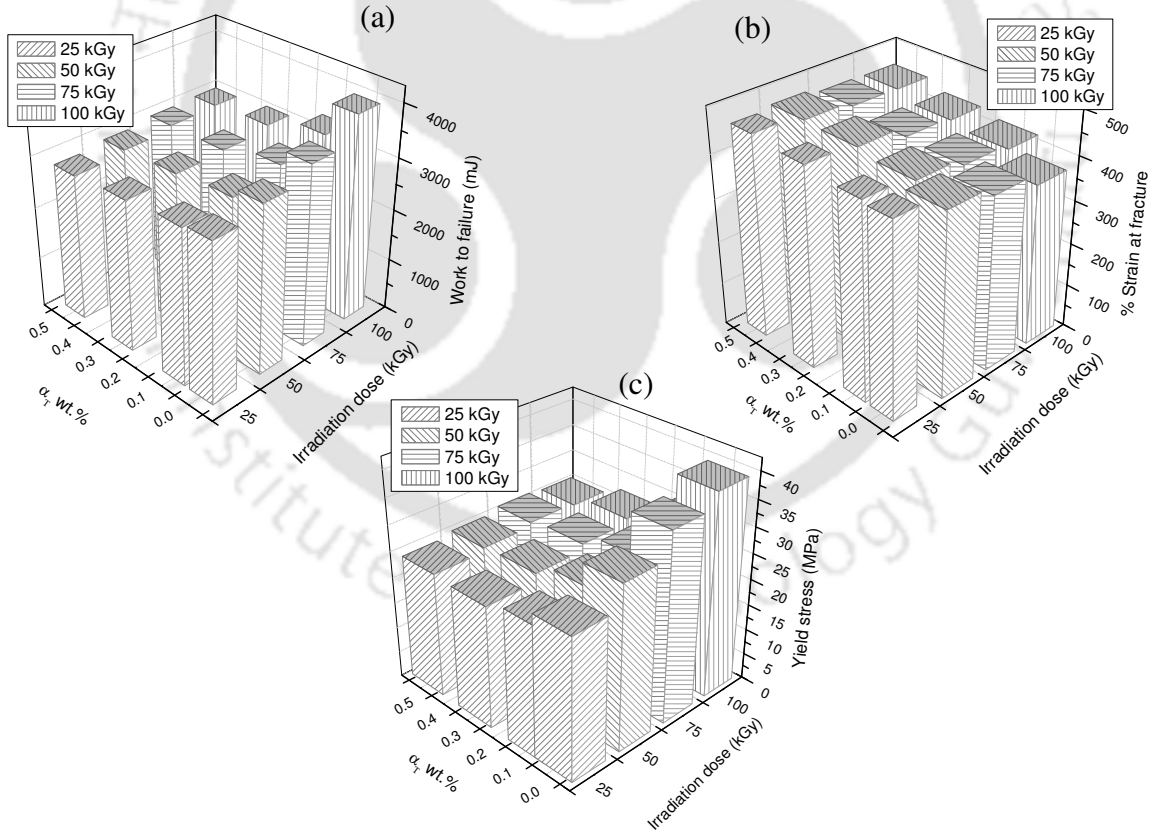

Figure 4.16. Mechanical properties of α_T blends within 10 days after irradiation a) Work to failure b) Strain at fracture c) Yield stress

In general, it is observed that the strain at fracture of α_T blended samples was reduced with an increase of irradiation dose but it was increased with α_T content in UHMWPE. It is observed that the fracture strain of GI25α_T0.1 was found to be 447 %, which was reduced to 420 % upon irradiation at 100 kGy dose corresponding to the reduction of 6 %. In case of GI25α_T0.5, the strain at fracture was observed to be the same as that of unirradiated virgin polymer, i.e. 466 %. However, it was reduced by 3.5 % upon 100 kGy irradiation. An increase of strain at fracture with α_T content is due to the fact that α_T content in UHMWPE restricted the CLD during irradiation. The presence of α_T in UHMWPE is not interfered with the length and mass of the molecular chains, and it led to improved chain mobility of the polymer, Lerf et al. [2010]. However, the elongation of the test material was restricted with an increase of irradiation dose due to increased CLD.

Figure 4.16c shows the yield stress of the α_T blend samples. It is observed that the yield stress was increased with irradiation dose but decreased with raise in α_T concentration. The yield stress of GI25α_T0.1 was observed to be 25 MPa, which was increased to 31.2 MPa at 100 kGy dose corresponding to 23.8 % enhancement. However, the yield stress of GI100α_T0.5 was observed to be 25.6 MPa, which is about 10 % less than that of the same sample irradiated at 25 kGy. It is due to the fact that α_T reacted with primary free radicals formed in the UHMWPE chains during the irradiation process, thereby decreasing the amount of free radicals available for the formation of crosslinks, Oral et al. [2008]. When the α_T concentration was increased from 0.1 to 0.5 wt. %, it left with fewer primary free radicals available for crosslinking leading to the reduction of overall crosslinking of UHMWPE. However, when the irradiation dose of the test sample was increased at a given α_T concentration, the number of free radicals available in the

polymer is increased and helped to form crosslinks leading to increased yield stress of the test sample.

4.2.2 Mechanical properties of composites and α_T blends after 60 days of irradiation

4.2.2.1 Mechanical properties of composites

The load vs. displacement plots of composites at 25 and 100 kGy doses are shown in Figures 4.17a and 4.17b, respectively. It is observed that the trend followed by the composites was similar to that of results observed within 10 days after irradiation shown in Figure 4.13. The mechanical properties of composites after 60 days of irradiation at different doses were obtained from the load vs. displacement plots and are shown in Figures 4.18a - 4.18c. It is observed from Figure 4.18a that the work to failure of the test sample was reduced with an increase of irradiation dose but it was increased with MWCNTs concentration. The work to failure of GI25NC0.0 was 2056 mJ, which was reduced to 1595 mJ at GI100 corresponding to the reduction of 22.4 %, whereas the reduction was found to be only 17 % for NC2.0 sample when the irradiation dose was increased

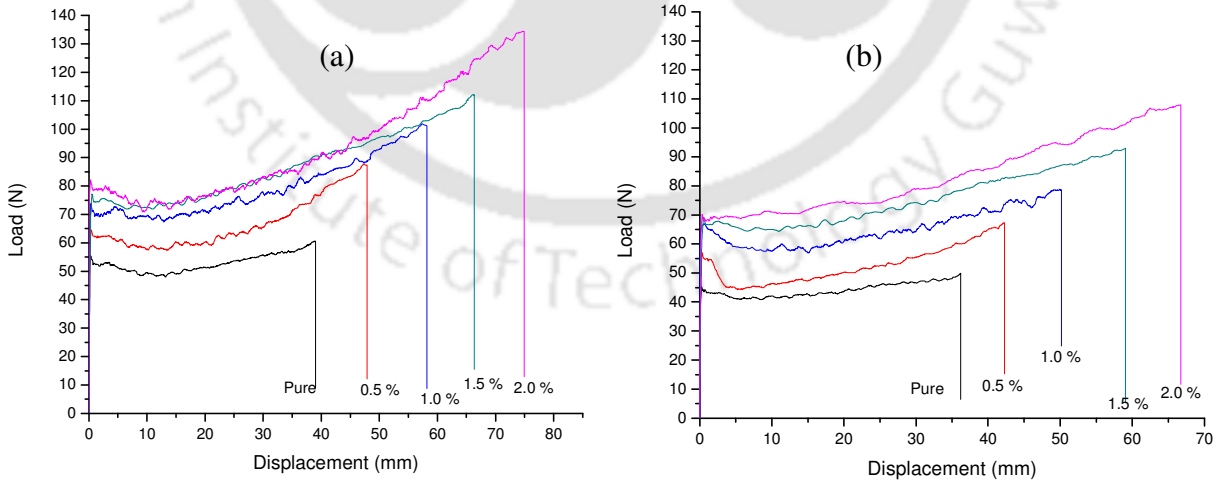

Figure 4.17. Load vs. displacement plots of composites at a) 25 kGy dose b) 100 kGy dose after 60 days of irradiation

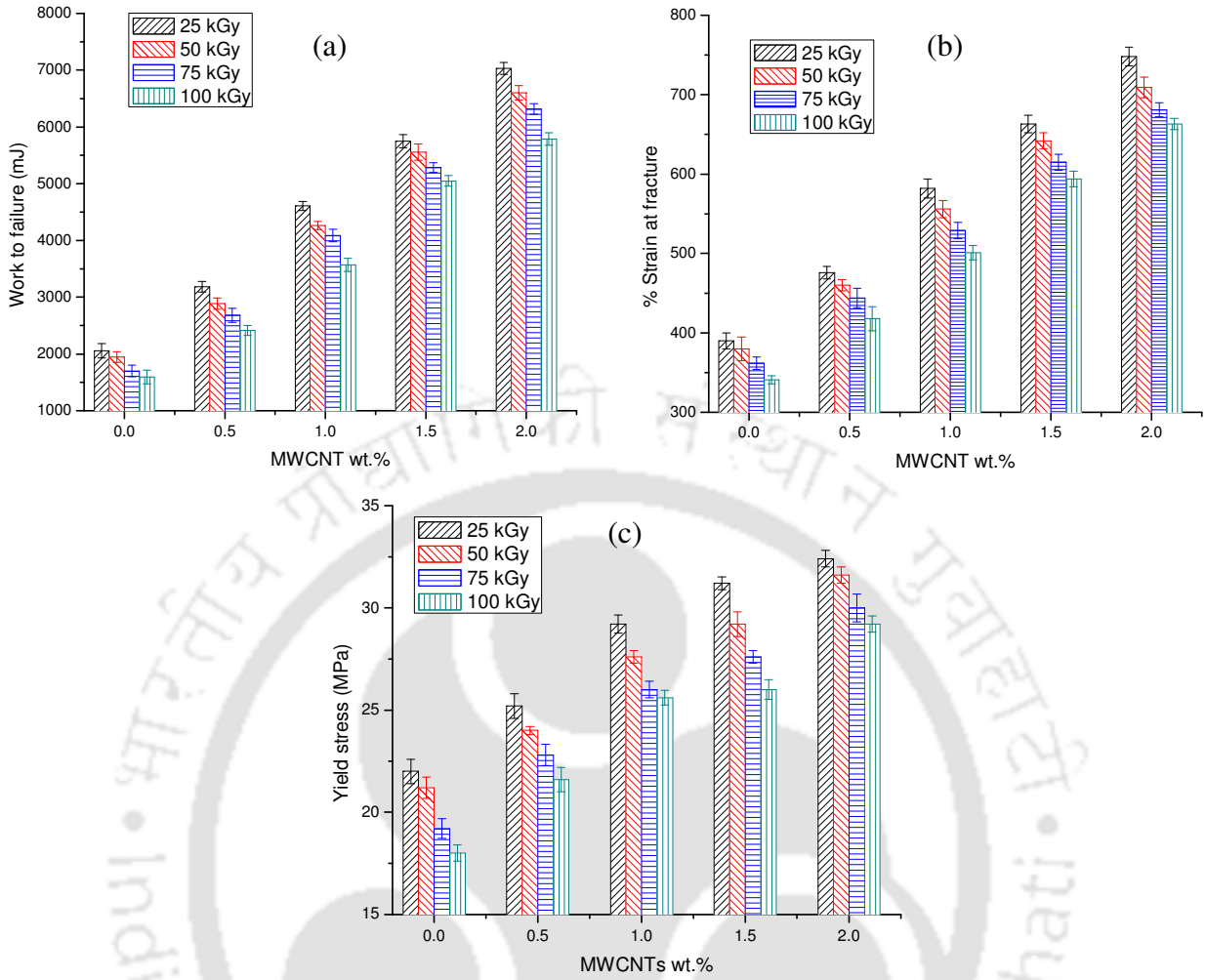

Figure 4.18. Mechanical properties of composites after 60 days of irradiation a) Work to failure b) Strain at fracture c) Yield stress

from 25 to 100 kGy. It is also observed that when the concentration of MWCNTs was increased from 0 to 2 wt. % at 100 kGy irradiation dose, the work to failure of polymer was increased from 1595 to 5789 mJ corresponding to an enhancement of 263 %, whereas the enhancement was found to be 240 % at 25 kGy irradiation dose. The general trend of strain at fracture after 60 days of irradiation remained the same as that of the results obtained within 10 days after irradiation, i.e., it was increased with MWCNTs concentration but reduced with an increase of irradiation dose. It is observed from Figure 4.18b that the strain at fracture of GI25NC0.0 was increased

from 390 to 748 %, when the MWCNTs concentration was increased to 2 wt. % corresponding to an enhancement of 92 %. Similarly, the strain at fracture of NC0.0 and NC2.0 at 100 kGy was found to be 341 and 663 %, respectively and the enhancement was found to be 94 %. However, the strain at fracture was reduced with an increase of irradiation dose at a given concentration of MWCNTs. The strain at fracture of GI25NC2.0 was found to be 748 %, which was reduced by 11.4 % at 100 kGy dose.

The yield stress of composites tested after 60 days of irradiation is shown in Figure 4.18c, where it is observed that it was increased with MWCNTs concentration but reduced with an increase of irradiation dose. The yield stress of pure polymer was reduced from 22 to 18 MPa corresponding to 18 % reduction, when the irradiation dose was increased from 25 to 100 kGy. In case of NC2.0 test sample, the reduction was limited to 10 % for the same condition. When the concentration of MWCNTs in UHMWPE was increased from 0 to 2.0 wt. %, the yield stress at 25 kGy was increased from 22 to 32.4 MPa corresponding to 47 % enhancement. For the same condition, the yield stress was increased by 62 % at 100 kGy irradiation dose.

4.2.2.2 Mechanical properties of α_T blends

The load vs. displacement plots of α_T blends at 25 kGy and 100 kGy irradiation dose are shown in Figures 4.19a and 4.19b, respectively, where the trend was similar to that of results observed within 10 days after irradiation but with reduced magnitude. The mechanical properties, which are derived from the load vs. displacement plots, are shown in Figures 4.20a-4.20c. Figure 4.20a shows that the work to failure of α_T blends was reduced with an increase of irradiation dose at a given concentration of α_T but it was increased with α_T concentration at any given irradiation dose. The work to failure of α_T0.1 was reduced by 17 % upon increasing the irradiation dose from 25 to 100 kGy and it was increased by 15 % at 100kGy for α_T0.5

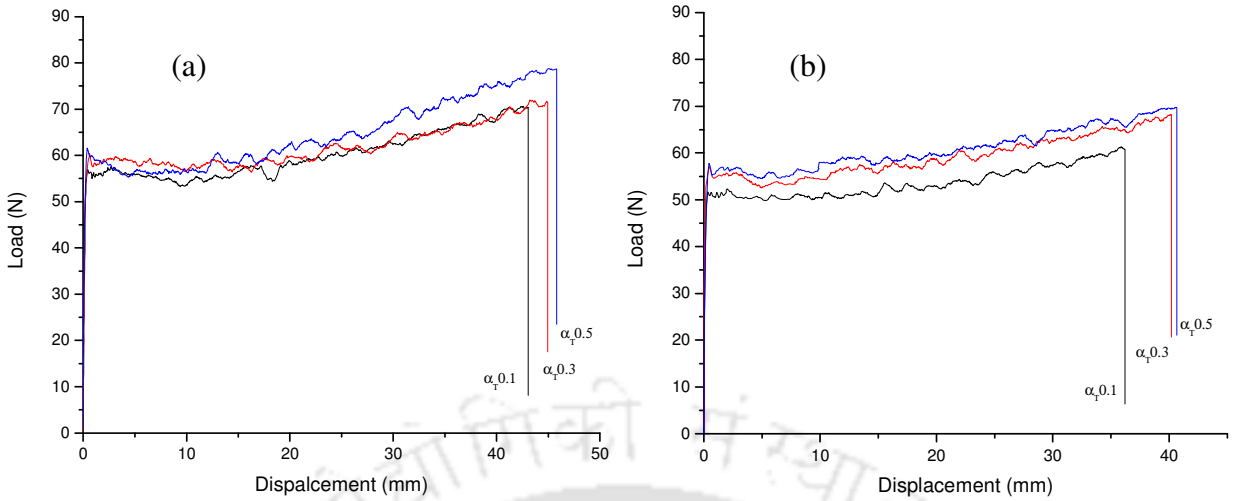

Figure 4.19. Load vs. displacement plots of α_T blends at a) 25 kGy dose b) 100 kGy dose after 60 days of irradiation

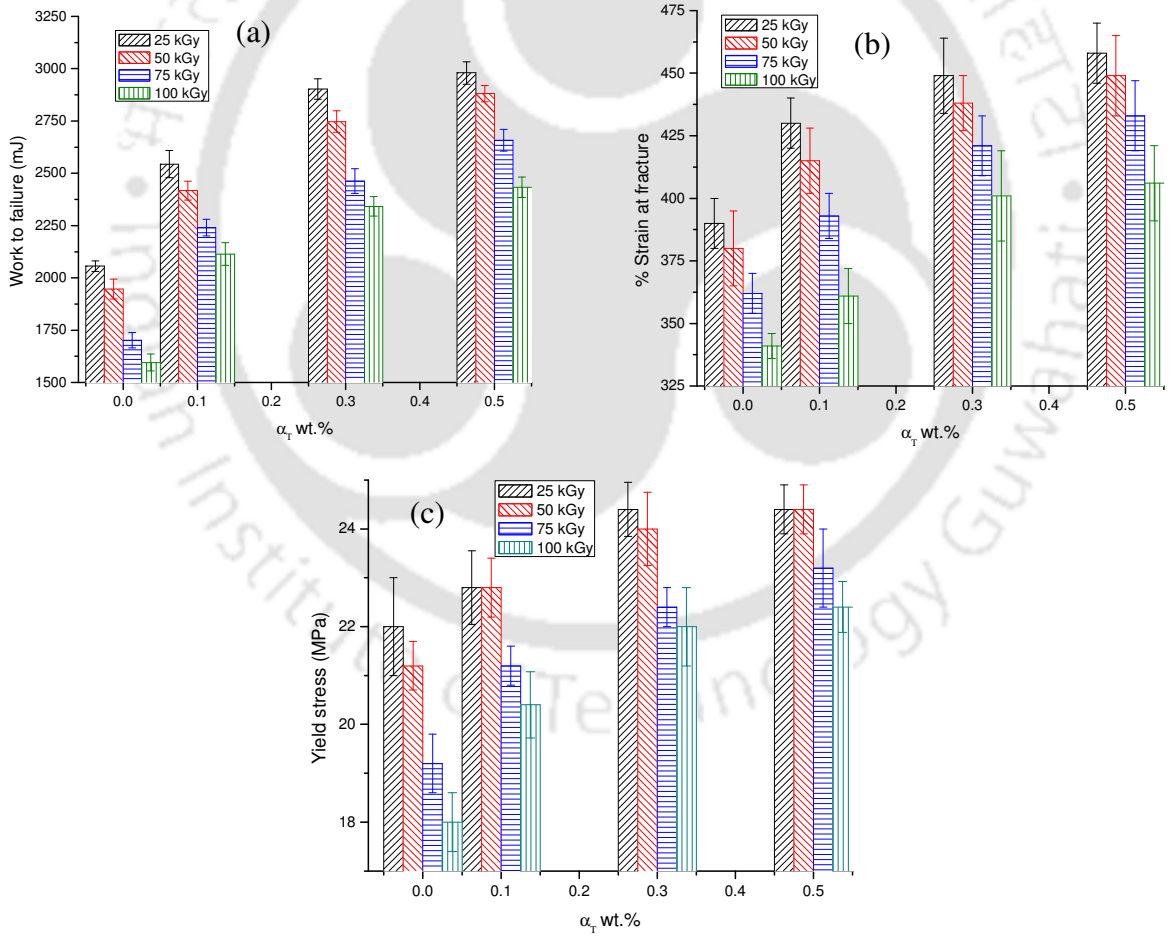

Figure 4.20. Mechanical properties of α_T blends after 60 days of irradiation a) Work to failure b) Strain at fracture c) Yield stress

It is observed from Figure 4.20b that the strain at fracture of α_T blends was reduced with an increase of irradiation dose but it was increased with α_T concentration. The strain at fracture at 100 kGy dose was increased from 361 to 406 %, when the α_T concentration was increased from 0.1 to 0.5 wt. % corresponding to an enhancement of 12.5 %. Similarly, when the irradiation dose was increased from 25 to 100 kGy, the strain at fracture of α_T0.1 and α_T0.5 sample was reduced by 16 and 11 %, respectively.

Figure 4.20c shows the yield stress of α_T blends, which was reduced with an increase of irradiation dose but slightly increased with α_T concentration. The yield stress of GI25α_T0.1 was reduced from 22.8 to 20.5 MPa, i.e. ~10 %, when the irradiation dose was increased to 100 kGy. At 100 kGy dose, the yield stress of 0.1, 0.3 and 0.5 wt. % α_T in UHMWPE was found to be 20.4, 22 and 22.4 MPa, respectively and the respective enhancement was found to be 10, 3.5 and 1.7 % in comparison with 100 kGy irradiated pure polymer. It is noted that the influence of irradiation dose was found to be negligible at 0.3 and 0.5 wt. % of α_T in UHMWPE.

4.2.3 Mechanical properties of composites and α_T blends after 120 days of irradiation

4.2.3.1 Mechanical properties of composites

The load vs. displacement plots of composites at 25 and 100 kGy doses are shown in Figure 4.21a and 4.21b, respectively, where a similar trend as that of 60 days after irradiation was observed. The mechanical properties of composites after 120 days of irradiation are shown in Figures 4.22a-4.22c. It is observed from Figure 4.22a that the work to failure of UHMWPE was increased with MWCNTs concentration but it was reduced with an increase of irradiation dose. The work to failure of GI25NC0.0 sample was reduced by 53 % when the irradiation dose was increased to 100 kGy, whereas the corresponding reduction was limited to only 24 % in case of GI25NC2.0 sample.

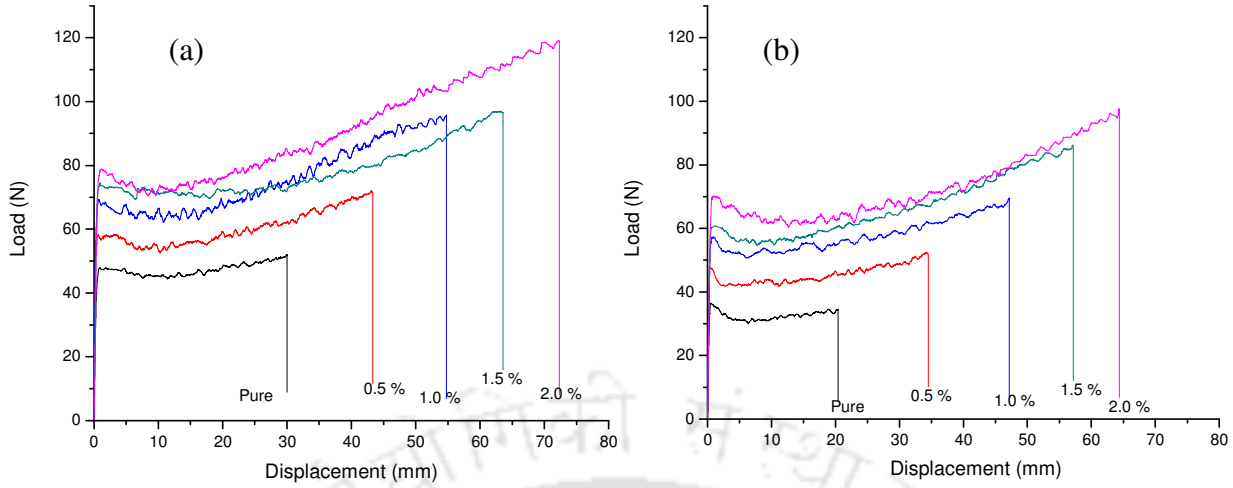

Figure 4.21. Load vs. displacement plots of composites at a) 25 kGy dose b) 100 kGy dose after 120 days of irradiation

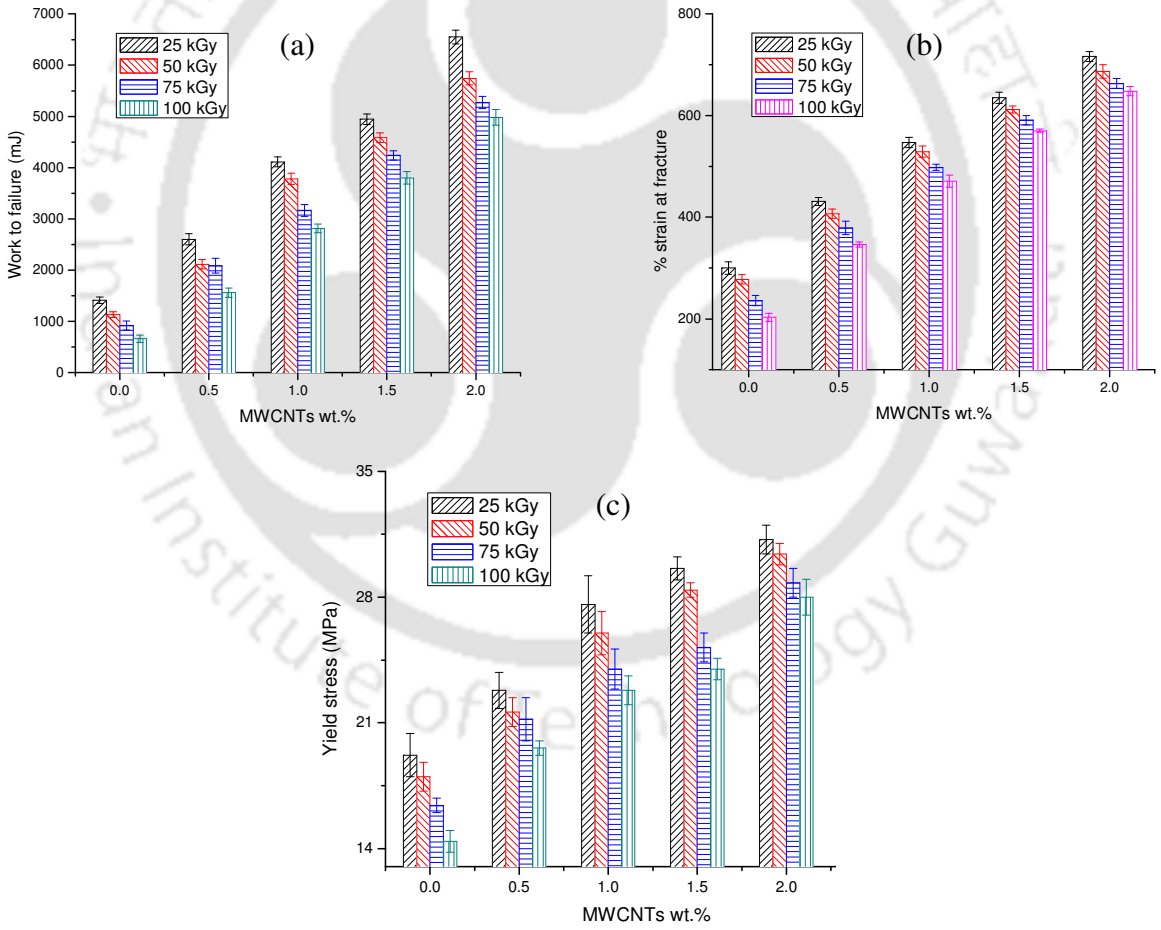

Figure 4.22. Mechanical properties of composites after 120 days of irradiation a) Work to failure b) Strain at fracture c) Yield stress

Figure 4.22b shows the strain at fracture, which was decreased with an increase of irradiation dose but increased with MWCNTs concentration. It is observed that the pure UHMWPE has become less ductile after 120 days of irradiation due to its severe degradation. The GI25NC0.0 sample has shown the strain at fracture of 300 % against 203 % for GI100NC0.0 sample corresponding to the reduction of 32 %, whereas GI100NC2.0 has shown the reduction of only 9.5 % compared to GI25NC2.0 test sample.

The trend observed for the yield stress of composites was found to be the same as that of strain at fracture, and the results are shown in Figure 4.22c. The yield stress of GI25NC0.0 test sample was found to be 19.2 MPa, which was increased by 62.5 % for the GI25NC2.0 sample, in case of GI100NC0.0 sample, the corresponding enhancement was 94.4 %. It is noted that the yield stress of pure UHMWPE was reduced by 25 %, when the irradiation dose was increased from 25 to 100 kGy. In case of NC2.0 sample, the reduction was observed to be only 10.2 % for the same dosage enhancement. A significant observation is that the reduction of work to failure, strain at fracture and yield stress was significantly less for irradiated composites compared to that of irradiated virgin UHMWPE due to ageing.

4.2.3.2 Mechanical properties of α_T blends

The load vs. displacement plots and mechanical properties of α_T blends after 120 days of irradiation are shown in Figure 4.23, where the trend observed was similar to that of results obtained after 60 days of irradiation. Figure 4.24a shows the work to failure of α_T blends. It is observed that the trend observed for the work to failure with irradiation dose and α_T concentration is similar to that of the results obtained after 60 days of irradiation. The work to failure of GI25α_T0.1 was found to be 2311 mJ, which was reduced by 23 % at 100 kGy dose. When the concentration of α_T was increased from 0.1 to 0.5 wt. % at 100 kGy dose, the

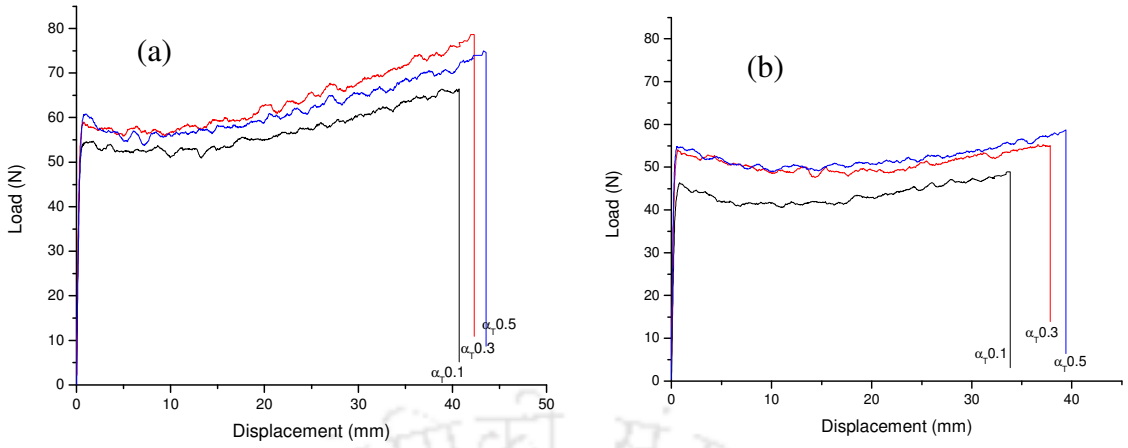

Figure 4.23. Load vs. displacement plots of α_T blends at a) 25 kGy dose b) 100 kGy dose after 120 days of irradiation

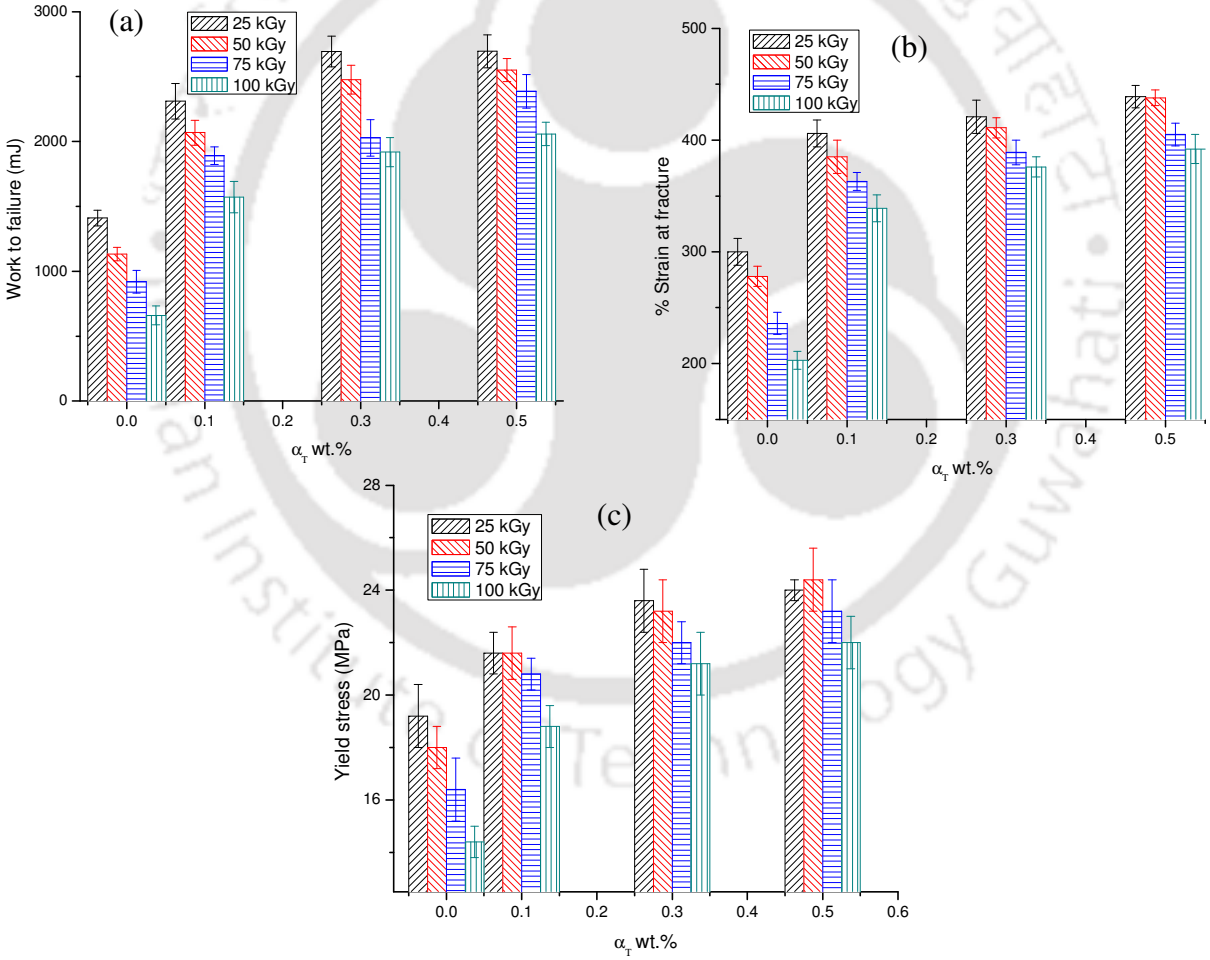

Figure 4.24. Mechanical properties of α_T blends after 120 days of irradiation a) Work to failure b) Strain at fracture c) Yield stress

work to failure was increased by 16 %. It is to be noted that the work to failure of α_T blends was significantly higher than that of virgin UHMWPE at same irradiation dose. The work to failure of GI100α_T0.1 was found to be 168 % more than that of 100 kGy irradiated virgin UHMWPE. It confirms that the presence of α_T has limited the loss of work to failure of irradiated UHMWPE.

Figure 4.24b shows the strain at fracture of α_T blends, where it is observed that it was increased with α_T concentration but decreased with irradiation dose. At 100 kGy irradiation dose the strain at fracture of α_T0.1blend was 67 % higher compared to that of pure UHMWPE. it is noted that the trend followed by strain at fracture after 60 days of irradiation is similar to that observed within 10 days. Figure 4.24c shows the yield stress of α_T blends. The yield stress of α_T0.1 at 100 kGy was found to be 45 % higher than that of virgin UHMWPE at same irradiation condition. In general, it can be inferred that the trend followed by all the mechanical properties of the composites and blends after 60 and 120 days of irradiation was found to be identical.

4.2.4 Comparison of the mechanical properties of composites and α_T blends on a time scale

Figure 4.24a shows the influence of ageing on the work to failure of composites on a time scale at 100 kGy irradiation dose. The work to failure of the sample at unirradiated condition is also given for the comparison purpose. It is observed from Figure 4.25a that the work to failure of all the composites was increased significantly within 10 days after irradiation compared to their respective unirradiated test sample. However, it was found to be decreased after 60 and 120 days of irradiation. The work to failure of unirradiated UHMWPE was found to be 2938 mJ, which was increased by 35 % within 10 days after irradiation and then later it was reduced by 45 and 77.5 % after 60 and 120 days of irradiation, respectively. Similarly, the work to failure of unirradiated 2 wt. % composite was increased from 8111 to 9936 mJ within 10 days after

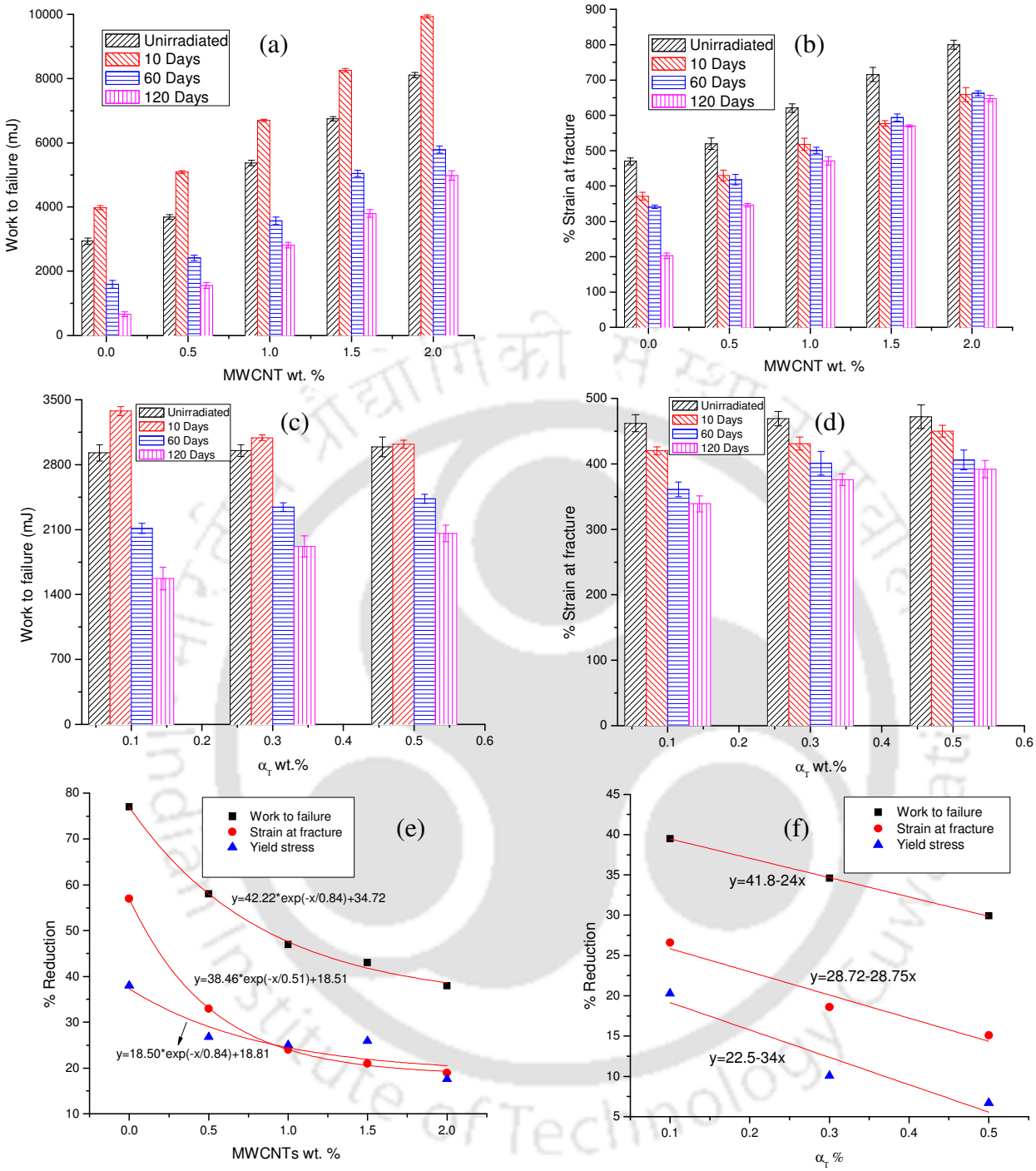

Figure 4.25. Comparison of the properties at 100 kGy irradiation dose on a time scale a) Work to failure of composites b) Strain at fracture of composites c) Work to failure of α_T blends d) Strain at fracture α_T blends e) Percentage reduction of the mechanical properties of composites after 120 days of irradiation f) Percentage reduction of the mechanical properties of α_T blends after 120 days of irradiation

irradiation corresponding to 22.5 % enhancement. However, the same was reduced by 28 and 38 % after 60 and 120 days of irradiation, respectively.

The reason for the enhancement of work to failure immediately after the irradiation process and the reduction thereafter is explained as follows. The irradiation leads to crosslinking of the polymer and composites. As discussed earlier, the crosslinks act as stiffeners between two individual polymer chains and thus it demands higher loads to deform and consequently the material becomes tougher. Moreover, the free radicals that are formed in the amorphous region of the polymer during the irradiation process have higher mobility and hence they recombine to form new crosslinks in the amorphous region leading to increased crystallinity of the polymer, Premnath et al. [1999]. As the mechanical properties of the polymer depend on its crystallinity, Perepechko [1981], it leads to the enhancement of the work to failure immediately after irradiation. However, the radicals generated in the crystalline phase of the polymer lacked sufficient mobility and thus they were trapped in the polymer. The trapped radicals slowly diffused into the amorphous region leading to oxidation of the polymer, Lewis [2001]. The free radicals in the polymer reacted with diffused atmospheric Oxygen forming peroxides, which increased the severity of oxidation. It led to the formation of new radicals that continued the chain scission process resulting to degradation of material properties and the formation of various oxidation products. Thus, the work to failure of the test material was decreased after 60 and 120 days of irradiation. It is observed from Figure 4.25b that the strain at fracture of UHMWPE has shown a decreasing trend with ageing upto 1 wt. % of MWCNTs, but thereafter no significant influence of ageing was observed. It is due to the fact that the polymer reduced its mobility immediately after irradiation due to infinitely long molecular chains and large molecular mass. In addition to that the irradiated polymer is easily prone to oxidation due to the

reaction of free radicals formed during the irradiation process with atmospheric Oxygen and thus the ability of elongation of test sample was reduced after 60 and 120 days of irradiation. In case of composites, such a trend was not observed beyond 1 wt. % of MWNCTs. Because of the radical scavenging ability of MWCNTs, which will be discussed later, the degradation of the composites is restricted and it leads to the preservation of their ductility.

Figure 4.25c shows the comparison of the work to failure of α_T blends. The work to failure of α_T0.1 sample was found to be increased by 15 % within 10 days after irradiation. However, it is decreased with ageing. It is also noted that the enhancement of work to failure of irradiated pure polymer was increased by 36 %, whereas it was restricted to 15 % by the addition of 0.1 wt. % α_T. It is due to the fact that the presence of α_T restricted the crosslinking of UHMWPE and thus the work to failure of the polymer was not found to be increased significantly after irradiation. However, the crosslinking effect in α_T blends is relatively higher at 0.1 wt. %. Though the presence of α_T in UHMWPE delayed the oxidation process but it is not completely eliminated, and hence the work to failure was reduced significantly after 60 and 120 days of irradiation irrespective of α_T concentration. It is also observed that the work to failure of irradiated α_T0.3 and α_T0.5 test sample was decreased continuously with ageing. Figure 4.25d shows the strain at fracture of the α_T blend samples. It is observed that the strain at fracture of the test sample was reduced with ageing irrespective of the presence of α_T but it was slightly increased with α_T concentration. The discussion regarding the reduction of work to failure against Figure 4.25c is applicable for the above observation in connection with reduction of strain at fracture with ageing.

The degradation of mechanical properties of irradiated polymer is an inevitable event due to the reaction of free radicals. However, it is observed from Figure 4.25e that the percentage of

reduction of properties of composites was exponentially reduced with an increase of MWCNTs concentration in UHMWPE. The work to failure, strain at fracture and yield stress of GI100NC0.0 and GI100NC2.0 were reduced by 77, 57 and 38 %, and 38, 19 and 17.5 %, respectively after 120 days of irradiation in comparison with their respective unirradiated test sample. The reason for the reduction of properties degradation of the polymer is due to the presence of MWCNTs. The interaction of MWCNTs with gamma irradiation produces defects on their surfaces, Krasheninnikov et al. [2004]. Along with simple defects, more complex defects like pentagon, Stone Wales defects can also be formed. According to Zeynalov et al. [2008], the surface induced defects on MWCNTs exhibited high electron affinities, and hence they act as radical traps. Thus, it reduces the amount of free radicals in the polymer and the oxidation associated with it. It was also reported by Galano [2010] that the antioxidant activity of MWCNTs was increased and the scavenging processes were occurred faster through the functionalized side walls. In the present study, the MWCNTs used for the preparation of composites were functionalized and thus it is expected to reduce the number of free radicals. In addition to that the irradiation induced defects on MWCNTs could result in pinning of them to the polymer substrates through the formation of chemical bonds between them, Krasheninnikov et al. [2002, 2004], and thus it is expected to compensate the loss of mechanical properties at higher irradiation doses. It is observed that the loss of mechanical properties of pure UHMWPE was severe after 120 days of irradiation, but the presence of MWCNTs has significantly counteracted the degradation and the maximum reduction of degradation was observed at 2 wt. % composite. According to Sreekanth et al. [2012], a strong network of MWCNTs and polyethylene was formed due to the reaction between the radicals and MWCNTs in order to improve the properties of the composites.

Figure 4.25f shows the reduction of mechanical properties of α_T blends and it is observed that the degradation of properties of the UHMWPE/α_T blends was reduced linearly with an increase of α_T content in UHMWPE. The work to failure, strain at fracture and yield stress of GI100α_T0.1 were reduced by 39.5, 26.6 and 20.3 %, respectively after 120 days of irradiation, whereas the reduction of same properties of GI100α_T0.5 was limited to 30, 15 and 6.7 %, for the same ageing period in comparison with their respective unirradiated test sample. It is due to the fact that α_T is a conventional antioxidant material used to prevent the oxidation of polymer and it reacts with free radicals formed during the irradiation process, which was also confirmed by Kurtz [2009]. The reduction of degradation of the mechanical properties of GI100NC2.0 and GI100α_T0.1 after 120 days of irradiation was compared, which are shown in Figure 4.25e and Figure 4.25f, respectively. It is clearly observed that the antioxidant activity exhibited by 2 wt. % MWCNTs in UHMWPE is similar to that of 0.1 wt % α_T in UHMWPE. However, the equivalence between them is a mere indication of their similarity, because the antioxidant activity of MWCNTs depends on several parameters such as synthesis route, associated defects due to irradiation, geometrical parameters and the type of functionalization of MWCNTs, Galano [2010].

4.2.5 Summary of the mechanical properties of irradiated UHMWPE/MWCNTs composites and UHMWPE/α_T blends

The composites and α_T blends were subjected to gamma irradiation at different irradiation doses and the mechanical properties of the test specimens were assessed at different time intervals such as within 10 days, 60 and 120 days after irradiation. It was observed that the properties, except strain at fracture, of all the test samples were increased immediately after irradiation, but reduced after 60 and 120 days of irradiation process. However, the strain at

fracture of the sample was reduced with ageing. It was also observed that the deterioration of properties after irradiation process was reduced with an increase of MWCNTs and α_T concentration. The reduction of work to failure, strain at fracture and yield stress of 100 kGy irradiated UHMWPE after 120 days irradiation was reduced exponentially with an increase of MWCNTs concentration, whereas a linear reduction trend was observed in case of α_T blends. The restriction of property degradation by the 2 wt. % MWCNTs in UHMWPE was found to be similar to that of 0.1 wt. % α_T in UHMWPE. It is well understood that the presence of MWCNTs could restrict the degradation of the mechanical properties of irradiated UHMWPE.

4.3 Studies on network parameters and radical scavenging capability of composites and α_T blends

Based on the above results, it was inferred that the defects formed on the surface of MWCNTs during the irradiation process bond with most of the free radicals present in the polymer. In order to confirm the same and understand the synergic effect of MWCNTs reinforcement/α_T blend and gamma irradiation in reducing the degradation of mechanical properties of UHMWPE, a systematic study was proposed to (i) identify the defects on MWCNTs, (ii) study crosslink density and (iii) quantify the relative radical concentration of composites and α_T blends.

4.3.1 Studies on irradiation induced defects on the surface of MWCNTs

In order to understand the influence of irradiation on the structure of MWCNTs at different doses, different analytical techniques were used. The FTIR spectra of MWCNTs after gamma

irradiation at different doses such as 25, 50, 75 and 100 kGy are shown in Figure 4.26. It is observed that the position of all the prominent peaks remains unchanged even after irradiation

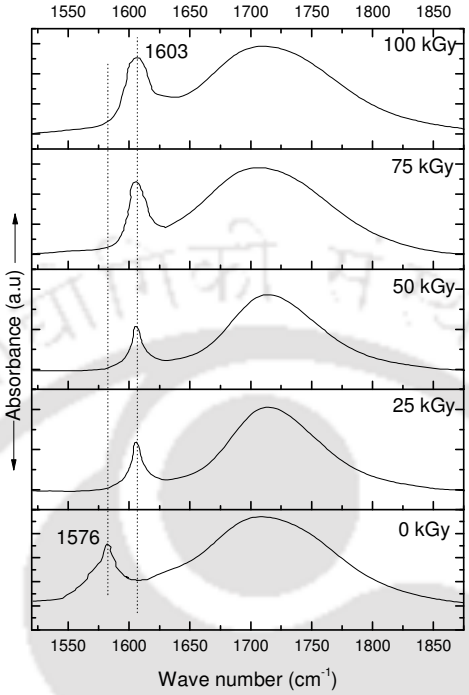

Figure 4.26. FTIR spectra of gamma irradiated MWCNTs at different doses

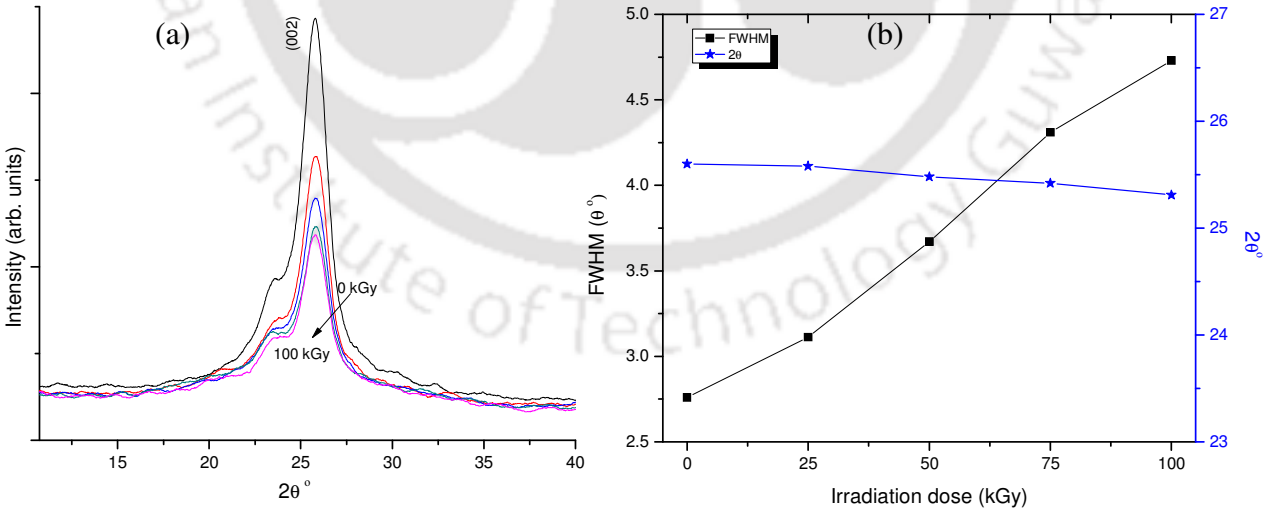

Figure 4.27. (a) X-Ray Diffractogram and (b) FWHM and peak position of MWCNTs at different irradiation doses

except for the peak corresponding to C=C. It is appeared at 1576 cm^{-1} for an unirradiated sample, and shifted to 1603 cm^{-1} upon irradiation, which is represented by a dotted line in Figure 4.26. The shift in peak may suggest a change in the structure of MWCNTs, Zhang et al. [2003], which may have resulted due to the impingement of high energy γ photons on the MWCNTs surface during the irradiation process. Such change leads to the generation of defects on MWCNTs. The formation of defects on MWCNTs during irradiation was confirmed by quantitatively and qualitatively using XRD, Raman spectroscopy and TEM techniques.

Figure 4.27a shows the X-Ray Diffractogram, where it is observed that the intensity of the peak corresponding to (002) plane was reduced with an increase of irradiation dose. Figure 4.27b shows that the full width at half maximum (FWHM) of the sample was increased from 2.76^o for unirradiated sample to 4.73^o for 100 kGy irradiated sample. An increase of FWHM indicates micro straining of the MWCNTs, which confirmed the generation of defects in the structure, Singh et al. [2010]. It is also observed that the variation of diffraction angle is considered to be negligible against irradiation dose.

Raman spectroscopy technique was used to confirm the irradiation induced defects on MWCNTs by quantitative analysis. The assessment of defects on the surface of MWCNTs was done by calculating the ratio of the intensity of the defect induced double resonant D band and the in-plane vibration of sp^2 carbon atoms resulting in G band, i.e. (I_D/I_G), from the Raman spectra of MWCNTs, Mu et al. [2009]. The Raman spectra and the I_D/I_G ratio of irradiated MWCNTs are shown in Figure 4.28a and 4.28b, respectively. It is observed from Figure 4.28a that the intensity of D band was increased with irradiation dose, confirming the increased disordered carbon in the irradiated MWCNTs. The I_D/I_G ratio of MWCNTs was increased from 0.47 for unirradiated sample to 0.97 at 100 kGy irradiation dose, where a linear trend between

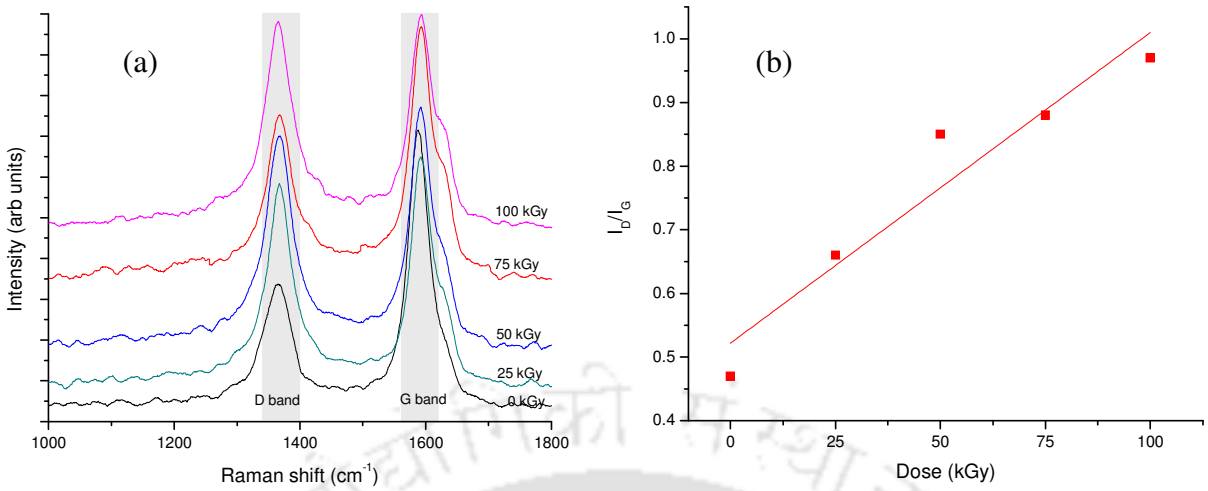

Figure 4.28. (a) Raman spectra of irradiated MWCNTs (b) I_D/I_G ratio of MWCNTs at different irradiation doses

the I_D/I_G ratio and the irradiation dose was observed and it is shown in Figure 4.28b. The defects are usually formed on the surface of MWCNTs during their synthesis process due to disordered carbonaceous and amorphous carbon compounds, which contributed to the Raman peaks in the spectra, Pimenta et al. (2007). An increase of I_D/I_G ratio indicates that the number of defects on the MWCNTs surface increased with irradiation dose.

The formation of defects on the surface of MWCNTs is due to the fact that the gamma irradiation in solids caused radiolysis leading to occurrence of various chemical reactions and ionization. The damage induced mechanism was caused by the high kinetic energy electrons ejected from the atoms by γ-photons, which led to the formation of interstitial atoms and other kind of defects, Cataldo [2000]. Figure 4.29 shows the TEM micrographs and Selective Area Electron Diffraction (SAED) patterns of untreated, chemically treated and gamma irradiated MWCNTs. Figure 4.29a shows the untreated MWCNTs, where the presence of amorphous carbon is observed prominently. The SAED pattern of untreated MWCNTs is shown in Figure 4.29b, where a diffused halo pattern was observed indicating the presence of large quantities of

amorphous carbon. Figure 4.29c shows MWCNT after chemical treatment, which removed the amorphous carbon and traces of substrate metallic impurities from it and thus the SAED pattern showed a sharp ring pattern. It is shown in Figure 4.29d, where the prominent (002) and (100) planes are also observed. Figure 4.29e shows the 100 kGy irradiated MWCNT, which showed

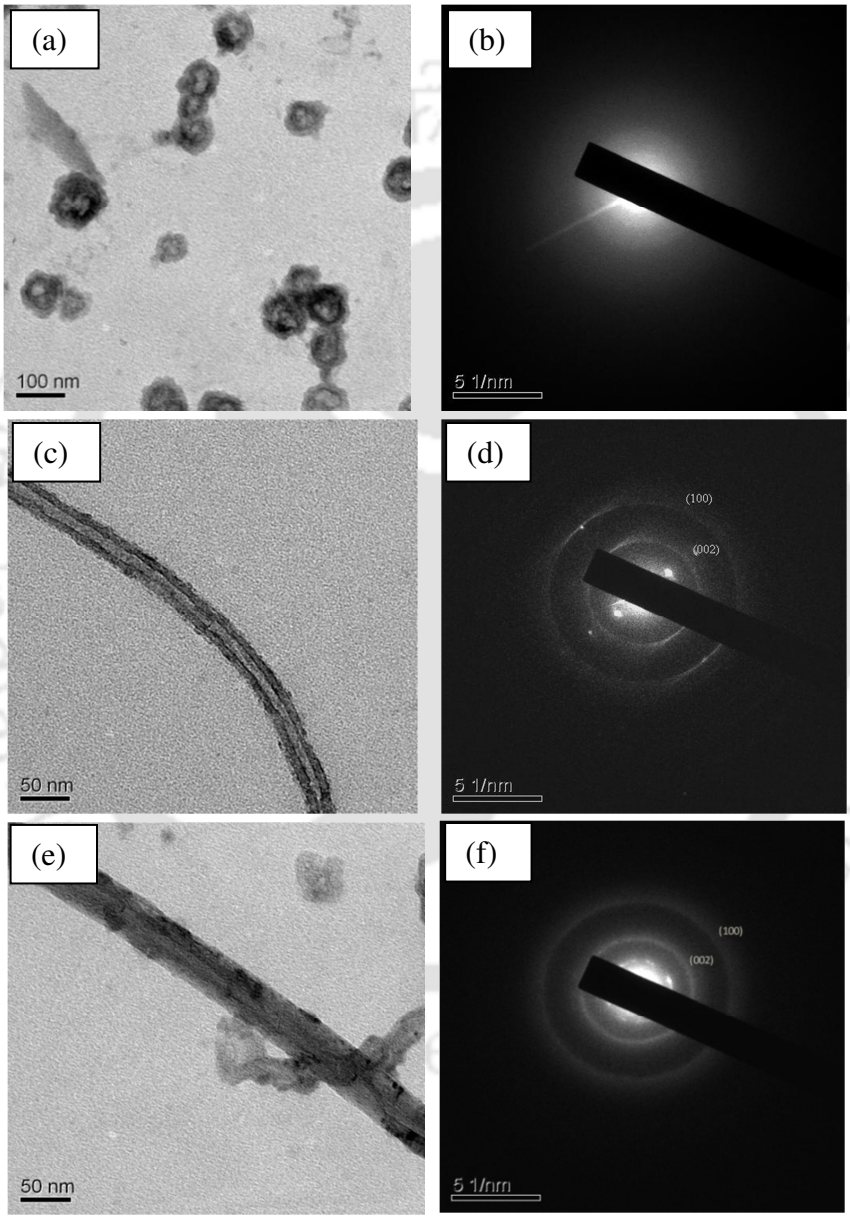

Figure 4.29. a) Amorphous carbon in untreated MWCNTs b) SAED pattern of (a) c) Chemically treated MWCNT d) SAED pattern of (c) e) 100 kGy irradiated MWCNT f) SAED pattern of (e)

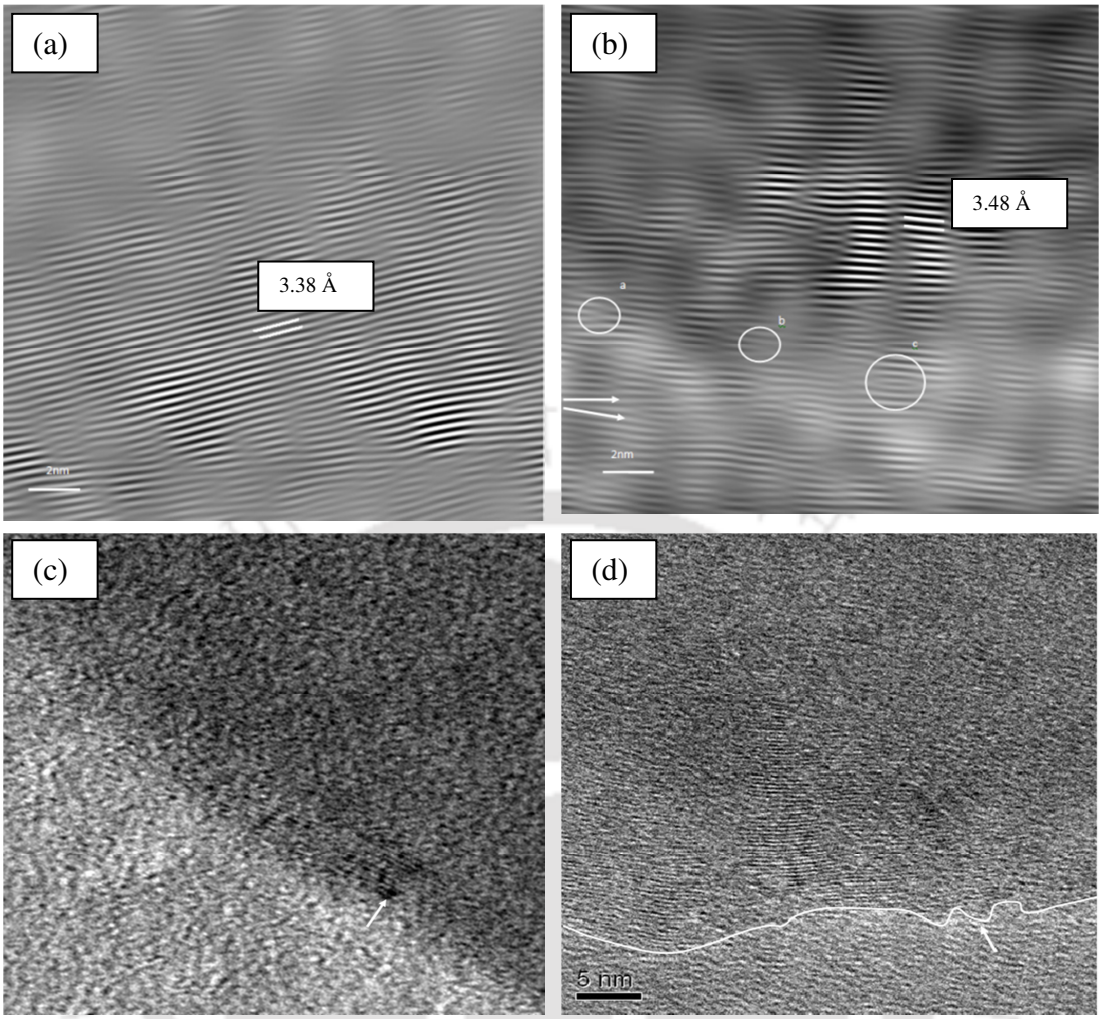

Figure 4.30. a) Interplanar spacing of (002) plane in an unirradiated MWCNT b) Interplanar spacing of (002) plane and the defects in 100 kGy irradiated MWCNT c) Formation of amorphous carbon on the outer walls d) Damage on the outer walls and the formation of curved graphitic structure after 100 kGy irradiation

the presence of amorphous carbon on the outer walls of MWCNT. The SAED pattern of irradiated MWCNT is shown in Figure 4.29f**,** where it is observed that the sharpness of the ring pattern was reduced compared to that of the results observed in Figure 4.29d. It indicates that the amorphous content was increased in the MWCNTs after the irradiation process due to the damage on their structure.

In order to visualize the formation of defects, the surface of MWCNT was observed under HRTEM. Figure 4.30a shows the interplanar spacing of unirradiated MWCNT, where it is observed that the interplanar spacing was found to 3.38 Å and most of the planes are found to be perfect without any distortion. Figure 4.30b shows that the interplanar spacing of 100 kGy irradiated MWCNT was increased to 3.48 Å. The defects in the planes are shown in the encircled regions, as a, b and c. The changes in the orientation are also indicated by arrows confirming the distortion of the structure of MWCNT due to irradiation. Figure 4.30c shows the damages on the outer walls of MWCNT and the formation of amorphous carbon, indicated by the arrow. Figure 4.30d shows the defects or vacancies on the outer wall of MWCNT, indicated by an arrow. The formation of curved graphitic structure also confirms the structural changes on the MWCNT surface.

Figure 4.31 shows the typical irradiation generated defects on MWCNT at 50 and 100 kGy doses. Figure 4.31a shows the MWCNT irradiated at 50 kGy**,** where the negative inclination indicated the presence of heptagon ring or various ring members resulting the formation of curvature of sharp bend, Ebbesen [1997]. It is also clearly observed that the diameter of the nanotube varied considerably after the sharp bend. It can also be noted that the deposition of amorphous carbon at the vertex of the bend is observed indicating a major structural damage and modification of MWCNT due to the irradiation**.** A similar type of observation can also be seen in Figure 4.31b, where a local modification of the pheriphery was occurred, and indicated by arrows. Such local modifications in the pheriphery of nanotubes occured due to tetra vacancy collapsing into 5-7-7-5 ring structure, Krasheninnikov et al. [2007]. It also shows the surface defects, wall damage and the formation of amorphous carbon, as indicated by the arrows. Figure 4.31c shows the changes in internal and external diameter of MWCNT irradiated at 100 kGy,

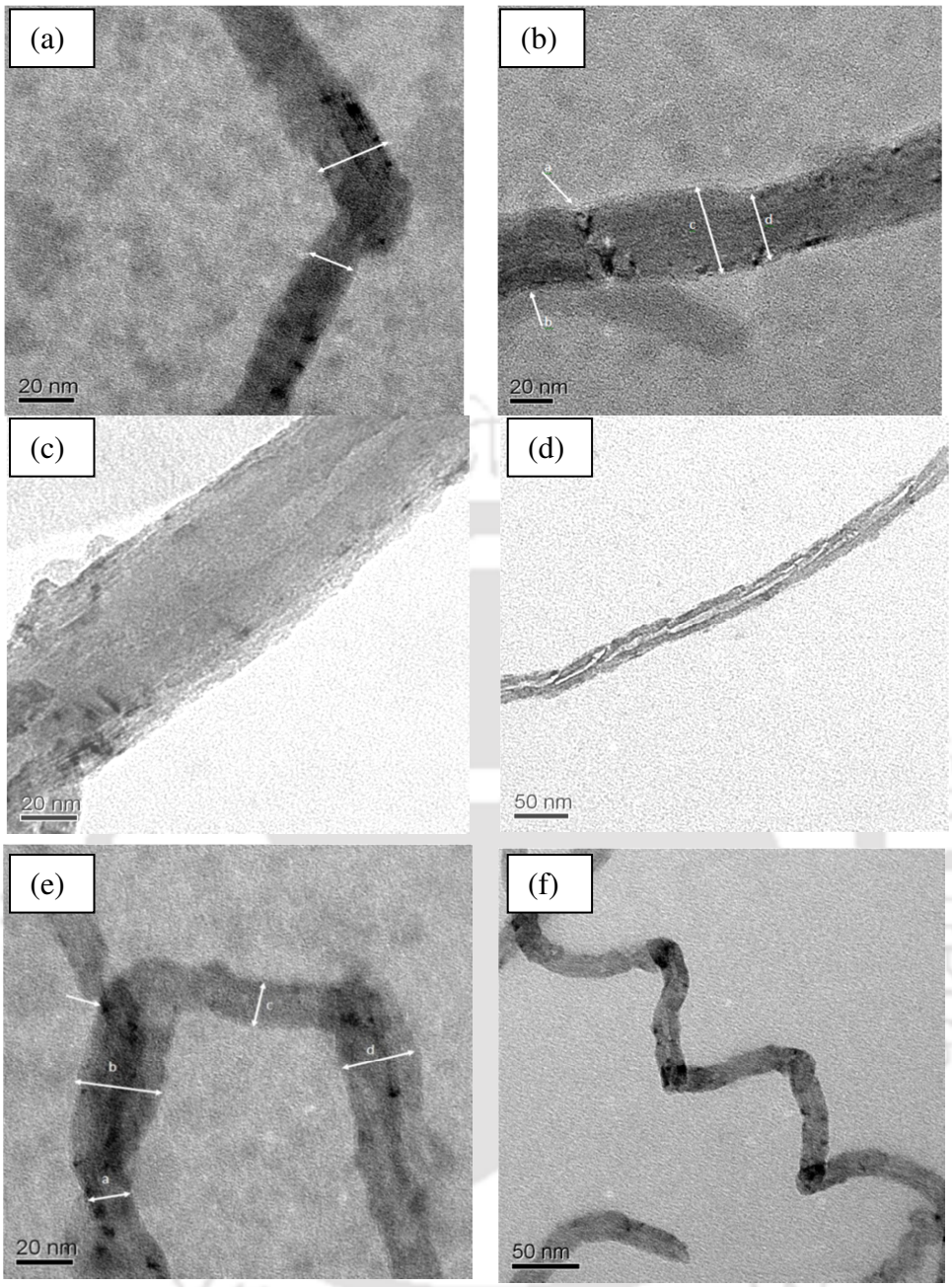

Figure 4.31. Formation of defects on gamma irradiated MWCNT at 50 and100 kGy irradiation doses (a,b - 50 kGy and c,d,e,f - 100 kGy) a) Sharp bend and sudden variation of diameter b) Surface defects and variation of diameter c) Variation of internal diameter d) wall breakage e) Typical bend defects, variation of diameter and formation of amorphous carbon f) Zig-Zag bends

which can be attributed to the presence of ring structure. Figure 4.31d shows the discontinuities in the inner wall of 100 kGy irradiated MWCNT. Figure 4.31e shows a wide variety of defects

such as sharp 90^{o} bends, variation of diameter, indicated by arrows labeled as 'a' and 'b', and the deposition of amorphous carbon at the sharp bends of 100 kGy irradiated MWCNT. Figure 4.31f shows a severely damaged MWCNT irradiated at 100 kGy dose. Several Zig-zag bends were observed indicating the damage and the presence of defects. Such bends with different angles were formed in the presence of various ring members, and such sharp bends were resulted due to the presence of tetragonal rings or vacancies, Ouyang et al. [2001]. There is also a finite possibility of the formation of point defects, which are difficult to observe under TEM.

4.3.2 Studies on crosslink density (CLD) of composites

As the irradiation induced defects on MWCNTs are expected to react with the free radicals in the polymer, the presence of MWCNTs is likely to influence the crosslink density of the UHMWPE and its composites. In order to confirm the same, swell test was conducted on the irradiated polymer and composite samples. The CLD of the test samples was calculated using the equation 3.7 and the variables used in the equation were obtained from the swell test. The swell ratio of irradiated sample is inversely proportional to the crosslinks in the polymer, Ganji et al. [2010]. A crosslinked polymer, when immersed in a solvent, swells by absorbing the solvent. The extent of swelling depends on two forces: i) elongation of the polymer chains by the swelling action, ii) reactive elastic forces generated due to crosslinks. When these forces balance each other, the swelling of the polymer attains equilibrium. It leads to an understanding that if the number of crosslinks is more, the extent of swelling in the polymer is less due to large reactive elastic forces. Figure 4.32 shows the CLD of composites at different MWCNTs

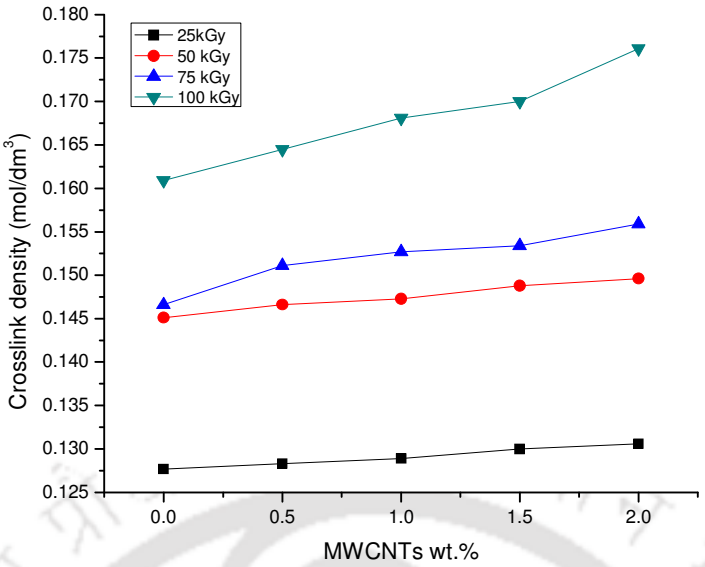

Figure 4.32. Crosslink density of composites

concentrations and irradiation doses. It is observed from Figure 4.32 that a significant enhancement of CLD of test sample was observed when both MWCNTs concentration and irradiation dose were increased. The CLD of pure UHMWPE at 25 kGy was found to be 0.1277 mol/dm^3, which was increased to 0.1306 mol/dm^3 at 2 wt. % composites corresponding to an enhancement of 2.5 %. In case of 100 kGy irradiated test sample, the enhancement of CLD was observed to be about 10 %. The enhancement of CLD of NC0.0 and NC2.0 samples was found to be highest at 100 kGy dose compared to any other irradiation dose used in this study. The CLD of GI100NC2.0 test sample was found to be 34.8 % higher than that of GI25NC2.0 test sample. In case of pure polymer, the CLD was enhanced by 25 %.

Based on the above results, it is clear that the presence of MWCNTs in UHMWPE has increased its CLD by reacting with the free radicals generated during irradiation process. The mechanism of how MWCNTs influence the CLD of polymer is graphically represented in Figures 4.33a to 4.33e. A normal polyethylene chain structure is shown in Figure 4.33a. Figure 4.33b shows the irradiation generated radicals resulting from C-C and C-H cleavages. Figure

4.33c shows the MWCNTs acting as a chain scission inhibitor by reacting with the free radicals formed from the C-C cleavage. A crosslink formed between two adjacent polyethylene chains as a result of C-H cleavage is also shown in Figure 4.33c. Figure 4.33d shows the MWCNTs acting as a crosslink promoter by reacting with the radicals in the two adjacent chains forming an intermediate crosslink. Figure 4.33e shows the MWCNTs bonding with free radicals generated from both C-C and C-H cleavages. Though Figure 4.33 shows the schematic representation in 2D view, both the polyethylene chains and MWCNTs originally exist in a 3-dimensional network and hence the bonding can be more effective. It is expected that all the free radicals formed during the irradiation process are not taking part in bonding with MWCNTs and the unbonded free radicals led to the formation of oxidation products resulting to degradation of the properties of test samples.

(a)

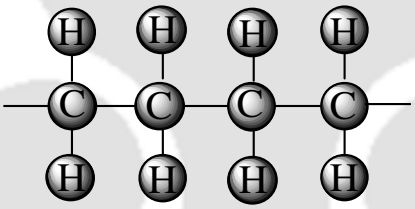

Polyethylene chain.

(b)

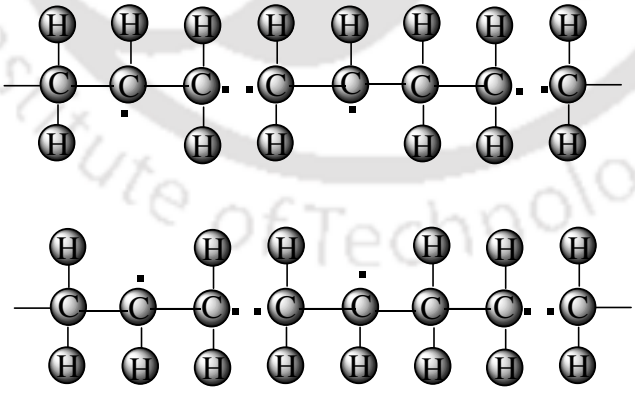

Polyethylene chain showing radicals resulting from C-C cleavage and C-H cleavage.

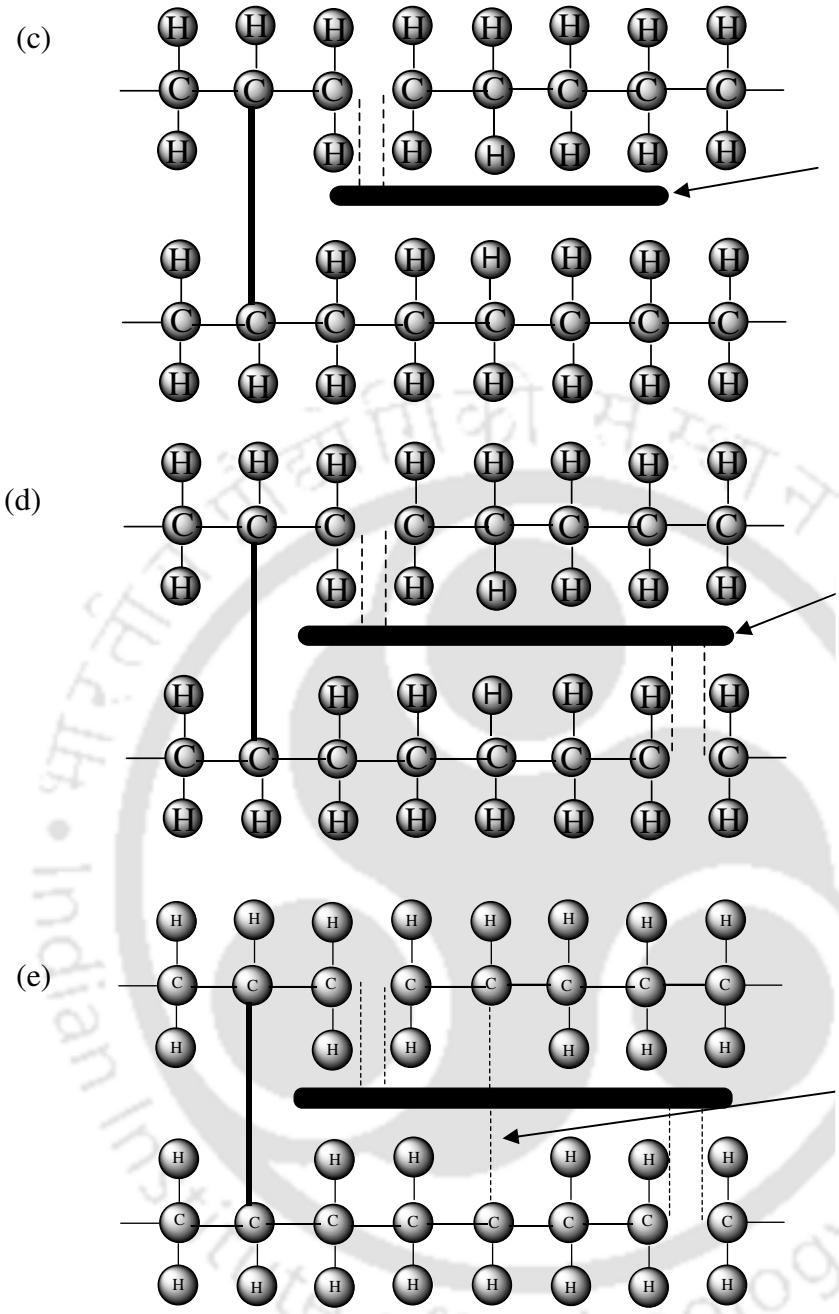

Figure 4.33. a) Structure of polyethylene molecule b) Polyethylene chains with irradiation generated free radicals c) MWCNT acting as chain scission inhibitor d) MWCNT acting as crosslink promoter e) MWCNT acting as both crosslink using C-C and C-H cleavage

Based on the above observation and the reduction of degradation of the mechanical properties of composites by the presence of defects on the surface of MWCNTs, as discussed in Section 4.2, it can be inferred that MWCNTs acted as both crosslink promoters and chain scission inhibitors using the irradiation induced defects.

4.3.3 Studies on CLD of α_T blends

α_T is being used as a standard antioxidant additive in orthopedic applications since 2003, Kurtz [2009]. However, the use of α_T possesses certain limitations such as reduced crosslinking, as it absorbs the free radicals generated during the irradiation process, Oral et al. [2005]. Figure 4.34 shows the CLD of the α_T blends. It is observed that the CLD of UHMWPE/α_T blends was reduced with an increase of α_T content. The pure UHMWPE has higher degree of CLD, which varied between 0.1277 mol/dm^3 at 25 kGy to 0.1609 mol/dm^3 at 100 kGy. However, the CLD of α_T0.1 blend was reduced to 0.1118 mol/dm^3 at 25 kGy and 0.132 mol/dm^3 at 100 kGy. However, there was no influence of the irradiation dose on CLD of blends having 0.3 and 0.5 wt. % α_T in UHMWPE. It is also observed that there was about 26 % enhancement of CLD of pure polymer, when the irradiation dose was increased from 25 to 100 kGy, but the

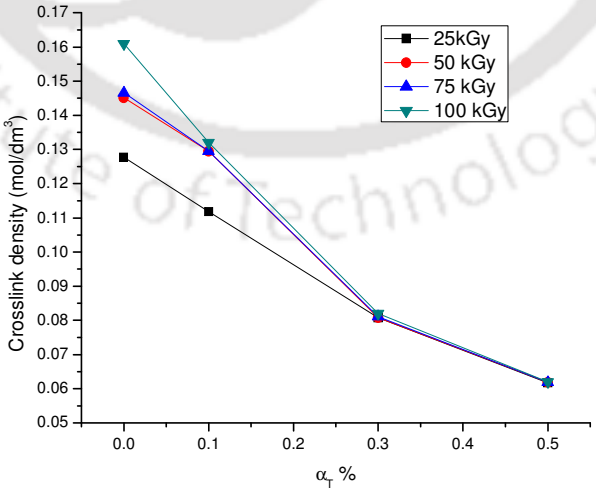

Figure 4.34. Crosslink density of UHMWPE/α_T blends

enhancement was reduced to 18 % for 0.1 wt. % α_T. However, it becomes negligible when the α_T concentration was increased to 0.3 wt. % and beyond.

4.3.4 ESR studies on composites and UHMWPE/α_T blends

The ESR studies were used to quantify the free radicals present in the composites and α_T blends. Although MWCNTs and α_T reacted with the free radicals in the polymer, there will be good amount of unbounded free radicals left over in the polymer. The free radicals that are trapped in the crystalline phases of the UHMWPE slowly diffuse towards amorphous regions and they react with atmospheric Oxygen leading to the formation of peroxy radicals. They abstract a hydrogen atom from the polyethylene chain leading to the generation of further new radicals, Oral et al. [2006], and finally it leads to the shelf ageing induced degradation of the mechanical properties. Figures 4.35a, 4.35b and 4.35c show the ESR spectra of 100 kGy irradiated composites within 10 days, 60 and 120 days after irradiation, respectively. It is observed from the spectra of irradiated samples obtained at different ageing periods that the intensity of the ESR signal is reduced with an increase of MWCNTs concentration. It indicates that the number of free radicals present in the polymer causing the degradation of its

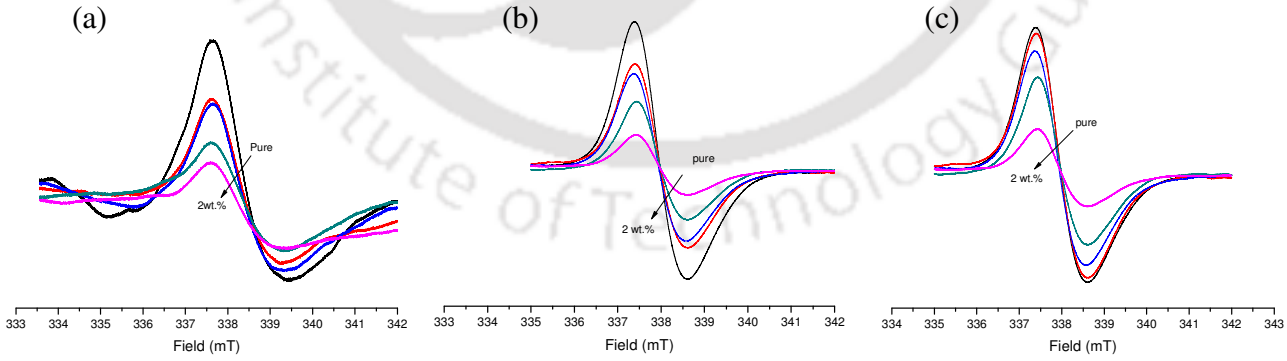

Figure 4.35. ESR spectra of 100 kGy irradiated composites at different periods of ageing a) Within 10 days b) 60 days c) 120 days after irradiation

mechanical properties reduced with an increase in MWCNTs concentration in UHMWPE.

An asymmetric broad singlet at room temperature serves as an indicator of the presence of peroxy radicals, Jahan et al. [2001]. The number of free radicals present in the test samples at any given time is proportional to the intensity of the spectrum. The spectral splitting factor (g) is evaluated from the equation 3.5 in order to confirm the formation of peroxy radicals because it is a characteristic value for a certain species of free radicals. In the present study, the obtained g-value varied between 2.003 to 2.005 (when H is app. 338.43 mT), where the usual range of 'g' for a peroxy radical is 2.001 to 2.005, Pedro et al. [2008].

The experimentally recorded first derivative of ESR spectrum, shown in Figure 4.35, is integrated to obtain the absorption curve. The absorption curve of 100 kGy irradiated composites after 120 days of irradiation is shown in Figure 4.36a. The area under the absorption curve is proportional to the radical concentration present in the test sample. It is observed from Figure 4.36a that the intensity of the absorption curve is reduced with an increase of MWCNTs

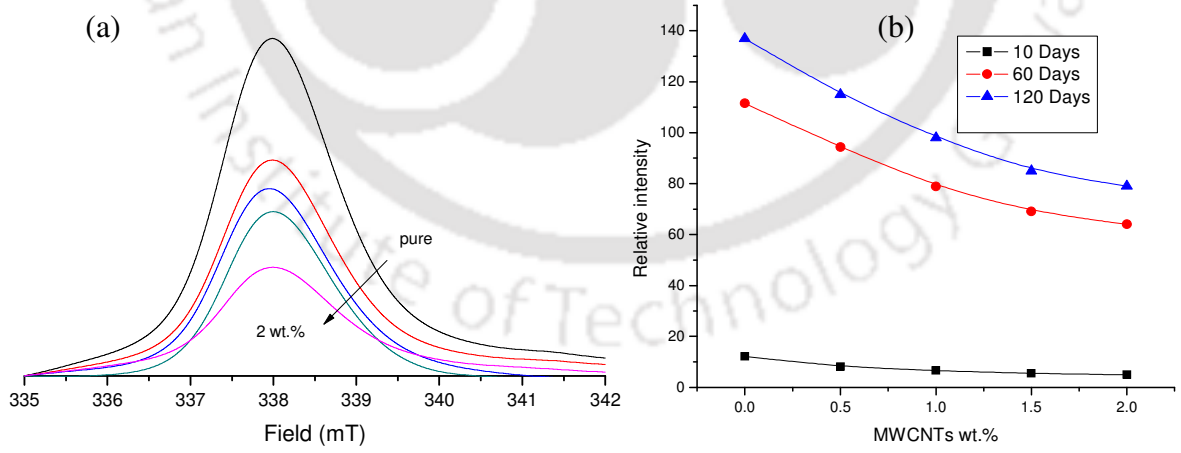

Figure 4.36. a) Absorption spectra of the ESR signal obtained from 100 kGy irradiated composites after 120 days of irradiation b) Relative intensity of the irradiated composites at different periods of ageing

concentration. The relative intensity of composites at different ageing periods at 100 kGy dose was obtained by normalizing the area under the absorption curve of each composite with that of an unirradiated sample, Suarez et al. [2003] and it is shown in Figure 4.36b. It is observed from Figure 4.36b that the reduction of relative intensity of free radicals present in the composites followed a linear trend upto 1 wt. %, beyond which the reduction rate was negligible. The relative radical intensity of pure UHMWPE after 10 days of irradiation was found to be 12.1, which was reduced to 4.9 at 2 wt. % MWCNTs corresponding to a reduction of 59 %. In case of irradiated pure UHMWPE after 120 days of irradiation, the relative radical concentration was calculated to be 137, and it was reduced to 79 for 2 wt. % composite corresponding to the reduction of 42.3 %. The presence of MWCNTs has effectively restricted the concentration of radicals present in the composites against ageing compared to that of virgin UHMWPE. It can be inferred from the above studies that the presence of MWCNTs reduced the number of free radicals in UHMWPE and thus it helps to restrict the deteriorating effects of oxidation.

The ESR spectra of 100 kGy irradiated UHMWPE/α_T blends within 10 days, 60 and 120 days after irradiation are shown in Figures 4.37a, 4.37b and 4.37c, respectively. It is observed from the spectra that the intensity was reduced with an increase of α_T concentration at any given shelf ageing period. Being an antioxidant material, α_T reacts with free radicals present in the polymer and thus reduces its radical concentration. The absorption curve of 100 kGy irradiated UHMWPE/α_T blends after 120 days of irradiation is shown in Figure 4.38a. Figure 4.38b shows the relative intensity of blends after different periods of irradiation. The relative intensity of pure polymer was found to be 137, which was reduced to 63 and 45 for GI100α_T0.1 and GI100α_T0.5 after 120 days of irradiation. The relative intensity was reduced exponentially from 0 to α_T 0.5

wt. % α_T for 60 and 120 days aged samples. However, there was no significant influence of α_T concentration on the relative intensity of the sample within 10 days after irradiation.

A comparison of the relative intensity of radical concentration of 100 kGy irradiated composites and UHMWPE/α_T blends after 120 days of irradiation is shown in Figure 4.37. It is observed that the radical intensity of virgin UHMWPE was found to be 137, which was reduced to 79 and 63 for NC2.0 and α_T0.1 blend, respectively. The relative intensity of NC2.0 and α_T0.1 was found to be reduced by 43 and 54 %, respectively compared to that of virgin UHMWPE.

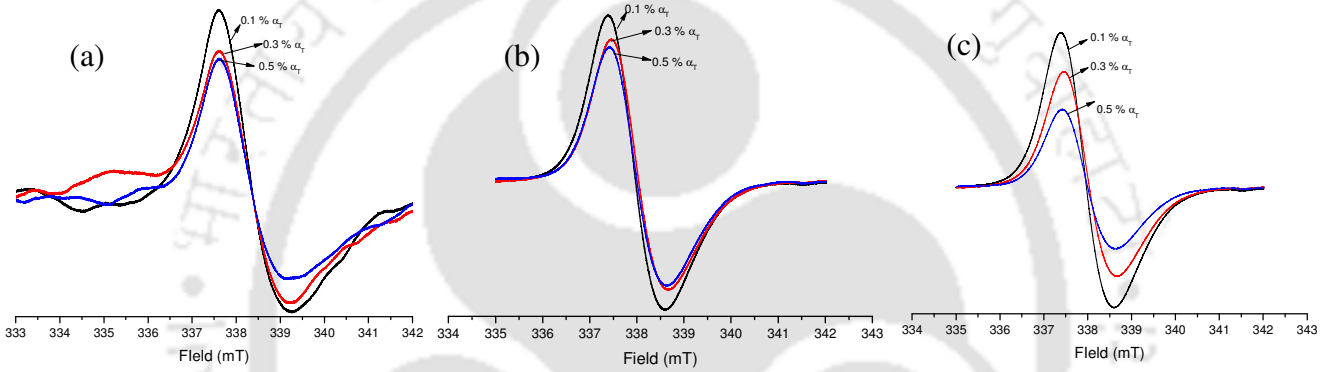

Figure 4.37 ESR spectra of 100 kGy irradiated UHMWPE/α_T blends at different periods of ageing a) Within 10 days b) 60 days c) 120 days after irradiation

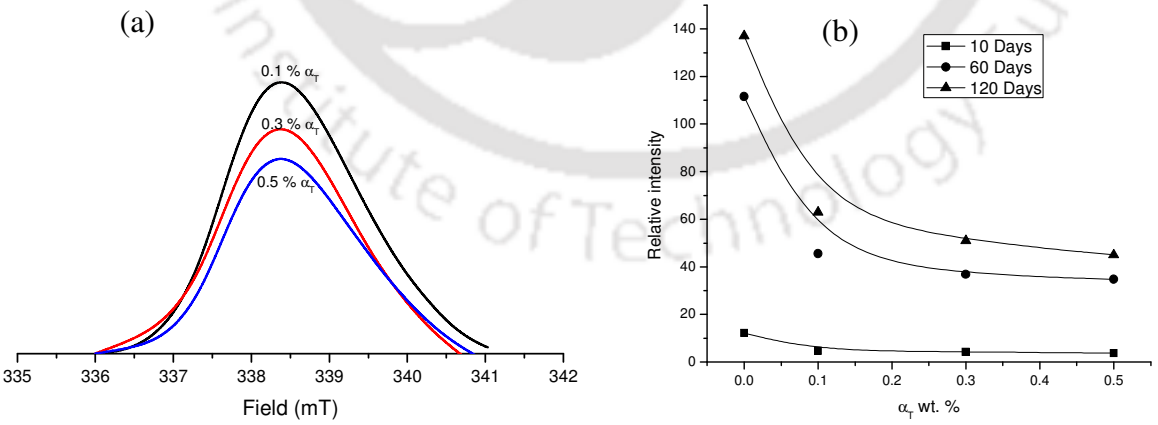

Figure 4.38. a) Absorption spectra of the ESR signal of 100 kGy irradiated UHMWPE/α_T blends after 120 days of irradiation b) Relative intensity of the UHMWPE/α_T blends at different periods after irradiation

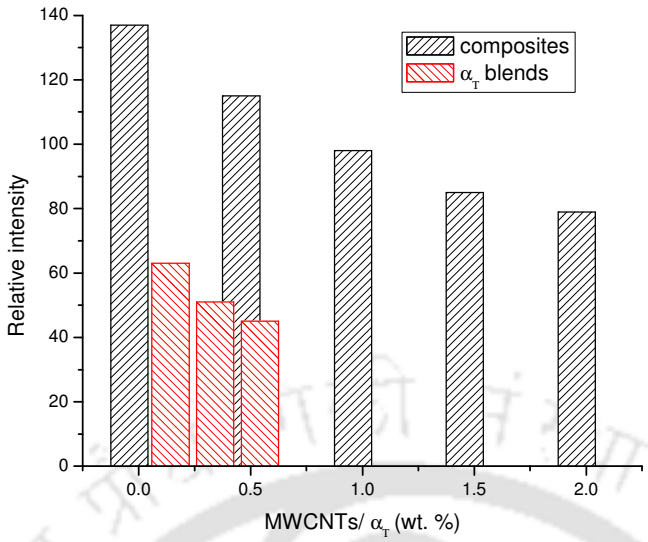

Figure 4.39. Comparison of relative intensity of 100 kGy irradiated composites and UHMWPE/α_T blends after 120 days of irradiation

Based on the above studies related to the defects formed on MWCNTs surface, CLD and ESR spectra, it is concluded that the role of 2 wt. % composites is similar to that of α_T0.1 in restricting the degradation of mechanical properties after irradiation. The defects formed on the surface of MWCNTs due to irradiation act as strong radical traps due to their high electron affinity and thus reduce the radical intensity. The defective sites tend to easily trap the free radicals present in the polymer generated during the process of irradiation. Thus, the presence of MWCNTs minimized the degradation of UHMWPE and restricted the loss of mechanical properties. In case of α_T blends, the free radicals absorbed by the α_T leading to the reduced content of them causing the reduction of degradation of mechanical properties.

4.3.5 Summary of the studies on network parameters and radical scavenging capability of composites and α_T blends

The irradiation induced defects on the surface of MWCNTs were identified using suitable analytical techniques. It was observed that the number of defects observed in the MWCNTs

increased with irradiation dose. The crosslink density of composites and α_T blends was assessed using swell test according to ASTM F 2214-02 standards. It was observed that the crosslink density of composites was increased with irradiation dose and MWCNTs concentration. In case of α_T blend samples, the crosslink density was reduced with an increase of α_T concentration. The electron spin resonance studies showed a decrease in relative radical intensity with an increase of MWCNTs and α_T concentration in UHMWPE. The reduction of free radicals in UHMWPE due to the presence of MWCNTs and α_T led to the reduction of degradation of properties of the polymer. Based on the obtained results, a schematic molecular structure model was proposed to elucidate how the presence of MWCNTs in UHMWPE could reduce the degradation of properties by acting as a crosslink promoter and a chain scission inhibitor using the irradiation induced defects. It is concluded that the defects generated on the surface of MWCNTs have high electron affinities and are responsible for trapping the free radicals in the polymer. Thus, the presence of MWCNTs has reduced the deteriorating effects of irradiation on the reduction of mechanical properties of UHMWPE.

4.4 Studies on wear behaviour of composites and UHMWPE/α_T blends before and after irradiation

4.4.1 Hardness of composites and α_T blends before and after irradiation

As the hardness of the test surface strongly influences its wear performance, the hardness of all the samples at different irradiation doses and MWCNTs concentration is obtained and it is shown in Figure 4.40. It is observed that the hardness of composites was increased with both MWCNTs concentration and irradiation doses, but the enhancement of irradiation induced hardness was not as significant as that of MWCNTs concentration. The hardness of unirradiated NC0, NC0.5, NC1.0, NC1.5, and NC2.0 composites was found to be 26.1, 29.1, 38.2, 41.2 and

45.7 MPa, respectively and the corresponding enhancement was 0, 11.5, 46.4, 57.8 and 75 %. The reason for the improved hardness of UHMWPE with an increase of MWCNTs concentration is due to increase of its crystallinity, which was also confirmed by the DSC studies and supported by Perepechko [1981]. As higher crystallinity of the polymers also makes them harder and rigid, Crompton [2006], the hardness of polymer was increased with MWCNTs concentration. A similar type of observation was also found in the literature, where the hardness of epoxy, PMMA and UHMWPE was increased by 30%, [Wang et al. [2008]], 50 %, [Jia et al. [1999]], and about 12%, [Bakshi et al. [2007]], respectively by the reinforcement of MWCNTs. The hardness of UHMWPE obtained from the present study was 26.1 MPa, which is approximately closer to the value reported by Wang et al. [2007], i.e. 28.5 MPa. Such deviations in polymer are expected due to the differences in processing conditions and operating parameters. The hardness of virgin UHMWPE and NC2.0 sample was enhanced by 16.5 and 7.5 %, respectively when the irradiation dose was increased from 0 to 100 kGy. The hardness of GI100NC2.0 test sample was increased by 89 % compared to that of unirradiated virgin polymer. An increase of hardness of UHMWPE with irradiation dose was expected due to restructuring of the polymer network caused by the crosslinking and oxidation process, Benson [2002]. The presence of MWCNTs in UHMWPE during the irradiation process was expected to reduce the oxidation induced degradation due to their ability to react with the free radicals in the test sample, which was also confirmed earlier, and thus it helped to reduce the severity of polymer oxidation. The oxidation index of irradiated polyethylene was also found to be significantly reduced by the reinforcement of MWCNTs, Sreekanth et al. (2012). Thus, the increase of hardness of irradiated NC2.0 test sample was relatively less compared to that of virgin UHMWPE.

The hardness of α_T blended UHMWPE before and after irradiation process is shown in Figure 4.40b**.** The hardness of the UHMWPE was found to be unaffected by the presence of α_T prior to irradiation. However, it has shown a decreasing trend with an increase of α_T content in UHMWPE after the irradiation process. The hardness of virgin UHMWPE at 100 kGy was found to be 30.4 MPa, which was reduced to 29.3, 28.2 and 26.3 MPa at 0.1, 0.3 and 0.5 wt. % of α_T concentration, respectively. Although the hardness of 100 kGy irradiated UHMWPE was increased by 16 % compared to unirradiated polymer, the hardness of α_T0.1, α_T0.3 and α_T0.5 was about 3.7, 8 and 14 % lower than that of GI100NC0.0. The reason for the reduction of hardness is due to the fact that α_T reduced the CLD of the polymer. In addition to that the presence of α_T in UHMWPE during the irradiation process acted as a plasticizer, Tomita et al. [1999] causing the reduction of hardness of UHMWPE.

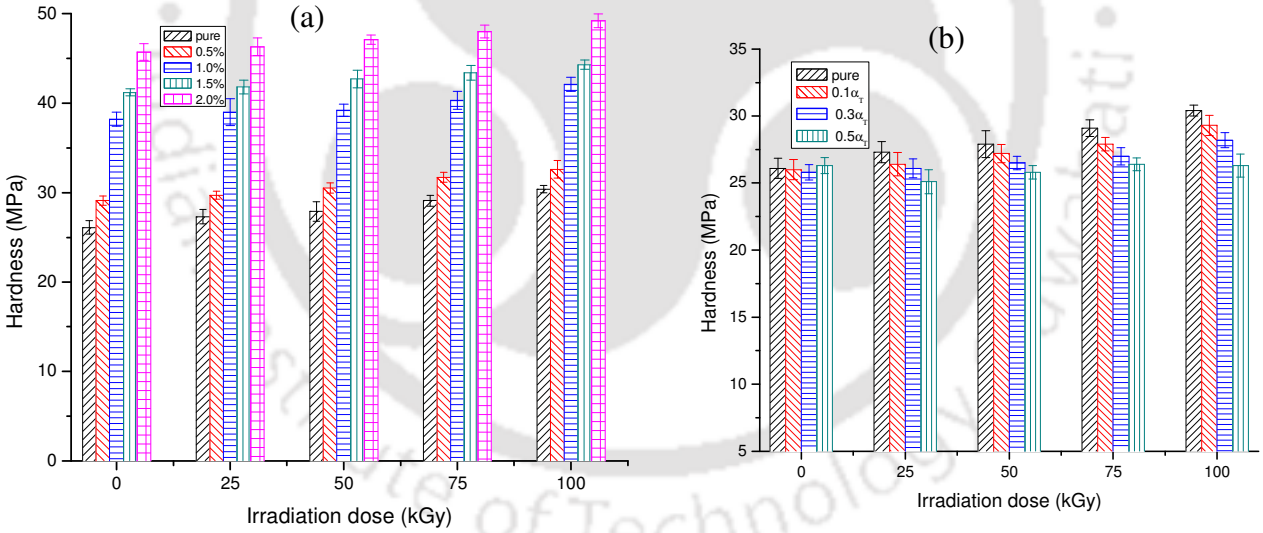

Figure 4.40. Hardness of a) Composites b) α_T blends at different irradiation doses

4.4.2 Wear studies on unirradiated composites and α_T blends

Figure 4.41a shows the wear volume of UHMWPE and its composites against sliding distance. The total wear volume of the test sample is contributed by the transient wear (initial

wear) and the linear wear (steady state). The initial wear of the test samples was found to be very high and non-linear nature, where the surface irregularities were flattened when the traction force was applied. The steady state wear of the samples was reached after the transient effects, where the wear volume was increased linearly with sliding distance. It is also observed that the steady state wear rate of all the test samples was observed to be the same. However, the final wear volume of the test sample was lowest for a composite having 2 wt. % MWCNTs. It is due to the

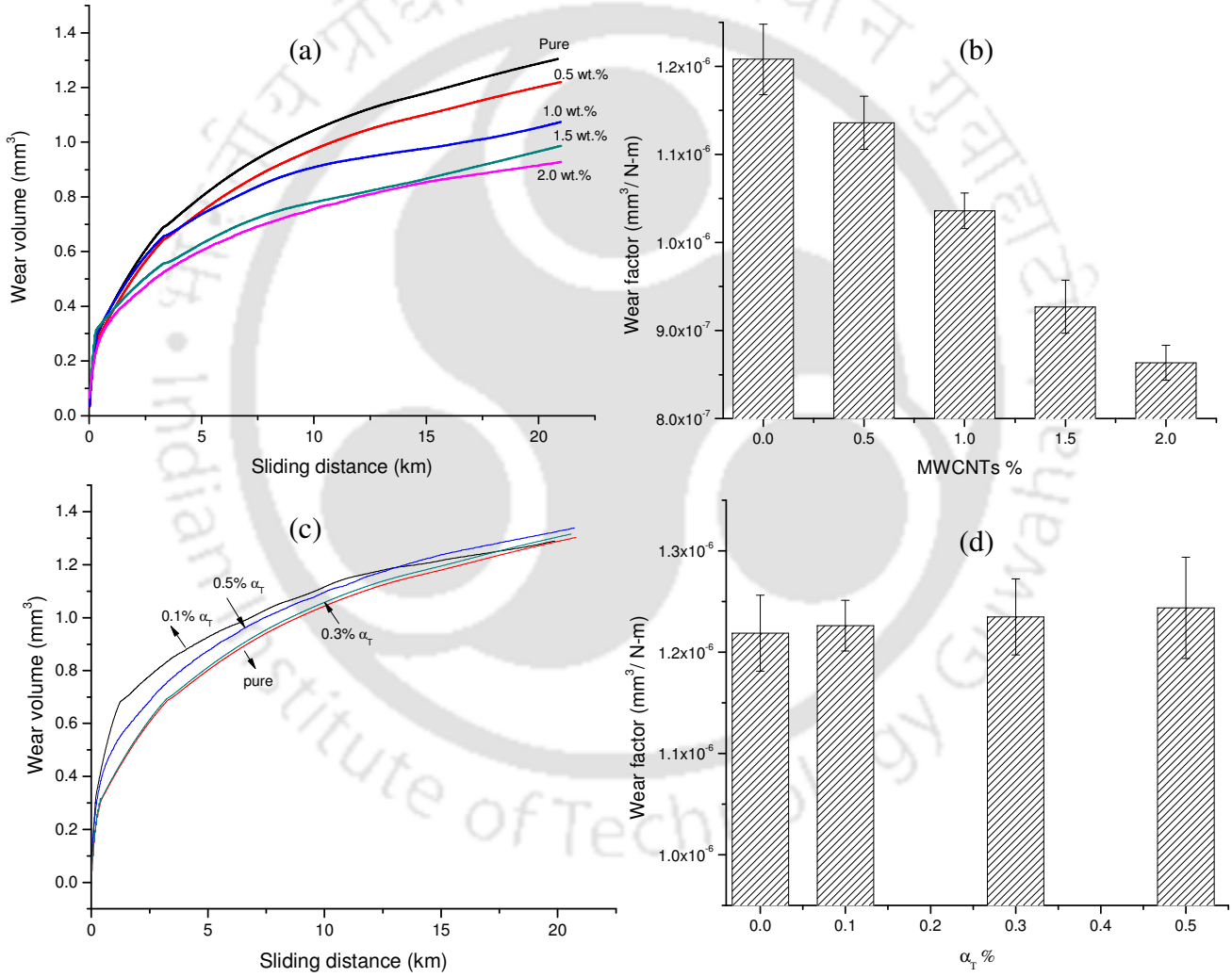

Figure 4.41. a) Wear profile of composites b) Wear factor of composites c) Wear profile of α_T blends d) Wear factor of α_T blends (under unirradiated condition)

fact that the initial wear of the composites was significantly influenced by the concentration of MWCNTs. It is observed from the previous results that the hardness of UHMWPE was increased with MWCNTs concentration leading to the significant reduction of the severity of initial wear of UHMWPE. It is also observed from Figure 4.41a that the wear volume of pure UHMWPE sample was found to be 1.33 mm^3 after 20 km sliding distance, which was reduced to 1.25, 1.14, 1.02, and 0.92 mm^3 for NC0.5, NC1.0, NC1.5 and NC2.0 sample, respectively and the corresponding reduction of wear volume is 7, 18.6, 26 and 31 %. The wear factor, which is defined as the volume of the material worn per one Joule of work done, is calculated for all the irradiated test samples and it is shown in Figure 4.41b. The wear factor was found to be reduced with increasing concentration of MWCNTs in UHMWPE and it was found to be the lowest for NC2.0 composite compared to that of pure UHMWPE. It was observed that the wear factor of virgin UHMWPE was found to be 1.208×10^{-6} mm^3/N-m, which was reduced to 8.63×10^{-7} mm^3/N-m by incorporating 2 wt. % MWCNTs. The reason for increased wear resistance of composites is due to their higher work to failure and hardness compared to that of pure UHMWPE.

The wear volume of α_T blend samples against sliding distance is shown in Figure 4.41c. It is observed that the there was no significant difference in the wear volume of the blends after the sliding distance of 20 km. Though minor deviations were observed during the transient wear stage, but it has not affected the final wear volume of the α_T blends attained during the steady state. The wear factor of all the α_T blended samples is shown in Figure 4.41d, where it is observed that the presence of α_T in UHMWPE prior to irradiation process did not have any influence on the wear factor of the blends. This is due to the fact that α_T is used only as an additive to prevent the oxidation during the irradiation process.

The variation of coefficient of friction of the unirradiated composite samples with sliding distance is shown in Figure 4.42. The direction of the arrow in the plot indicates the increase of MWCNTs from 0 to 2 wt. %. It is observed that the coefficient of friction was decreased initially with sliding distance during the run-in stage for all the materials and it was not significantly changed during the later stages from the average value. The initial reduction of coefficient of friction is due to shearing of the interlocked surface asperities and smoothening of the surfaces in contact. It is also observed from Figure 4.42 that the coefficient of friction in the steady state period was reduced with an increase of MWCNTs concentration. The coefficient of friction of pure UHMWPE was found to be 0.125 at steady state condition, which was reduced to 0.12, 0.117, 0.115 and 0.112 at 0.5, 1.0, 1.5 and 2 wt. % MWCNTs, respectively. The reduction of coefficient of friction with an increase of MWCNTs concentration can be attributed to their self-lubricating characteristics, Qianming et al. [2008]. A similar observation was made by Chen et al. [2003] and Cai et al. [2004] for PTFE/CNT and polyimide/CNT composites, respectively.

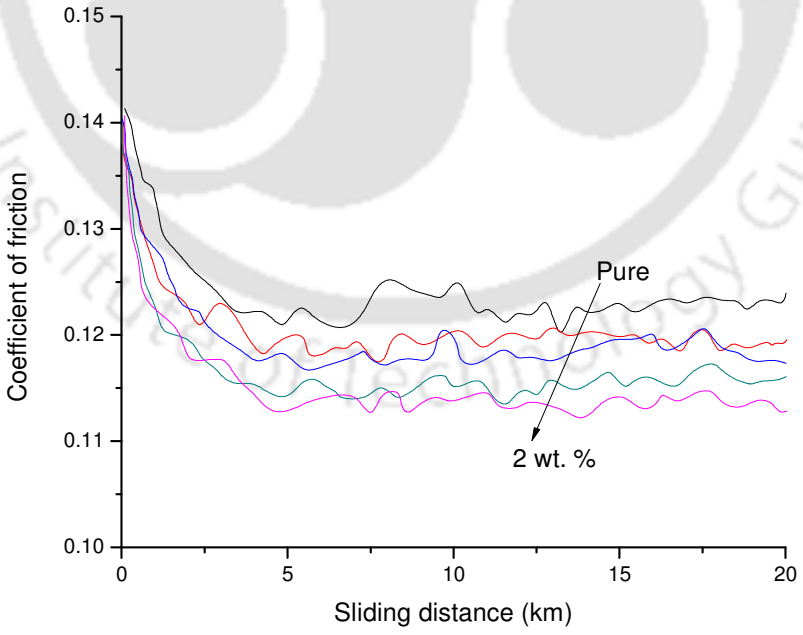

Figure 4.42. Coefficient of friction of unirradiated composites against sliding distance

Figure 4.43 shows the representative SEM and optical microscopic images of the wear debris and wear tracks of the test sample. The wear mechanisms were explained based on the observation made from these figures. Figure 4.43a shows the wear debris of NC0.0, where both long needle like fibrils and particulate wear debris were observed. Figure 4.43b shows the wear debris produced from the NC2.0 test sample. It is observed from Figures 4.43a and 4.43b that the size of most of the wear debris obtained from the pure polymer and 2 wt. % composite sample was approximately 10 µm or less and very few particles were observed to be outside the range. The length of long needle like fibrils, which are indicated in Figure 4.43a, varied between 50 to 90 µm. However, these type of fibrils were not observed in NC2.0 sample. Although the size of the particulate wear debris generated from the pure polymer and composites was not varied, the particulate density was found to be less in case of NC2.0 sample compared to that of virgin UHMWPE. Figures 4.43c and 4.43d show the formation of wear craters resulted due to initial adhesive wear on the surface of pure polymer and NC2.0 test samples, respectively. The wear craters are indicated by an arrow in Figure 4.43c and encircled in Figure 4.43d. In addition to wear craters, the abrasive wear furrows were also observed on the test surface. The generation of craters is resulted due to the relative motion between the counterface and test surface.

Polyethylene underwent deformation at the asperity contact due to the normal force, which led to the reduction of the height of asperities and consequently an adhesive bond was created at the interface of the materials in contact. If the relative motion is continued, a portion of the soft material is pulled off leaving behind a crater or cavity, Bhushan [1999]. If the pulled off material continues to bond with the counterface material, it forms a transfer film or wear debris if it is slipped off. Although the wear craters observed in both polymer and composites, the dimension and number of craters observed in the composites are found to be less than that of virgin

UHMWPE and it is shown in Figure 4.43d. It may be due to the fact that MWCNTs have strong bond with polyethylene due to the chemical groups attached on their surface. Thus, the amount of adhesive force required to pull off the soft material is increased significantly, and resulted in fewer wear craters on the composites.

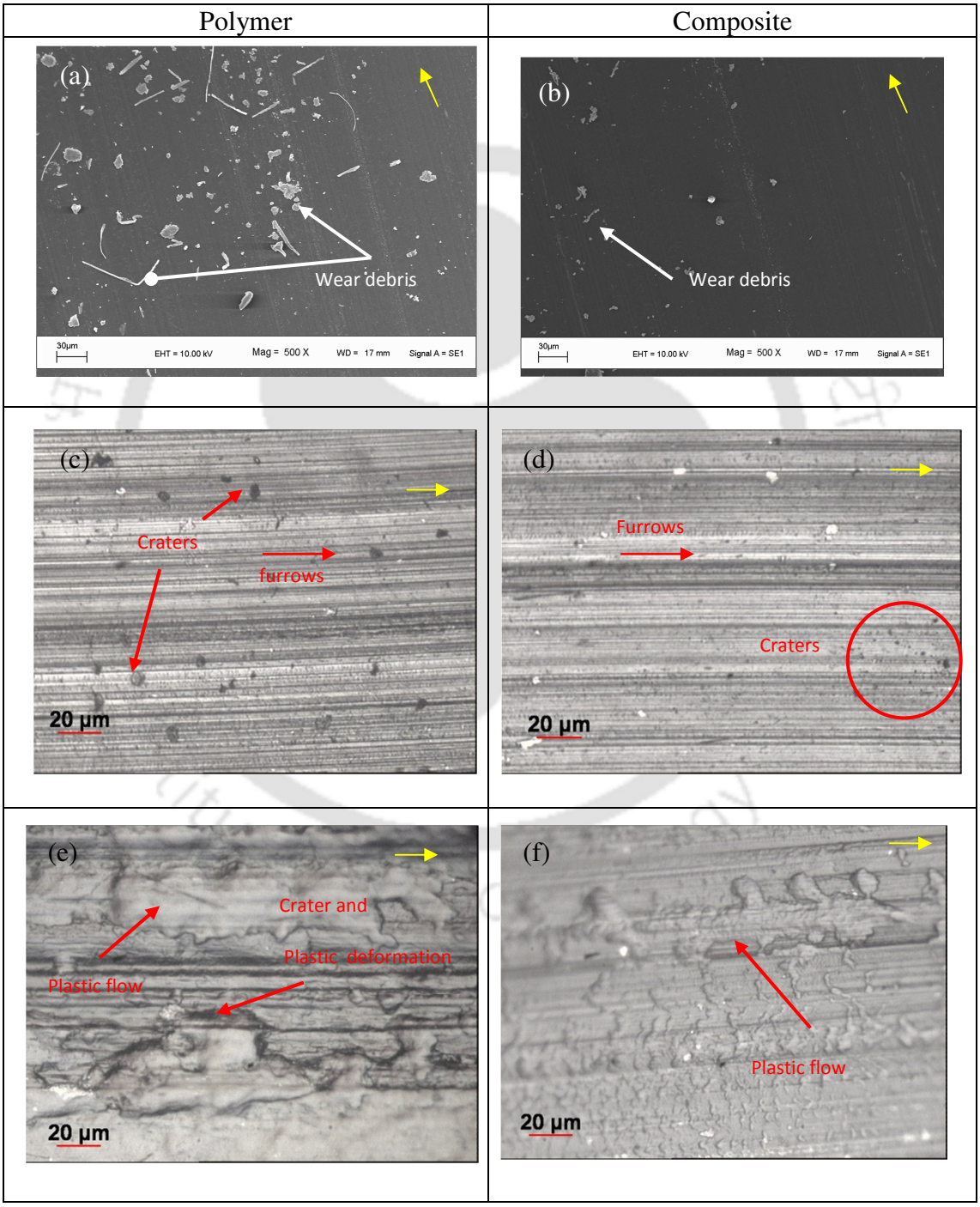

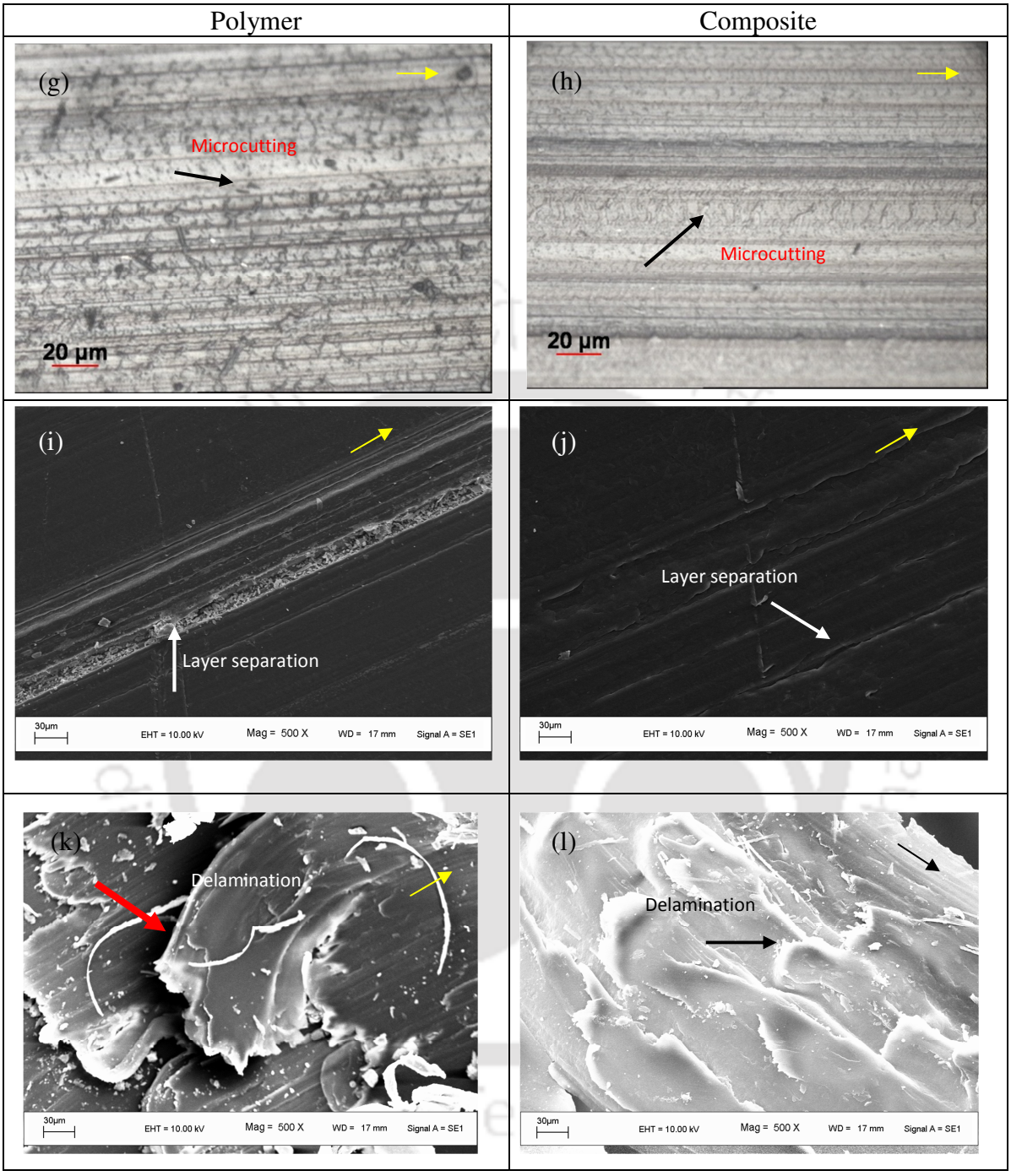

Figure 4.43. Representative SEM and optical microscopy images of the test samples before irradiation showing different wear mechanism. (a, b) Wear debris showing micron particulate and fibrils (c, d) Wear craters due to initial adhesive friction e) Plastic flow and wear craters f) Plastic flow (g, h) Micro cutting and abrasive wear furrows (i, j) Cracks and layer separation (k, l) Delamination of fibrils from underlying test sample

Figure 4.43e shows the wear crater on the surface of UHMWPE, which was further aggravated by the plastic flow and deformation resulted due to frictional heating of the test sample. Figure 4.43f shows the intensity of plastic flow resulted in the NC2.0 test sample, which is found to be less than that of virgin UHMWPE. It may be due to the fact that MWCNTs have superior thermal properties compared to that of polymer. The thermal conductivity of MWCNTs is 3000 W/m-K, Yang et al. [2009]; while the same for UHMWPE is 0.41 W/m-K, Ticona data sheet [2010]. The temperature of polymer raised due to frictional heating leading to its softening and thus it influenced the plastic flow. Due to higher thermal conductivity of MWCNTs, a significant portion of heat generated due to frictional heating was dissipated by them and thus it reduced the plastic flow and deformation of the composites. Figures 4.43g and 4.43h show the surface of the UHMWPE and NC2.0 test samples, respectively, subjected to microcutting. This type of wear mechanism primarily occurs due to the abrasive action of the generated wear particles, which cut the polymer surface, Imbeni et al. [2001]. It is observed from Figure 4.43h that the severity and intensity of microcutting in the composites are observed to be less than that of virgin UHMWPE. It is due to the fact that the hardness of NC2.0 sample was 75 % higher than that of pure polymer and it is a known fact that the harder materials offer better resistance against cutting than the soft materials. Figure 4.43i shows the cracks formed on the polymer surface, which was further aggravated by third body wear leading to separation of a layer. In case of NC2.0 composite, the cracks were found to be mild and the separation of a layer due to third body wear was not much significant compared to that of pure polymer and it is shown in Figure 4.43j. Figures 4.43k and 4.43l show the delamination of the fibrils from the underlying material of pure polymer and NC2.0 test samples, respectively. The primary mechanism for the delamination wear of the test sample is that the hard asperities of the metal counterface

penetrated into the soft material leading to its plastic deformation or fracture. It proceeded in an incremental way till the relative motion at their interface continued. Due to severe fatigue resulting from the repeated loading and plastic deformation, the cracks were formed at the subsurface of the test materials, which propagated due to the combined effect of compressive loading on the crack and shear deformation at the crack tip, Qianming et al. [2008]. These cracks were expected to propagate and join among them, which eventually formed a long and thin sheet of delamination, as observed in Figure 4.43k. The delamination wear of pure UHMWPE was significantly reduced by the reinforcement of MWCNTs as shown in Figure 4.43l due to their superior properties and interfacial bonding between polymer and MWCNTs.

Figure 4.44 shows the surface topography and typical wear profile of the test samples. Figure 4.44a shows the topography of pure polymer and it is observed that the material on the surface of polymer was piled up due to its plastic flow. The height of the piled up material was observed to be 0.542 μm above the mean level, and it is shown in Figure 4.44b. Figure 4.44c shows the formation of wear crater on the pure polymer, where the depth of the wear crater was about 0.40 μm and it is shown in Figure 4.44d. Figure 4.44e shows the stacking up material on NC2.0 test sample. The plastic flow of the material caused by frictional heating and subsequent pushing under compressive force were expected to influence the formation of stacked layers. The surface profile of the stacks is shown in Figure 4.44f. It is observed that the height of the stacks reduced gradually in a sequential order confirming their formation. Figures 4.44g and 4.44h show the typical wear furrows formed on the NC0.0 and NC2.0 test samples, respectively, where the corresponding wear furrow was observed to be 3.35 and 1.95 μm. The images observed in AFM are strongly supporting the observation and discussion made against wear mechanism shown in Figure 4.44.

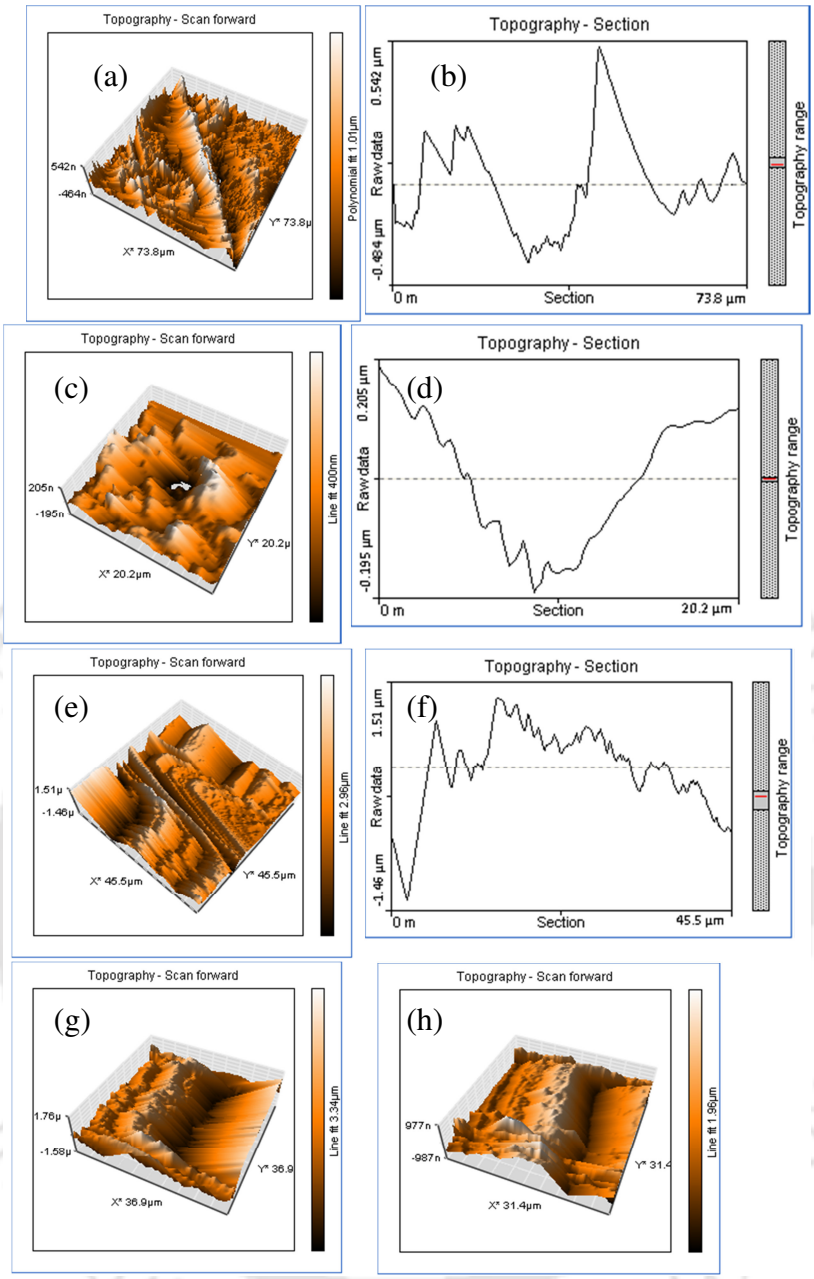

Figure 4.44. Surface topography and typical wear profiles observed on the test samples (a, b, c, d and, g corresponds to polymer; e, f and, h corresponds to 2 wt. % composite) a) Plastic deformation b) Surface profile of (a) c) Wear crater d) Surface profile of (c) e) Piling of material due to plastic flow f) Surface profile of (e) g and h) Wear furrow

4.4.3 Wear studies on irradiated composites and α_T blends

4.4.3.1 Wear studies on irradiated composites

Wear studies were performed on both composites and α_T blends after irradiation. The wear volume of the composites against sliding distance at 25 and 100 kGy irradiation doses is shown in Figures 4.45a and 4.45b, respectively. It is observed that the trend of wear volume was similar to that of unirradiated samples. It is also observed that the wear volume of virgin UHMWPE at 25 kGy was found to be 1.29 mm^3, which was reduced to 0.88 mm^3 by reinforcing 2 wt. % MWCNTs corresponding to a reduction of 31 %. In addition to that the GI100NC2.0 composite exhibited 40 and 73 % reduction of wear volume compared to that of GI100NC0.0 and unirradiated pure polymer samples, respectively. Figure 4.45c shows the wear factor of polymer and its composites at different irradiation doses and MWCNTs concentration. It is observed that the wear factor of the test samples was reduced with an increase of irradiation dose and MWCNTs concentration. The wear factor of GI25NC0.0 test sample was found to be 1.036×10^{-6} mm^3/N-m, which was reduced to 5.363×10^{-7} mm^3/N-m upon irradiation at 100 kGy corresponding to almost 50 % reduction. Similarly, the wear factor of GI25NC2.0 sample was also reduced by 50 % at 100 kGy irradiation dose. The combined effect of 2 wt. % MWCNTs reinforcement and 100 kGy irradiation was observed to be considerably more than that of the individual effects due to defect mediated crosslinks in the polymer.

The coefficient of friction of 100 kGy irradiated UHMWPE and composite test samples against sliding distance is shown in Figure 4.45d and it is found to be decreased initially with sliding distance during the run-in stage similar to that of unirradiated samples. At 100 kGy irradiation dose, the average coefficient of friction was found to be 0.110, 0.109, 0.104, 0.098, and 0.093 for pure polymer, 0.5, 1.0, 1.5 and 2.0 wt. %, respectively. The coefficient of friction

of 100 kGy irradiated sample was decreased compared to that of unirradiated test sample, which was discussed against Figure 4.42. The reduction of coefficient of friction at 100 kGy irradiation dose is attributed to the generation of less wear debris due to increased crosslink density, Zhou et al. [2005]. It could also be due to molecular chain rearrangement and restructuring of the lamellae below the articulating surface parallel to the sliding direction, Klapperich et al. [1999].

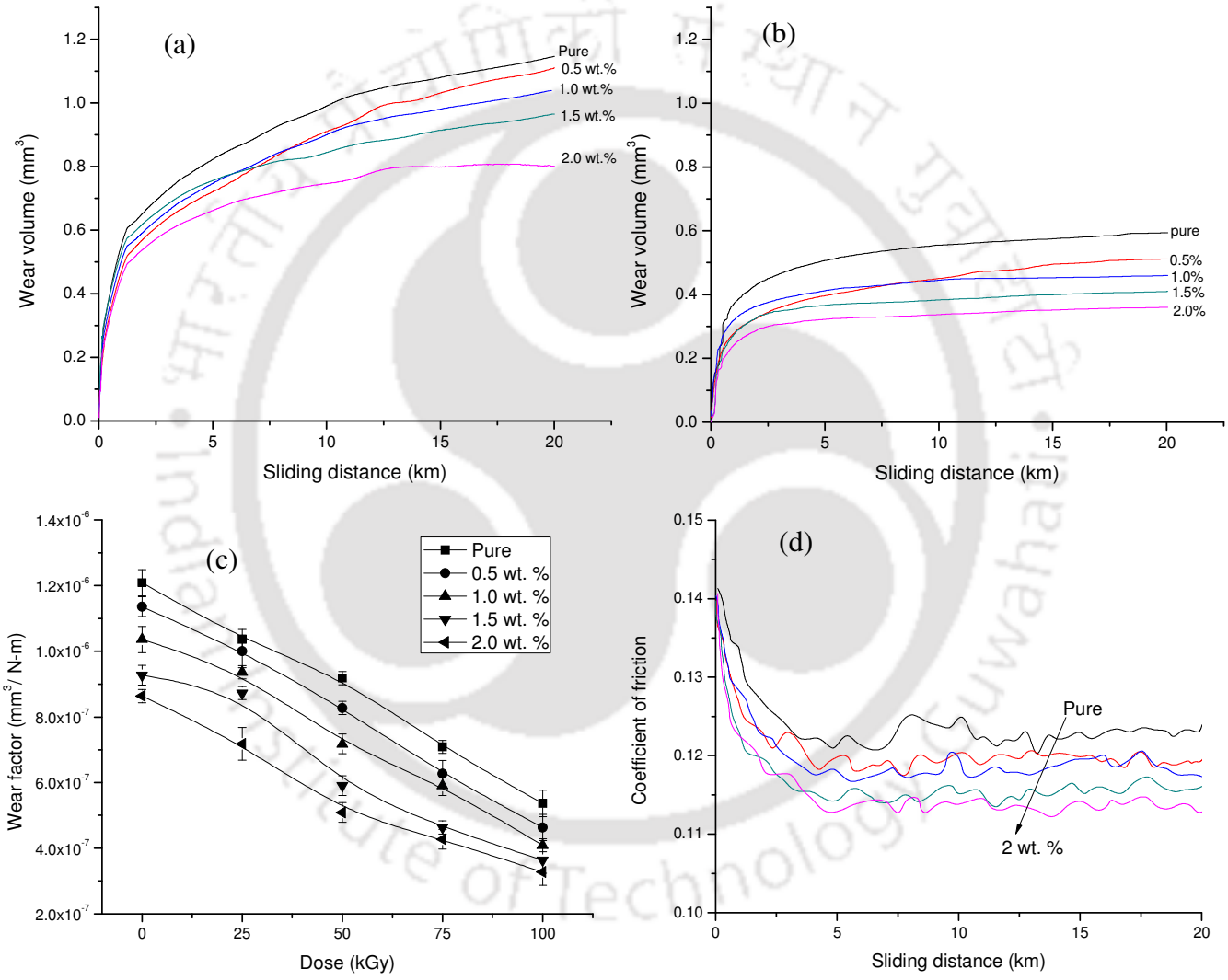

Figure 4.45. Sliding distance vs. wear volume at a) 25 kGy b) 100 kGy c) Wear factor of composites at different irradiation doses d) Coefficient of friction of composites at 100 kGy dose

Figure 4.46 shows the surface morphology of 100 kGy irradiated wear test samples. It is observed from Figure 4.46a that the wear debris formed on the GI100NC0.0 test sample was found to be very fine powder of less than 1 μm size. It is due to the fact that UHMWPE reduced its ductility due to irradiation induced oxidation. The wear debris generated from the test sample may possibly be trapped and leading to third body wear between the test sample and the counterface material. During the process, the particles were pulverized into fine wear debris. Figure 4.46b shows the size of the wear debris of the composites, which was not varied significantly before and after gamma irradiation. Figures 4.46c and 4.46d show the plastic flow and deformation caused by the frictional heating on the 100 kGy irradiated NC0.0 and NC2.0 samples, respectively. It is observed that the intensity of plastic flow and deformation was less in case of composite compared to that of pure polymer. Moreover, the severity of plastic flow of both UHMWPE and composites under irradiated condition was found to be less than that of unirradiated condition. It is due to the fact that the irradiation of UHMWPE led to increase of its surface hardness, which was also confirmed in section 4.4.1. Figures 4.38e and 4.38f show the microcutting and wear furrows in NC0.0 and NC2.0 wear test sample, respectively. It is observed that the irradiation of test samples reduced the effect of microcutting due to increase of their hardness. It is also observed that the wear mechanism of UHMWPE is not affected by the irradiation dose and the presence of MWCNTs but its severity was significantly reduced.

Figure 4.47 shows the AFM images of 100 kGy irradiated samples. Figures 4.47a and 4.47b show the deformation due to plastic flow in the NC0.0 and NC2.0 test sample, respectively. It is observed that the deformation was more severe in NC0.0 sample compared to NC2.0 sample. Figures 4.47c and 4.47d show the wear craters on NC0.0 and NC2.0 test sample, respectively. The depth of wear craters in NC0.0 and NC2.0 was observed to be 0.3 and0.23 μm, respectively.

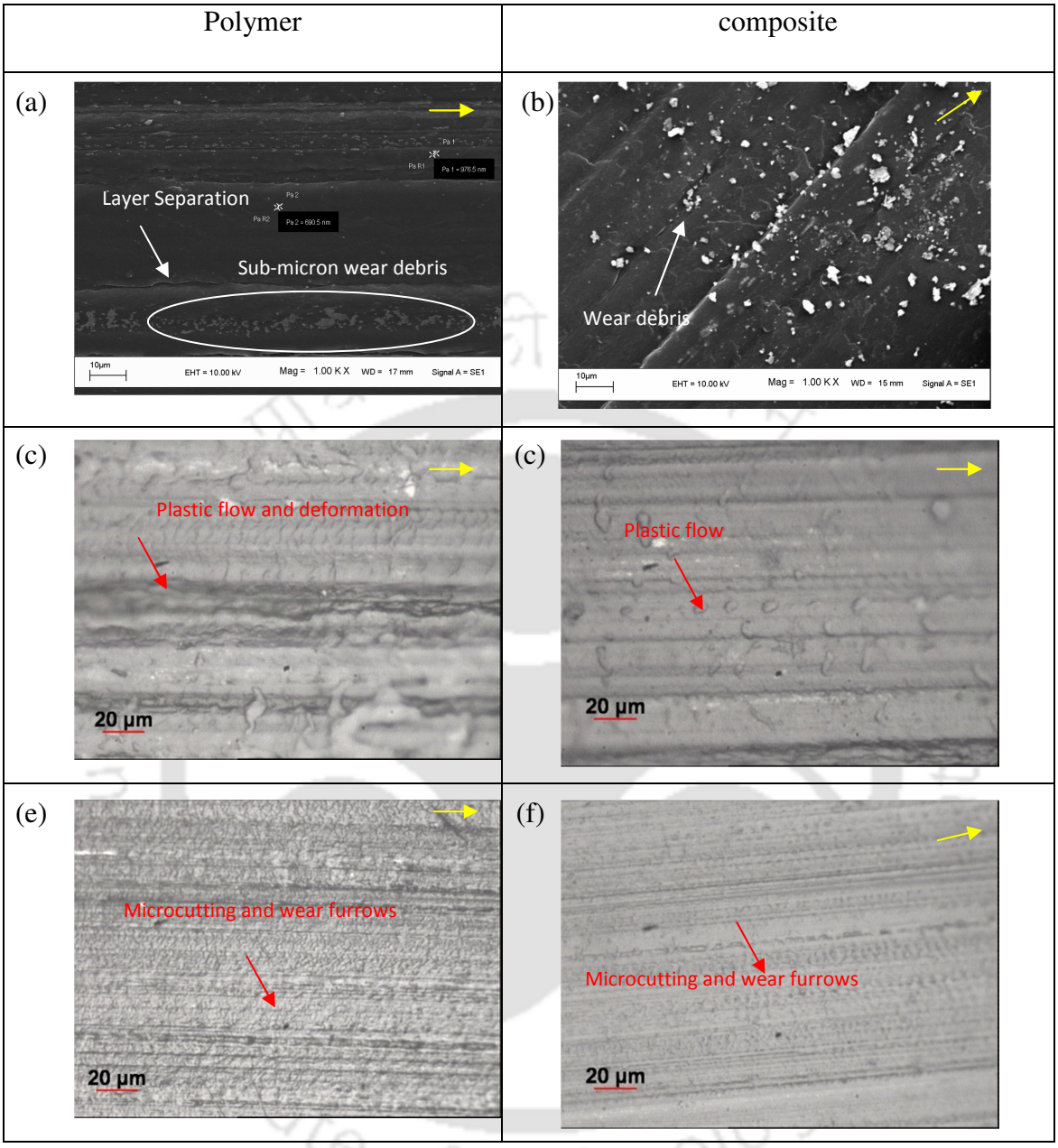

Figure 4.46. Representative SEM and optical microscopy images of the test samples after 100 kGy gamma irradiation showing different wear mechanisms. (a, c, e - for NC0.0; b, d, f – for NC2.0 samples). (a, b) Wear debris and cracks formed on the test surface (c, d) Plastic flow and deformation (e, f) Micro-cutting and wear furrows on the test surface

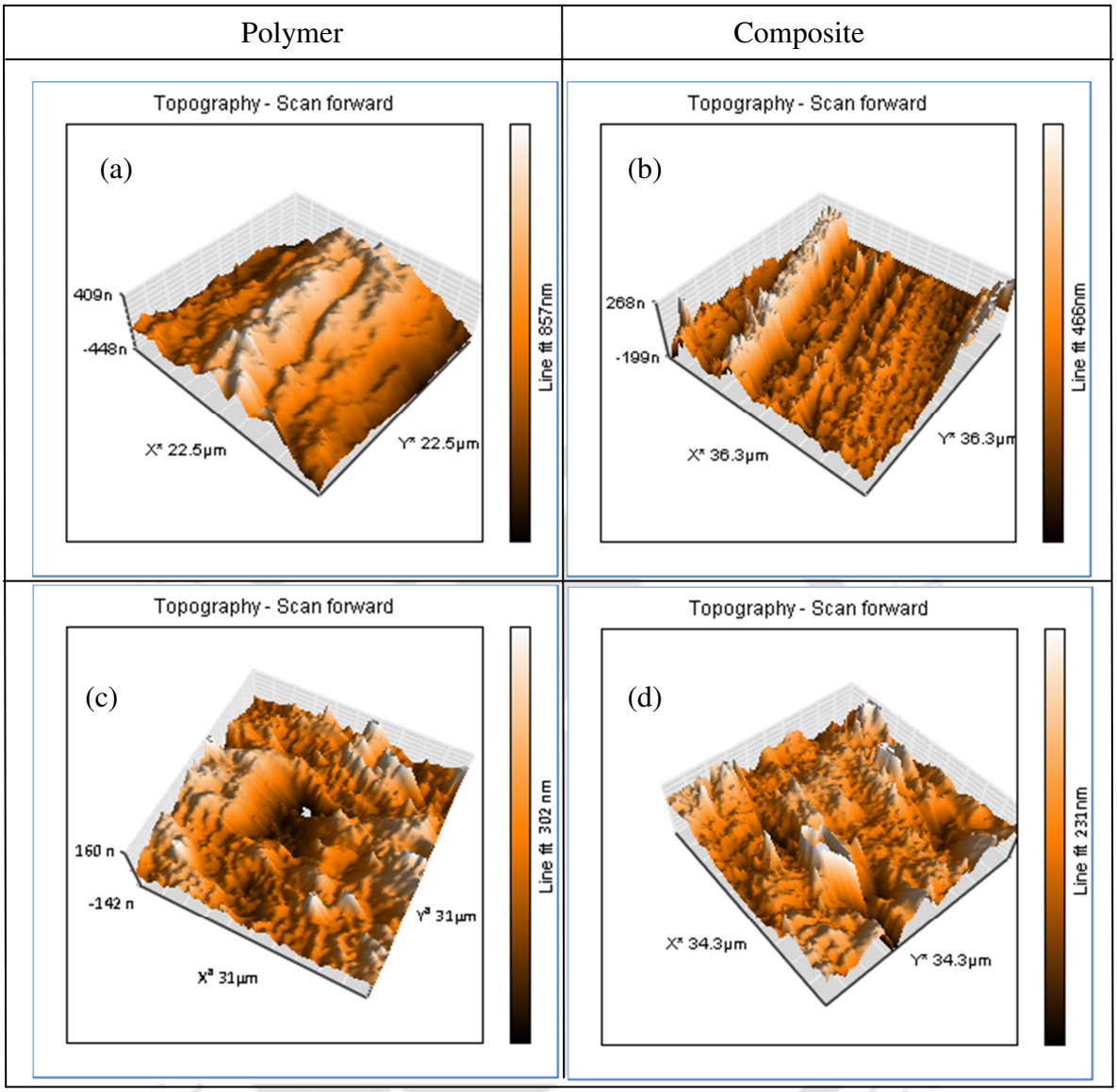

Figure 4.47. Surface topography of the 100 kGy irradiated test samples (a and c correspond to polymer; b and d correspond to 2 wt. % composite). (a,b) Plastic flow and deformation (c,d) Formation of wear craters

4.4.3.2 Wear studies on irradiated α_T blends

As the work to failure of 25, 50 and 75 kGy α_T blends was found to be within the experimental deviation as that of unirradiated pure polymer, which is discussed in detail in

section 4.2.1, and a noticeable enhancement of the work to failure of the sample was observed only at 100 kGy irradiation dose, the sample irradiated at 100 kGy was tested and reported. Figure 4.48a shows the wear volume pattern of 100 kGy irradiated α_T blended UHMWPE against sliding distance. It is observed that the wear volume of 100 kGy irradiated UHMWPE sample was increased from 0.59 mm^3 to 0.73, 0.91 and 0.93 mm^3 by the addition of 0.1, 0.3 and 0.5 wt. % α_T, respectively, corresponding to an increase of 23.7, 54.2 and 57.6 %. It is due to the fact that the presence of α_T restricted the process of crosslinking and the plasticizer effect of α_T caused the softening of the polymer leading to reduced work to failure of UHMWPE. The wear factor of α_T blend samples after a sliding distance of 20 km is shown in Figure 4.48b and the results are compared with that of pure polymer. The wear factor of 100 kGy irradiated pure UHMWPE was found to be 5.363×10^{-7} mm^3/N-m, which was increased to 8.453×10^{-7} mm^3/N-m for GI100α_T0.5 sample. It is observed that the wear factor of pure UHMWPE at 100 kGy dose was found to be increased with α_T concentration.

Assuming that the wear volume of unirradiated virgin UHMWPE as 100 percent, the percentage wear volume of the unirradiated and irradiated composites and α_T blends is calculated and the corresponding wear factor was also inscribed in the plot and it is shown in Figure 4.49. It is observed that the wear volume of NC2.0, GI100α_T0.1, GI100NC0.0, and GI100NC2.0 test samples, respectively, after 20 km sliding distance was reduced to 71, 59, 44 and 27 % of the wear volume of unirradiated virgin UHWMPE. It can be concluded that the combined effect of MWCNTs reinforcement and 100 kGy irradiation reduced the wear factor of UHMWPE significantly.

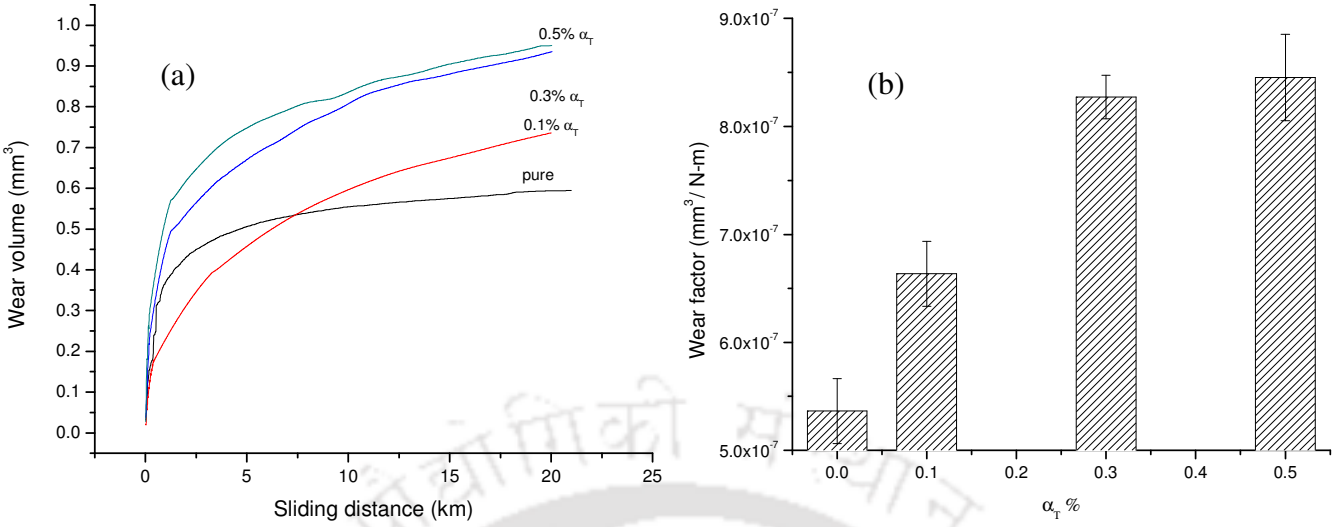

Figure 4.48. a) Sliding distance vs. wear volume of 100 kGy irradiated α_T blends b) Wear factor of 100 kGy irradiated α_T blends at a sliding distance of 20 km

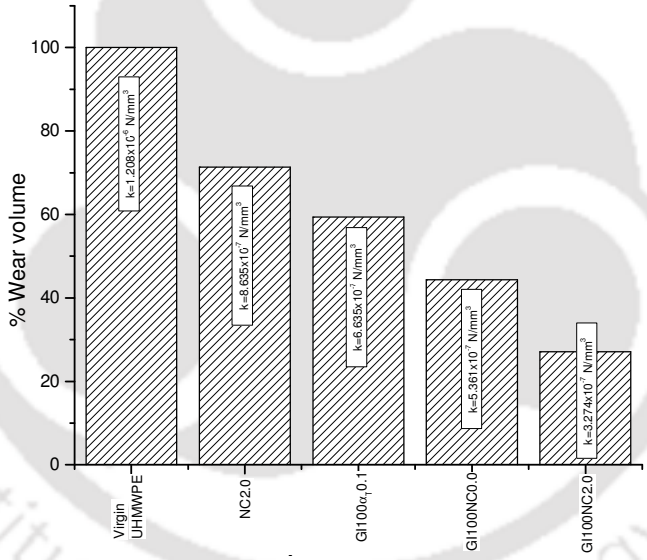

Figure 4.49. Percentage wear volume and wear factor of unirradiated, irradiated composites and α_T blends

The wear results obtained from the present study were compared with the literature. Comparison would be very difficult in the wear studies as the sliding conditions such as sliding distance, sliding velocity, lubricant etc would be varied. However, the same was made to the extent possible. Comparison of wear results from different literature is a mere indication to estimate the

feasibility of the developed composite. It is to be noted that there are significant differences in the wear testing conditions, which influence the wear characteristics of the materials.

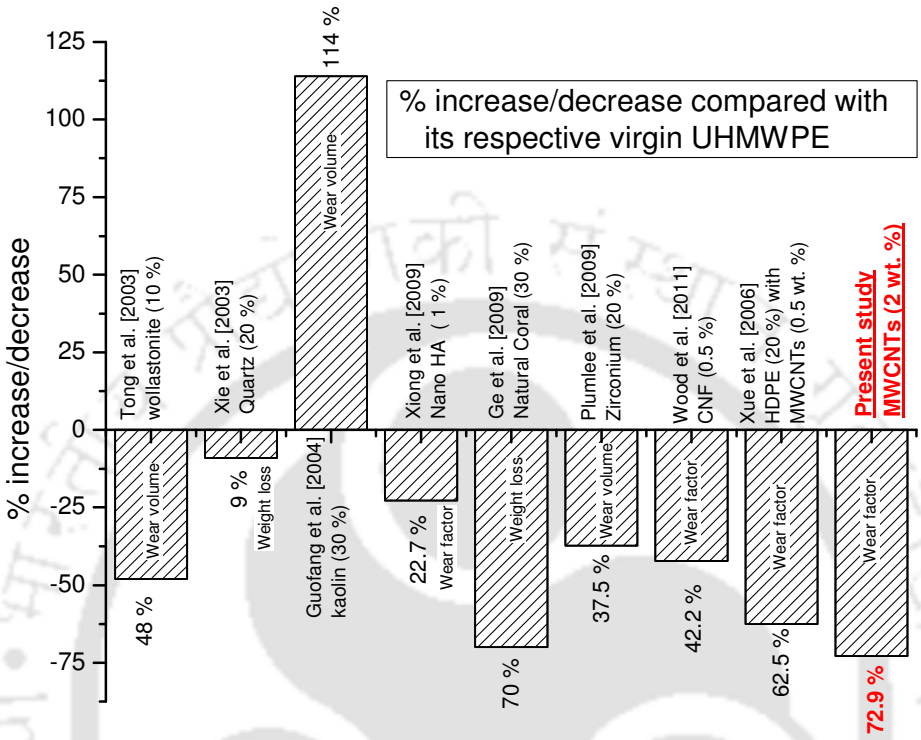

Figure 4.50. Comparison of wear results obtained from literature with the present study

Figure 4.50 shows the percentage/increase of wear volume/wear factor/mass loss of different composites compared with its respective virgin UHMWPE. It is observed from Figure 4.50 that the wear volume/wear factor/mass loss of UHMWPE was reduced by reinforcing different fillers.

4.4.4 Summary of the studies on wear behaviour of composites and UHMWPE/α_T blends before and after irradiation

Wear primarily depends on surface hardness and roughness of the test samples. As the roughness of the test sample was kept constant, the hardness of all the test composites and α_T blends was

studied using the Nanoindenter. It was observed that the hardness of the sample was increased with MWCNTs concentration and irradiation dose. In case of α_T blends, the hardness was reduced with an increase of α_T concentration but increased with irradiation dose. The wear studies on composites and α_T blend samples were performed over a sliding distance of 20 km under dry sliding conditions against SS316L disc conforming to ISO-5832-1 standards. It was observed that the wear volume and the coefficient of friction of UHMWPE were reduced with an increase of MWCNTs concentration. Different wear mechanisms such as microcutting, ploughing, plastic flow, wear crater formation, and delamination were observed in the test samples. However, the severity of these effects was found to be reduced in case of irradiated composites compared to that of virgin UHMWPE. In case of α_T blends, the wear volume was increased with α_T concentration. The wear volume of both composites and α_T blends was reduced with an increase of irradiation dose. The wear volume of NC2.0, GI100α_T0.1, GI100NC0.0, and GI100NC2.0 test samples, respectively, after 20 km sliding distance was reduced to 71, 59, 44 and 27 % of the wear volume of virgin UHWMPE.

4.5 Biocompatibility studies on composites

The success of any material intended for biomedical application depends on its biocompatibility. Thus, some preliminary biocompatibility tests such as simulated body fluid test, platelet adhesion test and *in vivo* subcutaneous tests were conducted. In order to reduce the number of animals involved in the study for *in vivo* characterization, the test was performed only on the 2 wt. % composite.

4.5.1 Simulated body fluid (SBF) studies

The composites were soaked in the SBF solution for a predefined period and incubated at 37 ^{0}C to replicate the human body temperature. The weight of the samples was monitored at predefined regular intervals after soaking them in SBF to assess the coating of HA. The effect of immersion time of the samples on the pH value of SBF solution was also studied. Figure 4.51a shows the percentage enhancement of weight of the sample at different soaking time with respect to its initial weight, where a rapid enhancement of the sample weight was observed during the initial period of soaking. The sample weight was increased by 11.7 % after 7 days of soaking, but it was limited to 12.9 and 13.2 % after 15 and 30 days of its immersion, respectively. It indicates that the deposition rate of apatite has attained an equilibrium after 15 days of the sample immersion in SBF. The Ca and P required for the apatite formation were extracted from the SBF solution. The formation of apatite layer on the surface of composites was a dynamic process, where the apatite layers were initially precipitated on the material surface and then dissolved. The precipitation and dissolution of the salts on the surface of the composites occurred simultaneously. During the initial period of time, the amount of dissolution was very slow as it was proportional to the surface area of the precipitated salts and thus the rate of increase of weight of the sample was high. The surface area of the precipitated salts increased with time and the dissolution rate was also increased consequently. The process of dissolution and precipitation reached an equilibrium over the time and thus, the enhancement of the sample weight attained a constant value, which is shown in Figure 4.51a. Figure 4.51b shows the influence of the immersion time of composites on the pH value of SBF. It is observed that the pH value of SBF solution was 7.35 before immersion of the test sample, which is similar to that of human blood plasma, Xin et al. [2009]. The pH value of SBF solution was increased slightly with immersion time of the sample during the early stage, which was resulted from the accumulation of OH^- in

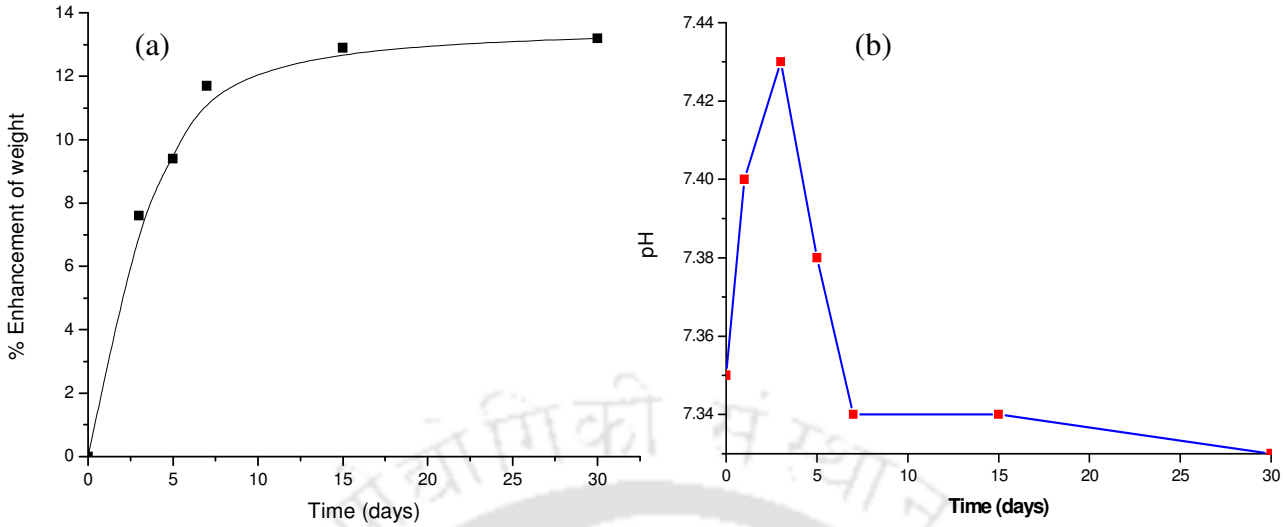

Figure 4.51. a) Enhancement of the sample weight against soaking period in SBF b) pH value of SBF solution at different soaking periods of the test sample

the solution due to the deposition of Ca^{+2} ions on the test surfaces. Thus, the pH value of SBF solution reached its maximum i.e. ~ 7.43 on the 3rd day, which is slightly higher than the normal value of human blood plasma. After immersion of the sample for 30 days, the pH value of SBF was reduced to 7.33 which is equivalent to the normal value of human blood plasma. Due to the deposition of Ca and P on the surface, OH^- is now extracted from the SBF solution to form apatite and thus the pH value decreased gradually during the later stages of sample immersion.

The SEM images of the apatite layer formed on the surface of composites are shown in Figures 4.52a-4.52f. Figure 4.52a shows the apatite layer formed on the composite surface with few uncovered regions of the test sample. A very thin layer of HA was observed on the test sample after one day of soaking. The leaf like apatite disappeared with an increase of soaking time and the number of thicker and denser spherical crystals was increased after 3 and 7 days of soaking period, which is shown in Figure 4.52b and 4.52c, respectively. It is clearly observed that the density of the coating was increased with the soaking period of the test sample. Figure

4.52d shows the test surface after 15 days of soaking period, where the apatite layer grew very thick and no crystals were visible but a dense film of apatite was formed and covered the surface

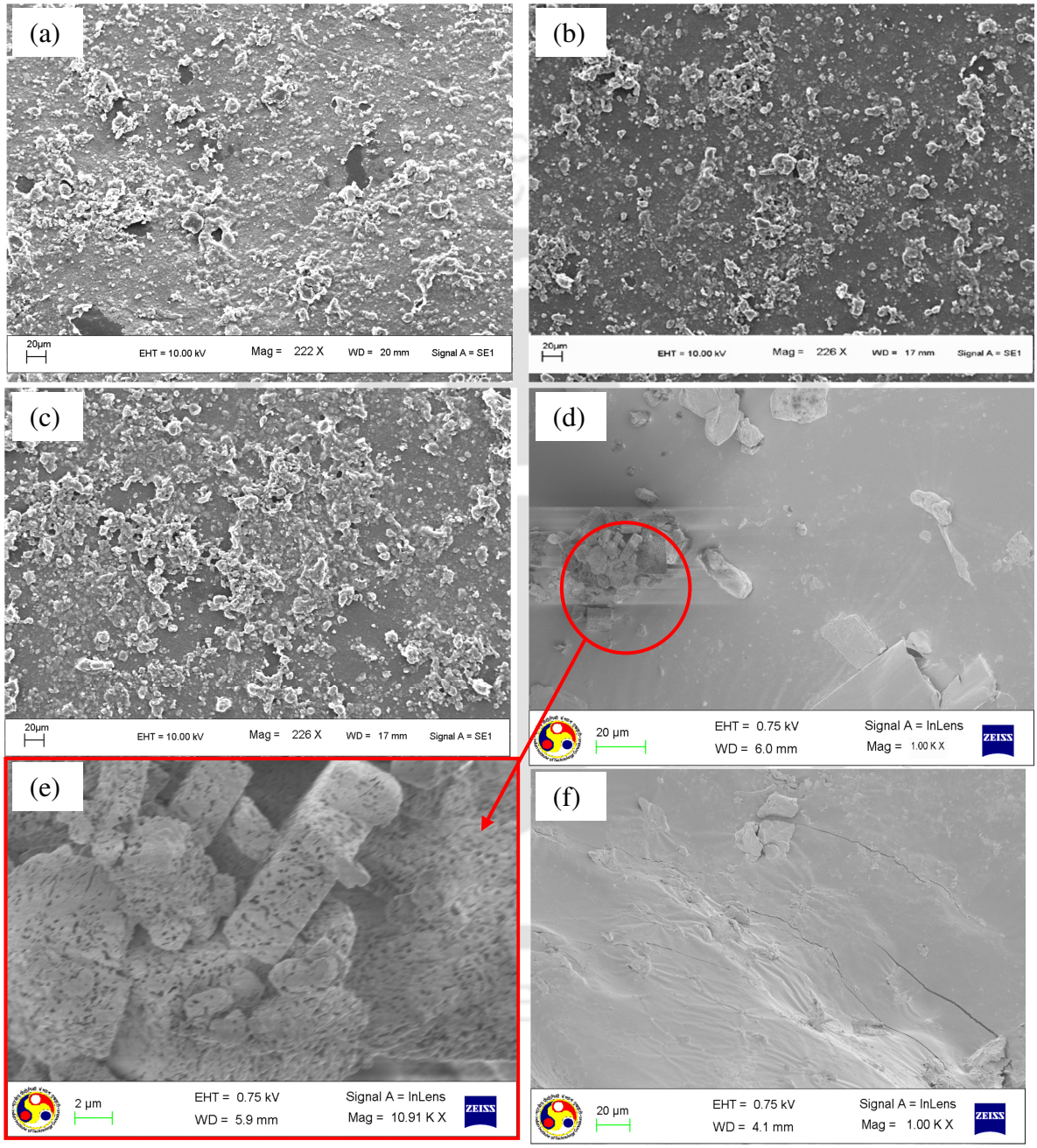

Figure 4.52. Formation of apatite layer on the surface of composites after different periods of soaking a) 1 day b) 3 day c)7 day d) 15 day e) magnified view of a particle observed on 15 day f) 30 days

of the sample. Figure 4.52e shows the magnified view of the apatite particles, where pores are observed. As the duration of soaking period increased, the thickness of the apatite layer formed on the test surface was also increased. Few cracks were observed on the apatite layer, shown in Figure 4.52f, due to its brittle nature and poor mechanical properties, Sousa et al. [2003].

The sequence of formation of the apatite layer described above agrees well with the mechanics of formation of bone-like apatite as described by Eichert et al. [2005] and Kokubo et al. [2004]. In order to further confirm the formation of apatite, EDAX and micro-Raman spectra were obtained and shown in Figures 4.53a and 4.53b, respectively. The formation of Ca and P was confirmed by EDAX spectra, which is shown in Figure 4.53a. Figure 4.53b shows the Raman spectra confirming the presence of mineral phase of the hydroxyapatite. Raman peaks are observed at 962 and 3576 cm^{-1} corresponding to PO_4^{3-} symmetric stretching modes and OH^- stretching, respectively. The band observed in the range of 400- 490 cm^{-1} also corresponds to internal PO_4^{3-} modes. It is noted from Reisel et al. [2002] that the formation of peak at 962 cm^{-1} is a strong indication of the formation of HA and broadening of the same indicates the presence of amorphous region of calcium phosphate.

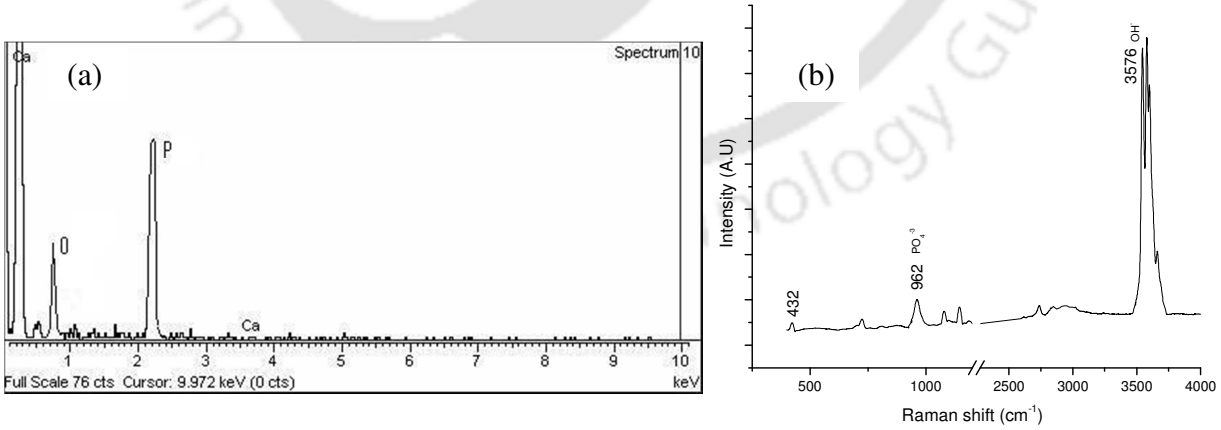

Figure 4.53. a) EDAX b) Raman spectra of the apatite layer formed on the composites

4.5.2 Platelet adhesion test

The potential blood compatibility of the composites was tested by assessing its anti-thrombus characteristics by observing the platelets adhered on the surface of the test material. The platelets adhered on the surface of pure UHMWPE and 2 wt. % composites under the same conditions were shown in Figures 4.54a-4.54d. It is observed from Figures 4.54a and 4.54b that the number of adhered platelets on composites was lesser compared to that of pure UHMWPE. However, the shape of platelets was not varied significantly for 2 wt. % composite after 30 minutes of incubation. It can also be observed that the adhered platelets were not conglomerated and most of them fall in the range of single platelet having the dimension of 2-4 μm and it was also supported by Ren et al. [2005]. When the incubation period was increased to 3 hours, the number of adhered platelets was also found to be increased for both pure polymer and 2 wt. % composite, which are shown in Figures 4.54c and 4.54d, respectively. There was no change in the shape of the platelets in both cases. It is also observed that there was no severe conglomeration of platelets even after 3 hours of incubation, which confirmed that the platelets were not in activated state. Figure 4.54e and 4.54f show the number of platelets adhered on the test sample, where it is observed that the presence of MWCNTs has slightly reduced the number of adhered platelets. After 30 min. of incubation, the number of platelets adhered on the surface of UHMWPE per 1000 μm^2 was 56, which was reduced to 45 for 2 wt. % composite corresponding to 20 % reduction. The number of platelets adhered after 3 hrs of incubation was reduced from 142 to 129 for pure UHMWPE and 2 wt. % composite, respectively corresponding to 9.1 % reduction. From the above study, it is observed that the addition of MWCNTs has not affected the anti-thrombic nature of UHMWPE. According to Ko et al. [1993], the qualitative assessment score of activation status of adhered platelets varied from 1 (unactivated) to 5 (highly

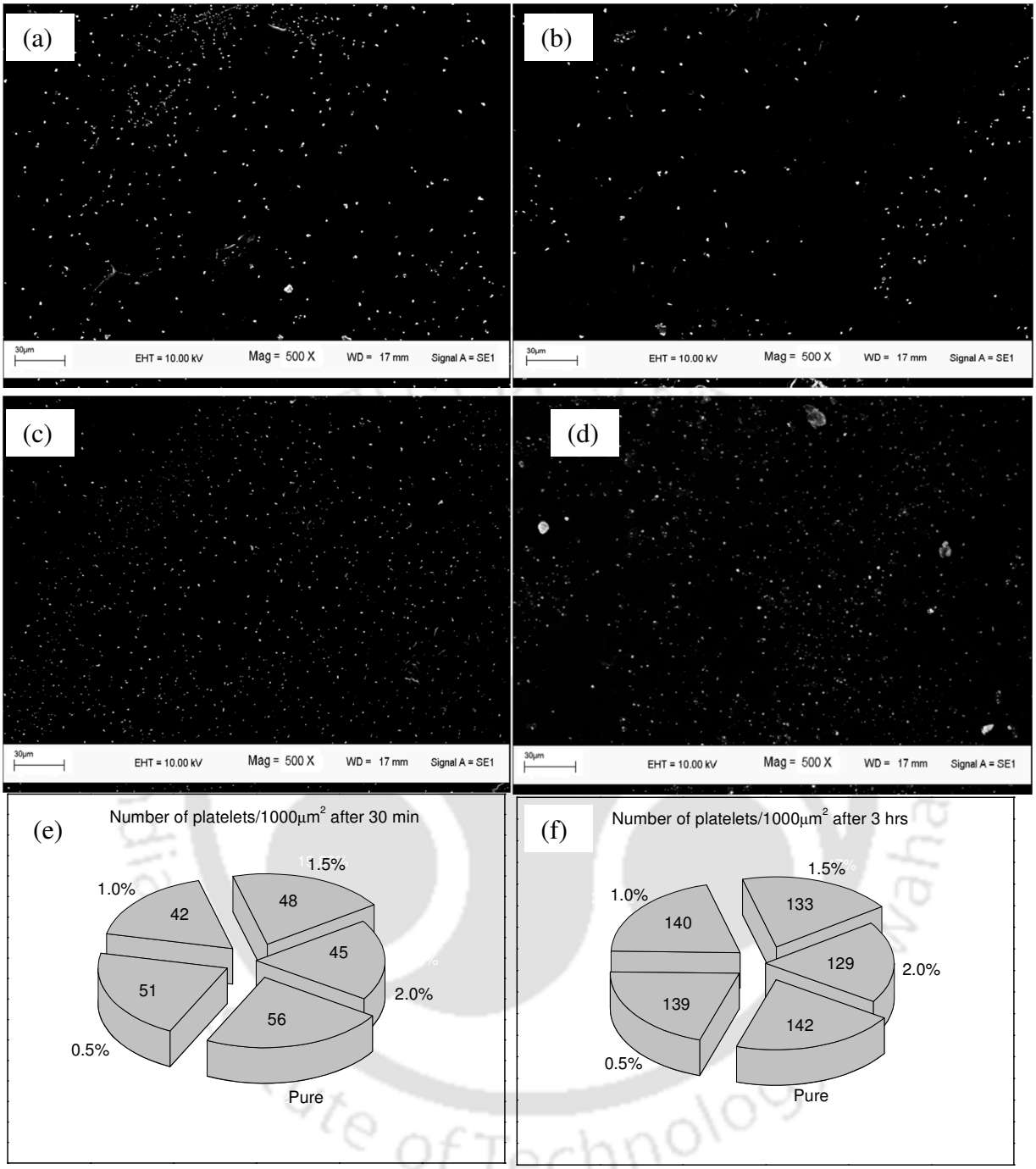

Figure 4.54. (a) SEM images of platelets adhered on UHMWPE within 30 min. b) SEM image - 2 wt. % composite within 30 min. c) SEM image - UHMWPE after 3 hrs d) SEM image 2 wt. % composite after 3 hrs e) Number of platelets adhered on test samples after 30 min. f) Number of platelets adhered on test samples after 3 hrs

activated). The same classification was further elaborated by Rhodes et al. [2007] based on the shape of the platelet, which are described as follows: 1- round; 2- dendritic; 3- spread-dendritic; 4- spreading and 5- fully spread. It is observed that most of the platelets were found to be round in shape (score 1), confirming their unactivated state. A few platelets with a very mild dendritic shape were also observed occasionally, hence a score of 1.5 was given for the 2 wt. % composite. It is concluded that the anti-platelet adhesion characteristics of pure UHMWPE was not affected by the reinforcement of MWCNTs.

4.5.3 *In vivo* subcutaneous test

All the animals survived during the entire test period and no abnormal behavioral changes in animals were observed. The histopathology slides of UHMWPE and 2 wt. % composite are shown in Figures 4.55a – 4.55e. The inflammatory mediators were released after implantation of test and reference materials in experimental animals. The inflammatory mediators were polymorphonuclear (PMN), macrophages, lymphocytes, plasmacells that were examined and quantified depending on their occurrence in the slide: Nil (0), occasional (0.5), mild (1) moderate (2) and severe (3). After quantification of these values according to the method given by Upman et al. [1998], the nature of the material is identified as non-irritant (0-2.9), slight irritant (3-8.9), irritant (9-15) and severely irritant (>15) characteristics.

PMN plays an important role in both acute and chronic inflammation and it is crucial for defense mechanism in the host, Khan et al. [2001]. PMN cells assume different shapes, regulate immune responses, participate in angiogenesis and play a crucial role in tumor biology. Different types of cells that are observed in the histopathological slides were represented in Figure 4.55a. In the present study, these cells occasionally observed in some test slides as well as in reference slides. Plasma cells were also observed in few slides occasionally, and their primary function is

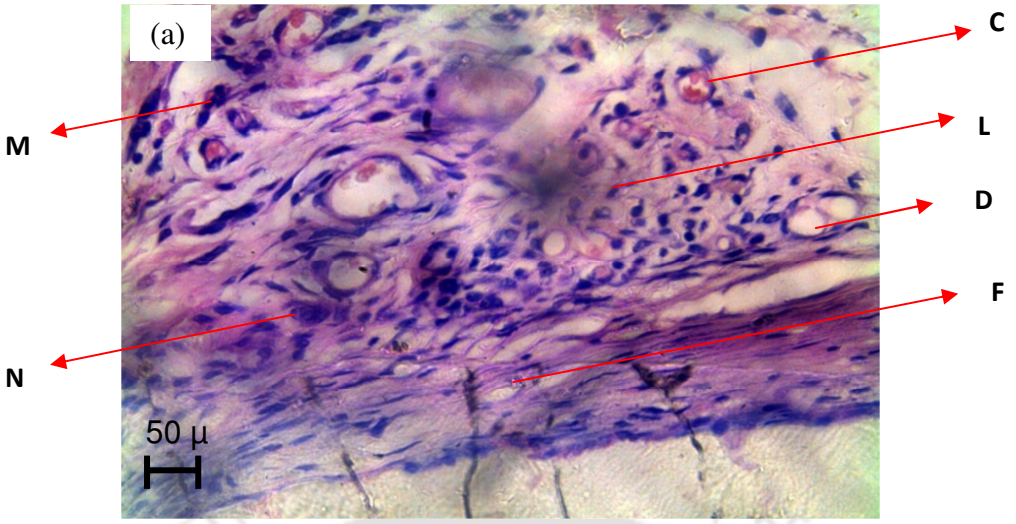

C-Capillaries, D- dilatation of blood capillaries, F- Fibrosis, L- Lymphocytes, M- Macrophages, N- Polymorphonuclear cells (Neutrophils or PMN).

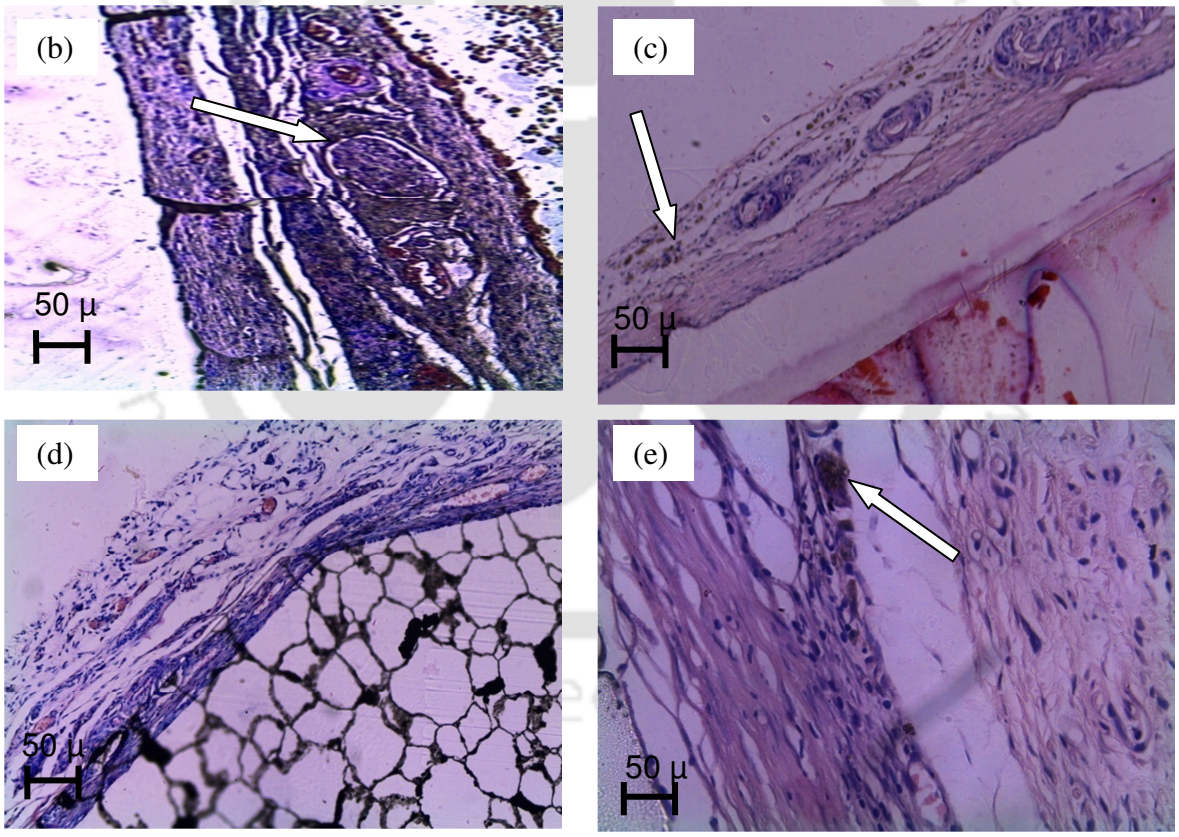

Figure 4.55. a) Histopathological slide of UHMWPE showing different elements b) Arrow indicating granulomatous inflammation with macrophages in UHMWPE c) Arrow showing macrophages d) Pathological slide of 2 wt. % composite e) Macrophages observed in 2wt. % composite indicated by the arrow

to produce antibodies and thus form an important part of immune system, Sato et al. [2008]. Lymphocytes, responsible for immune responses, were seen predominantly in all the slides. Lymphocytes are primarily two types and the secretions from them stimulate the functional activities of other type of cells and thus these are very frequently present at the sites of chronic inflammation indicating an allergic response to foreign material, Cassatella [2003]. Differentiation of monocytes in tissues produces macrophages, which function in both specific and nonspecific type of defense and their principal role is to engulf and then digest the cellular debris or any other foreign material. Giant cell is produced by the fusion of many cells and usually 2 to 3 macrophages are fused to form a giant cell to engulf the large particles, Kapoor et al. [2009]. Giant cells and necrosis are not observed in any slide, either in test or in reference sites. Mild fibrosis was observed in all the slides, whereas fatty infiltrate was not observed in any of the slides.

Table 4.2 Scoring based on the occurrence and presence of different cells at the site of implantation

2 wt.% composite (TEST)						UHMWPE (STANDARD)				
Animal No:	1	2	3	4	5	1	2	3	4	5
Inflammation PMN	1	0	0	1	0	1	0	1	0	0
Lymphocytes	1	2	1	2	1	1	1	2	1	2
Plasma cells	0	0	1	0	1	0	0	0	1	0
Macrophages	1	2	1	2	1	1	2	1	3	1
Giant cells	0	0	0	0	0	0	0	0	0	0
Subtotal x 2	6	8	6	10	8	6	6	8	10	6
Necrosis	0	0	0	0	0	0	0	0	0	0
Fibrosis	1	1	1	1	1	1	1	1	1	1
Fatty infiltrate	0	0	0	0	0	0	0	0	0	0
Sub total	1	1	1	1	1	1	1	1	1	1
Total	7	9	7	11	9	7	7	9	11	7
Group Total	43					41				
Average = TEST – Standard = 43-41=2										

Table 4.1 shows the scoring given for composite and UHMWPE reference based on the occurance of different types of cells as observed in the histo-pathological slides shown in Figures 4.55b- 4.55e . As observed from Table 4.2, the average scoring was calculated to be 2, indicating the non-irritant characteristics of the developed composites. Under the above discussed experimental conditions, it is concluded that composites made by UHMWPE/MWCNTs will not trigger any severe biological responses.

4.5.4 Summary of the biocompatibility studies on composites

As biocompatibility forms an important component in the success of the developed composites, preliminary biocompatibility studies such as simulated body fluid, platelet adhesion test and *in vivo* subcutaneous studies were performed. It was concluded that the bone bonding ability and non thrombogenic characteristics of UHMWPE were not affected by the presence of MWCNTs. Local effects after *in vivo* subcutaneous implantation revealed that the developed composites were non-irritant in nature. However, some more in depth *in vivo* studies as per ISO 10993 standards are required to be carried out prior to any clinical trials.

Chapter 5

Conclusions and future scope

5.1 Conclusions

UHMWPE/MWCNTs composites have been prepared and studied their mechanical properties at 0.5, 1.0, 1.5, 2.0, 2.5 and 5.0 wt. % of MWCNTs and the optimum concentration of filler was obtained. The various mechanisms involved for the enhancement of mechanical properties upto an optimum concentration and the reduction thereafter were suggested and confirmed. Further studies on the composites were limited upto an optimum concentration of MWCNTs. UHMWPE/α_T blends were also studied with 0.1, 0.3 and 0.5 wt. % and compared with MWCNTs reinforced composites in order to study the influence of ageing on the mechanical properties. The composites and UHMWPE/α-T blends were subjected to gamma irradiation at 25, 50, 75 and 100 kGy irradiation doses. The mechanical properties of irradiated samples within 10 days, and 60 and 120 days after irradiation were studied. The presence of MWCNTs in UHMWPE reduced the deteriorating effects of irradiation. Network parameters and the free radical concentration of composites and pure polymer were also identified. The reduction of mechanical properties of MWCNTs reinforced composites was compared with that of α-T blended UHMWPE. An attempt was also made to identify the irradiation induced defects on the MWCNTs. Wear studies on unirradiated and irradiated composites and α_T blends were also performed and the different wear mechanisms were confirmed and identified. Finally, an attempt was made to study the preliminary biocompatibility studies on the developed composites.

The specific conclusions of the present work are summarized as follows.

A. Properties of MWCNTs composites and α_T blends before irradiation

- The optimum concentration of MWCNTs in UHMWPE was found to be 2 wt. %. The work to failure, fracture stress, fracture strain and yield stress of the medical grade UHMWPE were enhanced by 176, 93, 70 and 44 %, respectively at an optimum concentration of MWCNTs.
- The reasons for the enhancement of mechanical properties of composites upto an optimum concentration of reinforcement were attributed to (i) inherent properties of the reinforcement; (ii) homogeneous dispersion of MWCNTs in UHMWPE matrix; (iii) increased crystallinity of the composites and (iv) the effective stress transfer from matrix to filler.
- The rheological percolation threshold was obtained at 0.4 wt. % of MWCNTs, which indicates better debundling and homogeneous dispersion of them in UHMWPE.
- Though the mechanical properties were observed to be reduced beyond 2 wt. % composites, the crystallinity of them was increased till 5 wt. % of reinforcement.
- The reasons for the reduction of mechanical properties of composites beyond optimum concentration of reinforcement were ascertained to (i) the increased viscosity of composite melt; (ii) the reduced amount of polymer available to wet the increased surface area of MWCNTs and (iii) the large difference in thermal properties of the matrix and filler. The above said reasons caused incomplete consolidation of the polymer leading to large number of voids which act as defective zones.
- The surface hardness and Young's modulus of UHMWPE were increased with MWCNTs concentration, while the plasticity index was found to be reduced.

- The mechanical properties of unirradiated UHMWPE were not influenced by the presence of α_T.

B. Properties of MWCNTs composites and α_T blends after irradiation at different time periods

- The work to failure and yield load of the composites and α_T blends were increased with irradiation dose immediately after irradiation due to irradiation induced crosslinks between the polymer chains whereas the strain at fracture of both test samples was reduced with an increase of irradiation dose.
- The work to failure and yield load of composites were increased with MWCNTs concentration, whereas the same was found to be reduced with an increase of α_T concentration in an irradiated UHMWPE.
- The mechanical properties of composites and α_T blends were decreased after 60 and 120 days of irradiation due to free radical induced oxidation. The degradation of properties was found to be increased with irradiation dose. However, it was restricted with an increase of both MWCNTs and α_T concentration in UHMWPE.
- There was no influence of ageing on fracture strain of composites having more than 1 wt. % of MWCNTs.
- The degradation of mechanical properties of UHMWPE was found to be decreased exponentially with an increase in MWCNTs concentration, whereas a linear trend was observed for the same in case of α_T blends.

C. Studies on crosslink density, radical intensity and MWCNT defects

- The crosslink density (CLD) of the UHMWPE was increased with irradiation dose and MWCNTs concentration. In case of α_T blends, the CLD was reduced with an increase of α_T concentration.
- The free radical concentration present in the irradiated sample was found to be reduced with an increase of MWCNTs and α_T concentration in UHMWPE.
- The antioxidant activity exhibited by 2 wt. % MWCNTs is similar to that of 0.1 wt. % α_T in UHMWPE. MWCNTs act as crosslink promoters and chain scission inhibitors in UHMWPE and the same has been schematically represented.
- The d-spacing of MWCNTs was increased with irradiation dose confirming its irradiation induced micro straining. In addition to that the presence of amorphous carbon was also found to be increased with irradiation dose.

D. Wear studies on composites and α_T blends

- The hardness of UHMWPE was increased with MWCNTs reinforcement and irradiation dose. However, the same was reduced with an increase of α_T concentration.
- The wear factor of UHMWPE was reduced with an increase of irradiation dose and MWCNTs concentration. In case of α_T blends, the wear factor of UHMWPE was increased with α_T concentration.
- The coefficient of friction of UHMWPE was reduced with an increase in MWCNTs concentration. It was also found to be reduced with an increase of irradiation dose.
- The severity of plastic flow, deformation and wear delamination of irradiated composites was found to be reduced compared to pure polymer.

- The wear mechanism of unirradiated pure polymer was not affected either by the irradiation dose or MWCNTs reinforcement but the severity of wear was significantly reduced by both variables.
- The wear factor of unirradiated UHMWPE was reduced to 71, 59, 44 and 27 % upon adding 2 wt. % MWCNTs, 100 kGy irradiated 0.1 wt. % α_T, 100 kGy irradiation and a combination of 2 wt. % MWCNTs and 100 kGy irradiation, respectively.

E. Biocompatibility studies on composites

- Preliminary *in vitro* biocompatibility studies revealed that
  (i) The formation of HA on the composites was found to be same as that of pure UHMWPE,
  (ii) The non-thrombic characteristics of UHMWPE were not affected by the presence of MWCNTs.
- *In vivo* subcutaneous studies revealed that the developed composites were non-irritant and not expected to trigger any biological reactions.

In general, it is concluded that the MWCNTs reinforced UHMWPE composites can be explored as a potential alternative for total joint replacements to enhance the longevity of the implant material. Further, the results present in the thesis will also be useful to fine tune the properties of composites after post irradiation heat treatments. In addition to that an elaborate *in vivo* studies in animal models are required to be performed according to ISO 10993 standards prior to any clinical trials.

Schematic illustration showing the influence of γ-irradiation and MWCNTs on different properties of composites.

5.2 Scope of future work

The work presented in this thesis opens up several avenues for further development of the composites for future application of carbon nanotube based composites for orthopedic application. The scope of future work is outlined as follows:

1. The effect of different aspect ratio of MWCNTs on the properties of the composites can be studied. Such studies would provide a better insight into the proper selection of MWCNTs for optimum mechanical properties of the composites.
2. Sandwich composites can be prepared with MWCNTs composite as core and virgin UHMWPE as skin to improve the fracture toughness. The same can also be explored by varying the concentration of α_T at skin and core prior to irradiation.
3. The influence of ion irradiation can be compared with that of gamma irradiation in composites/polymer by following accelerated ageing protocol.
4. Wear studies can be performed under simulated body fluid or bovine calf serum lubricating condition to replicate the human physiological condition in a pin-on-disc machine. Such a study would enable to assess the wear performance of the composites in a more realistic human body environment.
5. Hip simulator studies can be performed to exactly replicate the physiological loading conditions, which can influence the wear mechanisms. Such a study would greatly enhance to envisage the performance of the developed composites.
6. Elaborate biocompatibility studies can be performed confirming to ISO 10993 standards to completely assess the behaviour of developed composites in a biological system.

Schematic illustration of influence of γ- irradiation

Polymer

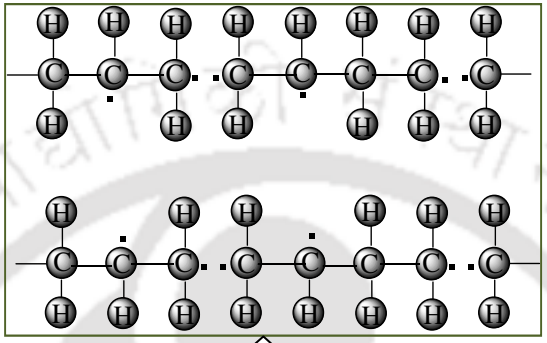

Wear volume

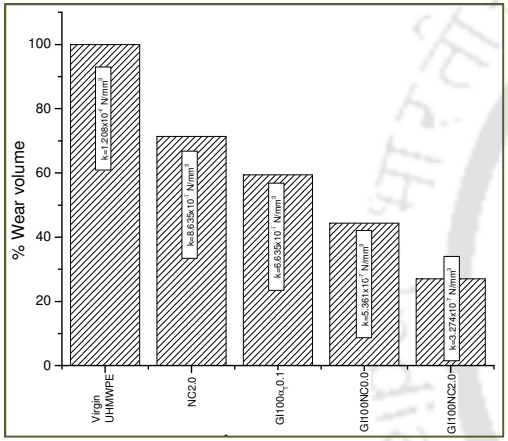

Crosslink density

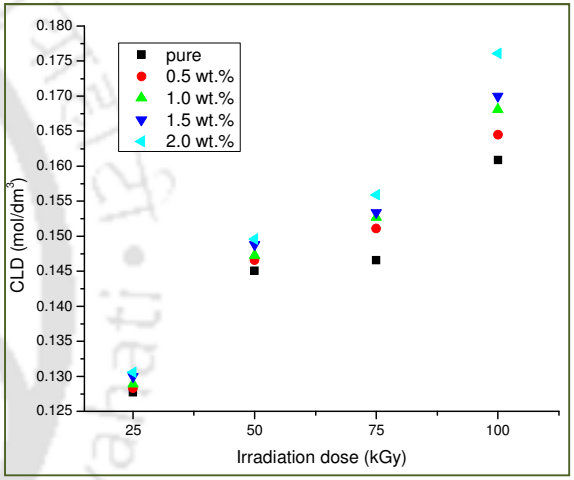

Influence of γ- irradiation

Mechanical properties

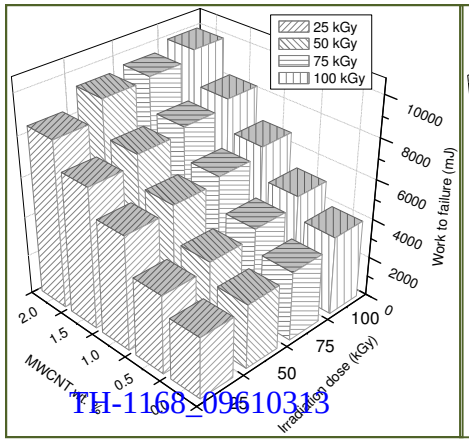

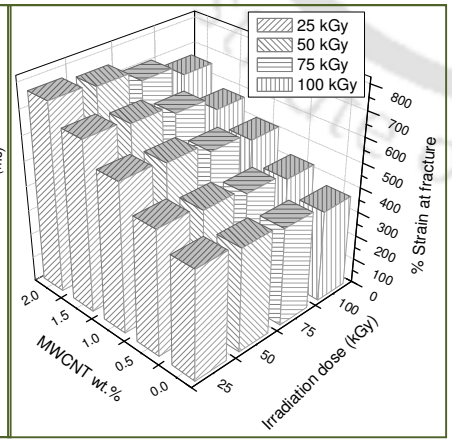

MWCNTs morphology

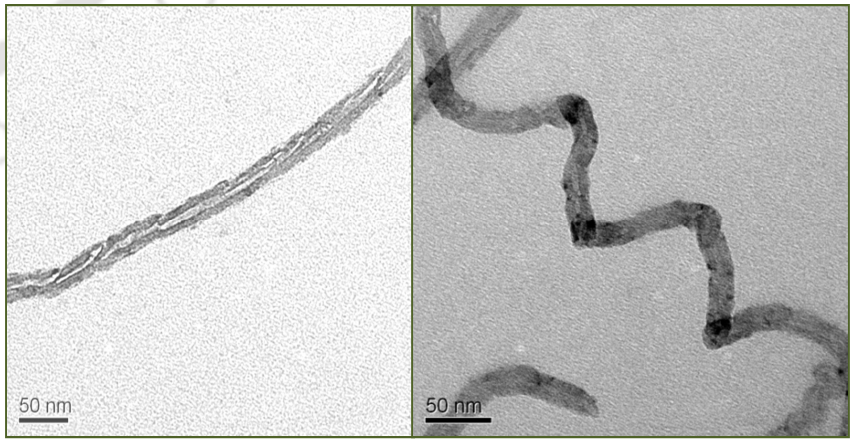

Schematic illustration of influence of MWCNTs

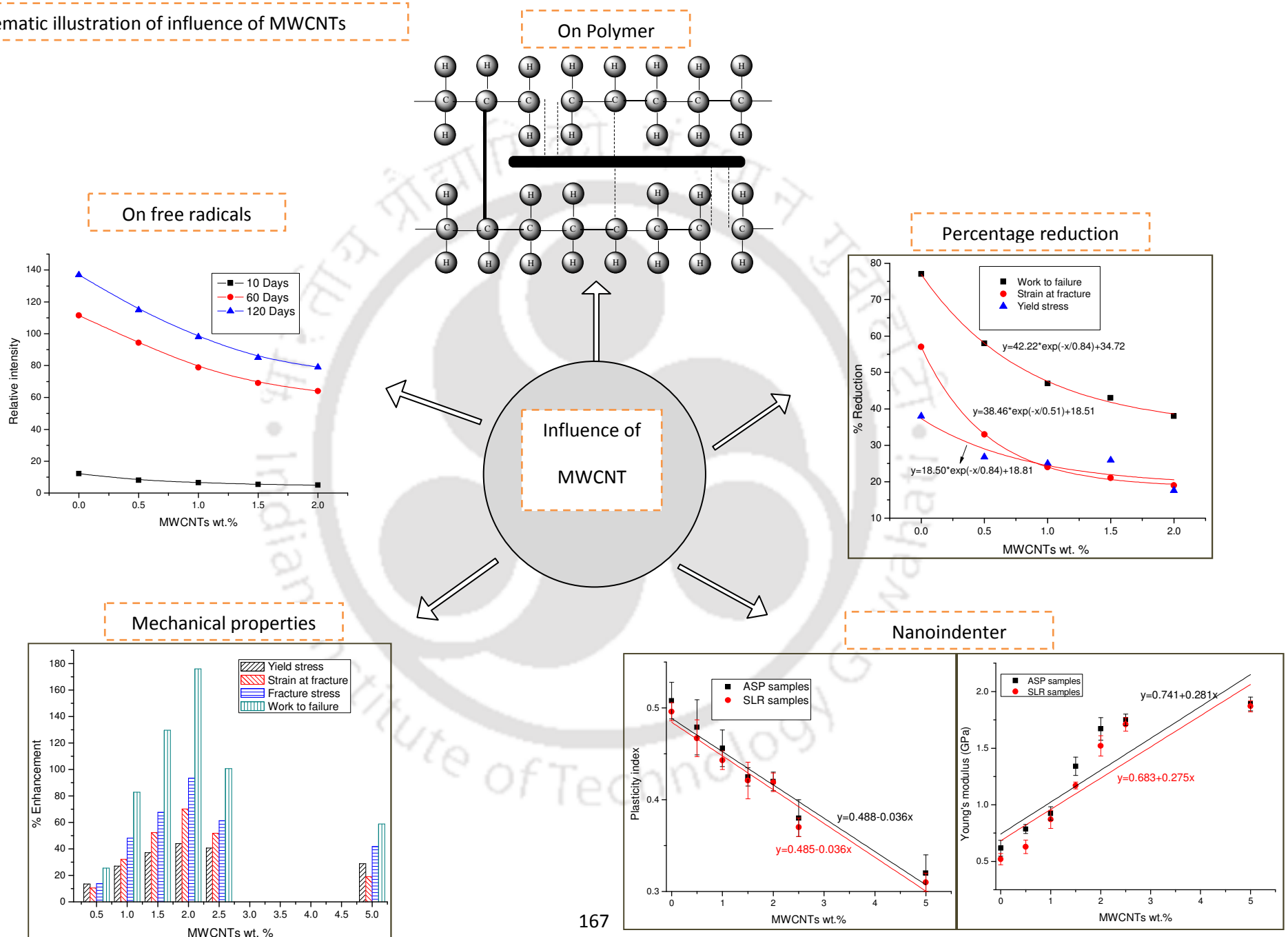

References

1 Amstutz H, Campbell P, Kossovsky N, Clarke I. Mechanism and clinical significance of wear debris-induced osteolysis. Clinical Orthopaedics and Related Research 1992; 276: 7-18.

2 Aquino KAS. Strerilization by gamma irradiation. In Gamma irradiation. Ed Adrovic F, Intech publishers, Croatia, 2012.

3 ASTM F2214–02, Standard test method for *in situ* determination of network parameters of crosslinked ultra high molecular weight polyethylene (Reapproved 2008).

4 ASTM F2625 – 10. Standard test method for measurement of enthalpy of fusion, percent crystallinity, and melting point of ultra-high-molecular weight polyethylene by means of differential scanning calorimetry [Reapproved 2010]

5 ASTM D1708-10, Standard test method for tensile properties of plastics by use of microtensile specimens.

6 Bakshi SR, Tercero JE, Agarwal A. Synthesis and characterization of multiwalled carbon nanotube reinforced ultra high molecular weight polyethylene composite by electrostatic spraying technique. Composites: Part A 2007; 38:2493–2499.

7 Bakshi SR, Balani K, Laha T, Tercero J, Agarwal A. The nanomechanical and nanoscratch properties of MWNT reinforced ultrahigh-molecular weight polyethylene coatings. Journal of the Minerals, Metals and Materials Society 2007a; 59:50-53.

8 Bashyal RK, Eberhardt J, Malchau H. Highly crosslinked ultrahigh molecular weight polyethylene in total hip arthroplasty: no further concerns-affirms. Seminars in arthroplasty 2011; 22:79-81.

9 Belluci S. Carbon nanotubes:Physics and applications. Physica Status Solidi C 2005; 2(1):34-47.

10 Benson RS. Use of radiation in biomaterials science. Nuclear Instruments and Methods in Physics Research B 2002; 191:752–757.

11 Bhushan B. Principles and Applications of Tribology. New York: Wiley, 1999.

12 Bianco A, Kostarelos K, Partidos CD, Prato M. Biomedical applications of functionalized carbon nanotubes. Chemical Communications 2005; 5: 571-577.

13 Black J. Biological performance of materials: Fundamentals of biocompatibility. 2nd ed. Marcel Dekker, New York, 1992.

14 Bracco P, Brunella V, Zanetti M, Luda MP, Costa L. Stabilisation of ultra-high molecular weight polyethylene with Vitamin E. Polymer Degradation and Stability 2007; 92:2155-2162.

15 Briscoe BJ, Fiori L, Pelillo E. Nanoindentation of polymeric surfaces. Journal of Physics. D: Applied Physics 1998; 31:2395–2405.

16 Burger NDL, Vaal de PL, Meyer JP. Failure analysis on retrieved ultra high molecular weight polyethylene (UHMWPE) acetabular cups. Engineering Failure Analysis 2007; 14: 1329-1345.

17 Burroughs BR, Blanchet TA, The effect of pre-irradiation vacuum storage on the oxidation and wear of radiation sterilized UHMWPE. Wear 2006; 261:1277–1284.

18 Burton G, Ingold K. Autoxidation of biological molecules. 1. The antioxidant activity of vitamin E and related chain-breaking phenolic antioxidants in vitro. Journal of American Chemical Society 1981; 103:6472–6477.

19 Cai H, Yan F, Xue Q. Investigation of tribological properties of polyimide/carbon nanotube nanocomposites. Materials Science and Engineering A 2004; 364: 94–100.

20 Cassatella MJ. The neutrophil: An emerging regulator of inflammatory and immune response, Chemical Immunology and Allergy, Vol.83, Karger publishers: Switzerland, 2003.

21 Cataldo F. A Raman study on radiation-damaged graphite by γ-rays. Carbon 2000; 38: 623– 641.

22 Chakrapani N, Zhang YM, Nayak SK, Moore JA, Carroll DL, Choi YY, Ajayan PM. Chemisorption of acetone on carbon nanotubes. Journal of Physical Chemistry B 2003; 107: 9308-9311.

23 Chand N, Dwivedi UK, Sharma MK. Development and tribological behaviour of UHMWPE filled epoxy gradient composites. Wear 2007; 262:184–190.

24 Charlier JC. Defects in carbon nanotubes. Accounts of Chemical Research 2002; 35:1063-1069.

25 Chatterjee T, Yurekli K, Hadjiev VG, Krishnamoorti R. Single-walled carbon nanotube dispersions in poly (ethylene oxide). Advanced Functional Materials 2005; 15(11): 1832-1838.

26 Chen WX, Li F, Han G, Xia JB, Wang LY, Tu JP, Xu ZD. Tribological behavior of carbon-nanotube-filled PTFE composites. Tribology Letters 2003; 15(3): 275-278.

27 Cherukuri P, Gannon CJ, Leeuw TK, Schmidt HK, Smalley RE, Curley SA, Weisman RB. Mammalian pharmacokinetics of carbon nanotubes using intrinsic near-infrared fluorescence. Proceedings of National Academy of Science 2006; 103:18882-18886.

28 Cohen Y, Rein MD, Vaykhansky L. A novel composite based on ultra high molecular-weight polyethylene. Composites Science and Technology l997; 57:1149-1154.

29 Cooper CA, Cohen SR, Barber AH, Wagner HD. Detachment of nanotubes from a polymer matrix. Applied Physics Letters 2002; 81:3873-3875.

30 Costa L, Luda MP, Trossarelli L, Prever EMB, Crova M, Gallinaro P. Oxidation in orthopaedic UHMWPE sterilized by gamma-radiation and ethylene oxide. Biomaterials 1998; 19:659-668.

31 Costa L, Luda MP, Trossarelli L. Ultra-high molecular weight polyethylene: I. Mechano-oxidative degradation. Polymer Degradation and Stability 1997; 55:329-338.

32 Costa L, Luda, MP, Trossarelli L. UHMWPE.2. Thermally and photo initiated oxidation. Polymer Degradation and Stability 1997a; 58: 41-54.

33 Crompton TR. Polymer reference book. Shawbury: Rapra Technology Limited; 2006.

34 Cronin SB, Swan AK, Unlu MS, Goldberg B, Dresselhaus MS, Tinkham M. Measuring uniaxial strain in individual single-wall carbon nanotubes: resonance Raman spectra of AFM-modified SWNTS. Physical Review Letters 2004; 93: 167401/1- 4.

35 Dangsheng X. Friction and wear properties of UHMWPE composites reinforced with carbon fiber. Materials Letters 2005; 59:175–179.

36 Datsyuk V, Kalyva M, Papagelis K, Parthenios J, Tasis D, Siokou A, Kallitsisa I, Galiotis C. Chemical oxidation of multiwalled carbon nanotubes. Carbon 2008; 46:833–840.

37 Davidson D, Graves S, Batten J, Cumberland W, Harris J, Morgan. National joint replacement registry, Australian Orthopaedic Association, 2003.

38 Deng M, Shalaby SW. Properties of self-reinforced ultra high molecular weight polyethylene composites. Biomaterials 1997; 18:645-655.

39 Dorr LD, Wan Z, Longjohn DB, Dubios B, Murken R. Total hip arthroplasty with use of the metasul metal-on-metal articulation. Journal of Bone & Joint Surgery 2000; 82-A: 789–798.

40 Dresselhaus MS, Dresselhaus G, Avouris P. Carbon nanotubes synthesis, structure, properties and applications. Springer, Germany, 2001.

41 Drexler KE. Nanosystems, Molecular Machinery, Manufacturing and Computation. Wiley & Sons, New York, 1992.

42 Du, FM, Scogna, RC, Zhou W, Brand S, Fischer JE, Winey KI. Nanotube networks in polymer nanocomposites: Rheology and electrical conductivity. Macromolecules 2004; 37 (24): 9048- 9055.

43 Ducheyne P. Prosthesis fixation for orthopedics. In: Encyclopedia of medical devices and instrumentation. Ed. J. G. Webster, Wiley-Interscience, New York, 1988.

44 Dumbleton JH. Tribology of natural and artificial joints. Tribology series-3, Elsevier scientific publishing company, New York, 1981.

45 Ebbesen TW. Carbon nanotubes preparation and properties. CRC Press, Florida, 1997.

46 Edidin AA, Jewett CW, Kalinowski A, Kwarteng K, Kurtz SM. Degradation of mechanical behavior in UHMWPE after natural and accelerated aging. Biomaterials 2000; 21:1451-1460.

47 Eichert D., C. Combes, C. Drouet and C. Rey, Formation and evolution of hydrated surface layers of apatites, Key Engineering Materials 2005; 284(3/6): 105-108.

48 Essner A. Hip simulator wear comparison of metal-on-metal, ceramic-on-ceramic and crosslinked UHMWPE bearings. Wear 2005; 259:992-995.

49 Esumi K, Ishigami M, Nakajima A, Sawada K, Honda H. Chemical treatment of carbon nanotubes. Carbon 1996; 34:279-281.

50 Fang L, Leng Y, Gao P. Processing of hydroxyapatite reinforced ultrahigh molecular weight polyethylene for biomedical applications. Biomaterials 2005; 26: 3471–3478.

51 Fang L, Leng Y, Gao P. Processing and mechanical properties of HA/UHMWPE nanocomposites. Biomaterials 2006; 27:3701–3707.

52 Farling G. Human body implant of graphitic carbon fiber reinforced ultra-high molecular weight polyethylene. United States Patent No. 4,055,862; 1977.

53 Fonseca A, Kanagaraj S, Oliveira MSA, Simões JAO. Optimization of compression moulded UHMWPE/CNT composites for medical applications. Proceedings of Rapid Product Development 2008; 3015:1-5.

54 Fonseca A, Kanagaraj S, Oliveira MSA, Simões JAO. Enhanced UHMWPE reinforced with MWCNT through mechanical ball-milling. Defect and Diffusion Forum 2011; 312-315:1238-1243.

55 Galano A. Carbon nanotubes: promising agents against free radicals. Nanoscale 2010; 2: 373–380.

56 Ganji F, Samira VF, and Ebrahim VF. Theoretical description of hydrogel swelling: A Review. Iranian Polymer Journal 2010; 19 (5):375-398.

57 Ge S, S Wang, X Huang. Increasing the wear resistance of UHMWPE acetabular cups by adding natural biocompatible particles. Wear 2009; 267:770-776.

58 Gencur SJ, Rimnac CM, Kurtz SM. Fatigue crack propagation resistance of virgin and highly crosslinked, thermally treated ultra-high molecular weight polyethylene, Biomaterials 2006; 27:1550–1557.

59 Grady BP. Carbon Nanotube-Polymer Composites: Manufacture, Properties and Applications. John Wiley & Sons, New Jersey, 2011.

60 Guofang G, Huayong Y, Xin F. Tribological properties of kaolin filled UHMWPE composites in unlubricated sliding. Wear 2004; 25:688–694.

61 Guzman LA, Labhasetwar V, Song C, Jang Y, Lincoff AM, Levy R, Topol EJ. Local intraluminal infusion of biodegradable polymeric nanoparticles. A novel approach for prolonged drug delivery after balloon angioplasty. Circulation 1996; 94(6):1441-1448.

62 Haider H, Weisenburger JN, Kurtz SM, Rimnac CM, Freedman J, Schroeder DW, Garvin KL. Does vitamin E stabilized ultrahigh-molecular- weight polyethylene address concerns of cross-linked polyethylene in total knee arthroplasty?. The Journal of Arthroplasty 2012; 27(3): 461-469.

63 Hallab NJ, Jacobs JJ. Biologic effects of implant debris. Bulletin of the NYU Hospital for Joint Diseases 2009; 67(2):182-188

64 Harris WH. The problem is osteolysis. Clinical Orthopedics 1995; 311:46–5

65 Hashmi SAR, Neogi S, Pandey A, Chand N. Sliding wear of PP/UHMWPE blends: effect of blend composition, Wear 2001; 247:9–14.

66 Hench LL, Ethridge EC. Biomaterials- An interfacial approach, Academic Press, London, 1982.

67 http://advancedpt.patientsites.com/Injuries-Conditions/Ankle/Ankle Anatomy /a~47/article.html,http://lifepositiveayurveda.com/joint_pain.html, http://caretipsvilla.com/ tips/exercises-for-loosening-the-hip-joint-hamstring-calf muscles, referred on 27/11/11.

68 Hu Y, Jang I, Sinnott SB. Modification of carbon nanotube-polystyrene matrix composites through polyatomic-ion beam deposition: predictions from molecular dynamics simulations. Composites Science and Technology 2003; 63:1663 -1669.

69 Huang YY, Ahir SV, Terentjev EM. Dispersion rheology of carbon nanotubes in a polymer matrix. Physical Review B 2006; 73:125422 -1-9.

70 Iijima S, Ichihashi T, Ando Y. Pentagons, heptagons and negative curvature in graphite microtubule growth. Nature 1992; 356:776-778.

71 Imbeni V, Martini C, Lanzoni E, Poli G, Hutchings IM. Tribological behaviour of multi-layered PVD nitride coatings. Wear 2001; 251:997–1002.

72 Jacobs O, Mentz N, Poeppel A, Schulte K. Sliding wear performance of HDPE reinforced by continuous UHMWPE fibres. Wear 2000; 244:20–28.

73 Jahan MS, King MC, Haggard WO, Sevo KL, Parr JE. A study of long-lived free radicals in gamma-irradiated medical grade polyethylene. Radiation Physics and Chemistry 2001; 62:141–144.

74 Jia Z, Wang Z, Xu C, Liang J, Wei B, Wu D, et al. Study on poly (methyl methacrylate)/carbon nanotube composites. Material Science and Engineering A 1999; 271: 395-400.be composites. Composites Science and technology 2007, 67:3071-3077.

75 Kanagaraj S, Vardana FR, Zhiltsova TV, Oliveira MSA, Simoes JAO. Mechanical properties of high density polyethylene/carbon nanot

76 Kang PH, Nho YC. The effect of g-irradiation on ultra-high molecular weight polyethylene recrystallized under different cooling conditions. Radiation Physics and Chemistry 2001; 60:79-87.

77 Kang L, Galvin Al, Thomas D, Jina Z, Fisher J. Quantification of the effect of cross-shear on the wear of conventional and highly cross-linked UHMWPE. Journal of Biomechanics 2008; 41(2):340-346.

78 Kapoor G, Verma V, Rengaswamy V. Cells involved in immune system. Advanced Biotech Journal 2009; 9:1-12.

79 Khan IA, Murphy PM, Casciotti L, Schwartzman JD, Collins J, Gao JL, Yeaman GR. Mice lacking the chemokine receptor CCR1 show increased susceptibility to *toxoplasma gondii* infection. The Journal of Immunology 2001; 166:1930-1937.

80 Kilgour A, Elfick A. Influence of crosslinked polyethylene structure on wear of joint replacements. Tribology International 2009; 42:1582–1594.

81 Kim S. Changes in surgical loads and economic burden of hip and knee replacements in the US: 1997-2004. Arthritis and Rheumatism 2008; 59(4):481-488.

82 Kis A, Csányi G, Salvetat JP, Lee TN, Couteau E, Kulik AJ, Benoit W, Brugger J, Fórro L. Reinforcement of single-walled carbon nanotube bundles by intertube bridging. Nature Materials 2004; 3:153 – 157.

83 Klapperich C, Komvopoulos K, Pruitt L. Tribological properties and microstructure evolution of ultra high molecular weight polyethylene. Journal of Tribology 1999; 121: 394–402.

84 Ko T, Cooper S. Surface properties and platelet adhesion characteristics of acrylic acid and allalamine plasma-treated polyethylene. Journal of Applied Polymer Science 1993; 47:1601–1619.

85 Kogut L, Etsion I. A static friction model for elastic-plastic contacting rough surfaces. Transactions of the ASME 2004; 126: 34-40.

86 Kokubo T, Hanakawa M, Kawashita M, Minoda M, Bbeppu T, Miyamoto T, Nakamura T. Apatite formation on non-woven fabric of carboxymethylated chitin in SBF. Biomaterials 2004; 25: 4485-4488.

87 Koutsky J, Kocik J. Radiation damage of structural materials, Elsevier, Amsterdam, 1994.

88 Koyama S, Kim YA, Hayashi T, Takeuchi K, Fujii C, Kuroiwa N, Koyama H, Tsukahara T, Endo M. *In vivo* immunological toxicity in mice of carbon nanotubes with impurities. Carbon 2009; 47: 1365–1372.

89 Koyama S, Endo M, Kim YA, Hayashi T, Yanagisawa T, Osaka K, Koyama H, Haniu H, Kuroiwa N. Role of systemic T-cells and histopathological aspects after subcutaneous implantation of various carbon nanotubes in mice. Carbon 2006; 44:1079–1092.

90 Krasheninnikov AV, Nordlund K, Keinonen J. Production of defects in supported carbon nanotubes under ion irradiation. Physical Review B 2002; 65:165423–165428.

91 Krasheninnikov AV, Nordlund K. Irradiation effects in carbon nanotubes. Nuclear Instruments and Methods in Physics Research Section B 2004; 216:355–366.

92 Krasheninnikov AV, Banhart F. Engineering of nanostructured carbon materials with electron or ion beams. Nature Material 2007; 6:723-733.

93 Kurtz SM, Mowat F, Ong K. Prevalence of primary and revision total hip and knee arthroplasty in the United States from 1990 through 2002. Journal of Bone &Joint Surgery 2005; 87:1487-1497.

94 Kurtz SM, Ong K, Lau E, Halpern M. Projections of primary and revision hip and knee arthroplasty in the United States from 2005 to 2030. Journal of Bone & Joint Surgery 2007; 89:780-785.

95 Kurtz SM. UHMWPE Hand book. Second edition, Academic Press, Paris, 2009.

96 Lacerda L, Bianco A, Prato M, Kostarelos K. Carbon nanotubes as nanomedicines: from toxicology to pharmacology. Advanced Drug Delivery Reviews 2006; 58:1460–1470.

97 Lam CW, James JT, McCluskey R, Hunter RL. Pulmonary toxicity of single-wall carbon nanotubes in mice 7 and 90 days after intratracheal instillation. Toxicological Sciences 2004; 77:126-134.

98 Lavernia CJ, Hernandez VH, Rossi MD. Payment analysis of total hip replacement. Current Opinion in Orthopedics 2007; 18:23–27.

99 Lee R, Essner A, Wang A, Jaffe WL. Scratch and wear performance of prosthetic femoral head components against crosslinked UHMWPE sockets. Wear 2009; 267:1915–1921.

100 Lerf R, Zurbru D, Delfosse D. Use of vitamin E to protect cross-linked UHMWPE from oxidation. Biomaterials 2010; 31:3643-3648.

101 Lewis G. Properties of crosslinked ultra-high-molecular-weight polyethylene. Biomaterials 2001; 22:371-401.

102 Liu C, Ren L, Arnell RD, Tong J. Abrasive wear behavior of particle reinforced ultrahigh molecular weight polyethylene composites. Wear 1999; 225–229:199–204.

103 Long LJ, Yuan ZY, Qingliang W, Shirong GE. Biotribological behavior of ultra high molecular weight polyethylene composites containing bovine bone hydroxyapatite. Journal China University of Mining & Technology 2008; 18:0606–0612.

104 Lucas AA, Ambrósio JD, Otaguro H, Costa LC, Agnelli JAM. Abrasive wear of HDPE/UHMWPE blends. Wear 2011; 270:576–583.

105 Maksimkin AV, Kaloshkin SD, Kaloshkina MS, Gorshenkov MV, Tcherdyntsev VV, Ergin KS, Shchetinin IV. Ultra-high molecular weight polyethylene reinforced with multi-walled

carbon nanotubes: Fabrication method and properties. Journal of Alloys and Compounds 2012; 536: 538–540.

106 Ma'adeed MAA, Al-Qaradawi IY, Madi N, Al-Thani NJ. The effect of gamma irradiation and shelf aging in air on the oxidation of ultra high molecular weight polyethylene. Applied Surface Science 2006; 252:3316–3322.

107 McKellop H, Shen FW, Lu B, Campbell P, Salovey R. Development of an extremely wear resistant ultra-high molecular weight polyethylene for total hip replacements. Journal of Orthopedics Research 1999; 17(2):157-167.

108 Medel F, Barrena EG, Alvarez FG, Rıos R, Villa LG, Puertolas JA. Fractography evolution in accelerated aging of UHMWPE after gamma irradiation in air. Biomaterials 2004; 25:9–21.

109 Minfang M, Osswald S, Gogotsi Y, Winey KI. An in situ Raman spectroscopy study of stress transfer between carbon nanotubes and polymer. Nanotechnology 2009; 20: 335703-335710.

110 Morlanes MJM, Castell P, Nogués VM, Martinez MT, Alonso PJ, Puértolas JA. Effects of gamma-irradiation on UHMWPE/MWNT nanocomposites. Composite Science Technology 2011; 71:282–288.

111 Morlanes MJM, Castell P, Alonso PJ, Martinez MT, Pue´rtolas JA. Multi-walled carbon nanotubes acting as free radical scavengers in gamma-irradiated ultrahigh molecular weight polyethylene composites. Carbon 2012; 50:2442 –2452.

112 Morley KS, Webb PB, Tokareva NV, Krasnov AP, Popov VK, Zhang J, Roberts CJ, Howdle SM. Synthesis and characterisation of advanced UHMWPE/silver nanocomposites for biomedical applications. European Polymer Journal 2007; 43:307–314.

113 Mu M, Osswald S, Gogotsi Y, Winey KI. An in situ Raman spectroscopy study of stress transfer between carbon nanotubes and polymer. Nanotechnology 2009; 20:335703-335710.

114 Muratoglu OK, Bragdon CR, O'Connor DO, Jasty M, Harris WH, Gul R, McGarry F. Unified wear model for highly crosslinked ultrahigh molecular weight polyethylenes (UHMWPE). Biomaterials 1999; 20(16):1463-1470.

115 Muratoglu OK, Bragdon CR, O'Connor DO, Jasty M, Harris WH. A novel method of crosslinking UHMWPE to improve wear, reduce oxidation and retain mechanical properties. Journal of Arthroplasty 2001; 16(2):149-160.

116 Muratoglu OK, O'Connor DO, Bragdon CR, Delaney J, Murali J, Harris WH, Merrill E, Venugopalan P. Gradient crosslinking of UHMWPE using irradiation in molten state for total joint arthroplasty. Biomaterials 2002; 23:717–724.

117 Nakajima A, Mawatari T. Effects of surface topography and running-in upon rolling contact fatigue life - evaluation by plasticity index, in: Dowson, D., (Eds), Tribology for Energy Conservation, Elsevier science B V, Netherlands, pp 291-299, 1998.

118 Nakamura K, Ogata S, Ikada Y. Assessment of heat and storage conditions on c-ray and electron beam irradiated UHMWPE by electron spin resonance. Biomaterials 1998; 19 2341-2346.

119 Narayan R. Biomedical materials. Springer, New york, 2009.

120 Nel A, Xia T, Maedler L, Li N. Toxic potential of materials at the nanolevel. Science 2006; 311:622-627.

121 Oliver WC, Pharr GM. An improved technique for determining hardness and elastic modulus using load and displacement sensing indentation experiments. Journal of Materials Research 1992; 7:1564-1583.

122 Oliver WC, Pharr GM. Measurement of hardness and elastic modulus by instrumented indentation: Advances in understanding and refinements to methodology. Journal of Materials Research 2004; 19:3-20.

123 Oonishi H. Long term clinical results of THR. Clinical results of THR of an alumina head with a cross-linked UHMWPE cup. Orthopedic Surgery and Traumatology. 1995; 38:1255-1264.

124 Oonishi H, Kunot M, Tsujit E, Fujisawa A. The optimum dose of gamma radiation–heavy doses to low wear polyethylene in total hip prostheses, Journal of Materials Science: Materials in Medicine 1997; 8:11-18.

125 Oral E, Wannomae KK, Hawkins N, Harris WH, Muratoglu OK. α-Tocopherol-doped irradiated UHMWPE for high fatigue resistance and low wear. Biomaterials 2004; 25:5515–5522.

126 Oral E, Greenbaum ES, Malhi AS, Harris WH, Muratoglu OK. Characterization of irradiated blends of α-tocopherol and UHMWPE. Biomaterials 2005; 26:6657–6663.

127 Oral E, Rowell SL, Muratoglu OK. The effect of α-tocopherol on the oxidation and free radical decay in irradiated UHMWPE. Biomaterials 2006. 27:5580–5587.

128 Oral E, Malhi AS, Muratoglu OK. Mechanisms of decrease in fatigue crack propagation resistance in irradiated and melted UHMWPE. Biomaterials 2006a; 27:917–925.

129 Oral E, Orhun K. Muratoglu, Radiation cross-linking in ultra-high molecular weight polyethylene for orthopaedic applications. Nuclear Instruments and Methods in Physics Research B 2007; 265:18–22

130 Oral E, Christine Godleski Beckos , Arnaz S. Malhi , Orhun K. Muratoglu. The effects of high dose irradiation on the cross-linking of vitamin E-blended ultrahigh molecular weight polyethylene. Biomaterials 2008; 29:3557–3560.

131 Oral E, Beckos CAG, Lozynsky AJ, Malhi AS, Muratoglu OK. Improved resistance to wear and fatigue fracture in high pressure crystallized vitamin E containing ultra-high molecular weight polyethylene. Biomaterials 2009; 30:1870–1880.

132 Ormsby R, McNally T, O'Hare P, Burke G, Mitchell C, Dunne N. Fatigue and biocompatibility properties of a poly (methyl methacrylate) bone cement with multi-walled carbon nanotubes. Acta Biomaterialia 2012; 8:1201–1212.

133 Ouyang M, Huang JL, Cheung CL, Lieber CM. Energy gaps in "Metallic" single walled carbon nanotubes. Science 2001; 292:702-705.

134 Park JB. Orthopedic prosthesis fixation. Annals of Biomedical Engineering 1992; 20(6):583-594.

135 Park JB, Bronzino JD. Biomaterials principles and applications, CRC Press, London, 2003.

136 Park J, Lakes RS. Biomaterials - an introduction. 3rd edition, Springer publications, New York, 2007.

137 Pedro S, Albano C, Perera R. Use of electron paramagnetic resonance to evaluate the behavior of free radicals in irradiated polyolefins. Revista Latinoamericana de Metalurgiay Materiales 2008; 28:79-90.

138 Perepechko II. An introduction to polymer physics. Mir Publishers, Moscow, 1981.

139 Peter DF, Campbell PA, Amstutz HC. Metal versus polyethylene wear particles in total hip replacements: A review. Clinical Orthopaedics & Related Research 1996; 329: S206-S216.

140 Pharr GM, Oliver WC, Brotzen FR. On the generality of the relationship among contact stiffness, contact area, and elastic-modulus during indentation. Journal of Materials Research 1992; 7:613-617.

141 Pimenta A, Dresselhaus G, Dresselhaus MS, Canc¸ado LG, Jorio A, Saito R. Studying disorder in graphite-based systems by Raman spectroscopy. Physical Chemistry Chemical Physics 2007; 9:1276–1290.

142 Plumlee K, Schwartz CJ. Improved wear resistance of orthopaedic UHMWPE by reinforcement with zirconium particles. Wear 2009; 267:710–717.

143 Poland CA, Duffin R, Kinloch I, Maynard A, Wallace WAH, Seaton A, Stone V, Brown S, MacNee W, Donaldson K. Carbon nanotubes introduced into the abdominal cavity of mice show asbestos-like pathogenicity in a pilot study. Nature Nanotechnology 2008; 3:423-428.

144 Pradhan SK, Dwarakadasa ES, Reucroft PJ. Processing and characterization of coconut shell powder filled UHMWPE. Materials Science and Engineering A 2004; 36:757–762.

145 Pradhan NR, Duan H, Liang J, Iannacchione GS. The specific heat and effective thermal conductivity of composites containing single-wall and multi-wall carbon nanotubes. Nanotechnology 2009; 20: 1-7.

146 Premnath V, Bellare A, Merrill EW, Jasty M, Harris WH. Molecular rearrangements in ultra high molecular weight polyethylene after irradiation and long-term storage in air. Polymer 1999; 40: 2215–2229.

147 Puertolas JA, Larrea A, Barrena EG. Fracture behavior of UHMWPE in non-implanted, shelf-aged knee prostheses after gamma irradiation in air. Biomaterials 2001; 22:2107-2114.

148 Qianming G, Dan L, Zhi L, Xiao Y, Li L.. Tribology properties of carbon nanotube reinforced composites. in: Friedrich, K., Schlarb, A.K., (Eds.) Tribology of polymeric nanocomposites: Tribology and interface engineering series -55, Elsevier, London, p. 245-270, 2008.

149 Ratner BD, Allan S. Hoffman, Frederick J. Schoen, Jack E. Lemons. Biomaterials Science, An Introduction to Materials in Medicine, 2nd ed. Elsevier Academic Press. USA, 2004.

150 Reis J, Kanagaraj S, Fonseca A, Mathew MT, Silva FC, Potes J, Oliveira MSA, Simoes JAO. *In vitro* studies on multiwalled carbon nanotubes/ultrahigh molecular weight polyethylene nano composites. Brazilian Journal of Medical and Biological Research 2010; 43:476-482.

151 Reisel AD, Klemm V, Irmer G, Muller E. Nano and microstructure of short fiber reinforced and unreinforced hydroxyapatite. Biomedical Technology 2002; 47:397-400.

152 Ren Y, Yang K, Zhang B. In vitro study of platelet adhesion on medical nickel-free stainless steel surface. Materials Letters 2005; 59:1785–1789.

153 Reno F, Mario Cannas. UHMWPE and vitamin E bioactivity: An emerging perspective. Biomaterials 2006; 27(16):3039-3043.

154 Rhodes NP, Wilson DJ William RL. The effect of gas plasma modification on platelet and contact phase activation processes. Biomaterials 2007; 28: 4561–4570.

155 Ridley MD, Jahan MS. Measurements of free radical in vitamin E-doped ultra-high molecular weight polyethylene: Dependence on materials processing and irradiation environments. Nuclear Instruments and Methods in Physics Research B 2007; 265:62–66

156 Rieker CB, Konrad R, Schon R, Schneider W, Abt NA. *In Vivo* and *In Vitro* Surface Changes in a Highly Cross-linked Polyethylene. The Journal of Arthroplasty 2003; 18: 48-54.

157 Ritter MA. All polyethylene versus metal backing. Clinical Orthopedics and Related Research 1995; 311: 69-75.

158 Ritter U, Scharff P, Siegmund C, Dmytrenko OP, Kulish NP, Prylutskyy YI, Belyi NM, Gubanov VA, Komarova LI, Lizunova SV, Poroshin VG, Shlapatskaya VV, Bernas H. Radiation damage to multi-walled carbon nanotubes and their Raman vibrational modes. Carbon 2006; 44:2694–2700.

159 Ruan SL, Gao P, Yang XG, Yu TX. Toughening high performance ultrahigh molecular weight polyethylene using multiwalled carbon nanotubes. Polymer 2003; 44:5643–5654.

160 Samad MA, Sinha SK. Mechanical, thermal and tribological characterization of a UHMWPE film reinforced with carbon nanotubes coated on steel. Tribology International 2011; 44:1932–1941.

161 Samad MA, Sinha SK. Dry sliding and boundary lubrication performance of a UHMWPE/CNTs nanocomposite coating on steel substrates at elevated temperatures. Wear 2011a; 270:395–402.

162 Sammalkorpi M, Krasheninnikov A, Kuronen A, Nordlund K, Kaski K. Mechanical properties of carbon nanotubes with vacancies and related defects. Physical Review B 2004; 70: 245416-1-8.

163 Samrutishika B. Experimental study of mechanical and electrical properties of carbon nanofiber/ epoxy composites. Journal of Materials Design 2010; 31: 2406-2413.

164 Sato Y, Yokoyama A, Shibata K, Akimoto Y, Ogino S, Nodasaka Y, Kohgo T, Tamura K, Akasaka T, Uo M, Motomiya K, Jeyadevan B, Ishiguro M, Hatakeyama R, Watari F, Tohji K. Influence of length on cytotoxicity of multiwalled carbon nanotubes against human acute monocytic leukemia cell line THP-1 in vitro and subcutaneous tissue of rats in vivo. Molecular Biosystems 2005; 1:176-182.

165 Sato Y, Yokoyama A, Kasai T, Hashiguchi S, Ootsubo M, Ogino S, Sashida N, Namura M, Motomiy K, Jeyadevan B, Tohji K. *In vivo* rat subcutaneous tissue response of binder-free multi-walled carbon nanotube blocks cross-linked by de-fluorination. Carbon 2008; 46: 1927–1934.

166 Schultz RML, Moore VC, Leonard AD, Price BK, Kosynkin DV, Lu M, Partha R, Conyers JL, Tour JM. Antioxidant Single-Walled Carbon Nanotubes. Journal of American Chemical Society 2009; 131:3934-3941.

167 Schwartz CJ, Bahadur S, Mallapragada SK. Effect of crosslinking and Pt–Zr quasicrystal fillers on the mechanical properties and wear resistance of UHMWPE for use in artificial joints. Wear 2007; 263:1072-1080.

168 Shen FW, McKellop HA, Salovey R. Irradiation of chemically crosslinked ultrahigh molecular weight polyethylene. Journal of Polymer Science Part B: Polymer Physics 1996; 34:1063-1077.

169 Shibata N, Tomita N. The anti-oxidative properties of a-tocopherol in g-irradiated UHMWPE with respect to fatigue and oxidation resistance. Biomaterials 2005; 26:5755–5762.

170 Singh BP, Singh D, Mathur RB, Dhami TL. Influence of surface modified MWCNTs on the mechanical, electrical and thermal properties of polyimide nanocomposites. Nanoscale Research Letters 2008; 3: 444–453.

171 Singh DK, Iyer PK, Giri PK. Diameter dependence of interwall separation and strain in multiwalled carbon nanotubes probed by X-ray diffraction and Raman scattering studies. Diamond & Related Materials 2010; 19:1281–1288.

172 Smith BW, Luzzi DE. Electron irradiation effects in single wall carbon nanotubes. Journal of Applied Physics 2001; 90:3509-3515.

173 Sokoloff L. The Joints and synovial fluid - Volume 1, Academic Press, New York, 1978.

174 Sousa RA, Oliveira AL, Reis RL, Cunha AM, Bevis MJ. Bi-composite sandwich moldings: processing, mechanical performance and bioactive behavior. Journal of Materials Science Materials in Medicine 2003; 14:385-397.

175 Sreekanth PSR, Naresh Kumar N, Kanagaraj S. Improving post irradiation stability of high density polyethylene by multi walled carbon nanotubes. Composites Science and Technology 2012; 72:390–396.

176 Stoller AP, Johnson TS, Popoola OO, Humphrey MS, Blanchard RC. Highly crosslinked polyethylene in posterior-stabilized total knee arthroplasty. The Journal of Arthroplasty 2011, 26(3):483-491.

177 Suarez JCM, de Biasi RS. Effect of gamma irradiation on the ductile-to-brittle transition in ultra-high molecular weight polyethylene. Polymer Degradation and Stability 2003; 82:221–227.

178 Sugano N, Saito M, Yamamoto T, Nishii T, Yau SS, Wang A. Analysis of a retrieved UHMWPE acetabular cup crosslinked in air with 1000 kGy of gamma radiation. Journal of Orthopaedic Research 2004; 22:828–831.

179 Sui G, Zhong WH, Ren X, Wang XQ, Yang XP. Structure, mechanical properties and friction behavior of UHMWPE/HDPE/carbon nanofibers. Materials Chemistry and Physics 2009; 115:404–412.

180 Tong J, Ma Y, Jiang M. Effects of the wollastonite fiber modification on the sliding wear behavior of the UHMWPE composites. Wear 2003; 255:734–741.

181 Ticona data sheet, http://tools.ticona.com/tools/mcbasei/product- tools.php?sProduct=GUR, referred on 20/02/2010

182 Tomita N, Kitakura T, Onmori N, Ikada Y, Aoyama E, Prevention of fatigue cracks in ultrahigh molecular weight polyethylene joint components by the addition of vitamin E, Journal of Biomedical Materials Research 1999;48(4):474-478.

183 Treacy MMJ, Ebbesen TW, Gibson JM. Exceptionally high Young's modulus observed for individual carbon nanotubes. Nature 1996; 381:678–680.

184 Upman PJ. Toxicity Testing (of medical devices), Handbook of Biomaterials Evaluation, (Ed) A. VonRecum, 2nd ed. Taylor & Francis: Philadelphia, 1998.

185 Wang A, Schmidig G. Ceramic femoral heads prevent runaway wear for highly crosslinked polyethylene acetabular cups by third-body bone cement particles. Wear 2003; 255:1057-1063.

186 Wang HF, Wang J, Deng XY, Sun HF, Shi ZJ, Gu ZN, Liu Y, Zhao Y. Biodistribution of carbon single-wall carbon nanotubes in mice. Journal of Nanoscience Nanotechnology 2004; 4:1019-1024.

187 Wang S, Ge S. The mechanical property and tribological behavior of UHMWPE: Effect of molding pressure. Wear 2007; 263:949–956.

188 Wang A, SS Yau, A Essner, L Herrera, M Manley, J Dumbleton. A highly crosslinked UHMWPE for CR and PS total knee arthroplasties. The Journal of Arthroplasty 2008; 23(4): 559-566.

189 Wang H, Changjian L, Ren H. Effects of structure and composition of the CaP composite coatings on apatite formation and bioactivity in simulated body fluid. Applied Surface Science 2009; 255:4074–4081.

190 Wang Q, Liu J, Ge S. Study on Biotribological Behavior of the Combined Joint of CoCrMo and UHMWPE/BHA Composite in a Hip Joint Simulator. Journal of Bionic Engineering 2009a; 6:378–386.

191 Watts PCP, Fearon PK, Hsu WK, Billingham NC, Kroto HW, Walton DRM. Carbon nanotubes as polymer antioxidants. Journal of Materials Chemistry 2003; 13:491–495.

192 Wood WJ, Maguire RG, Zhong WH. Improved wear and mechanical properties of UHMWPE–carbon nanofibers composites through an optimized paraffin-assisted melt-mixing process. Composites: Part B 2011; 42:584–591.

193 Wong JY, Bronzino JD. Biomaterials, CRC Press, USA, 2007.

194 Xie XL, Tang CY, Chan KYY, Wu XC, Tsui CP, Cheung CY. Wear performance of ultrahigh molecular weight polyethylene/quartz composites. Biomaterials 2003; 24:1889–1896.

195 Xin F, Chen J, Zou JP, Wan Q, Zhou ZC, Ruan JM. Bone-like apatite formation on HA/316L stainless steel composite surface in simulated body fluid. Transactions of nonferrous Metals Society of China 2009; 19: 347-352.

196 Xiong L, Xiong D, Jin J. Study on tribological properties of irradiated crosslinking UHMWPE nano-composite. Journal of Bionic Engineering 2009; 6:7–13.

197 Xu Z, Chen L, Liu L, Wu X, Chen L. Structural changes in multi-walled carbon nanotubes caused by c-ray irradiation. Carbon 2011; 49:339–351.

198 Xue Y, Wu W, Jacobs O, Schadel B. Tribological behaviour of UHMWPE/HDPE blends reinforced with multi-wall carbon nanotubes. Polymer Testing 2006; 25:221–229.

199 Yang K, Mingyuan G, Yiping G, Xifeng P, Guohong M. Effects of carbon nanotube functionalization on the mechanical and thermal properties of epoxy composites. Carbon 2009; 47:1723 –1737.ubes. Topics applied Physics 2001; 80:287-327.

200 Yakobso BI, Avouris P. Mechanical properties of carbon nanot

201 Zeynalov EB, Friedrich JF. Antioxidative activity of carbon nanotube and nanofiber. The Open Mater Science Journal 2008; 2: 28–34.

202 Zhang J, Zou H, Qing Q, Yang Y, Li Q, Liu Z, Guo X, Du Z. Effect of chemical oxidation on the structure of single-walled carbon nanotubes. Journal of Physics Chemmistry B 2003; 107:3712-3718.

203 Zhang QH, Lippits DR, Rastogi S. Dispersion and rheological aspects of SWNTs in ultrahigh molecular weight polyethylene. Macromolecules 2006; 39: 658-666.

204 Zhou LG, Shi SQ. Adsorption of foreign atoms on Stone–Wales defects in carbon nanotube. Carbon 2003; 41:579-625.

205 Zhou J, Komvopoulos K. Wear mechanisms of untreated and gamma irradiated ultra-high molecular weight polyethylene for total joint replacements. Journal of Tribology 2005; 127: 273-279.

206 Zhu YH, Chiu KY, Tang WM. Review Article: Polyethylene wear and osteolysis in total hip arthroplasty. Journal of Orthopaedic Surgery 2001; 9: 91-99.

List of Publications

Journal papers

1. P. S. Rama Sreekanth, S. Kanagaraj Restricting the ageing degradation of the mechanical properties of gamma irradiated UHMWPE using MWCNTs. Journal of Mechanical Behavior of Biomedical Materials .21, 57-66, 2013.
2. P. S. Rama Sreekanth, S. Kanagaraj. Biocompatibility studies on MWCNTs reinforced ultra high molecular weight polyethylene nanocomposites. 27(1), 2013. (Accepted-Trends in Biomaterials and Artificial organs)
3. P. S. Rama Sreekanth, S. Kanagaraj. Assessment of bulk and surface properties of medical grade UHMWPE based nanocomposites using Nanoindentation and microtensile testing. Journal of Mechanical Behavior of Biomedical Materials 18, 140-151, 2013.
4. P. S. Rama Sreekanth, S. Kanagaraj. Influence of MWCNT and gamma irradiation on thermal characterization of medical grade UHMWPE. Bulletin of material science, 2013 (accepted)
5. N. Naresh Kumar, P. S. Rama Sreekanth, S. Kanagaraj. Effect of γ-irradiation on thermal properties of MWCNTs reinforced HDPE. Advanced Nanoscience and Nanotechnology-Springer Proceedings in Physics 143, 408-418, 2013.
6. P. S. Rama Sreekanth, N. Naresh Kumar, S. Kanagaraj. Improving post irradiation stability of high density polyethylene by multi walled carbon nanotubes. Composites Science and Technology 72, 390-396, 2012.
7. P. S. Rama Sreekanth, N. Naresh Kumar, S. Kanagaraj. Effect of MWCNT on mechanical properties of γ -irradiated UHMWPE during shelf ageing process. Advanced Materials Research 410, 160-163, 2012.

8. P. S. Rama Sreekanth, K. Acharyya, I. Talukdar, S. Kanagaraj. Studies on gamma irradiation induced defects on the surface of multi wall carbon nanotubes. Proceeding of Processing and Fabrication of Advanced Materials, 21: 1081-1086, 2012.
9. P. S. Rama Sreekanth, S. Kanagaraj. UHMWPE for total joint replacements: A review on trends and developments. NE Orthoscan 7, 87-99, 2011.
10. P. S. Rama Sreekanth, S. Kanagaraj. Influence of γ-irradiation and MWCNT reinforcement on the wear behavior of UHMWPE under dry sliding condition. (under preparation), 2013.
11. P. S. Rama Sreekanth, S. Kanagaraj. Comparison of multiwall carbon nanotubes and alpha-tocopherol in limiting the age degradation of the mechanical properties of gamma-irradiated ultra high molecular weight polyethylene. (under preparation), 2013.

Book chapter

1. P. S. Rama Sreekanth and S Kanagaraj. Wear of Biomedical implants, in: Tribology for Scientists and Engineers: From Basics to Advanced Concepts, editors: Sudeep I, Michael N, Kailas SV, Lovell MR, Menezes PL. Springer publications, USA (Accepted), 2012.

Papers presented in international conferences:

1. P. S Rama Sreekanth, S. Kanagaraj, Feasibility studies on UHMWPE/MWCNTs nanocomposites for total joint replacements-A Pre and Post gamma irradiation study. Intl conference on design of biomaterials, IISc Bangalore*, India, December 9-11, 2012.
2. P. S. Rama Sreekanth, S. Kanagaraj. Studies on UHMWPE/MWCNT nanocomposites for total joint replacements. Adv. Nano Materials, Chennai*, IIT Madras, October 17- 19, 2012.

3. P. S. Rama Sreekanth, S. Kanagaraj. Antioxidant activity of carbon nanotubes in preventing the loss of mechanical properties of γ irradiated UHMWPE/MWCNT nanocomposites used in orthopedic application. 9th World Biomat. Congress, Chengdu, China, June 1– 5, 2012.
4. P. S. Rama Sreekanth, N. Naresh Kumar, Ravindra Reddy, Mangala Lahkar, B. Bhaskar, S Kanagaraj. A study on the bioactive and hemocompatibility of UHMWPE/MWCNT nanocomposites. 9th World Biomat. Congress, Chengdu, China, June 1–5, 2012.
5. P. S. Rama Sreekanth, N. Naresh Kumar and S. Kanagaraj. Effect of MWCNT on Mechanical Properties of γ-irradiated UHMWPE during Shelf Ageing Process. 20th Intl. Symp. on Processing and Fabrication of Adv. Mat., Hong Kong*, December 15-18, 2011.
6. P. S. Rama Sreekanth, S. Kanagaraj. Thermal characterization of gamma irradiated medical grade UHMWPE reinforced with multiwalled carbon nanotubes. International Conference on Advanced Nanomaterials and Nanotechnology, IIT Guwahati, India, December 8-10, 2011.
7. N. Naresh Kumar, P. S. Rama Sreekanth, S Kanagaraj. Effect of gamma-irradiation on thermal properties of multi walled carbon nanotubes reinforced HDPE. Intl. Conference on Advanced Nanomaterials and Nanotechnology, IIT Guwahati, India, December 8-10, 2011.
8. P. S. Rama Sreekanth, N. Naresh Kumar, S Arun, P Madhusoodanan, S Kanagaraj. Role of carbon nanotubes in preventing shelf aging of gamma irradiated polyethylene. Intl. conf. on Biomat. and Implants: Prospects and Possibilities in the New Millennium at CGCRI, Kolkata, July 21-23, 2011.
9. P. S. Rama Sreekanth, S. Kanagaraj. Feasibility study on carbon nanotubes and polyethylene nanocomposite for acetabular cup in THR. IORACON-2011, NEIGRIHMS, Shillong, India, April 9-10, 2011.

10. N. Naresh Kumar, P. S. Rama Sreekanth, S Kanagaraj. Biocompatibility and morphology studies on ultrahigh molecular weight polyethylene/multi walled carbon nanotubes nanocomposites. 4th Indo-Australian Conf. on Biomat., Tissue Engg. and Drug Delivery Systems, Ahmedabad*, India, February 10-12, 2011.
11. P. S. Rama Sreekanth and S.Kanagaraj. Miniaturized disc technique for mechanical characterization of carbon nanotubes/high density polyethylene nanocomposites. Intl. conf. on Nanosci., Nanotech., and Adv. Mat., Visakhapatnam, India, December 17-19, 2010.

*presented by supervisor/colleague